DEVELOPMENT OF A NOVEL PRIME-BOOST IMMUNOTHERAPY FOR DEDIFFERENTIATED LIPOSARCOMA

ANNA JIROVEC

Thesis submitted to the University of Ottawa
in partial Fulfillment of the requirements for the
Doctorate of Philosophy in Microbiology and Immunology

Department of Biochemistry, Microbiology and Immunology
Faculty of Medicine
University of Ottawa

Abstract

Cancer is a multifaceted and intricate disease that poses a significant global health burden and impacts millions of individuals worldwide. Among the diverse subtypes of cancer, sarcoma stands out as a rare yet highly aggressive malignancy originating from connective tissues such as bone, cartilage, and muscle, and presents challenges in diagnosis and treatment. Despite remarkable progress in cancer research and therapy, the prognosis for sarcoma patients remains low, requiring development of novel therapeutic avenues.

Cancer immunotherapies focused on generating tumor-specific responses are emerging as promising alternatives to traditional cancer treatments. T cell-based immunotherapies, such as cancer vaccines and CAR-T cells, are designed to target tumor antigens and generate long term immune memory capable of constant surveillance against recurrence. Therefore, the objective of this study is to establish the groundwork for a novel T cell-based immunotherapeutic approach tailored specifically to sarcoma.

Throughout the study, we explored various critical aspects associated with the development of immunotherapy. First, we conducted a proof-of-concept study, evaluating a novel prime-boost vaccine combination employing anti-DEC205 and oncolytic rhabdoviruses targeting a model antigen in a pre-clinical model of melanoma. This study showed that using the DEC205 dendritic cell-targeting antibody as a vector for antigen delivery is a promising alternative to other prime-boost strategies being evaluated in the clinic (NCT02285816).

To facilitate the translation of this therapeutic approach to clinical applications, a comprehensive understanding of the human sarcoma tumor immune microenvironment and the identification of a suitable target antigen are essential. Therefore, we conducted an in-depth immune profiling of a high grade and aggressive dedifferentiated liposarcoma (DDLS) using gene expression profiling and immunohistochemistry. We gained valuable insights into the tumor biology and the complex immunological mechanisms within the tumor immune microenvironment. Notably, we

identified a novel antigen that is highly expressed in human DDLS and absent in normal tissues, that could be used as a potential antigenic target for immunotherapy.

Finally, we evaluated a range of prime and boost vaccine vectors targeting the newly discovered target antigen in pre-clinical murine sarcoma models. Ultimately, we found that an oncolytic rhabdovirus prime and a modified vaccinia Ankara virus boost targeting the sarcoma antigen generates strong antigen specific cellular and humoral responses and protects against tumor growth in a prophylactic model of sarcoma. Altogether, this study lays the foundations for the development of a T cell-based immunotherapy employing an oncolytic rhabdovirus and targeting a novel antigen for the treatment of sarcoma.

Acknowledgements

I wish to extend my sincere thank you to all those whose support and mentorship have been instrumental in the completion of this work. While this acknowledgment inevitably falls short of my gratitude, I hope to one day return the favor somehow.

Firstly, I would like to thank my supervisor Dr. Jean-Simon Diallo for providing an ideal research environment and support throughout my studies, and for mentoring me since my Undergraduate Honors Project. I am grateful to Dr. Fanny Tzelepis, whose passion for immunology kindled my own curiosity and drove me to embark on this PhD journey. Fanny's mentorship and encouragement have undoubtedly shaped the scientist I am today.

I extend my thanks to the members of my thesis advisory committee: Dr. Michele Ardolino, Dr. Bryan Lo, and Dr. Joel Werier. Their guidance and invaluable feedback have been instrumental in refining my research. Dr. Werier, your unwavering support in facilitating my engagement with the scientific and clinical community through travel is deeply appreciated; may our collaborative efforts continue to bridge the gap between laboratory research and clinical practice.

To my lab colleagues—Andrew Chen, Anne Landry, Max Thomson, Nouf Alluqmani, Akram Alwithenani, Zaid Taha, and Dr. Rozanne Arulanandam, thank you for all your support. Special thank you to Dr. Elena Godbout, Dr. Daniel Serrano, Dr. Nicole Forbes, for our in-depth troubleshooting and lengthy scientific discussions in small group meetings, this project wouldn't have come this far without you. A heartfelt thank you to Michael Phan, Dr. Anabel Bergeron, and Boaz Wong, whose friendship helped me get through some challenging times. And of course, thank you to Dr. Samriti Birdi, with whom my immunology journey started and blossomed into a cherished friendship.

Finally, thank you to my parents, Katerina and Petr, and to my sister, Elise, whose unwavering support has been a cornerstone of my journey. Elise, I hope that the knowledge gained during my studies will contribute meaningfully to your own scientific pursuits.

Table of Contents

List of Abbreviations

3-methylcholanthrene	MCA
adenovirus	Ad
adenovirus serotype 5	Ad5
antibody-dependent cellular toxicity (ADCC)	ADCC
antigen presenting cell	APC
C-type multilectin receptor	CLR
Cancer-testis antigen	CTA
carcinoembryonic antigen	CEA
CD4+ helper T cells	Th
CD4+ regulatory T cells	Tregs
central memory T cell	T_{CM}
cyclin-dependent kinase 4	CDK4
Cytotoxic CD8+ T cells	CTL
cytotoxic T-lymphocyte associated protein 4	CTLA-4
damage-associated molecular proteins	DAMPs
dedifferentiated liposarcoma	DDLS
dendritic cells	DC
epidermal growth factor	EGFR
Herpes simplex virus 1	HSV-1
hepatitis B viruses	HBV
human immunodeficiency virus	HIV
human papillomavirus	HPV
immune checkpoint blockade	ICB
infected cell vaccine	ICV
interferon gamma	IFNγ
interleukin	IL
low-density lipoprotein	LDL
low-density lipoprotein receptor	LDLR
lymphocyte activation gene-3	LAG3
Lymphokine-activated killer T-cell-originated protein kinase	PBK
macrophage mannose receptor	MMR
major histocompatibility complex	MHC
Maraba virus	MG1
melanoma-associated antigen-A3	MAGE-A3
memory T cells	T_{MEM}
modified vaccinia Ankara	MVA
myeloid-derived suppressor cell	MDSC
New York esophageal squamous cell carcinoma 1	NY-ESO-1
Natural killer cells	NK cells
Oncolytic viruses	OV
pattern-associated molecular proteins	PAMP
phospholipase A2 receptor PLA2R	PLA2R
plaque-forming units	PFU
platelet-derived growth factor	PDGF
programmed cell death protein	PD-1
programmed cell death protein ligand	PD-L1

prostate-specific antigen	PSA
prostatic acid phosphatase	PAP
pattern recognition receptors	PRR
RNA dependent RNA polymerase	RdRp
Sperm Autoantigenic Protein 17	SPA17
synovial sarcoma X chromosome breakpoint	SSX2
T cell receptors	TCR
Talimogene laherparepvec	T-vec
Toll-like receptor	TLR
transforming growth factor beta	TGF-β
TTK protein kinase	TTK
tumor associated antigen	TAA
tumor associated macrophage	TAM
Tumor microenvironment	TME
tumor mutational burden	TMB
tumor necrosis factor alpha	TNFα
tumor specific antigens	TSAs
vascular endothelial growth factor	VEGF
Vesicular Stomatitis Virus	VSV
well-differentiated liposarcoma	WDLS

List of Figures

List of Tables

Chapter 1 - General Introduction

1.1 Cancer and sarcoma

Cancer remains the leading cause of death in Canada, where an estimated 2 in 5 Canadians are predicted to develop cancer during their lifetime, and one in four individuals will die from the disease.[1] Despite significant improvement in the survival rates of many cancer subtypes, the incidence of cancer in Canada continues to rise and presents a significant burden on the healthcare system. Low survival rates of some cancer subtypes and high rates of recurrence show a need for more effective therapeutic options.

Cancer is a multifaceted disease resulting from the accumulation of genetic and epigenetic alterations that enable cells to acquire oncogenic properties and form malignant tumors. Dr. Hanahan and Dr. Weinberg have delineated a set of functional capabilities associated with all cancers, known as the hallmarks of cancer.[2] These include sustained proliferative signalling, evasion of growth suppressors, resistance to cell death, stimulation of angiogenesis, reprogramming of cellular metabolism, evading immune destruction, and activating tumor invasion and metastasis.[2] Continuous research into the mechanisms of cancer has led to the establishment of four new emerging hallmarks described as; senescent cells, phenotypic plasticity, non-mutational epigenetic reprogramming, and polymorphic microbiomes.[3] The hallmarks of cancer represent the complex nature of this disease, this framework has been instrumental in our understanding of cancer biology and has paved the way for remarkable progress in the development of novel cancer treatments. For instance, Health Canada has granted approval for use first-line use of treatments such as atezolizumab (antibody against programmed cell death protein ligand (PD-L1)) for NSCLC and pembrolizumab (antibody against programmed cell death protein (PD-1)) for metastatic or unresectable recurrent head and neck cancer. Additionally, combination treatments such as trastuzumab (anti-HER2) for HER2 positive breast cancer in combination with chemotherapy or surgery, and bevacizumab (antibody against vascular

endothelial growth factor-A (VEGF-A)) in combination with chemotherapy for metastatic colon carcinoma are both indicated for first-line treatment. Although few newly approved cancer therapeutics change first-line treatment, many are helpful as second and third-line treatment options. Despite these significant advances, tumor resistance to chemotherapy and radiation therapy, and recurrence and metastasis continue to present challenges in cancer treatment.

Certain cancer types, such as sarcoma, continue to pose significant challenges to clinicians and researchers. Sarcoma is a rare and highly heterogenous cancer that arises from mesenchymal tissues and comprises over 100 histological subtypes of both soft tissue and bone sarcoma. Sarcoma accounts for less than 1% of adult cancer in Canada, but soft-tissue and other extraosseous sarcomas represent 6% of pediatric cancers.[4] First-line sarcoma treatment options remain limited to traditional surgery, chemotherapy and radiation; however, these are largely ineffective due to disease resistance. In addition, high rates of recurrence and metastasis make this cancer subtype difficult to treat. The overall survival rate of patients with metastatic or recurrent sarcoma remains low (16-30%)[5], suggesting that novel treatment is required to improve outcome in these high-risk patients. An increasing knowledge of sarcoma biology could lead to new and more effective therapeutic strategies for sarcoma treatment. Indeed, several molecular aberrations that are characteristic of certain sarcoma subtypes have been identified, but few can be effectively therapeutically targeted. For example, Ewing's sarcoma is characterised by an EWS-FL1I translocation that results in a fusion oncogene. Although this may seem like an ideal target for therapeutic application, EWS-FL1 directed therapies have failed to reach the clinic.[6] Synovial sarcoma is another sarcoma that harbours a translocation, however the SYT-SSX1 fusion product has shown little therapeutic benefit as a target for immunotherapy.[7–9] Finally, the oncogenic driver cyclin-dependent kinase 4 (CDK4) is found to be expressed in 95% of liposarcomas, however, the used of CDK4 inhibitors has led to mixed clinical results.[10] Overall, the rarity and heterogeneity of sarcoma has led to challenges in treatment development, highlighting the need for a better understanding of tumor biology and the tumor microenvironment.

1.2 Tumor Immune Microenvironment

The tumor microenvironment (TME) comprises proliferating malignant cells and non-transforming cells such as vascular endothelial cells, fibroblasts, and pericytes, as well as several immune system components. The interactions between these cell types and structures promote tumorigenesis and metastasis and form the complex, constantly evolving tumor microenvironment. Understanding the rapidly changing intercellular interactions between the components of the TME will help to identify novel therapeutic targets, and to better understand and predict therapeutic outcome.

The immune component of the TME includes immune cells, cytokines, and chemokines, which can be divided into anti-tumor and pro-tumor components. Anti-tumor immune cells consist of effector T cells, including cytotoxic CD8+ T cells and effector CD4+ T cells, natural killer cells (NK), dendritic cells (DC), and M1-polarized macrophages. Cytotoxic CD8+ T cells (CTLs) play a pivotal role in tumor elimination by functioning as the immune systems primary effectors against cancer. T cell receptors (TCR) of activated CTLs recognize tumor antigens presented through major histocompatibility complexes (MHC)-I, engagement of MHC triggers cytoplasmic degranulation of cytotoxic granules at the immune synapse, thereby releasing perforin and granzymes toward the target cells. Perforin forms pores in the target cell's plasma membrane, allowing granzyme (e.g., granzyme B) to enter and initiate apoptotic cell death pathways.[11] Activated CTLs also secrete cytokines such as interferon gamma (IFNγ), tumor necrosis factor alpha (TNFα), and interleukin-2 (IL-2) which can further activate immune cells.

NK cells can induce cytotoxic cell death by recognizing membrane-bound ligands on target cells and detect tumors through stress-induced autologous proteins. Notably, NK cells are inhibited by MHC-I molecules, enabling preferential killing of MHC-I deficient tumor cells.[12] NK cells express various receptors that can activate NK cell responses, among which engagement of CD16 and CD32

high-affinity Fc receptors trigger antibody-dependent cellular toxicity (ADCC), characterized by secretion of cytotoxic molecules and cytokine release.

CD4+ T cells exhibit diverse functions than can support the activities of CTLs, DCs and B-cells - making them crucial regulators of both cellular and humoral immunity. CD4+ T cells recognize peptides presented on MHC-II complexes on antigen presenting cells. Upon activation, naïve CD4+ T cells differentiate into distinct subsets of CD4+ helper T cells (Th), a process influenced by the cytokine milieu at the site of activation: Th1 differentiation relies on local IL-12, whereas Th2 is driven by IL-4 in the absence of IL-12.[13] Th1 cells are characterized by the production of cytokines such as IFNγ, TNFα and Il-2, and primarily support cell-mediated responses by aiding in the activation of CTLs, NK cells, and antigen presenting cells (APCs).[13] Th2 cells facilitate humoral immune responses and contribute to B-cell development into antibody-producing plasma cells by secretion of cytokines such as IL-4, IL-5 and IL-13.[14] Much like CD4+ T cells, tumor associated macrophage (TAM) differentiation into the M1 subset is driven by signals derived from the TME. M1 macrophages are pro-inflammatory and can drive an anti-tumor immune response by the production of TNFα, IFNγ and IL-12. However, the TME is known to polarize TAMs towards the M2 anti-inflammatory phenotype predominantly.[15]

Pro-tumor immune components include CD4+ regulatory T cells (Tregs), M2-polarized macrophages and myeloid-derived suppressor cells (MDSCs), among others. Tregs are crucial for preventing autoimmunity but also suppress effector T cell responses against tumors. Tregs develop from CD4+ T cell differentiation in the thymus, or by activation of naïve CD4+ T cells in peripheral organs in the presence of transforming growth factor beta (TGF- β) and IL-2. Within the context of a tumor, Tregs inhibit anti-tumor responses through the production of immunosuppressive cytokines (such as TGF- β and IL-10) which have a wide range of effects on anti-tumor immune cells such as the inhibition of CTL activity through TGF-β, and polarization of tumor macrophages to an M2 phenotype by inhibition of IFNγ secretion from CTLs. Furthermore, interaction of Treg cell surface molecules

with receptors on other immune cells can trigger further immune inhibition. For example, binding of lymphocyte activation gene-3 (LAG3) or cytotoxic T-lymphocyte associated protein 4 (CTLA-4) on Tregs to MHC-II, or CD80/CD86 costimulatory molecules on DCs can inhibit their activation. The TME is known to polarize TAMs towards the M2 phenotype by secretion of factors such as IL-10, VEGF and platelet-derived growth factor (PDGF). M2-polarized macrophages are characterized as anti-inflammatory and release cytokines such as IL-6, IL-10 and TGF-β.[15] In addition to having anti-inflammatory characteristics, M2 macrophages can promote tumor progression by favoring angiogenesis and promoting metastasis.[16] Finally, MDSCs create an immunosuppressive microenvironment by inducing anergy of T cells through depletion of essential factors for T cell activation and proliferation, and the expression of immunosuppressive molecules such as PD-L1.[17]

In addition to the diverse array of pro- and anti-inflammatory immune cells present in the TME, immune cells and tumor cells express various immune checkpoint molecules that play a role in suppressing intra-tumoral T cell responses. One of these checkpoints is programmed death-ligand (PD-L1), which is frequently upregulated in the TME and binds to the programmed cell death protein (PD-1) on T cells, resulting in impaired anti-tumor responses.[18] Another checkpoint, CTLA-4, expressed on Tregs competes with CD28 for binding to CD80 or CD86 on antigen presenting cells, reducing APCs' ability to activate CD8+ T cells.[19] Additional checkpoints that inhibit T cell activation include TIGIT; expressed on T cells and binding to CD155 on APCs, and TIM3; highly expressed by CD8+ T cells and interacting with CEACAM1 on APCs.[20]

1.3 Immune Classification of Tumors

The described complex immune mechanisms significantly contribute to the heterogeneity observed within the tumor microenvironment, resulting in diverse inflammatory phenotypes between tumors. Tumors can generally be categorized into 'hot,' 'intermediate,' or 'cold' based on their immune characteristics. Hot tumors are characterized by a high infiltration of cytotoxic T lymphocytes (CTLs)

expressing PD-1, along with tumor cells expressing PD-L1. Conversely, cold tumors lack CTL infiltration into the tumor core and show no expression of PD-L1. Intermediate tumors exhibit either low CTL infiltrate or CTLs localized at the tumor periphery. While there is a consensus that the immune contexture strongly influences clinical outcomes of cancer patients, this classification system falls short in meeting clinical needs. As a result, various efforts have been made to establish an immune-based cancer classification that provides prognostic value and helps stratify patients for optimal therapeutic benefits.

The first standardized tumor classification system integrating immune composition is the Immunoscore—a pathology-based assay quantifying CD3+ and CD8+ T cells within both the tumor core and margins. Successfully integrated into clinical practice, the Immunoscore has emerged as a prognostic marker in colorectal cancer, effectively predicting high-risk patients with stage II colon cancer at risk of recurrence.[21,22] Ongoing studies seek to understand the prognostic implications of the Immunoscore across various indications, aiming to enhance patients' prognostic and therapeutic management in clinical settings.

Given the intricate nature of tumor-immune interactions, efforts to capture this complexity using single analytes such as PD-L1, CD3 or CD8 expression, yields limited and incomplete information about the TME. Recent immune profiling studies across diverse cancer types have revealed a far more intricate inflammatory characterization than traditional classifications.[23–26] For example, The Tumour Inflammation Signature (TIS) is an 18-gene signature measuring pre-existing but suppressed adaptive immune responses within tumors, that and has been show to enrich for patients who respond to anti-PD1 therapy in a Pan-cancer analysis.[27] Another classification focuses on the composition of the TME, including malignant cells, non-transforming cells and immune cells. Clustering of tumors based on gene expression levels identified five distinct phenotypes of soft-tissue sarcoma: immune-desert, immune-low, immune-high, vascularized, immune and tertiary lymphoid structure high.[26] The latter group demonstrated improved survival and a high response rate to PD1

blockade with pembrolizumab in a phase 2 clinical trial. This sheds light on the potential of B-cell-rich tertiary lymphoid structures in guiding clinical decision-making and treatments. Altogether, the collective body of studies highlight the evolving landscape of immune-based classification in cancer research.

1.4 Cancer immunotherapy

The ability of the immune system to eliminate infected or aberrant cells has long been recognized in the scientific community and forms the foundation of immunotherapy. One of the earliest documented instances of immunotherapy can be attributed to William Coley, who observed spontaneous tumor regression following bacterial, viral, and fungal infections. Inspired by these observations, Coley injected patients with heat-killed *Streptococcus pyogenes* and *Serratia marcescens*, a treatment that came to be known as "Coley's toxins", in an effort to treat unresectable sarcomas. While some patients experienced complete remission, the precise mechanisms underlying tumor regression were never fully understood, although it was hypothesized that inflammation played a role. Over a century later, our understanding of the immune system's role in tumor control and progression has significantly advanced, leading to the development of immune checkpoint inhibitors that have revolutionized the field of cancer immunotherapy. Immune checkpoints, such as PD-1/PD-L1 and CTLA-4, play a crucial role in regulating immune responses. Blockade of these checkpoints using antibodies can unleash the activity of tumor specific T cells, leading to enhanced immune responses against cancer cells. This work was recognised by the awarding of the Nobel Prize in Physiology to Dr. Allison and Dr. Honjo. Ongoing research continues to provide novel therapeutic strategies, paving further advancements in the field of cancer immunotherapy.

Cancer immunotherapies aim to leverage the immune system and activate components of innate and adaptive immune system against malignant cells. As described above, the tumor microenvironment is a complex system comprising various immune components which can be targeted for therapeutic

interventions. In particular, CD8+ T cells play a central role in anti-cancer immunity by recognizing tumor associated antigens presented as MHC-I-peptide complexes. This recognition triggers the activation of cytotoxic T lymphocyte effector functions, leading to destruction of malignant cells and suppression of tumor growth. A number of studies in humans have demonstrated a positive correlation between the presence of tumor infiltrating lymphocytes and tumor regression, as well as improved patient outcomes.[28,29] Additional components of the immune system such as Th1, NK cells and memory T cells (T_{MEM}) also play a role in anti-cancer immunity. Despite host cancer immune surveillance by a functioning immune system, disease progression is often observed and can be attributed to the tumors ability to evade these anti-tumor responses.

The recognition and elimination of malignant cells by innate and adaptive immune responses form a critical defense against cancer. However, immune pressure imposed on the tumor trigger mechanisms of tumor immune evasion by a process called immunoediting, and involves cancer cells as well as cells composing the tumor microenvironment.[30] Firstly, immunoediting promotes tumor growth by natural selection of tumor clones that have evaded immune recognition. These cancer cells are often characterized by reduced immunogenicity due to defects in antigen processing,[31] decrease or loss of MHC-I expression,[32–35] or increased expression of immune inhibitory molecules such as PD-L1.[36] These "immunoedited" tumors enter a growth phase where they are no longer controlled by innate and adaptive immune mechanisms. Furthermore, the tumor microenvironment includes immune regulatory cells, such as myeloid-derived suppressor cells and tumor associated macrophages, which actively supress anti-tumor responses mediated by T cells. [37] Moreover, tumor cells themselves secrete immunosuppressive factors such as TGF-β and IL-10, further compromising T cell function and facilitating tumor growth.[38] To overcome the immunosuppressive mechanisms imposed by tumors, developing novel approaches that can induce a broad and strong immune response is crucial.

T cell focused cancer immunotherapies based on the induction of large CD8+ T cell populations specific to tumor cells and generation of long-term anti-tumor immune surveillance are an attractive

approach to cancer immunotherapy. There are several immunotherapeutic approaches that harness the power of T cells against cancer; immune checkpoint blockade (ICB) designed to "take the brakes off" T cell responses, adoptive cellular therapies that consist of infusion of tumor specific T cells/CAR-T cells, and finally cancer vaccines, designed to stimulate a tumor antigen specific response.

1.4.1 Cancer Vaccines

Therapeutic cancer vaccines are a promising approach to cancer immunotherapy and are designed to stimulate an immune response against tumor antigens and to eliminate malignant cells. There are several types of cancer vaccines, including peptide-based vaccines, cell-based vaccines, nucleic acid-based vaccines, and viral vector-based vaccines. Each of these approaches involves the presentation of tumor antigens to immune cells to boost a pre-existing response against tumor cells.

One of the most promising approaches to vaccination are recombinant viral vector-based vaccines. These types of vaccines use a virus to deliver an antigenic payload that is presented to the immune system. Viral vectors offer several advantages over other vaccine modalities, notably, viral vectors can deliver large antigenic payloads and induce robust immune responses without the need for additional adjuvants. Upon vaccination, viral vectors can infect local cells at the site of injection, as well as antigen-presenting cells like dendritic cells to produce the encoded antigen. Infection of antigen presenting cells ensures antigen processing and presentation through MHC-I and MHC-II, thus initiating a potent cytotoxic CTL response.

Viruses possess inherent immunogenic properties that elicit diverse immune responses. Key among these responses is the activation of the innate immune system through recognition of pathogen-associated molecule patterns (PAMPs), such as viral RNA or DNA or viral glycoproteins, by pattern recognition receptors (PRRs) including toll-like receptors (TLRs) expressed on immune cells. Engagement of PRRs triggers a signalling cascade mediated by NF-κB, leading to downstream expression of pro-inflammatory cytokines, particularly type I IFNs (IFN-α and IFN- β). Type I IFNs

are vital cytokines the mediate both the innate immune responses and the development of adaptive immunity. Namely, type I IFNs promote the maturation of DCs by upregulating the expression of co-stimulatory molecules (CD80, CD86 and CD40), and MHC-I and -II molecules. This functional maturation of DCs is essential for the successful priming of naïve T cells. Furthermore, recognition of viral PAMPS by TLR7/8 (RNA) and TLR9 (DNA) leads to the expression of inflammatory cytokines such as IL-2, IL-6, IL-8 and TNF-α and IFNγ. These cytokines promote the recruitment and activation of components of the adaptive immune system. The viral vectors immunostimulatory effects promote the generation of robust antibody responses, and long-lasting cellular immune responses.

A commonly used viral vector in antitumor immunotherapy belongs to the Poxviridae family. Poxviruses are enveloped dsDNA viruses capable of infecting mammalian cells and carrying large DNA inserts for efficient delivery of transgenes. Among the Poxviridae family, vaccinia virus stands out as a prominent viral vector used in cancer vaccines. Live attenuated recombinant vaccina virus encoding tumor antigens such as carcino-embryonic antigen (CEA) and prostate specific antigen (PSA) have been evaluated in several studies.[39–41] The modified vaccinia Ankara (MVA) virus MVA is an attenuated strain of vaccinia, initially intended for Smallpox vaccination, that has also been engineered for cancer vaccine applications. MVA has been armed with a variety of immunostimulatory cytokines in combination with tumor-associated antigens such as IL-2 and MUC1 antigen for non-small cell lung cancer[42], or melanoma antigens gp100 or MART-2 and CD80 and CD86 for melanoma.[39,43] In addition to poxviruses, replication-deficient adenovirus (Ad) are valuable viral vectors for cancer therapy. The efficient gene delivery capabilities and the oncolytic properties of certain adenovirus subtypes make them valuable tools for cancer treatment. Several ongoing phase I/II trials are currently investigating adenovirus-based vaccines targeting carcinoembryonic antigen (CEA; ClinicalTrials.gov: NCT03563157) or melanoma-associated antigen-A3 (MAGE-A3; ClinicalTrials.gov: NCT02285816) tumor antigens, while others, such as Ad serotype 5-PSA, have completed phase II trials with promising results. [44] High levels of antigen-specific antibodies and the activation of CTLs has been documented

after the administration of these vaccines; however, despite successful induction of an antigen-specific humoral and cellular immune response, the lack of tumor regression in patients remains a significant hurdle.

1.4.2 Oncolytic Viruses

The existence of viruses with the unique ability to cause neoplastic death was first recognized when early case studies reported the regression of cancer during naturally acquired virus infections such as measles and infleunza[45–47] or following rabies vaccination[48] leading to the concept of "viral oncotropism". This led to several early patient studies that evaluated the oncolytic potential of virus strains such as adenoviruses, herpes simplex virus, paramyxoviruses, picornaviruses and mumps virus. With our increasing understanding of malignant cell transformation and viral infection, oncolytic viruses have emerged as a promising class of cancer therapeutics.

Oncolytic viruses (OV) mediate their anti-neoplastic activity through a multi-mechanistic approach encompassing direct lytic effects, induction of anti-tumor immunity, and vascular collapse. They can be further potentiated by transgene expression. OVs exhibit a unique ability to selectively infect and eliminate cancer cells while leaving healthy cells unharmed. Several inherent alterations within cancer cells, such as defective antiviral signalling pathways (i.e. type I IFN pathway), aberrant cell cycle control, and resistance to apoptosis, render them highly susceptible to OV infection and replication.

The therapeutic efficacy of OVs is further enhanced by their intrinsic capacity to induce both innate and adaptive antitumor immune responses (as described in Chapter 1.4.1). The presence of viral PAMPs, and the release of DAMPs from lysed tumor cells activate dendritic cells trough TLR signalling, triggering the production of pro-inflammatory chemokines and cytokines, such as type 1 IFN, TNF-a, and IL-2. These play a crucial role in the recruitment of neutrophils, NK cells and additional DCs to the site of infection. These responses to OV infection promote intra-tumoral

infiltration of immune cells, transforming an immunologically "cold" tumor "hot". Furthermore, immunogenic cell death triggered by OVs reveals tumor antigens to DCs, activating antigen specific T cell responses. Another important mechanism by which OVs promote an anti-tumor response is by inducing upregulation of MHC-I expression on tumor cells, driven by the signalling through cytokines produced as a result of infection.[49] Altogether, this leads to the generation of a systemic adaptive anti-tumor immune response that can mediate tumor destruction that persists even after viral clearance by establishing long-term anti-cancer immune surveillance mechanisms.

Third, OV infection mediates tumor vascular collapse through two distinct mechanisms. OVs can initiate the formation of micro clots within tumor vasculature in a neutrophil-dependent process, leading to irreversible damage to tumor vasculature. [50,51] Another mechanism involves the sensitization of vascular endothelial cells to OV infection mediated by VEGF. VEGF secretion within the tumor microenvironment suppresses antiviral IFN responses through the VEGF-A/VEGFR2/Erk/Stat3 signaling axis, which renders vascular endothelial cells susceptible to OV infection, in turn damaging blood vessels and promoting viral dissemination into the tumor bed.[52]

Finally, the capacity of viruses to produce substantial amounts of viral proteins upon infection can be harnessed for the expression of therapeutic transgenes, thereby enhancing the efficacy of viruses. As it became evident that OV mediated oncolysis released tumor antigens into the tumor microenvironment and initiated an immune response, strategies to maximize clinical benefit of OVs began to focus on the modulation of these immune responses. OVs can encode transgenes such as cytokines and chemokines to help modulate the immune response, or tumor antigens to promote a tumor-antigen specific immune response. An additional benefit of encoding cytokine and chemokines into OVs is the targeted delivery to the tumor site, as systemically administered chemokines and cytokines generally lead to unwanted side effects. A notable example of a transgene used in OV therapy is the granulocyte-macrophage colony-stimulating factor (GM-CSF), which has been employed as a transgene to improve the antitumor immune response in the clinically approved oncolytic virus therapy

T-Vec. Other potent anti-cancer cytokines, such as IL-12, have also been incorporated into oncolytic viruses for localized delivery to the tumor site, demonstrating promise in various cancer types. [53–56] The overexpression of tumor antigens encoded by OVs can further enhance the anti-tumor immune response, leading to long-term antitumor immunity and protection against cancer recurrence. One example of an OV therapy targeting a tumor antigen is the heterologous prime-boost using a replication-incompetent adenoviral vector together with the oncolytic Maraba MG1, both armed with a transgene expressing the antigen MAGE-A3. This combination significantly prolonged survival in murine models of cancer[57] and generated large tumor-specific responses in non-human primates.[58] These preclinical studies have led to evaluation of this therapy in human patients with MAGE-A3 positive tumors. (ClinicalTrials.gov: NCT02285816)

Some OVs are naturally occurring and have natural tropism for entry receptors that are abnormally upregulated in cancer cells, such as CD46 for measles virus, or nectin -1 and -2 by Herpes simplex virus 1 (HSV-1). OV infection of cancer cells is further enhanced by genetic modifications aimed at improving viral oncotropism. One strategy involves targeting viruses to tumor cells by fusing viral proteins with peptides known to bind to tumor-associated receptors, such as EGFR.[59] Additionally, viral genes that normally allow for virus infection of normal cells can be manipulated to enhance cancer selectivity.[60] Another approach to enhancing viral specificity involves genetic modification for the selective replication of viruses. This involves placing a promoter to permit expression of essential viral genes in tumor cells but not in normal cells. For example, the prostate-specific antigen (PSA) promoter in the E1A region of adenoviruses results in selective adenoviral proliferation and oncolysis exclusively in prostate cells.[61]

To date, there are four globally approved viruses for cancer treatment. The first approved oncolytic adenovirus H101, which received approval in China. Shortly after, ECHO-7 echovirus was approved in Latvia. Talimogene laherparepvec (T-vec or Imlygic) is an HSV-1 based OV that has been approved in multiple countries for the local treatment of unresectable melanoma. More recently,

teserapturev (Delytact), another HSV-1 based OV, was approved in Japan. These approvals mark significant milestones in the field of oncolytic virotherapy, demonstrating the clinical potential of these viruses as a novel approach to cancer treatment.

1.4.3 Vesicular Stomatitis Virus

Vesicular Stomatitis Virus (VSV) is a zoonotic virus that belongs to the rhabdoviridae family of viruses. VSV infects a wide variety of mammalian and insect cells, and while human VSV infections rarely occur; they are often completely asymptomatic. VSV is bullet shaped, enveloped virus containing a single negative-sense RNA virus that encodes five structural proteins: the glycoprotein (G), membrane (or matrix) protein (M), nucleoprotein (N), and two internal proteins (L and P). The 11-kb RNA genome is fully coated with N protein. It is associated with L and P proteins that form RNA dependent RNA polymerase (RdRp) involved in viral transcription, together forming the nucleocapsid. The M protein condenses the nucleocapsid into a tightly coiled helical structure and has also been described to play a role in later steps of VSV infectious cycle. Finally, the G protein is organized in the lipid bilayer of the viral membrane that is derived from the host during viral budding and plays a role in viral entry. VSV viral entry is mediated by G protein binding to the low-density lipoprotein (LDL) receptor (LDLR) via cysteine-rich LDLR domains CR2 and CD3.[62,63] Effective VSV infection has also been observed in cells devoid of LDLR, suggesting the potential role of other unidentified ubiquitous surface proteins in viral entry.[62] Upon binding to LDLR, VSV is internalized by receptor-mediated endocytosis into clathrin-coated pits, and transported to endosomal compartments where endosomal acidification triggers pH dependent viral fusion to the endosomal membrane and viral release into the cell cytosol.[64] Once in the cytosol, RdRp uses negative-sense RNA as a template for transcription of viral genes into positive sense mRNAs which are subsequently translated by host ribosomes. Newly formed viral progeny assembles at the host cell plasma membrane

and is released from the cell by viral budding. Newly formed viral progeny is released from the host cell 2-6 hours post initial VSV infection. [65]

1.4.3.1 VSV as an Oncolytic Virus

VSV represents a valuable vaccine vector due to its low pathogenicity in humans, lack of pre-existing immunity, and its ability to accommodate a 40% increase in genome size without a reduction in infectivity. VSV based recombinant viral vectors have demonstrated both safety and immunogenicity in pre-clinical and clinical trials and a VSV-based vaccine against Ebola virus has recently gained regulatory approval for use in humans. The recombinant VSV Ebola virus (rVSV-ZEBOV) expresses the Ebola glycoprotein in place of the G gene of VSV, resulting in a highly attenuated phenotype[66] and generation of glycoprotein neutralizing antibodies.[67,68] VSV is also being explored as a vaccine platform against viruses such as Zika virus and coronavirus. VSV has proven to be an effective vaccine vector for immunization against viral infection, and is being used as a vector to induce an immune response to self-tumor antigens.[69,70]

VSV exhibits not only promising characteristics as a vaccine vector, but also holds great potential as an oncolytic agent due to its high tropism for various cancer cell types. VSV has demonstrated high affinity for cancers including breast cancer[71], cervical cancer[72], glioblastoma,[73] melanoma[74] and osteosarcoma[75]. However, the broad tissue tropism of VSV poses a challenge to its clinical approval as an oncolytic virus. While systemic administration of oncolytic viruses is preferable for effectively targeting widespread tumors, metastasis, and brain tumors, the neurotoxicity of wild type VSV in non-human primates has limited extensive testing of this virus.[76–78] Several strategies have been explored to attenuate VSV pathogenicity in healthy cells and to enhance onco-specificity. One mechanism by which VSV achieves cancer specificity is through its sensitivity to antiviral IFN-I, a pathway that is often defective in many cancer types. The M protein of VSV plays a role in inhibiting innate antiviral responses, such as expression of antiviral IFNα and IFNβ, by disrupting host

transcription pathways and host translation. In addition, delayed activation of NF-κB, a factor required for IFN gene transcription, mediated by the viral M protein further contributes to the evasion of antiviral responses by VSV. [79,80] Mutations in the M protein can attenuate VSV pathogenicity in normal cells by preventing the blockade of host anti-viral responses in infected cells.[81] An example is the VSV variant VSVΔ51, which contains a deletion of the 51st methionine in the M protein. Similarly, the VSV-M51R variant is attenuated be targeting the M protein by an amino acid substitution from methionine to arginine at position 51.[82] By selectively attenuating VSV's interaction with host antiviral pathways, the specificity of VSV for cancer cells can be enhanced, increasing its potential as an oncolytic virus. [83] Alternatively, truncating the G protein or introducing a G deletion reduces or blocks the ability to produce infectious virus.[84] Finally, a VSV variant expressing human IFNβ is being evaluated in phase I human clinical trial (ClinicalTrials.gov: NCT01628640). The expression of IFNβ is designed to prevent viral replication in normal cells by promoting an antiviral immune response upon infection.

VSV has been successfully used in pre-clinical studies to generate anti-tumor responses and to prolong survival. Incorporation of a tumor-associated antigen (ovalbumin) into wild type VSV increased activation of antigen specific T cells which translated to prolonged survival in B16-OVA tumor bearing mice.[85] The immunogenicity of VSV encoding tumor associated antigen (TAA) was further enhanced when used in a heterologous prime-boost regimen, employing an adenoviral vaccine followed by VSV both expressing the same TAA.[86,87] Notably, this approach to OV therapy skews the T-cell response toward the encoded TAA as opposed to the virus, leading to enhanced antigen specific immunity.[86,87] The use of attenuated VSV has generated promising results. VSVΔ51 shows efficacy against models of C666-1 nasopharyngeal carcinoma,[88] or CT2A astrocytomas.[89] VSVΔ51 has been engineered to express different chemokines and cytokines. VSVΔ51 engineered to express murine IFNγ enhanced activation of dendritic cells and generated greater tumor-specific immune responses, and showed improved efficacy compared to parental virus for treatment of 4T1 adenocarcinoma.[90] Similarly, intra-tumoral administration VSVΔ51 expressing murine IL-12 (in combination with a viral

sensitizer) improved therapeutic outcomes in CT26WT colon cancer.[91] Another approach to OV therapy that is designed to enhance antitumor immunity by increasing the breadth of antigenic coverage is the use of an infected cell vaccine (ICV).[92] ICV consists of irradiated tumour cells that are infected with a virus, such as VSV, that acts as a potent adjuvant by inducing rapid innate immune activation and increasing T cell and NK cell tumor infiltration. [93,94] In a B16F10 model, tumor bearing mice treated with irradiated cell prime and ICV (VSVΔ51-GMCSF) boost showed significant delay in tumor growth.[93]

Maraba virus is another rhabdovirus that exhibits oncolytic properties and is closely related to VSV. Two mutations were introduced in the M and P proteins, generating Maraba MG1 variant with enhanced onco-selectivity and attenuated activity in normal cells.[95] This virus demonstrated superior oncolytic activity when compared to a panel of other OV strains, including VSVΔ51.[96] As mentioned above, this virus is being evaluated in a heterologous prime-boost vaccination using adenovirus and Maraba MG1 both encoding the target tumor antigen MAGE-A3 (ClinicalTrials.gov: NCT02285816).

1.4.4 Heterologous Prime-Boost Immunotherapy

Traditional vaccine strategies often require multiple doses to achieve optimal immune responses, however this approach is hindered by the phenomenon of epitope dominance of viral antigens that shift immune responses away from encoded transgenes. Additionally, the administration of the same viral vector for both prime and boost vaccination can result in reduced efficacy due to the development of anti-vector immunity that clears the virus before transgene expression can occur. A notable approach that overcomes the barrier of anti-vector immunity is a heterologous prime-boost vaccination utilising different prime and boost vectors that target the same antigen. Prime-boost combinations of various viral vectored vaccines have been explored in infectious disease and in cancer. The chimpanzee adenovirus and MVA encoding MAGE antigens in combination with anti-PD1 promoted CD8+ T cell infiltration in tumors and turned a “cold” tumor “hot” in murine models[97], this

combination has now entered Phase I/II clinical trials for NSCLC (ClinicalTrials.gov: NCT04908111). Similarly, a poxvirus based heterologous prime-boost using recombinant vaccinia and fowlpox viruses targeting CEA and MUC1 showed antigen specific immunity and clinical efficacy in some breast, ovarian, or colorectal cancer patients in Phase I/II trials.[98]

The use of an OV in a heterologous prime-boost regimen is not as widely explored. ORVs have been described to be potent vectors as they can directly infect follicular B cells in the spleen, providing an additional site for antigen presentation and large secondary CD8+ T cell expansion. As mentioned previously, a study by Pol *et al.* demonstrated that an oncolytic prime-boost vaccination employing a recombinant adenovirus (rAd-DCT) as prime and the MG-1 oncolytic virus targeting DCT as a boost generates a large population of DCT specific T cells and leads to tumor control in mice bearing B16-F10 tumors.[57] The induction of a potent T cell response against a tumor antigen in combination with tumour infection can break tumor immune tolerance, and subsequent contraction of this adaptive T cell response generates a high number of memory T cells that actively survey the host against recurrence. Other prime-boost combinations being explored in the clinic to treat synovial sarcoma and myxoid/round cell liposarcoma include an NY-ESO-1 targeted regimen using a dendritic-cell targeting lentiviral vector as a prime and peptide vaccine as a boost.[99] Given the number of immunotherapeutic approaches currently available, many different prime-boost combinations using oncolytic viruses are possible.

1.4.5 DEC205

Dendritic cells bridge the innate and adaptive immune responses by the activation of CD4+ and CD8+ T cells. Briefly, DCs constantly take up antigens and pathogens by endocytosis and phagocytosis which are processed and presented on MHC-peptide complexes. DCs migrate from the site of antigen acquisition to secondary lymphoid organs where they interact with T cells and stimulate clonal expansion. T cell activation occurs in three steps; signal one is the recognition of MHC-peptide

complexes via the TCR, signal 2 is the interaction of costimulatory molecules CD28 on T cells with CD80/CD86 on DCs, and the final third signal is the cytokine signal that polarizes naïve T cells into effector T cells. The central role DCs play in the initiation of T cell immunity has supported the development of DC-based vaccination strategies, one promising approach is the targeting of DCs by DEC205 receptor using antigen-conjugated antibodies.

1.4.5.1 DEC205 Receptor Structure and Function

DEC205 is a type I endocytic cell surface receptor that belongs to the category C-type multilectin receptor (CLR) family, sharing this classification with the macrophage mannose receptor (MMR) and phospholipase A2 receptor (PLA2R). The extracellular domain of DEC205 contains a cysteine rich N-terminal domain, a fibronectin type II domain, and multiple C-type lectin domains. DEC205 possesses a distinctive feature in comparison to other receptors in the C-type multilectin family as it contains a 10 membrane-external C-type lectin domain (as opposed to eight). The cytoplasmic domain contains an internalization sequence located at its cytoplasmic tail. DEC205 ligands have not been identified to date, however, its domain structure suggests the potential for recognition of multiple ligands. Initial studies aimed to determine the physiological ligand of DEC205 revealed that this receptor can recognize ligands expressed during apoptosis and necrosis in a pH dependent matter, and point to DEC205 being a recognition receptor for apoptotic and necrotic self.[100] Further studies showed that DEC205 can bind keratin of apoptotic or necrotic cells at acidic pH through its N-terminal domains.[101] Lahoud *et al.* further demonstrated that DEC205 is a key receptor involved in the uptake of synthetic phosphorothioated cytosine–guanosine oligonucleotides, a clinically used adjuvant that mimics motifs in bacterial DNA.[102] Structural comparisons between the homologous DEC205 and MMR provide further insights into potential binding ligands. The C-type lectin domains in MMR and PLA2 bind carbohydrates, however, the mannose contact residues that mediate this interaction are not conserved in DEC205, suggesting that either DEC205 cannot bind carbohydrates, or the additional C-type lectin domains present in DEC205 provide additional mechanisms for carbohydrate binding.[103] Finally, key

residues responsible for collagen reactivity in MMR are not available for ligand binding in DEC205's extracellular domain. [104] This same study showed that DEC205 exhibits pH-dependent oligomerization which has a functional role in ligand recognition. Data suggests that the monomeric form of DEC205 observed in higher pH is the ligand binding component, therefor changes in the pH can affect ligand binding.[104] Altogether, this data provides evidence that DEC205 could potentially serve as a versatile receptor, with many possible ligands at different pH levels.

1.4.5.2 DEC205 as a Therapeutic Target

DEC205 was originally found to be expressed on human dendritic cells and thymic epithelial cells,[103] and further studies noted abundant expression of DEC205 in the T cell areas of peripheral lymphoid organs, and B cells within B cell follicles, stroma of bone marrow, epithelia of pulmonary airways and capillaries of the brain.[105] Characterization of DEC205 expression on human leukocyte subsets showed high levels on myeloid DC and monocytes, moderate levels on B cells and low levels on NK cells, plasmacytoid DC and T cells. [106,107] DEC205 expression is also detected in granulocytes and macrophages. Despite its high expression on dendritic cells and in several other tissues, the biological function of DEC205 remains unclear.

DEC205 antibodies have been extensively used as surrogate ligands to study DEC205 mediated adsorptive endocytosis, antigen processing, and antigen presentation. DEC205 targets endocytosed antigen to late endosome or lysosome multivesicular compartments that are rich in MHC-II.[108] Mahnke *et al.* described the two functional regions of DEC205 responsible for the mechanism of late endosomal targeting; a membrane-proximal region with a coated-pit sequence for uptake, and an acidic EDE triad for efficient targeting of endocytosed DEC205 to late endosomes/lysosomal compartments high in MHC-II.[108] In addition to targeting antigen to MHC-II, DEC205 also mediates cross-presentation of antigen on MHC-I molecules.[109] Moreover, DEC205 can cross-present several peptides from a single protein.[110]

Dendritic cells play a pivotal role in initiating the adaptive immune response by serving as key antigen presentation cells, and present antigens in the form of MHC-peptide complexes to T cells, thereby initiation T cell responses. The unique ability of DEC205 to efficiently mediate antigen presentation on MHC-I and MHC-II molecules has generated significant interest in the targeting of this endocytic receptor for therapeutic purposes. Endocytic activity of DEC205 can be leveraged as a vaccine target for effective antibody mediated antigen delivery. Importantly, human DEC205 exhibits approximately 80% of protein identity to its mouse homolog, suggesting its function is conserved between species, and allowing for pre-clinical testing of DEC205 targeted therapies.

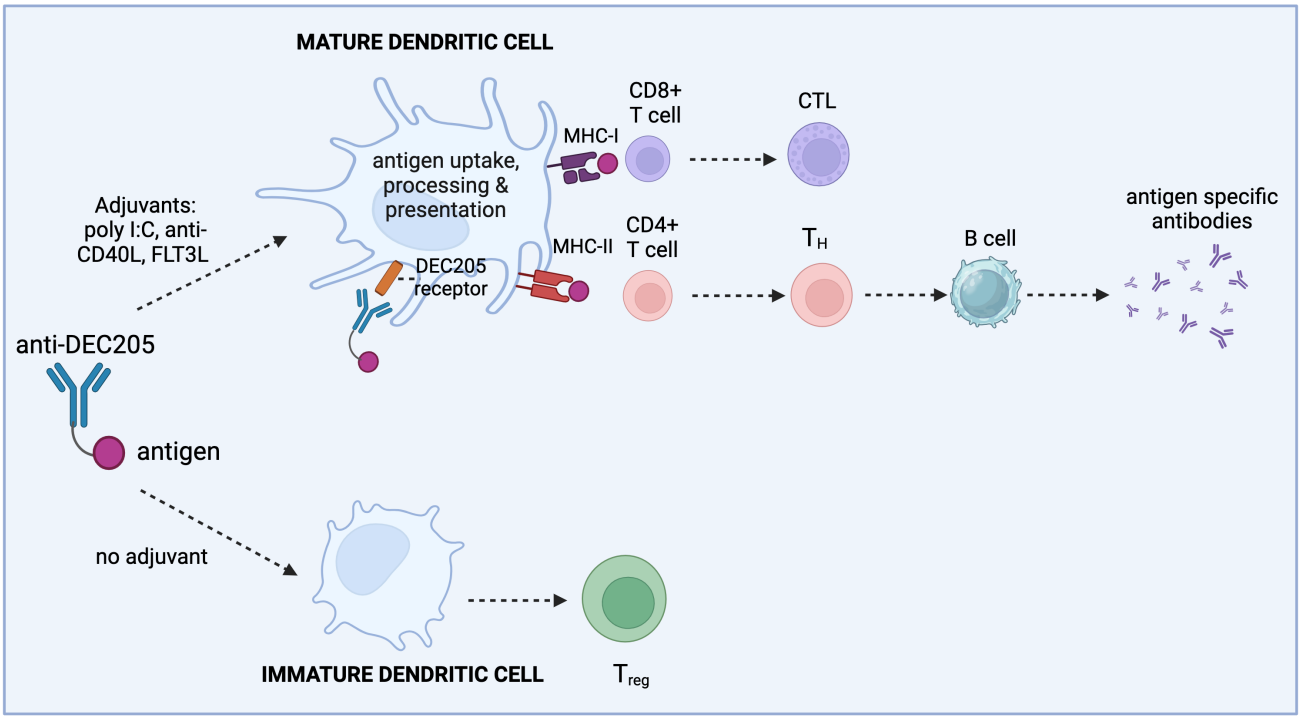

Figure 1.1 DEC205 directed antigen delivery using anti-DEC205. Administration of anti-DEC205 conjugated to an antigen in the presence of adjuvants leads to DEC205 receptor mediated antibody uptake, and antigen processing and presentation on MHC-I and MHC-II molecules, subsequently activating CD8+ T cells and CD4+ T cells. Conversely, the administration of anti-DEC205 in the absence of adjuvants will generate immune tolerance towards the antigen.

Early studies of antigen delivery to DC by targeting the DEC205 receptor involved using anti-DEC205 conjugated to ovalbumin (OVA) combined with anti-CD40 agonist as an adjuvant. These

studies demonstrated the generation of robust CD4+ and CD8+ T cell response against OVA epitopes.[109] Moreover, antigen targeting to DEC205 leads to 100x more efficient antigen presentation when compared to MMR targeting,[108] and proved superior to other techniques, such as targeting DC-SIGN[110], or DC peptide electroporation and DC peptide pulsing.[111] DEC205 targeted antigen delivery with the use of adjuvant poly-ICLC, have been employed in preclinical studies to elicit immune responses against various antigens, including those associated with Ebstein-Barr virus[112], HIV[113,114], and human papollomavirus[115], or cancer antigens such as MAGE-A3[116]. In clinical trials, the administration of DEC205 conjugated to NY-ESO-1, in combination with chemotherapy or checkpoint inhibitors, has been investigated for multiple malignancies (ClinicalTrials.gov: NCT02166905, NCT01834248, NCT03358719, NCT02129075). Studies with reported results demonstrate that the combined administration of the DEC205-NY-ESO-1 antibody with decitabine in myelodysplastic syndromes/acute myeloid leukemia patients,[117] or with Flt3 ligand in melanoma patients,[118] leads to the generation of antigen-specific adaptive and humoral responses. However, it is noteworthy that none of these studies have reported on outcomes such as response or survival.

In contrast to inducing strong antigen-specific T-cell responses, DC targeting using DEC205 without appropriate maturation stimuli is an effective strategy to induce tolerance against self-antigens and protect against autoimmunity. This approach has been used in pre-clinical studies of autoimmune encephalitis[119], arthritis[120], and diabetes[121], and have been shown to ameliorate symptoms or delay disease onset.

Altogether, the targeted delivery of antigens to DEC205 is an attractive approach to vaccination, as supported by both preclinical and clinical studies. These findings substantiate its potential as an approach for developing innovative therapeutic vaccines for cancer, and its use as a vector in a heterologous prime-boost vaccination.

1.5 Tumor antigens

The ability of the immune system to distinguish between normal and malignant cells is the foundation of a successful cancer immunotherapy and relies on the antigenicity of cancer cells. Tumors exhibit diverse antigens that can potentially provoke tumor-specific immune responses and serve as targets for immunotherapy. Tumor antigens can be broadly categorized as tumor associated antigens (TAAs) or tumor specific antigens (TSAs).

Table 1.1 Summary of tumor antigen classes and types of tumor antigens.

Tumor Antigen Classification	Antigen Type	Examples
Tumor Associated Antigen	Self-antigens	Survivin, ERBB2
	Differentiation antigens	MART-1, gp100, PAP, PSA,
	Cancer testis antigens	MAGE-A3, NY-ESO-1, SSX2,
Tumor Specific Antigen	Neoantigens	Unique to each patient
	Oncoviral proteins	HPV E6/E7, HBV X protein

1.5.1 Tumor Associated Antigens

Tumor associated antigens are frequently found to be upregulated by tumor cells while minimally expressed in healthy tissues, rendering them attractive targets for cancer therapeutic strategies. TAAs encompass various types; including normal self-antigens, differentiation antigens, and cancer testis antigens. Notable examples of well-characterized self-antigens that exhibit overexpression in cancer include ERBB2 (HER2/NEU) and survivin.

Differentiation antigens exhibit tissue-specific expression and are typically expressed in both tumor cells and their normal cell counterparts. Consequently, targeting these antigens carries the risk of low tumor specificity and the potential to induce autoimmune toxicity. Differentiation antigens were first described in melanoma, and include MART-1 and glycoprotein100 (gp100), which play essential roles in melanocyte differentiation and melanin biosynthesis. Targeting of differentiation antigens identified in prostate cancer include prostatic acid phosphatase (PAP) and prostate-specific antigen (PSA) hold

similar promise, notably, PAP targeting autologous active cellular immunotherapy (Sipuleucel-T) has received FDA approval. Altogether these results highlight the potential of using differentiation antigens as targets of appropriate cancer immunotherapies, however this approach can be faced with challenges such as on-target but off-tumor specificity.

Cancer-testis antigens (CTA) are a group of immunogenic tumor-associated proteins that elicit spontaneous humoral and cellular immune responses and are recognised as targets by CD8+ T cells.[122,123] CTA protein expression is restricted to immune privileged testicular germ cells that lack HLA expression and display aberrant expression in certain malignancies, making them an ideal candidate target for immunotherapy.[124] Unlike most self-antigens, CTAs are highly immunogenic. The identification of CTA specific T cells in patients suggests that CTA reactive T cells do not undergo negative selection in the thymus during the process of central tolerance, thereby adding CTA specific T cells to the immune repertoire.[125] Additionally, strong humoral and cellular immune responses against several CTAs in cancer patients suggests that the immune privileged expression of CTAs in germ line cells allows for decreased mechanisms of peripheral tolerance.[126,127] The first cancer testis antigen was identified in melanoma and was termed melanoma antigen family A,1 (MAGEA1)[128], this drove the discovery of other MAGE family members MAGE-A2 and MAGE-A3, as well as the novel antigens New York esophageal squamous cell carcinoma (NY-ESO-1)[124] and synovial sarcoma X chromosome breakpoint (SSX2).[129] These antigens were found to be expressed in a wide range of cancer types, providing promising antigenic targets for immunotherapy. Namely, MAGE-A3 antigen was targeted in a Phase III trial evaluating MAGE-A3 recombinant protein vaccine for lung cancer.[130] Despite demonstrating limited efficacy in this trial, CTAs continued to show promise as therapeutic targets. In the context of sarcoma, CTAs present an appealing target for an immunotherapy as sarcomas are generally driven by chromosomal translocations or copy number aberration, leading to low mutation rates and limiting the amount tumour-specific neoantigens available for targeting.[131] Several CTAs that are encoded by chromosome X genes are expressed in various malignancies due to

demethylation of promoter sequences.[132] Notably, the melanoma-associated antigen 3 (MAGE-A3), New York esophageal squamous cell carcinoma 1 (NY-ESO-1) and synovial sarcoma X chromosome breakpoint family of proteins (SSX) have been previously identified in sarcoma.[129,133–135]

One challenge to using TAAs as therapeutic targets for T cell-based immunotherapies reliant on the presentation of TAA as MHC-peptide complexes is the presence of central and peripheral tolerance mechanisms. These mechanisms regulate the ability of T cells and B cells to recognise self-antigens. Briefly, central tolerance is achieved during the development of thymic T cell receptors (TCR), where self-reactive TCRs are eliminated from the T cell repertoire through negative selection. However, a proportion of self-reactive T cells escape thymic selection, leading to the presence of these T cells in the periphery. Peripheral tolerance encompasses a broad range of mechanisms including signalling of tolerogenic DCs and CD4+ Tregs that can limit or prevent T cell activation in response to self-antigens.[136] Therefore, immunotherapies that induce a broad immune response that can overcome immune tolerance are advantageous for cancer patients.

1.5.2 Tumor Specific Antigens

The second class of antigens are tumour-specific antigens (TSA), which arise from genetic alterations such as mutations, insertion, deletions, and chromosomal rearrangements that result in non-synonymous amino acid sequences. These alterations are acquired during the transformation of tumor cells, rendering them unique to malignant cells and are termed “neoantigens”. Notably, neoantigens have been shown to exhibit enhanced binding affinity to MHC compared to self-antigens, and can elicit robust and tumor specific immune responses, making them an attractive target.[137] It is important to highlight that each tumor possesses a distinct repertoire of neoantigens, shaped by the genetic profile of each patient and the specific mutations acquired throughout tumor development. This unique characteristic poses a challenge to the development of effective therapies, particularly in personalised

therapeutic approaches that require the identification of neoantigens for each individual patient (and current methods of antigen discovery can be cost-prohibitive).

Tumor-specific antigens can also originate from oncoviral proteins. Viral infections have been recognized as potential contributors of several cancers, including cervical cancer, oropharyngeal, hepatocellular carcinoma and Kaposi's sarcoma. Oncogenic viruses, including human papillomavirus (HPV) and hepatitis B viruses (HBV), promote survival and proliferation of host cell through the expression of oncoviral proteins such as HPV E6 and E7, or HBV X protein. When expressed within tumor cells, these viral proteins can be presented on MHC molecules, thereby serving as foreign antigens that can be recognized and targeted by adaptive immune cells and present attractive targets for therapeutic interventions.

1.6 Rationale and goals

Cancer is a complex and multifaceted disease that affects millions of people worldwide. Sarcoma, a type of cancer that arises from connective tissues such a bone, cartilage, and muscle, represents a rare but aggressive form of cancer that poses significant challenges in both diagnosis and treatment. Despite substantial advances in cancer research and treatment, the prognosis of patients with sarcoma remains low, highlighting an urgent need for novel treatment modalities.

We propose that a T cell-based immunotherapy employing oncolytic rhabdoviruses and targeting a tumor antigen can be an alternative treatment for sarcoma patients. The overall objective of this research is to establish the foundations for a novel immunotherapeutic approach tailored to sarcoma.

Throughout this study, we investigated various critical aspects related to the development of immunotherapy. We conducted a proof-of-concept study evaluating a novel prime-boost combination using anti-DEC205 and Maraba MG1 targeting a model antigen. To facilitate the translation of this therapeutic approach to a clinical setting, a comprehensive understanding of the dedifferentiated

liposarcoma (DDLS) tumor immune microenvironment and the identification of a suitable target antigen is required. Therefore, we conducted in-depth immune profiling of DDLS, and gained a better understanding of DDLS tumor biology and the complex immunological mechanisms at play within the TME. Finally, we evaluated various prime and boost vaccine vectors employing the newly discovered antigen in pre-clinical models of murine sarcoma, and assessed the antigen specific and systemic immune responses following vaccination.

Chapter 2 – Oncolytic rhabdovirus vaccine boosts chimeric anti-DEC205 priming for effective cancer immunotherapy

Fanny Tzelepis[1]*, Harsimrat Kaur Birdi[1,2]*, Anna Jirovec[1,2]*, Silvia Boscardin[3,4], Christiano Tanese de Souza[1], Mohsen Hooshyar[1], Andrew Chen[1], Keara Sutherland[1,2], Robin Parks[2,6], Joel Werier[5], Jean-Simon Diallo[1,2]

* equal contribution

1. Centre for Innovative Cancer Research, Ottawa Hospital Research Institute, Ottawa, Ontario, Canada.

2. Department of Biochemistry, Microbiology and Immunology, University of Ottawa, Ottawa, Ontario, Canada.

3. Laboratory of Antigen Targeting to Dendritic Cells, Department of Parasitology, University of Sao Paulo, Sao Paulo, Brazil.

4. Institute for Investigation in Immunology (iii)-INCT, Sao Paolo, Brazil.

5. Department of Surgery, The Ottawa Hospital, Ottawa, Ontario, Canada.

6. Regenerative Medicine Program, Ottawa Hospital Research Institute, Ottawa, Ontario, Canada.

Published in: Molecular Therapy

Some modifications to the text and formatting of figures and tables have been made in this thesis.

The original article is attached as Appendix IV and is also available here:

https://doi.org/10.1016/j.omto.2020.10.007

2.1 Introduction

As knowledge of the important role played by the immune system in preventing tumor growth in healthy individuals has expanded over the last decades, immunotherapy has emerged as a viable treatment option for cancer.[138] One form of immunotherapy that has gained recent regulatory approval employs oncolytic viruses (OVs). OVs are live, replicating viruses selected or genetically modified to preferentially target and kill cancer cells while leaving healthy cells relatively unharmed.[139] This is possible owing to the fact that cancers exhibit many characteristics that are conducive to successful viral replication, such as resistance to apoptosis, increased nucleotide synthesis, and an impaired antiviral response.[140] OVs elicit their anti-cancer effects through multiple mechanisms and following tumor cell lysis and immunogenic cell death, can trigger anti-cancer immune responses.[141] In addition to Imlygic, an intratumorally delivered oncolytic herpes simplex virus 1 (HSV-1) strain approved for treatment of late-stage melanoma, many different viruses have been clinically evaluated for their potential as OVs, including many that can be delivered intravenously (i.v.), such as (but not limited to) measles virus,[142] coxsackie virus,[143] and rhabdoviruses, like vesicular stomatitis virus (VSV) and the closely related Maraba virus (MG1).[144] Additional attenuating genetic modifications are generally introduced into OVs in order to increase their safety profile. For example, oncolytic rhabdoviruses are attenuated by deletion of the matrix protein in VSV (termed VSVΔ51) and mutation of components of the matrix and glycoproteins in MG1.[145] In addition, OVs can be genetically manipulated to encode proteins that either help to establish a productive infection of cancer cells or encode cytokines and/or immunogenic antigens, such as cancer antigens.

It is known that OVs can elicit in situ cancer vaccine effects and relieve local immunosuppression through the induction of immunostimulatory cytokines. In this environment, dendritic cells (DCs) can phagocytose dead/dying infected tumor cells and prime an anti-tumor as well as antiviral immune response in the draining lymph node.[146] However, the heterogeneous nature of cancer has resulted in limited efficacy of OVs as monotherapies and has steered researchers to

investigate combinations of these biologics with other therapies that not only enhance OV infection of tumors but also enable anti-tumor immune responses.[147,148]

Typical vaccination regimens are generally not limited to a single dose and can be made more effective by multiple immunizations. This can involve the administration of additional homologous (matched vaccine) or heterologous (unmatched vaccine) doses.[149] In the context of cancer vaccines, it has been recently shown that a heterologous prime-boost strategy, where an initial priming dose of an adenovirus virus encoding a cancer antigen is administered, followed by a boosting dose of an oncolytic rhabdovirus encoding the same antigen, can be effective to eradicate tumors.[150] This strategy has been shown to induce robust and long-term effector T cell responses[69,96] and is currently undergoing clinical evaluation for multiple antigens and indications (ClinicalTrials.gov: NCT02285816, NCT02879760, NCT03618953, and NCT03773744).

As a boosting component, oncolytic rhabdoviruses are thought to be uniquely effective because in addition to infecting tumor and breaking local immunosuppression, they efficiently, but non-productively, infect splenic B cells, which provides an additional source for antigen presentation to DCs, resulting in secondary expansion of T cells.[151]

To prime the oncolytic rhabdovirus boost, current clinical trials employ a nonreplicating adenovirus serotype 5 (Ad5) vector expressing a shared cancer antigen (e.g., MAGE-A3, ClinicalTrials.gov: NCT02285816). Questions regarding the importance of vector seropositivity were raised recently following Merck's failed phase II clinical trial of a trivalent human immunodeficiency virus (HIV) vaccine delivered in an Ad5 vector.[152] Indeed, Ad5 seropositivity is sometimes an exclusion criterion in vaccine and gene-therapy clinical trials employing this vector.[153] Approximately 30%–40% of the North American population is seropositive for Ad5, and this proportion approaches an 85% average globally, posing a potential limitation to the widespread use of Ad5 as a priming vector for the oncolytic rhabdovirus heterologous prime-boost cancer immunotherapy strategy. [154–156]

DEC205 is a C-type lectin endocytic receptor highly expressed on certain DC subtypes. [157] Chimeric antibodies specific to DEC205 fused with an antigen of interest (anti-DEC205 [aDEC205]) have been shown to be an effective strategy to target fused antigens directly to DCs, inducing robust cellular and humoral responses when combined with adjuvants.[158,159] To overcome potential issues with Ad5 and other viruses that could be used as priming vectors but that may have the potential to be affected by pre-existing immunity, we hypothesized that chimeric aDEC205 antibodies could provide an effective alternative. In this study, we modeled and evaluated the impact of pre-existing immunity on Ad5-based priming. As proof of concept, we also evaluated a heterologous prime-boost vaccine strategy employing aDEC205-ovalbumin (OVA) as the priming agent, followed by a boost with OVA-expressing oncolytic rhabdoviruses in an experimental model of OVA-expressing B16 melanoma.

2.2 Results

2.2.1 Pre-existing Immunity to Wild-Type Ad5 (WTAd5) Impairs Generation of a SIINFEKL-Specific Immune Response to Recombinant Ad5-SIINFEKL (rAd5-SIINFEKL)

We hypothesized that pre-existing immunity to WTAd5 may negatively affect priming of the immune response induced by rAd5-expressing antigens. To investigate this, we evaluated the capacity of Ad5 encoding the OVA epitope rAd5-SIINFEKL to generate an antigen- specific immune response in mice with pre-existing immunity to WTAd5. To model pre-existing immunity, we immunized naive C57BL/6 mice with 10^{10} plaque-forming units (PFU) of the WTAd5 virus. After 35 days, mice were administered 10^{8} PFUs rAd5-SIINFEKL intramuscularly (i.m.) (Figure 2.1A). Generation of anti-adenovirus neutralizing antibodies (AdNAbs) in sera of preimmunized mice 40 days post-administration of WTAd5 was confirmed by neutralization assay and was elevated in preimmunized mice (Figure 2.1B). SIINFEKL-specific CD8+ T cell responses were measured 10 days after rAd5-SIINFEKL immunization, the peak time of the adaptive immune response elicited by adenovirus vectors.[160] We observed a statistically significant decrease from 10% to approximately 5% of splenic SIINFEKL-specific CD8+ T cells, depicted by H-2K^{b}-SIINFEKL pentamer staining, from preimmunized mice compared to control phosphate- buffered saline (PBS) mice (Figures 2.1C and 2.1D). To assess CD8+ T cell functionality, splenocytes from preimmunized mice and PBS mice were restimulated with SIINFEKL peptide *in vitro* and followed by intracellular cytokine staining (ICS) for interferon (IFN)-γ and tumor necrosis factor (TNF)-α. Again, there was a reduction from an average of 6% to 2% of IFN-γ- and TNF-α-producing CD8+ T cells specific to SIINFEKL detected in the splenocytes from preimmunized mice compared to control PBS (Figures 2.1E and 2.1F). Together, these results indicate that modeled pre-existing immunity to WTAd5 limits the generation of SIINFEKL-specific cellular responses following rAd5- SIINFEKL immunization in C57BL/6 mice.

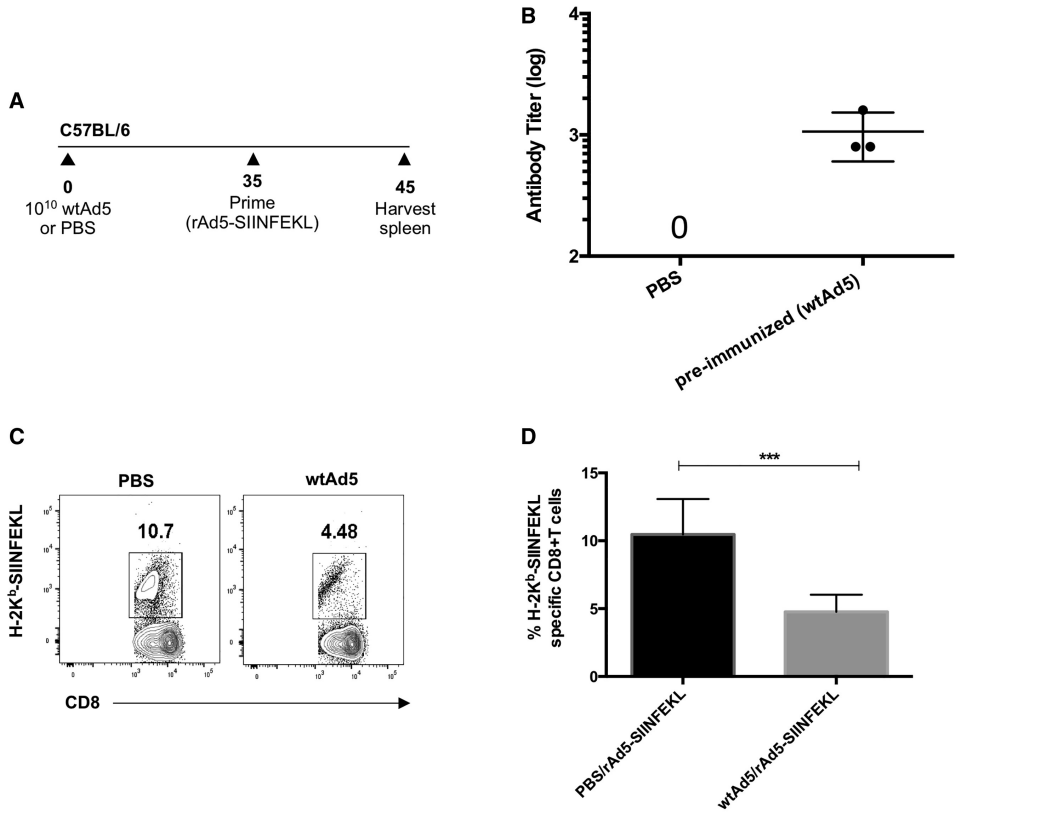
A
C57BL/6
0
10^10 wtAd5
or PBS
35
Prime
(rAd5-SIINFEKL)
45
Harvest
spleen
B
Antibody Titer (log)
4
3
2
0
PBS
Pre-immunized (wtAd5)
C
PBS
wtAd5
H-2K^b-SIINFEKL
10.7
4.48
CD8
D
% H-2K^b-SIINFEKL specific CD8+T cells
15
10
5
0
***
PBS/rAd5-SIINFEKL
wtAd5/rAd5-SIINFEKL
E
SIINFEKL
unstimulated
0.15
4.70
90.5
4.63
0.21
0.20
99.4
0.21
PBS/
rAd5-SIINFEKL
0.16
0.99
97.0
1.83
0.18
0.14
99.4
0.30
wtAd5/
rAd5-SIINFEKL
TNFα
IFNγ
F
PBS/rAd5-SIINFEKL
wtAd5/rAd5-SIINFEKL
%IFNg+ (CD8+ T cells)
20
15
10
5
0
****
unstimulated
SIINFEKL
%IFNg+TNFa+ (CD8+ T cells)
10
8
6
4
2
0
****
unstimulated
SIINFEKL

Figure 2.1 Comparing the SIINFEKL-Specific T Cell Response after i.m. Injection of Priming Agent Recombinant Adenovirus Expressing the SIINFEKL Transgene (rAd5-SIINFEKL) in Mice Modeling Pre-existing Immunity to WTAd5. **(A)** Naive C57BL/6 mice were injected i.m. on day 0 with 10^{10} PFUs of WTAd5 (n = 7) or PBS (n = 5). After 35 days, mice were injected i.m. with rAd5-SIINFEKL. **(B)** Anti-adenovirus neutralizing antibody (AdNAbs) titers in mouse sera (n = 3) were determined by neutralization assay, 40 days after administration of WTAd5.10 days after prime, the representative gating **(C)** and total percentage of **(D)** SIINFEKL-specific CD8+ T cells in the spleen was determined by H2-K^b-SIINFEKL pentamer staining. The representative gating **(E)** and percentage of **(F)** OVA-specific T cells producing IFN-γ and TNF-α in the spleen was evaluated by flow cytometry. Briefly, splenocytes were stimulated in vitro with MHC-I epitope (SIINFEKL) for 5 h, subsequently stained for intracellular production of IFN-γ and TNF-α, and assessed by flow cytometry. ***$p < 0.001$ and ****$p < 0.0001$ (two-way ANOVA).

2.2.2 Production and Characterization of aDEC205-OVA

Impaired SIINFEKL-specific immune responses following rAd5-SIINFEKL immunization of C57BL/6 mice modeling pre-existing immunity led us to consider employing an alternative priming agent that would be better able to overcome pre-existing immunity to WTAd5 and other potential alternative viral vectors. Several studies have shown the ability of chimeric aDEC205 antibodies fused to antigens, such as OVA (aDEC205-OVA) or tumor antigens, to elicit strong antigen-specific immune responses in mice when administered with an adjuvant.[109,161] To evaluate the use of antigen-fused aDEC205 antibodies as alternative priming agents for heterologous boosting with Oncolytic rhabdovirus (ORV) vectors, we used aDEC205 fused to the model antigen OVA.

To generate the aDEC205 antibodies used in this study, human embryonic kidney (HEK)293T cells were co-transfected with plasmids containing the mouse aDEC205-kappa light chain and the aDEC205 heavy chain fused to the full OVA protein sequence at the carboxyl terminus (or no antigen as a control [aDEC205-empty]). The recombinant antibodies produced following transient transfection in HEK293T cell were purified on protein G Sepharose columns.

The resulting antibodies were characterized by western blot using anti-immunoglobulin G (IgG) antibodies on SDS-PAGE under reducing conditions (Figure 2.2A). Figure 2A shows that heavy and light chains of the purified recombinant antibodies had the expected size for both the fused antibody (Ab) aDEC205-OVA (~95 kDa and 25 kDa, respectively) and control antibody aDEC205-empty (50 kDa and 25 kDa, respectively). The capacity of the aDEC205-OVA and aDEC205-empty antibodies to bind to its receptor on the surface of splenic DCs CD11c+CD8a+ was confirmed with a binding assay.[162] Incubation of splenocytes from naive C57BL/6 mice with different concentrations of aDEC205-OVA (0.1, 1, or 10 mg/mL) resulted in a dose-dependent binding (Figure 2B) on the surface of splenic CD11c+CD8a+ DCs (gating strategy shown in Supplemental Figure 9) expressing the DEC205 receptor. These results indicate that aDEC205-OVA and aDEC205-empty were successfully

purified from culture supernatants and that aDEC205-OVA and aDEC205-empty (Supplemental Figure 10) retain binding capacity to the DEC205 receptor as expected.

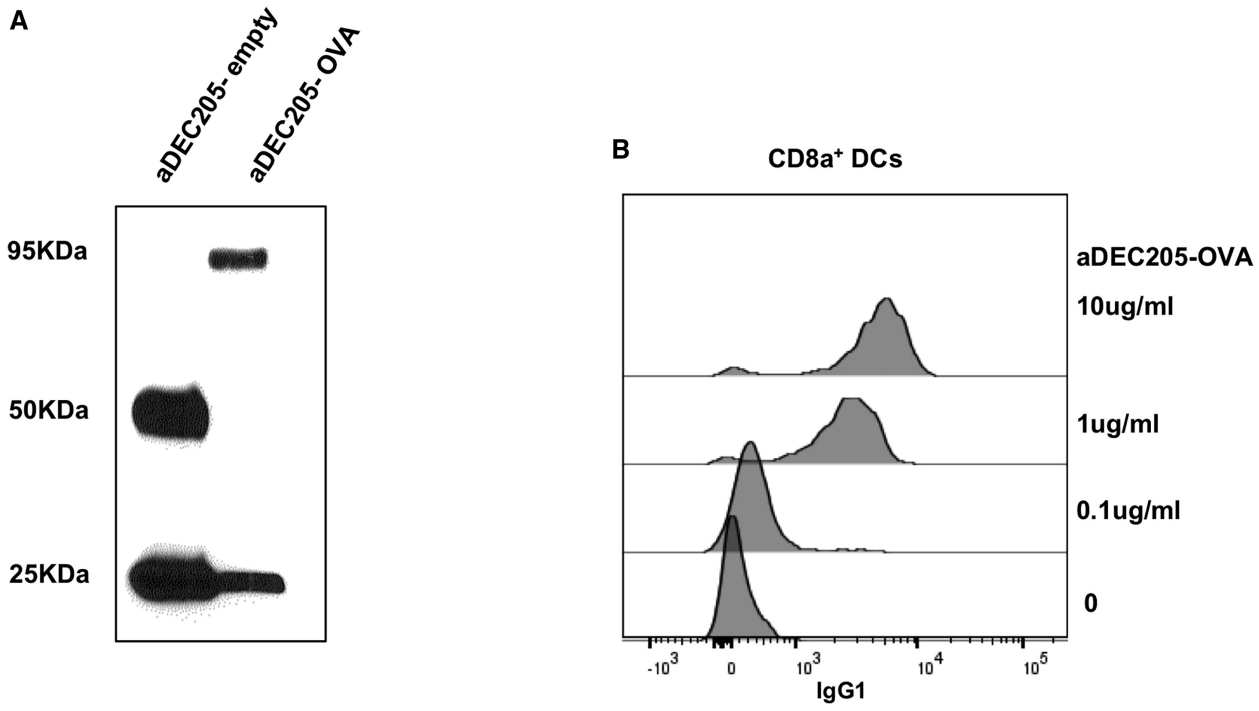
A
aDEC205- empty
aDEC205- OVA
95KDa
50KDa
25KDa
B
CD8a+ DCs
aDEC205-OVA
10ug/ml
1ug/ml
0.1ug/ml
0
-10^3
0
10^3
10^4
10^5
IgG1

Figure 2.2 Production and Characterization of aDEC205-OVA. aDEC205-OVA and aDEC205-empty were generated by transfection of 293T cells in vitro and subsequent purification of the antibody. **(A)** Final antibody product was reduced by β-mercaptoethanol and verified by immunoblotting for the heavy and light chains. aDEC205-empty shows a heavy chain at 50 kDa and light chain at 25 kDa. aDEC205-OVA shows the heavy chain linked with OVA at 95 kDa, indicating the presence of OVA antigen and a light chain at 25 kDa. **(B)** A binding assay was performed to verify effective binding of aDEC205-OVA to the DEC205 receptor on CD11c+CD8+ dendritic cells (DCs) isolated from murine splenocytes. aDEC205-OVA is probed with an anti-IgG1-APC antibody and detected by flow cytometry. The histogram overlay depicts high binding of aDEC205-OVA to CD11c+CD8+ DCs at concentrations of 10 μg/mL and 1 μg/mL and low binding at 0.1 μg/mL.

2.2.3 aDEC205-OVA Administered via Intraperitoneal (i.p.) and i.v. Routes Generates Cellular Immune Responses against SIINFEKL

Several studies demonstrated the influence of the route of immunization on immune response and disease outcome.[163] To determine which route of aDEC205-OVA administration leads to the most potent T cell response systemically, we immunized naive C57BL/6 mice i.p. or i.v. with 10 mg aDEC205-OVA or aDEC205-empty, both in combination with 50 mg poly(I:C) and 50 mg anti-CD40. SIINFEKL-specific T cells were evaluated by flow cytometry at 10 and 21 days postimmunization (Figure 2.3A; gating strategy shown in Supplemental Figure 7). After *in vitro* restimulation of lymphocytes with the SIINFEKL peptide, ICS showed that i.v. and i.p. routes of administration elicited statistically similar percentages of IFN-γ- and TNF-α- producing CD8+ T cells in the lung and spleen of mice immunized with aDEC205-OVA at days 10 and 21 postimmunization (Figures 3B–3D; Supplemental Figure 8). Additionally, staining with the H-2K^b-SIINFEKL pentamer showed statistically similar percentages of SIINFEKL-specific CD8+ T cells at day 21 in the spleen and lung of mice immunized with aDEC205-OVA when comparing i.v. and i.p. routes of administration (Figures 2.3E; Supplemental Figure 8). As expected, no SIINFEKL-specific CD8+ T cells were detected in the spleen or lungs of animals immunized with control aDEC205-empty. These results indicate that either route of administration elicits a strong anti-SIINFEKL primary immune response. Ultimately, to model a preferred route of administration in humans, we administered aDEC205-OVA i.v. for the remainder of this study.

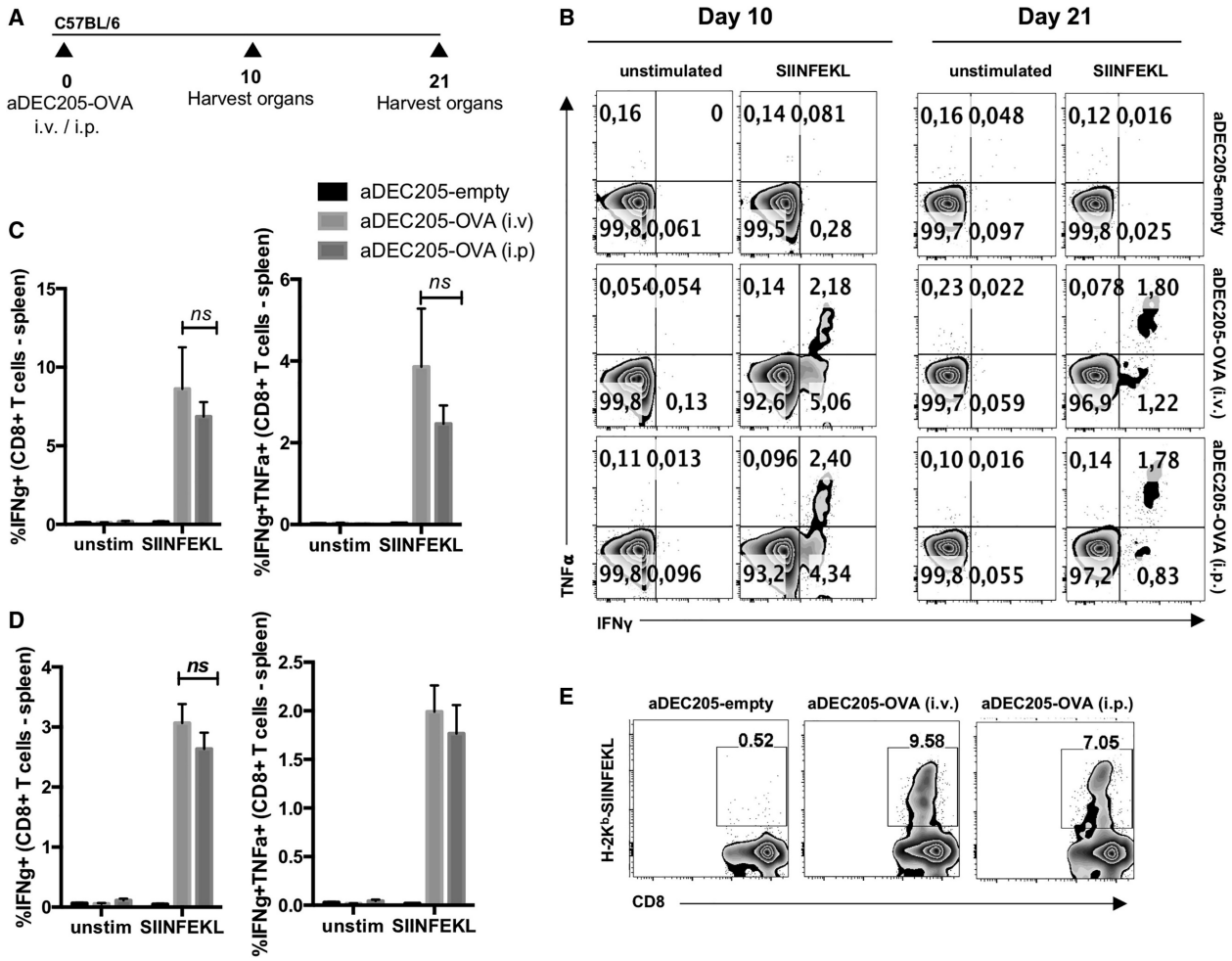
A
C57BL/6
0
aDEC205-OVA
i.v. / i.p.
10
Harvest organs
21
Harvest organs
B
Day 10
Day 21
unstimulated
SIINFEKL
aDEC205-empty
aDEC205-OVA (i.v.)
aDEC205-OVA (i.p.)
TNFα
IFNγ
C
aDEC205-empty
aDEC205-OVA (i.v)
aDEC205-OVA (i.p)
%IFNg+ (CD8+ T cells - spleen)
%IFNg+TNFa+ (CD8+ T cells - spleen)
ns
unstim
SIINFEKL
D
E
H-2Kb-SIINFEKL
CD8
0.52
9.58
7.05

Figure 2.3 aDEC205-OVA Administered i.v. or i.p. Elicits OVA-Specific T Cells in the Spleen of Immunized Mice (A) Naive C57BL/6 mice were primed with 10 μg of aDEC205-OVA or aDEC205-empty + 50 μg poly(I:C) + 50 μg anti-CD40 i.v. or i.p. The percentage of SIINFEKL-specific T cells producing IFN-γ and TNF-α in the spleen **(B)** on day 10 **(C)** and on day 21 **(D)** was evaluated by flow cytometry. **(E)** Quantification of SIINFEKL-specific T cells by pentamer staining (H-2K^{b}-SIINFEKL) was also assessed in the spleen by flow cytometry at day 21 post injection. p value was considered nonsignificant (ns) when >0.05 (two-way ANOVA).

2.2.4 aDEC205-OVA Overcomes Barriers Posed by Pre-existing Immunity and Generates Cellular and Humoral Immunity against OVA

We next evaluated the ability of aDEC205-OVA to overcome pre-existing immunity to WTAd5 in a C57BL/6 murine model. To model pre-existing immunity, all naive C57BL/6 mice were immunized with WTAd5 35 days prior to the injection of priming agents (Figure 2.4A). As previously observed, AdNAbs were detected by a neutralization assay in mouse sera 40 days post administration of WTAd5 and were elevated in preimmunized mice around time of prime (Figure 2.1B). Pre-existing immunity to WTAd5 did not affect priming with aDEC205-OVA; approximately 9% of SIINFEKL-specific CD8+ T cells were observed in the spleen of preimmunized mice and control PBS mice 10 days after prime (Figures 2.4B and 2.4C). Furthermore, a similar percentage of splenic IFN-γ- and TNF-α- producing CD8+ T cells specific to SIINFEKL was also detected by intracellular staining (Figures 2.4D and 2.4E). Together with Figure 1, these results suggest that adjuvanted aDEC205 is an effective prime in the face of pre-existing immunity to WTAd5.

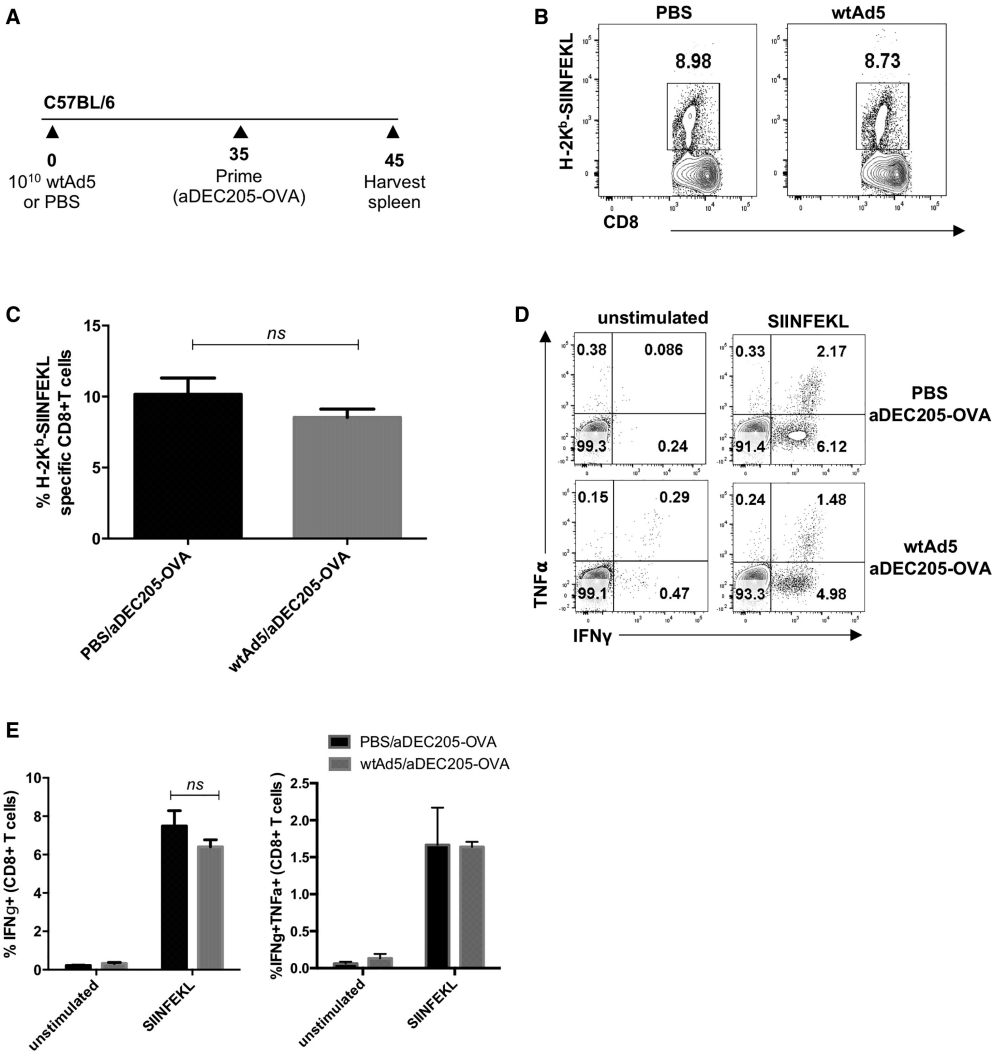
A
C57BL/6
0
10^{10} wtAd5
or PBS
35
Prime
(aDEC205-OVA)
45
Harvest
spleen
B
PBS
wtAd5
8.98
8.73
H-2K^b-SIINFEKL
CD8
C
% H-2K^b-SIINFEKL
specific CD8+T cells
ns
PBS/aDEC205-OVA
wtAd5/aDEC205-OVA
D
unstimulated
SIINFEKL
0.38
0.086
99.3
0.24
0.33
2.17
91.4
6.12
PBS
aDEC205-OVA
0.15
0.29
99.1
0.47
0.24
1.48
93.3
4.98
wtAd5
aDEC205-OVA
TNFα
IFNγ
E
PBS/aDEC205-OVA
wtAd5/aDEC205-OVA
% IFNg+ (CD8+ T cells)
ns
unstimulated
SIINFEKL
%IFNg+TNFa+ (CD8+ T cells)
unstimulated
SIINFEKL

Figure 2.4 Pre-existing Immunity to Adenovirus Does Not Affect an Immune Response Elicited by aDEC205-OVA Prime (A) Naive C57BL/6 mice were injected i.m. on day 0 with 10^{10} PFUs of WTAd5 or PBS. **(B and C)** After 35 days, mice were injected i.v. with 10 μg of aDEC205-OVA + 50 μg poly(I:C) + 50 μg anti-CD40. 10 days after priming, the representative gating **(B)** and percentage of **(C)** SIINFEKL-specific CD8+ T cells in the spleen was determined by H2-K^b-SIINFEKL pentamer staining. The representative gating **(D)** and percentage of **(E)** SIINFEKL-specific T cells producing IFN-γ and TNF-α in the spleen was also evaluated by ICS and flow cytometry. *p*-value was considered nonsignificant when >0.05 (two-way ANOVA).

2.2.5 Heterologous Boosting of aDEC205-OVA Prime with Rhabdovirus-Encoding OVA Potentiates a Cellular and Humoral Immune Response

Priming with Ad5 encoding a cancer antigen, followed by boosting with ORV vectors, such as MG1 or VSV, expressing the same antigen, induces strong antigen-specific responses, providing survival benefit in various tumor models.[69,96,148–150] Therefore, we tested the ability of the combination aDEC205-OVA prime and MG1-OVA boost in the generation of a SIINFEKL-specific T cell response. To this end, naive C57BL/6 mice were primed (i.v.) with 10 mg aDEC205-OVA or aDEC205-empty, both in combination with 50 mg poly(I:C) and 50 mg anti-CD40 and boosted (i.v.) 14 days later with 10^8 PFUs of MG1-OVA or 10 mg aDEC205-OVA with 50 mg poly(I:C) and 50 mg anti-CD40 or PBS. 7 and 14 days after boost, lymphocytes were harvested from the spleen and lung and then stained with the $H2K^b$-SIINFEKL pentamer. At days 7 and 14 post boost, the greatest expansion of SIINFEKL-specific T cells was observed in the spleen (Figures 2.5A–5E) and lungs (Supplemental Figure 9) of animals boosted with MG1-OVA. Similar results were obtained using VSV-OVA (Supplemental Figure 10A and 10B). Although boost with aDEC205-OVA expanded the antigen-specific cells compared to the group only primed with aDEC205-OVA, the level of expansion was significantly lower compared to MG1-OVA. Humoral immunity was also assessed using mouse sera to quantify OVA-specific IgG by ELISA. The combination of aDEC205-OVA/MG1-OVA prime-boost generated the highest anti-OVA antibody titers compared to other combinations and control groups (Figure 2.5F). Immunization with aDEC205-OVA/VSV-OVA prime-boost generated similar antibody titers compared to aDEC205-OVA/MG1-OVA prime-boost at day 7 post-boost (Supplemental Figure 10C).

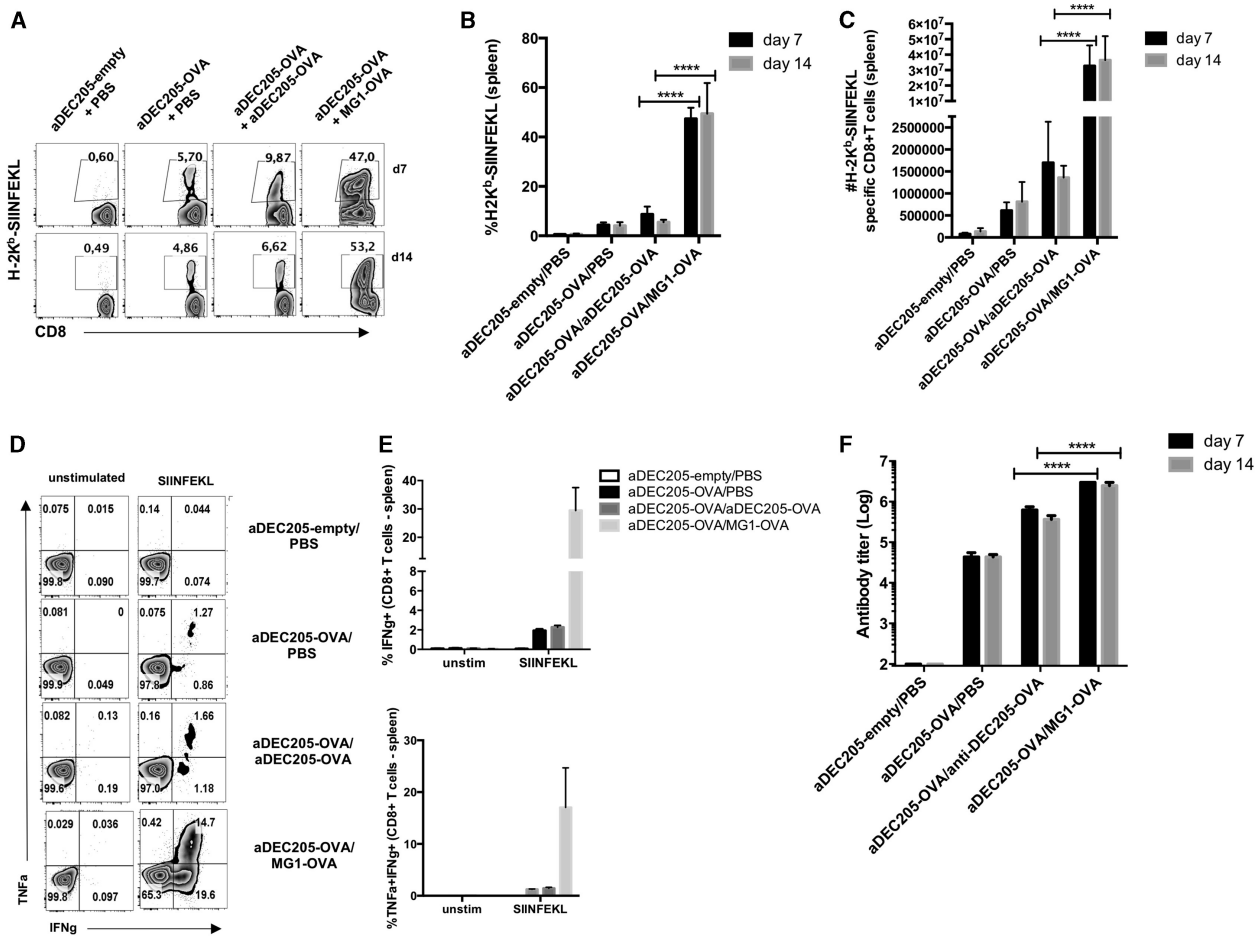
A
aDEC205-empty + PBS
aDEC205-OVA + PBS
aDEC205-OVA + aDEC205-OVA
aDEC205-OVA + MG1-OVA
H-2Kb-SIINFEKL
0,60
5,70
9,87
47,0
d7
0,49
4,86
6,62
53,2
d14
CD8
B
%H2Kb-SIINFEKL (spleen)
day 7
day 14
****
****
aDEC205-empty/PBS
aDEC205-OVA/PBS
aDEC205-OVA/aDEC205-OVA
aDEC205-OVA/MG1-OVA
C
#H-2Kb-SIINFEKL specific CD8+T cells (spleen)
day 7
day 14
****
****
aDEC205-empty/PBS
aDEC205-OVA/PBS
aDEC205-OVA/aDEC205-OVA
aDEC205-OVA/MG1-OVA
D
unstimulated
SIINFEKL
aDEC205-empty/ PBS
aDEC205-OVA/ PBS
aDEC205-OVA/ aDEC205-OVA
aDEC205-OVA/ MG1-OVA
TNFa
IFNg
E
% IFNg+ (CD8+ T cells - spleen)
aDEC205-empty/PBS
aDEC205-OVA/PBS
aDEC205-OVA/aDEC205-OVA
aDEC205-OVA/MG1-OVA
unstim
SIINFEKL
%TNFa+IFNg+ (CD8+ T cells - spleen)
unstim
SIINFEKL
F
Antibody titer (Log)
day 7
day 14
****
****
aDEC205-empty/PBS
aDEC205-OVA/PBS
aDEC205-OVA/anti-DEC205-OVA
aDEC205-OVA/MG1-OVA

Figure 2.5 Induction of a Potent Cellular and Humoral OVA-Specific Immune Response after aDEC205-OVA Prime and MG1-OVA Boost C57BL/6 mice were immunized i.v. with 10 μg of aDEC205-OVA or aDEC205-empty + 50 μg poly(I:C) + 50 μg anti-CD40 at day 0. 14 days later, mice were immunized with a boosting dose of PBS, 10 μg aDEC205-OVA i.v. + 50 μg poly(I:C) + 50 μg anti-CD40, or 10^8 PFUs of MG1-OVA. Spleens were harvested 7 and 14 days following boost to evaluate cellular immune response to prime-boost regimens by flow cytometry **(A)** The percentage **(B)** and total number of **(C)** SIINFEKL-specific CD8+ T cells were determined by H2-K^b-SIINFEKL pentamer staining. At day 14, the representative gating **(D)** percentage of **(E)** splenic IFN-γ and TNF-α-producing CD8+ T cells in response to in vitro stimulation with 5 μM SIINFEKL peptide was evaluated. **(F)** The titers of anti-OVA antibodies in the sera of mice were determined by ELISA at day 7 and day 14 after boost. These results are representative of two independent experiments. ∗∗∗∗$p < 0.0001$ (two-way ANOVA).

2.2.6 Heterologous Prime-Boost Vaccine with aDEC205-OVA and Rhabdovirus-Encoding OVA Confers a Survival Advantage in Tumor-Bearing Mice

We next evaluated the therapeutic efficacy of the aDEC205-OVA/MG1-OVA prime-boost vaccine in an experimental model of lung metastasis. Briefly, $3x10^5$ B16-OVA cells were injected i.v. in C57BL/6 mice, and different primes were administered 5 days post-B16-OVA tumor implantation (Figure 2.6A). Generation of SIINFEKL-specific T cell responses was evaluated by $H2K^b$-SIINFEKL pentamer staining of blood 7 days after boost. The heterologous prime-boost combination employing aDEC205-OVA or rAd5-OVA as a prime generated the greatest percentage of circulating antigen-specific T cells. Interestingly, whereas different routes of administration of the aDEC205-OVA prime (i.v. versus i.p.) did not significantly impact priming responses (Figure 2.3), there was a trend for a higher magnitude of a SIINFEKL- specific CD8+ T cell response generated after prime with aDEC205-OVA administered i.v. compared to aDEC205-OVA prime administered i.p. (Figures 2.6B and 2.6D). In general, all OVA-targeted heterologous prime-boost regimens led to improved survival of tumor-bearing mice, with rAd5-OVA/MG1-OVA and aDEC205- OVA/MG1-OVA regimens being the most effective (30% complete remission). The administering of a prime-boost of aDEC205-OVA/ VSV-OVA also resulted in the generation of greater SIINFEKL-specific CD8+ T cells and improved survival of tumor-bearing mice (Supplemental Figures 6B, 6D, and 6E). Cured mice were rechallenged with a subcutaneous injection of 2×10^6 B16-OVA cells (data not shown); no mice previously cured by any prime-boost regimen developed tumors, thus confirming that anti-SIINFEKL responses were long lasting and conferred protection against recurrent tumors.

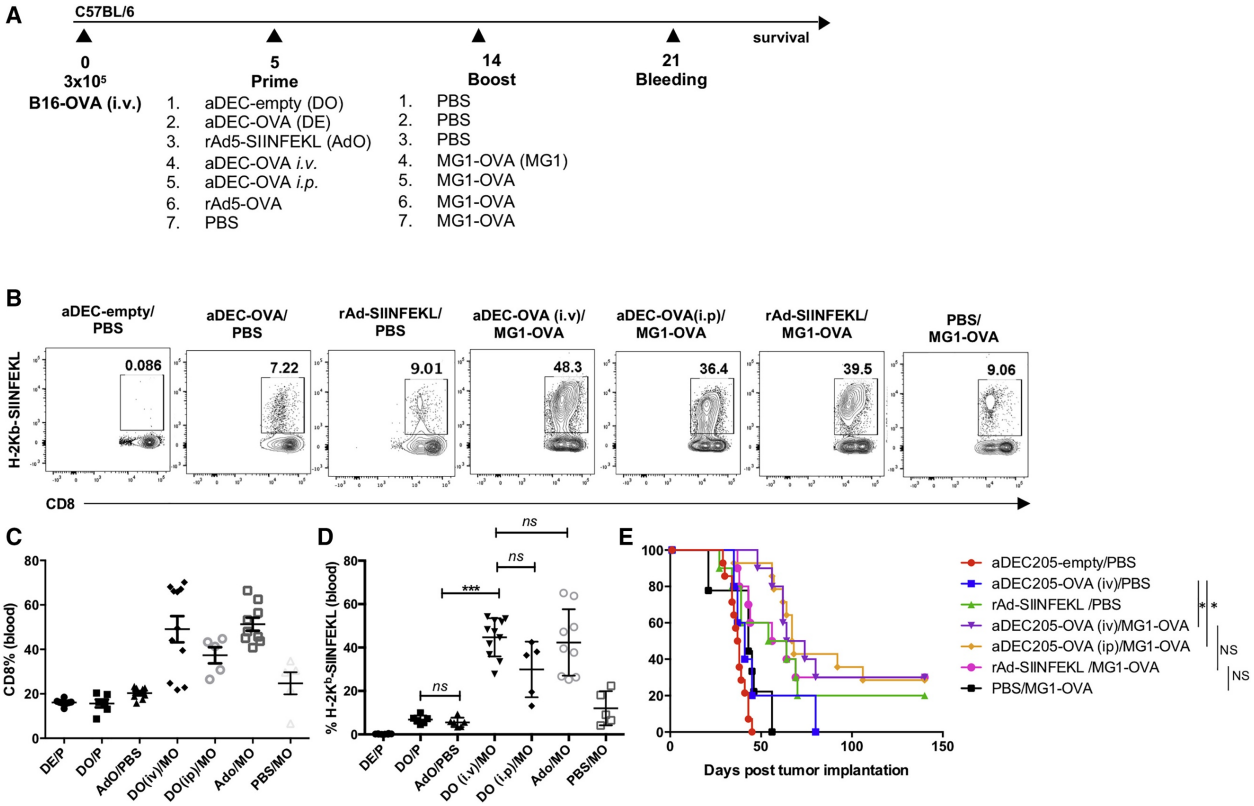
A
C57BL/6
survival
0
3x10⁵
B16-OVA (i.v.)
5
Prime
1. aDEC-empty (DO)
2. aDEC-OVA (DE)
3. rAd5-SIINFEKL (AdO)
4. aDEC-OVA i.v.
5. aDEC-OVA i.p.
6. rAd5-OVA
7. PBS
14
Boost
1. PBS
2. PBS
3. PBS
4. MG1-OVA (MG1)
5. MG1-OVA
6. MG1-OVA
7. MG1-OVA
21
Bleeding
B
aDEC-empty/ PBS
aDEC-OVA/ PBS
rAd-SIINFEKL/ PBS
aDEC-OVA (i.v)/ MG1-OVA
aDEC-OVA(i.p)/ MG1-OVA
rAd-SIINFEKL/ MG1-OVA
PBS/ MG1-OVA
0.086
7.22
9.01
48.3
36.4
39.5
9.06
H-2Kb-SIINFEKL
CD8
C
CD8% (blood)
DE/P
DO/P
AdO/PBS
DO(iv)/MO
DO(ip)/MO
Ado/MO
PBS/MO
D
% H-2Kb-SIINFEKL (blood)
ns
***
ns
ns
DE/P
DO/P
AdO/PBS
DO (i.v)/MO
DO (i.p)/MO
Ado/MO
PBS/MO
E
Days post tumor implantation
aDEC205-empty/PBS
aDEC205-OVA (iv)/PBS
rAd-SIINFEKL /PBS
aDEC205-OVA (iv)/MG1-OVA
aDEC205-OVA (ip)/MG1-OVA
rAd-SIINFEKL /MG1-OVA
PBS/MG1-OVA
**
NS
NS

Figure 2.6 Therapeutic Efficacy of an aDEC205/OVA Prime-Boost Vaccine (A) Schematic representation of immunization schedule. Briefly, C57BL/6 mice received 3×10^5 B16-OVA cells i.v. At day 5, mice were immunized i.v. or i.p. with 10 μg of aDEC205-OVA or aDEC205-empty + 50 μg poly(I:C) + 50 μg anti-CD40, 10^8 rAd5-SIINFEKL, or PBS. At day 14, mice were immunized with a boosting dose of either PBS or 10^8 MG1-OVA. **(B–D)** At day 21 saphenous (saph) bleeds were performed to assess the percentage, by flow cytometry **(B)**, of bulk-circulating CD8+ T cells **(C)** and SIINFEKL-specific CD8+ T cells **(D)**, the latter determined by $H2K^b$-SIINFEKL pentamer staining. p value was considered nonsignificant when >0.05; ∗∗∗p < 0.001 (one-way ANOVA). **(E)** Mice were monitored for survival 140 days post-B16-OVA implantation. Data from three independent survival experiments are pooled. *p* value was considered nonsignificant when >0.05; ∗p < 0.05 (log-rank Mantel-Cox).

2.3 DISCUSSION

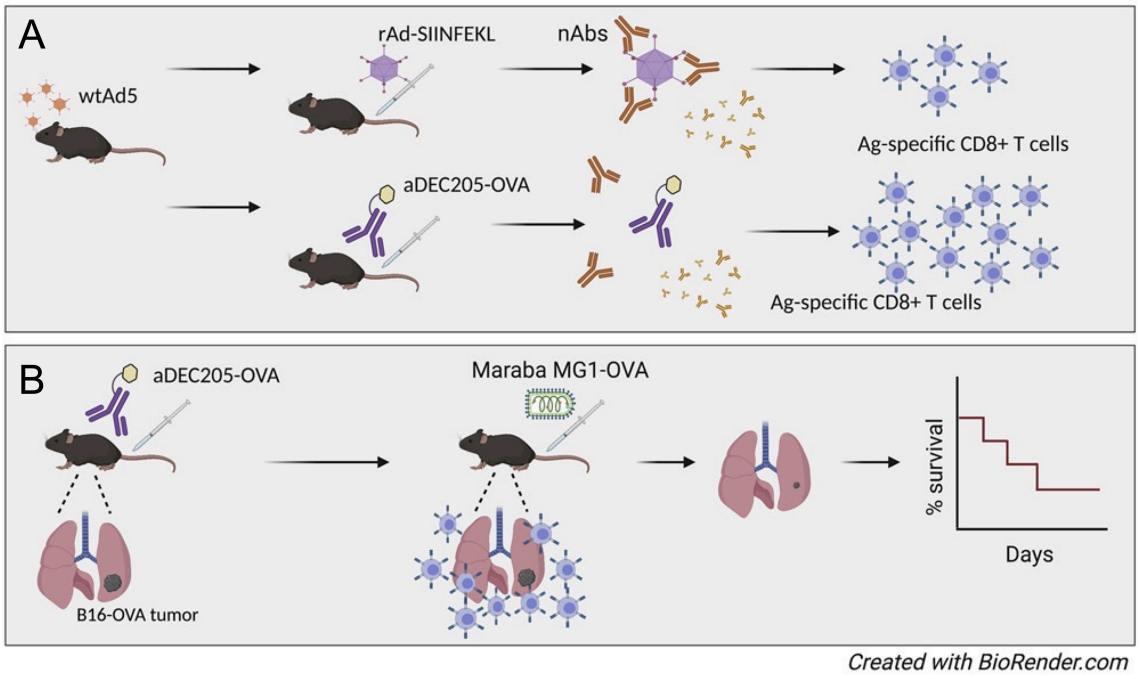

Figure 2.7 Schematic summary of Chapter 2 findings. We explored the potential use of DEC205-targeted antibodies as an alternative agent to prime antigen-specific responses ahead of boosting with an oncolytic rhabdovirus expressing the same antigen. **(A)** In a model of pre-existing immunity to Ad5, we found that a vaccination strategy consisting of an anti-DEC205 antibody fused to the model antigen ovalbumin (OVA) led to the formation of a robust antigen-specific immune response when compared to rAd5-SIINFEKL. **(B)** Furthermore, our prime-boost strategy improved survival in a B16-OVA tumor model.

Cancer immunotherapy has emerged as a promising alternative to conventional cancer treatments. Therapeutic strategies that actively stimulate the immune system to reject tumors have grown to include diverse platforms, including immune-modulating antibodies,[164] small molecules,[165,166] as well as genetically engineered bacteria,[167] cells,[168] and viruses.[144] OVs are attracting increasing interest as multi-mechanistic platforms for immunotherapy, owing, in part, to the recent approval of Imlygic for the treatment of melanoma and to the possibility of combining OVs with antibodies targeting immune checkpoints.[169] Indeed, it is increasingly recognized that OVs have significant potential as part of combination therapy regimens.[170]

In this study, we have further explored one such combination strategy consisting of a heterologous prime-boost, where the priming and boosting vectors share a similar tumor antigen and

where the boosting vector is an oncolytic rhabdovirus.[86] This is a strategy that is now under phase I/II clinical evaluation using a nonreplicating Ad5 as a priming vector and oncolytic MG1 as a boosting vector. In contrast with repeat dosing with the same vector (homologous vaccination), this heterologous prime-boost approach has been shown to skew the immune response from antiviral to anti-tumor, promoting long-lasting anti-tumor immunity.[58,149] The secondary immunization with rhabdovirus, which preferentially infects tumors, not only induces oncolysis but also boosts the primary anti-tumor adaptive immune response and breaks immune tolerance.[171]

Although nonreplicating Ad5 is an effective and well-validated vector for vaccination, pre-existing immunity to Ad5, resulting from prior exposure to WT adenoviruses in humans, can potentially limit its effectiveness in clinical trials.[151,152] Indeed, we found that administration of rAd5-SIINFEKL in preimmunized mice led to both significantly lower percentages of SIINFEKL-specific CD8+ T cells (Figures 1C and 1D) and a reduction in their functionality (Figures 2.1E and 2.1F).

As an alternative to Ad5, we demonstrate here, in line with other studies, that i.p. or i.v. administration of aDEC205-OVA generates antigen-specific and functionally robust anti-SIINFEKL T cells and humoral immunity toward OVA.[108,157,160] However, as a standalone vaccination agent, we observed that aDEC205-OVA did not perform as well as rAd5-SIINFEKL in terms of controlling B16-OVA tumors (Figure 2.6E) and generating activated (IFNγ+, TNFα+), SIINFEKL-specific CD8+ T cells, even though the numbers of SIINFEKL-specific T cells were similar with both primes (Figure 2.6B). This difference could relate to dosing inequivalence between aDEC205 relative to Ad5, however something that is difficult to establish, owing to differences in how immune responses are initiated with the two vaccination methods. However, the dose of aDE205-OVA used in this study is within the range of the human equivalent dose of what is being evaluated in clinical trials employing aDEC205 (ClinicalTrials.gov: NCT01834248 and NCT01127464).[172,173] In comparison, Ad5 was administered at a higher human equivalent dose than what is administered in current clinical trials, further illustrating the potential of aDEC205 over Ad5. Additionally, pre-existing immunity to WTAd5, as evidenced by

the presence of AdNAbs (Figure 2.1B), strongly decreased the ability of rAd5-SIINFEKL to produce an immune response against the SIINFEKL antigen but predictably bore no impact on the ability of aDEC205-OVA to generate functional anti-SIINFEKL CD8+ T cells.

Consistent with other studies, we found that heterologous boosting with an oncolytic rhabdovirus, such as MG1-OVA, amplifies antigen-specific immunity in the spleen at days 7 and 14 to a higher extent than homologous boosting, for example, with aDEC205-OVA (Figure 2.5; Supplemental Figure 9).[86,96] All heterologous regimens tested conferred a survival advantage in B16-OVA-bearing mice (Figure 2.6), and in this regard, primes using chimeric aDEC205 or Ad5 were essentially equivalent. This suggests that aDEC205 chimeric antibodies are a feasible alternative to Ad5 in the context of heterologous prime-boost with an oncolytic rhabdovirus. In addition to overcoming pre-existing immunity, which may be a barrier when using certain viral priming vectors, chimeric aDEC205 antibodies can provide additional practical advantages, including, but not limited to, ease of manufacturing, storage, and the possibility of repeat dosing. This last point is a notable limitation for viral vectors encoding antigens, which generally induce an antiviral immune response after the first dose.

Vaccines employing DCs loaded ex vivo with tumor lysate or major histocompatibility complex class I (MHC-I) peptides for re-administration to patients have been studied for decades and have been shown to generate robust memory CD8+ T cell responses.[174] Following research in the 1990s on antigen-loaded DC vaccines, many clinical trials carried out to this end have been unable to achieve significant clinical responses.[175,176] Objective response rates for a range of DC vaccines loaded with antigens, such as tyrosinase, gp100, MART-1, and MAGE-A3, and autologous peptides in melanoma patients did not exceed 5%–10%.[177] Considering limitations and logistical challenges in producing DC vaccines, DC targeting using chimeric antibodies, like aDEC205, may be more feasible for treating a diverse population of patients.[178] However, as observed in this study (Figure 2.6E), chimeric aDEC205 antibodies may be insufficient as stand- alone anti-cancer vaccines.

One key feature of chimeric aDEC205 antibodies is that they deliver a specific antigen directly to DCs, which in turn, present antigen and activate CD4+ T cells, as well as cross present antigen to CD8+ T cells. However, this approach is also not without limitations. For example, antibody/protein engineering challenges can restrict the choice of antigen and how many antigens can be fused to a given aDEC205 antibody. This can be somewhat addressed using more restricted epitopes in tandem or multiple different chimeric antibodies.

Another consideration for use of chimeric aDEC205 antibodies is the requirement for an adjuvant.[106] In our study, we found that aDEC205- OVA, administered with poly(I:C) and anti-CD40 adjuvants, was effective in generating anti-OVA responses in mice; however, whereas anti-CD40 antibodies (that target the costimulatory receptor CD40 on DCs to induce their maturation) are highly effective in mice, they have displayed severe toxicity in human cancer immunotherapy trials.[179,180] Although this regimen was selected for modeling purposes in mice, we expect adjuvants that are amenable to human use and that have been used in clinical trials (e.g., poly(I:C) stabilized with polylysine and carboxymethylcellulose [poly ICLC] Hiltonol) to be similarly effective in combination with aDEC205.[181] Indeed, many human-compatible adjuvants are known and available and routinely used in the context of cancer vaccines. These include, but are not limited to, alum, poly(I:C), CpG, lipopolysaccharide (LPS), T helper (Th)1- specific cytokines, and growth factors, like Flt3L, important for the development of classical DCs.[172,182] These adjuvants, cytokines, and growth factors may be further combined. For example, CDX-301, a soluble recombinant human (rhu)Flt3L, has been used in combination with poly ICLC in the context of a phase II human trial, testing an aDEC205-NY-ESO-1 melanoma vaccination strategy.[183]

Our study indicates that a vaccine consisting of an aDEC205-OVA prime, followed by a rhabdovirus boost, is a promising alternative to the current heterologous prime-boost that employs Ad5-OVA as a priming agent. To our knowledge, this study is the first of its kind to showcase a

combination of the well-studied aDEC205 antibody in combination with an OV. Additional studies in other tumor models and antigenic targets will be necessary to assess the applicability of this novel approach to a broad range of disease models.

2.4 Materials and Methods

2.4.1 Cell Lines

HEK 293T cells, kindly donated by the Oncolytic Virus Manufacturing Facility (OVMF; Ottawa, Canada) for antibody pro- duction and purification, were cultured in HyQ high-glucose Dulbecco's modified Eagle's medium (HyClone), supplemented with 10% ultra-low IgG fetal bovine serum (FBS; Gibco), 5% penicillin/ streptomycin (pen-strep; Gibco), and 5% L-glutamine (Gibco). B16- F10-OVA cells, kindly gifted by Dr. Yonghong Wan (McMaster University), were cultured in Roswell Park Memorial Institute (RPMI; HyClone), supplemented with 10% FBS, pen-strep, 1 M HEPES buffer, and 50 mg/mL geneticin sulfate (G148 sulfate) (Gibco). All cell lines were incubated at 37°C in a 5% CO_2 humidified incubator. All cells were tested by PCR and Hoechst staining to ensure that they are free of mycoplasma contamination.

2.4.2 Mice

6- to 8-week-old female C57BL/6J mice were obtained from Charles River Laboratories. All animals were handled in strict accordance with good animal practice and approved by the appropriate committee in collaboration with the Office of Animal Ethics and Compliance.

2.4.3 Antibody Production and Purification

The pcDNA plasmids expressing the heavy-chain aDEC205, aDEC205-OVA, and aDEC205-empty and the light-chain DEC205- kappa sequences were generated by Dr. Silvia Boscardin (University of São Paulo). The plasmid DNA was individually transformed in competent DH5-a, and DNA was purified using the QIAGEN Plasmid Maxi Kit (catalog [Cat.] 12165). Transfection of 90% confluent HEK293T cells in 150 mm tissue-culture dishes, antibody collection from culture supernatant, and antibody purification were performed as previously described.[184]

2.4.4 Peptides

Peptides corresponding to the immunodominant epitope of OVA (SIINFEKL) that binds to H-2K^b were synthesized by New England Peptide (lot number 3001-1/48-21) and have >95% purity.

2.4.5 Tissue Processing

SIINFEKL-specific T cell responses were measured in blood, spleen, and lung. Briefly, saphenous bleeds of mice from hindlimb were per- formed, and blood (70–100 mL) was collected in sterile heparin tubes. Red blood cells were lysed using ammonium-chloride-potassium (ACK) lysis buffer. Spleens were excised from sacrificed mice and filtered through a 100-mm plastic cell strainer (Fisherbrand; 352360, 22-363-549) for cell collection. The cell viability of the resulting white blood cells was determined using Trypan blue staining. Lungs were also excised from sacrificed mice after lung perfusion and dissociated using the Lung Dissociation Kit-Mouse (Miltenyi Biotec; 130-095-927), according to the manufacturer's instructions. Upon resuspension in R10 buffer (RPMI, 10% FBS), the cells from blood, spleen, and lung were counted, and 1 x 10^6 cells per condition were stained for flow cytometry.

2.4.6 Immunoblotting

After aDEC205-OVA antibody quantification by the NanoDrop ND- 1000 spectrometer, 1 mg of antibody was run on NuPAGE Novex 4%-12% Bis-Tris precast gels (Thermo Fisher Scientific) under reducing conditions using the XCell SureLock Mini-Cell System (Thermo Fisher Scientific) and transferred to nitrocellulose membranes (Hy- bond-C; Bio-Rad). Blots were blocked with 2% milk and probed with a goat anti-mouse peroxidase-conjugated antibody (1:2,000) (Jackson ImmunoResearch Laboratories). Bands were visualized using the SuperSignal West Pico Chemiluminescent substrate (Thermo Fisher Scientific).

2.4.7 ELISA

Murine serum was collected from blood for detection of OVA-specific antibodies. Briefly, blood (500 mL) from immunized mice was collected in sterile, 1.5 mL Eppendorf tubes. Collected blood was centrifuged for 10 min at 2,000 g, and the resulting serum in the supernatant was collected and frozen at 20°C for downstream use. Murine serum samples were evaluated for presence of OVA-specific antibodies by ELISA for all groups. 96-well enzyme immuno- assay (EIA)/radioimmunoassay (RIA) microplates (Corning; Cat. CLS3590) were coated with albumin (Sigma-Aldrich; A5503-1G) at a concentration of 2 ng/mL in PBS and incubated overnight at 4°C. Plates were washed twice with PBS-Tween 20 0.02% and blocked with blocking buffer (PBS-Tween 20 0.02%, 5% nonfat milk, and 1% BSA) for 1 h at room temperature (RT). Blocking buffer was removed, and serum dilutions (1:500–1:1,000,000 dilution in PBS- Tween 20 0.02%, 5% nonfat milk, and 0.25% BSA) were added to wells and incubated for 2 h at RT. Plates were washed three times with PBS- Tween 20 0.02%, and horseradish peroxidase (HRP)-AffiniPure goat anti-mouse IgG (Jackson ImmunoResearch), diluted 1:4,000, was added to wells and incubated for 1 h at RT. Plates were washed six times with PBS-Tween 20 0.02%, developed with substrate solution (R&D Systems; Cat. DY99), and incubated for 20 min in the dark (RT); development was stopped by addition of 2 N sulfuric acid, and absorbance was read at 510 nm on a Multiskan Ascent plate reader (Thermo LabSystems).

2.4.8 Neutralization Assay

A neutralization assay was performed to quantify the amount neutralizing antibodies against WTAd5, present in serum samples of preimmunized murine, and is based on the ability of serum antibodies to block adenovirus infection of A549 cells. Adenovirus used carries the firefly luciferase (Fluc) reporter gene, E1 deletion, and cytomegalovirus (CMV) promoter. 2-fold serum dilutions (1:100; 1:200; 1:400; 1:800; 1:1,600; 1:3,200; 1:6,400; 1:12,800; 1:25,600; 1:51,200; 1:102,400) were tested. In 96-well flat-bottom plates, the Ad-Fluc virus (MOI 100) was combined with different serum

dilutions and incubated for 1 h at 37°C. Contents of this plate were transferred to a 96-well flat-bottom plate, previously seeded with 2 x 10^5 A549 cells per well, washed 3 with PBS, and incubated for 48 h at 37°C. To read plate, luciferin was added at a final concentration of 2 mg/mL luciferin per well and imaged/read by the Biotek Synergy Mx Microplate Reader. The antibody neutralizing unit (NU) was defined as the minimum serum dilution required to achieve at least an 80% reduction in luciferase activity, which was assumed to correlate directly to an inhibition of vector infection.

2.4.9 Mouse Tumor Model and Injections

B16-OVA lung tumors were established in 8-week-old female C57BL/ 6 mice by i.v. injection of 3 x 10^5 cells in 100 mL PBS. For adenovirus injections, mice were anesthetized with 5% isoflurane. WTAd5 (10^{10} PFUs) and rAd5-SIINFEKL (10^8 PFUs) were administered i.m. in 50 mL PBS. For aDEC205 injections, a solution containing 10 mg of aDEC205, 50 mg poly(I:C), and 50 mg anti-CD40 ligand (CD40L) in 150 mL of PBS was administered either i.v. or i.p. Oncolytic rhabdoviruses (MG1-OVA and VSVΔ51-OVA) were administered i.v. in 100 mL of PBS.

2.4.10 Detection of Antigen-Specific T Cell Responses

OVA-specific T cell responses were measured 7 and 14 days post boost in blood, spleen, and lung. Splenocytes and lung-resident lymphocytes were isolated and stained for the presence of SIIN-FEKL-specific T cells using a H-2Kb-SIINFEKL pentamer. For SIINFEKL-specific CD8+ T cell in vitro restimulation, 1 x 106 splenocytes and lung-resident lymphocytes were incubated in RPMI medium, supplemented with 10% FBS and 5% pen-strep containing 5 mM of SIINFEKL peptide and brefeldin A (Golgi plug) for 4 h. ICS was per- formed as described below.

2.4.11 Virus Preparation

The adenoviruses were made using standard techniques.54 The Indi- ana serotype of VSV (VSVΔ51 or VSVΔ51-OVA) and the Brazilian MG1 (or MG1-OVA) were used throughout this study and were propagated in Vero cells. VSVΔ51-expressing and MG1-expressing OVA are recombinant

derivatives of VSVΔ51 and MG1, described previously.[83] All viruses were propagated on Vero cells and purified on 5%–50% OptiPrep (Sigma) gradient, and all virus titers were quantified by the standard plaque assay on Vero cells, as previously described.[185]

2.4.12 Antibody Binding Assay

A flow cytometry-based binding assay was performed to evaluate aDEC205-OVA and aDEC205-empty binding specificity to the target DEC205 receptor on DCs. Bulk splenocytes were isolated from spleens of naive C57BL/6J mice. Red blood cells were lysed, and $5x10^6$ bulk splenocytes were incubated with graded concentrations of antibody (0.1 mg/mL, 1 mg/mL, and 10 mg/mL) in a 96-well plate for 45 min (4°C). After incubation, cells were stained for flow cytometry.

2.4.13 Flow Cytometry

After processing the tissues as described above, cells were then stained with the FVS780 viability dye (BD Biosciences, San Jose, CA) PBS for 15 min at RT. Following washes, cells were incubated with anti- CD16/32 in 0.5% BSA/PBS at 4°C to block nonspecific antibody interaction with Fc receptors. Subsequently, the following protocols were used for staining.

2.4.14 Staining for Antibody Binding Assay

Anti-CD11c-phycoerythrin (PE)-Cy7, anti-MHC-I-PE, anti-CD8- PE-CF594, anti-IgG-allophycocyanin (APC), anti-CD3-fluorescein isothiocyanate (FITC), and anti-CD19-FITC antibodies were added to cells and incubated for 30 min (4°C).

2.4.15 Staining for ICS

First, $1x10^6$ cells were incubated with antibodies targeting T cell sur- face markers CD3-AF700 and CD8-PE-CF594 for 30 min (4°C). Cells were washed twice with fluorescence-activated cell sorting (FACS) buffer. Next, the mouse Cytofix/Cytoperm Plus (BD Bioscience) was used for permeabilization and ICS. Cells were incubated with Cytofix for 20 min to permeabilize cells for ICS (4°C). Cells were washed twice with PermWash and incubated with anti-IFN-g-BV650 and anti-TNF-a-AF647 diluted in PermWash for 30 min (4°C).

2.4.16 Staining for OVA-Specific T Cells/Pentamer Staining

Cells were washed with FACS buffer. In a 96-well plate, 3 mL of H-2K^b-SIINFEKL pentamer-APC (Proimmune) in 50 mL of FACS buffer was added per well and incubated for 10 min (RT) in the dark. Cells were washed twice with FACS buffer and stained with fixable viability stain for 30 min (4°C). Subsequently, the cells were washed with FACS buffer and incubated with anti-CD16/32 in FACS buffer for 5 min (4°C). Next, cells were stained with anti- CD8-PE-CF594 and anti-CD3-AF700 for 30 min (4°C). After staining, cells were washed with FACS buffer and fixed in 1% paraformaldehyde. Cells were acquired on Becton Dickinson (BD) flow cytometry (Fortessa), and analyses were performed using FlowJo software version (v.)9.

2.4.17 VSV-OVA Cloning and Rescue

Phagemid cloning vector, also known as BlueScribe SK (pBSSK)-VSVΔ51, plasmid-containing viral genome, was used to construct VSVΔ51-OVA. In brief, the OVA gene was PCR amplified from pcDNA expressing aDEC205-OVA using the following primers: for- ward: 50 -AATTCTCGAGATGGGCTCCATCG-30 and reverse: 50 -CATCGCTAGCTCACTACAGATCCTC-30 . PCR amplicon was digested by XhoI and NheI and cloned into the multiple cloning site (MCS) of pBSSK-VSVΔ51 between G and L open reading frames (ORFs). Positive clones were screened by restriction digestion map- ping and verified by sequencing.

2.4.18 Statistics

Statistical significance was calculated using Student's t-test or one-way or two-way ANOVA test, using Tukey's multiple comparison test, as indicated in the figure legends. The log-rank (Mantel-Cox) test was used to determine significant differences in plots for survival studies. Error bars represent the standard error of the mean. Significance is based on a p value <0.05. Statistical analyses were performed using Graph- Pad Prism 6.0 and Excel.

Chapter 3 – Immune profiling of dedifferentiated liposarcoma and identification of novel antigens for targeted immunotherapy

Anna Jirovec* [1,2], Ashley Flaman [3,4], Elena Godbout [2], Daniel Serrano [2], Joel Werier[4,5], Bibianna Purgina [3,4], Jean-Simon Diallo[1,2].

[1]Department of Biochemistry, Microbiology and Immunology, University of Ottawa, Ottawa, ON, Canada

[2] Centre for Innovative Cancer Research, Ottawa Hospital Research Institute, Ottawa, ON, Canada

[3] Department of Pathology and Laboratory Medicine, University of Ottawa, Ottawa, ON, Canada

[4] Department of Pathology and Laboratory Medicine, The Ottawa Hospital, Ottawa, ON, Canada

[5] Department of Orthopedic Surgery, The Ottawa Hospital, Ottawa, ON, Canada

This version of the manuscript was submitted to Scientific Reports and is under peer-review at the time of Thesis submission.

3.1 Introduction

Dedifferentiated liposarcoma (DDLS) is a rare high-grade mesenchymal-derived soft-tissue malignancy that originates from adipocytes, and typically occurs within the retroperitoneal region or the extremities. 90% of DDLS tumors arise *de novo*, with a minority of cases arising as a recurrence of well-differentiated liposarcoma (WDLS).[186] WDLS is a slow progressing low-grade sarcoma that can transition into DDLS by downregulation of adipocyte differentiation programs, resulting in tumors with a non-lipogenic DDLS adjacent to WDLS resembling mature adipose tissue. Surgical resection is the standard of care for DDLS, however tumor location, existence of metastasis, and tumor invasiveness have a significant impact on disease outcome.[187] Retroperitoneal liposarcomas are often large in size, and proximity to vital organs limits the ability to achieve negative surgical margins, leading to an 80% chance of local recurrence of DDLS.[188–190] Additionally, DDLS has high metastatic potential, with 30% of DDLS cases metastasizing to the lungs and negatively impacting patient prognosis.[191] The resistance of DDLS to chemotherapy and radiation limits the ability to control inoperable tumors or metastatic disease,[192] resulting in 5- and 10- year survival rates of 57.2% and 40.1%[193] and 5-year disease specific survival rates of 44%.[194] The low overall survival rate of patients with recurrent disease or metastasis highlights the necessity for the development of novel and effective therapeutic strategies against DDLS.[193,194]

As the role of the immune system in both tumor control and progression is becoming increasingly evident, modulation of the immune system has recently emerged as an alternative approach to cancer treatment.[3] Immunotherapies that have been evaluated in sarcoma include immune checkpoint inhibitors, and cancer testis antigen (CTA) targeted adoptive cellular therapies or vaccination strategies. [195–203] Despite progress of the development of immunotherapies in other cancer subtypes, immunotherapies have shown limited clinical responses in DDLS. For example, the monoclonal antibody pembrolizumab that blocks T cell inhibition by targeting immune inhibitory molecules PD1 was evaluated in several sarcoma subtypes, however, this treatment resulted in a

response rate of only 10% in DDLS patients.[204] Additionally, while CTAs are attractive targets, CTA targeted immunotherapies to date have been most effective in a small subset of sarcomas in which CTA expression is exceptionally high, such as NY-ESO-1 in synovial sarcoma.[196,198,205,206]

The poor clinical outcome of existing immunotherapy approaches can be attributed in part to tumor heterogeneity and significant variations in tumor immune microenvironment, thus impacting the efficacy of immunotherapy regimens.[26,207] We suggest that the characterization of the TME and determination of the underlying immunological mechanisms at play within the tumor microenvironment will guide in the development of specific and effective immunotherapies. Furthermore, CTAs remain to be promising immunotherapy targets as their expression is generally restricted to germ line cells but are aberrantly re-expressed and often up-regulated in various human cancers. However, no reliable antigen has been identified and characterized for application of antigen targeted therapies to DDLS; identifying a highly expressed tumor antigen may drive further development of novel immunotherapies for this sarcoma subtype. Furthermore, alongside their role as immunotherapy targets, CTAs are currently under investigation as promising predictive biomarkers for immunotherapy response. Notably, the expression of CTA SPA17 has been linked to tumor immune cell infiltration, and served as a predictive indicator for patient response to anti-PDL1 and anti-PD1 therapy in a Pan-Cancer analysis. [208] Similarly, in colon cancer, PBK expression has been found to correlate with heightened immune cell infiltrates, warranting additional research into PBK as a potential predictive biomarker for immunotherapy response.[209]

In this study, we set out to address these shortcomings in the specific context of DDLS and performed a comprehensive evaluation of the tumor immune microenvironment, using RNA-based immune profiling and immunohistochemistry. Furthermore, we screened for additional target antigens to further circumvent immune-evasion. Immune analysis of DDLS tumors revealed two distinct immune phenotypes; described as inflamed and non-inflamed within tumor specimens. Two novel antigens were identified that have not been previously reported as antigenic targets in DDLS.

3.2 Results

3.2.1 Patient Characteristics

We first set out to determine the immune profile and to identify antigens expressed in DDLS using an RNA-based tumor profiling method applied to archival tumor samples. RNA was extracted from formalin-fixed paraffin-embedded (FFPE) DDLS tumor samples selected from 29 patients (Table 3.1, Supplemental Table 1), and matched with healthy adipose tissue from the pannus fat of 10 patients, which were used as controls for antigen expression. The selection included twenty-four primary tumors (82.8%) and four recurrent tumors (13.7%). DDLS tumors occurred in the retroperitoneum in 9 patients (31%), trunk in 4 patients (13.7%) and 14 in distal extremities (48.3%). 8 patients in the study were only treated by surgical resection. 5 (17.2%) patients received neoadjuvant radiation therapy, 6 (20.7%) patients received adjuvant radiation therapy, and 1 (3.4%) patient received adjuvant chemotherapy and radiation therapy. Out of 29 patients, 11 patients (37.9%) were alive at the time of last follow-up.

Table 3.1 Patient characteristics of FFPE DDLS samples used in nCounter Nanostring analysis

Characteristic	N=29	%
Age		
Median	66	
Range	31-88	
Site Category		
Retroperitoneal	8	27.5
Trunk	6	20.7
Distal Extremity	14	48.3
Unknown	1	3.4
Primary Tumor	25	86.2
Metastasis present	6	20.6
Recurrence	4	13.7
Metastasis present	2	6.9
Treatment Prior to Surgery		
None	9	31
Chemo	3	10.3
RT	3	10.3
Chemo+RT	0	
Unknown	7	24.1
Treatment Post Surgery		
RT	6	20.7
Chemo + RT	1	3.4
Outcome		
Alive at time of last follow-up	11	37.9
Lost to follow-up	13	44.8
Deceased from disease	5	17.2
Deceased not from disease	1	3.4

3.2.2 Differential gene expression analysis revealed upregulation of genes associated with immune functions

To identify the key differences in gene expression between DDLS tumors and healthy adipose controls, mRNA expression of 770 genes was determined using the nCounter PanCancer Immune Profiling Panel on the nCounter SPRINT Profiler. Differential gene expression analysis was performed and a p-value <0.005 threshold was set for significant differences in gene expression. 51 genes that fall within this threshold were further analyzed and classified as genes involved in cytokine signaling, cell cycle, T cell function, adhesion and CTAs (Supplemental Table 2, Figure 3.1 A-D).

Genes that were upregulated in DDLS compared to healthy adipose controls include cytokines (*CXCL10, CCR5*), as well as genes involved in cell cycle (*CDK1, BIRC5, BAX*), T cell functions (*GZMA, CD8, IDO1*) and CT antigens (*TTK, PBK*) and others such as *ISG15, FN1, NEFL* and *NUP107* and *FCGR1A* (Figure 3.1 A,C). Together, upregulation of these genes is indicative of a tumor undergoing proliferation that is permissive to immune cell infiltration.

Genes that are downregulated in DDLS compared to healthy adipose controls include adhesion molecules *ITGA1, ITGB4, ICAM2* and *MCAM*. There is also downregulation of several cytokines and chemokines and their receptors, such as *IL-1b, CCL21, IL18RAP, TNFRSF1A*, and several members of the JAK/STAT pathway (*JAK2*, *NFKB1A* and *STAT5B*). Several downregulated genes are associated with loss of adipocyte function and include *SAA1*, *PPARG*, and *DUSP6* and the cytokines *CCL14*, *CXCL2* and *CCL2* (Figure 3.1A).

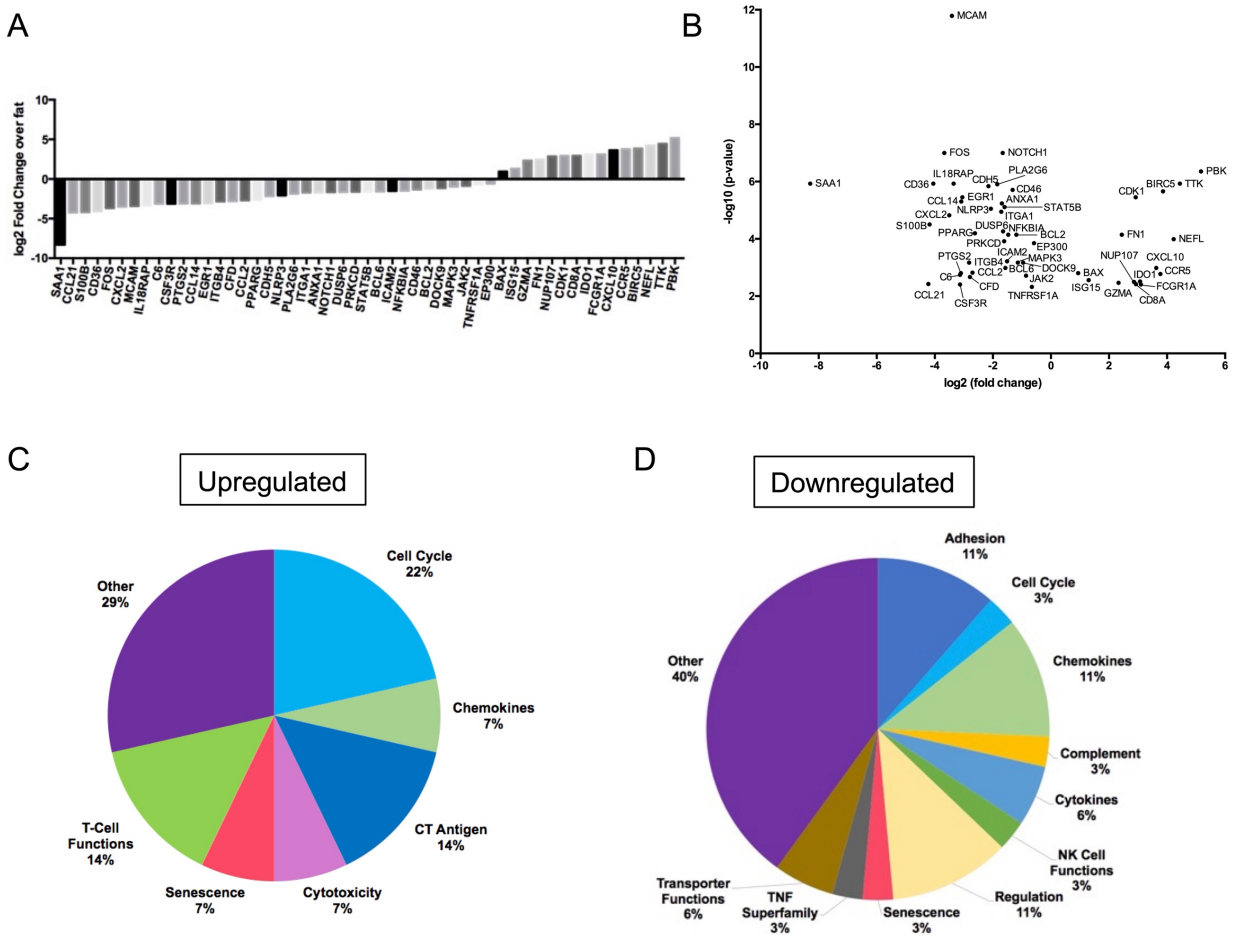
A
log2 Fold Change over fat
10
5
0
-5
-10
SAA1
CCL21
S100B
CD36
FOS
CXCL2
MCAM
IL18RAP
C6
CSF3R
PTGS2
CCL14
EGR1
ITGB4
CFD
CCL2
PPARG
CDH5
NLRP3
PLA2G6
ITGA1
ANXA1
NOTCH1
DUSP6
PRKCD
STAT5B
BCL6
ICAM2
NFKBIA
CD46
BCL2
DOCK9
MAPK3
JAK2
TNFRSF1A
EP300
BAX
ISG15
GZMA
FN1
NUP107
CDK1
CD8A
IDO1
FCGR1A
CXCL10
CCR5
BIRC5
NEFL
TTK
PBK
B
-log10 (p-value)
12
10
8
6
4
2
0
-10
-8
-6
-4
-2
0
2
4
6
log2 (fold change)
MCAM
FOS
NOTCH1
SAA1
IL18RAP
PLA2G6
CDH5
CD36
CD46
PBK
CDK1
BIRC5
TTK
CCL14
EGR1
ANXA1
NLRP3
STAT5B
CXCL2
ITGA1
S100B
DUSP6
NFKBIA
PPARG
BCL2
FN1
NEFL
PRKCD
EP300
PTGS2
ICAM2
MAPK3
NUP107
CXCL10
ITGB4
BCL6
DOCK9
C6
CCL2
BAX
IDO1
CCR5
JAK2
CFD
ISG15
GZMA
FCGR1A
CCL21
TNFRSF1A
CD8A
CSF3R
C
Upregulated
Cell Cycle
22%
Chemokines
7%
CT Antigen
14%
Cytotoxicity
7%
Senescence
7%
T-Cell
Functions
14%
Other
29%
D
Downregulated
Adhesion
11%
Cell Cycle
3%
Chemokines
11%
Complement
3%
Cytokines
6%
NK Cell
Functions
3%
Regulation
11%
Senescence
3%
TNF
Superfamily
3%
Transporter
Functions
6%
Other
40%

Figure 3.1 Distinct expression pattern characteristics of DDLS tumors compared to healthy adipose tissue. (A) Genes showing significant (p-value <0.005) fold change in expression compared to control tissue. Significance calculated using the Benjamini-Yekutieli procedure **(B)** Volcano plot showing statistical significance (-log10 p-value) versus fold change of differentially expressed genes. Overview of gene sets encompassing differentially expressed genes in DDLS compared to healthy adipose controls that are **(C)** upregulated and **(D)** downregulated

3.2.3 DDLS show large heterogeneity in active pathways and infiltrating lymphocytes

To obtain comprehensive information about the specific underlying molecular changes in DDLS, we assessed broadly active molecular pathways within DDLS. In this approach, the expression data of all genes in the nCounter panel was subjected to a pathway analysis performed by nSolver 4.0. Pathway scores are determined by nSolver Advanced Analysis Software 2.0 and are fit using the principal component of each gene set's data and are oriented such that increasing scores correspond to increasing expression of genes included within the pathway. Pathway scores were compared between DDLS and healthy adipose controls. The only pathway significantly downregulated in DDLS compared to healthy adipose controls was cell adhesion (Figure 3.2A). Within the adhesion pathway, *MCAM, ITGA1, ICAM2* and *ITGB4* demonstrate significant downregulation in DDLS compared to healthy adipose tissue (Figure 3.2B). The activated leukocyte cell adhesion molecule (*ALCAM*) was the sole gene within the adhesion pathway that demonstrated significant upregulation ($p<0.005$) in DDLS when compared to healthy adipose tissue (Figure 3.2B).

Despite the downregulation of several adhesion molecules in DDLS compared to healthy adipose tissue, several adhesion molecules were found to be expressed at the mRNA level in DDLS (Supplemental Figure 11A). We observed high expression of factors that make up the extracellular matrix; *FN1* and *COL3A1* in 100% of DDLS samples. We also observed the expression of several integrins. Integrins play a significant role in cell-cell adhesion within the extracellular matrix and leukocytes by binding a diverse array of ligands. In the context of tumor biology, integrins are implicated in tumor progression and metastasis. In our analysis, we observed the downregulation of several integrins such as *ITGA1*, *ITGB4*, *ITGAX* and *ITGA6* in DDLS compared to healthy adipose tissue (Figure 3.2B). This downregulation may be due to the loss of adipocyte function during DDLS dedifferentiation. Notably, specific integrin subunits, particularly *ITGB1*, have been found to be expressed in the adipose tissue in specimens from obese subjects. [210–213]

Integrins function as heterodimers and consist of alpha and beta subunits that form a functional transmembrane receptor. To further explore the functional integrins in DDLS, we performed correlation analysis between various known integrin heterodimer complex subunits (Supplemental Figure 11B, Supplemental Table 3). In our analysis, we discovered a positive and significant expression correlation between the following integrins (ITG) *A1/B1*, *A4/B1*, *AL/B2*, *AM/BA*, *AX/B2*, and *A6/B4*, suggesting their functional role as integrins in DDLS (Supplemental Table 3). We further investigated the correlation between integrin subunits and their natural ligands (Supplemental Figure 11B) and found a statistically significant positive correlation between *ITGB2* and *COL3A1* expression (Supplemental Figure 11C). ITGB2 is a subunit of the $\alpha 1\beta 2$ integrin activating ligand of collagen type III, suggesting a functional signaling unit. No correlation of expression was found between *FN1* and *ITGA4*, *ITGA5*, *ITGB1* or *ITGB3* subunits.

Furthermore, cell adhesion molecules such as integrins and members of the immunoglobulin superfamily (*VCAM, MCAM, ALCAM)* have been associated with metastatic behaviour in various cancer types.[214–216] Therefor, we explored the differential expression of adhesion molecules (Figure 3.2C) between primary tumors of patients with or without metastasis. We observed significantly increased expression of *ALCAM* in the primary tumors of patients with metastasis compared to those without metastasis. These findings offer valuable insights into the potential role of *ALCAM* as a contributing factor to metastasis in DDLS.

Next, we assessed immune cell types present in DDLS samples compared to healthy adipose controls. Cell type scores were calculated by nSolver Advanced Analysis Software 2.0 based on the expression levels of predefined genes previously shown to be characteristic of a cell population. Cell types that were detected by Nanostring are classified by nSolver as cytotoxic cell, DC, macrophages, T-cells, mast cells and CD8 T cells. Cytotoxic cells, DCs, macrophages, T-cells and CD8 T cells showed no significant differences in abundance compared to healthy adipose controls (Figure 3.2C).

Notably, we observed large standard deviations in cell type scores of all tumor-infiltrating cell types identified of DDLS compared to healthy adipose tissue.

The presence of mast cells was significantly higher in healthy adipose controls compared to DDLS. Mast cells, traditionally associated with allergic reactions, play an active role in adipose tissue development and metabolism and are abundantly found in fatty tissues alongside adipocytes.[217–221] The difference in mast cell abundance between DDLS and healthy adipose controls is possibly a result of the higher baseline levels of mast cells in fat tissue. Given that DDLS involves dedifferentiation from adipocytes and loss of adipocyte functions, it is rational to expect a lack of mast cell accumulation in tumor tissue.

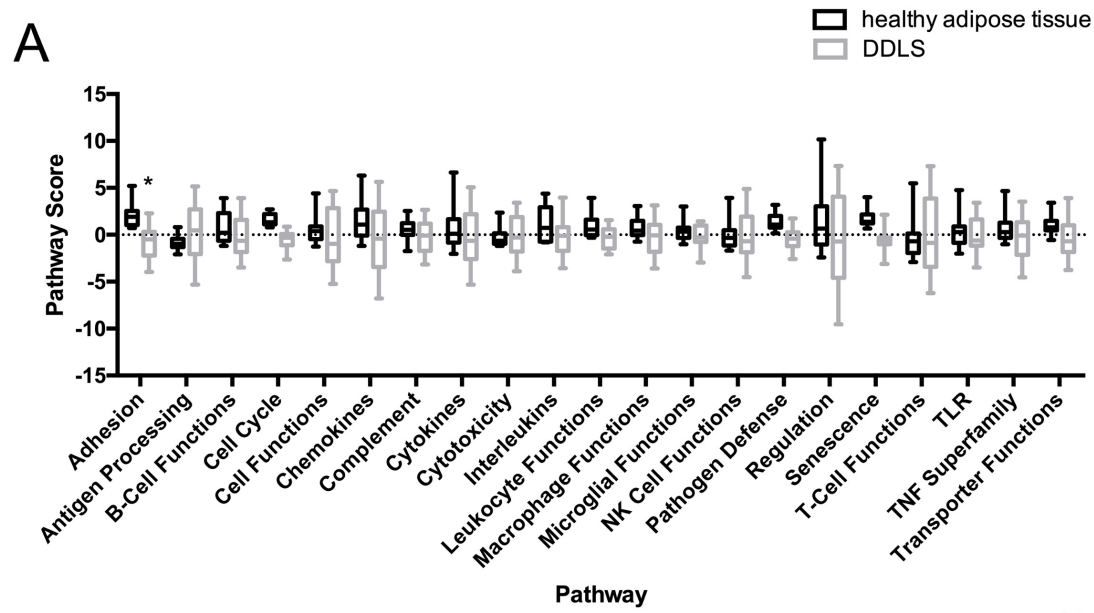
A
healthy adipose tissue
DDLS
Pathway Score
15
10
5
0
-5
-10
-15
*
Adhesion
Antigen Processing
B-Cell Functions
Cell Cycle
Cell Functions
Chemokines
Complement
Cytokines
Cytotoxicity
Interleukins
Leukocyte Functions
Macrophage Functions
Microglial Functions
NK Cell Functions
Pathogen Defense
Regulation
Senescence
T-Cell Functions
TLR
TNF Superfamily
Transporter Functions
Pathway

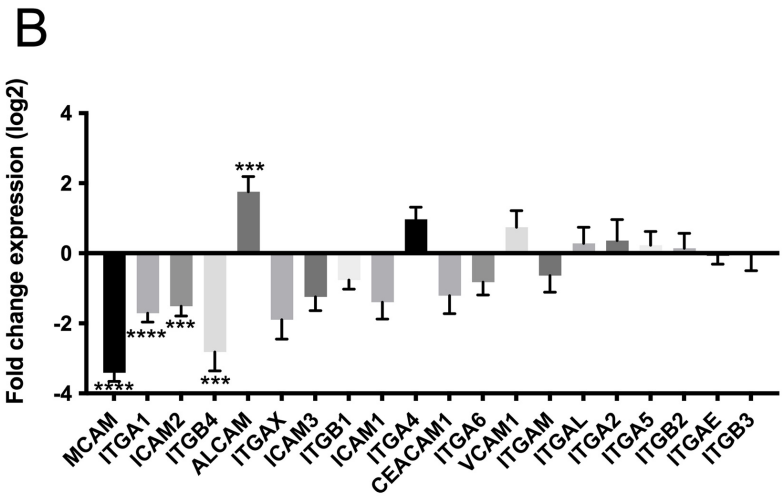
B
Fold change expression (log2)
4
2
0
-2
-4
***
****
***
***
****
MCAM
ITGA1
ICAM2
ITGB4
ALCAM
ITGAX
ICAM3
ITGB1
ICAM1
ITGA4
CEACAM1
ITGA6
VCAM1
ITGAM
ITGAL
ITGA2
ITGA5
ITGB2
ITGAE
ITGB3

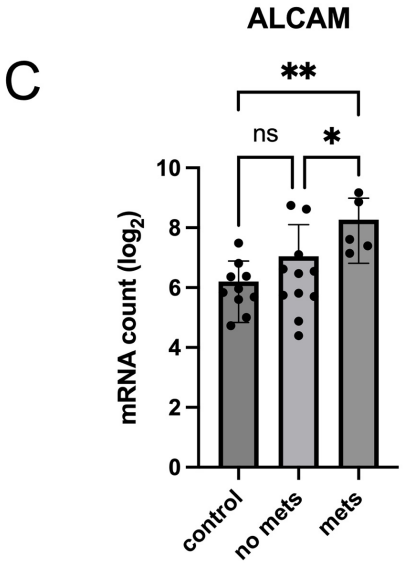
C
ALCAM
**
ns
*
mRNA count (log2)
10
8
6
4
2
0
control
no mets
mets

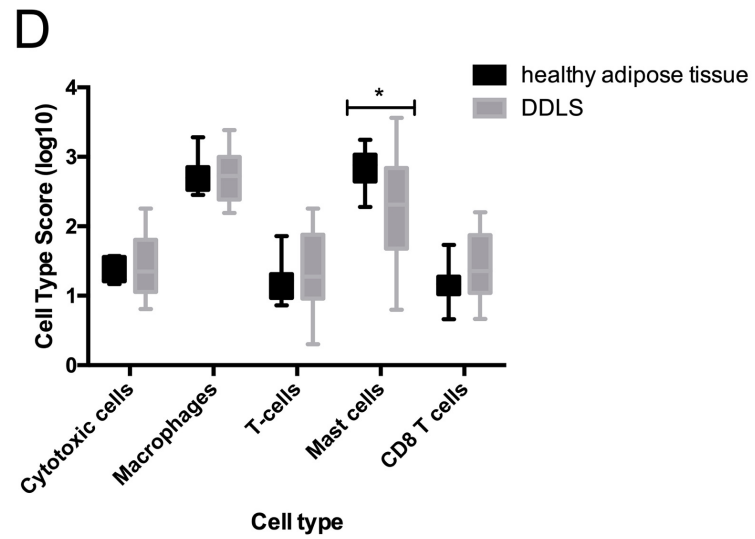
D
healthy adipose tissue
DDLS
Cell Type Score (log10)
4
3
2
1
0
*
Cytotoxic cells
Macrophages
T-cells
Mast cells
CD8 T cells
Cell type

Figure 3.2 Active molecular pathways and cell types within DDLS reveal tumor heterogeneity. **(A)** Overview of pathway scores in DDLS compared to healthy adipose tissue. Significance calculated using 2way ANOVA Sidak's multiple comparisons test. *= p-value<0.05, ** = p-value <0.01 **(B)** Log2 fold change in expression of individual genes within the adhesion pathway. Significance calculated using the Benjamini-Yekutieli procedure. *= p-value<0.05, ** = p-value <0.01, *** = p-value<0.001, ****= p-value < 0.0001 **(C)** log2 mRNA counts of ALCAM in healthy adipose tissue, primary tumors of patients with metastasis, and those without metastasis. Significance calculated using One way Anova, *= p-value <0.05, ** = p-value <0.01 **(D)** Cell type scores of different immune cells detected in DDLS.

3.2.4 Immune profiling reveals DDLS tumors have two distinct immune phenotypes

The observed heterogeneity in pathway scores and the abundance of various immune cell types in DDLS compared to healthy adipose controls prompted us to question whether DDLS tumors can be further subdivided into groups based on expression of inflammatory genes. To evaluate the immunological characteristics of DDLS tumors, we classified them using the 18-gene Tumor Inflammation Signature (TIS) that measures pre-existing but suppressed adaptive immune responses within tumors. [222] The TIS contains genes related to antigen presentation, chemokine expression, cytotoxic activity, and adaptive immune resistance. Hierarchical clustering based on expression levels of TIS genes revealed two distinct groups, consisting of 15 inflamed tumors and 14 non-inflamed tumors, demonstrating a dichotomy within the DDLS sarcoma subtype (Figure 3.3A, Supplemental Table 1). To validate the categorization of these tumors into the two distinct phenotypes, we conducted expression analysis of the immune cell marker CD45 between the newly classified groups. We found significant upregulation of CD45 expression in the inflamed group compared to non-inflamed group, confirming the accurate classification of tumors into the inflamed and non-inflamed phenotypes (Supplemental Figure 12A). In line with these findings, within the inflamed phenotype, the *CXCL13* marker of tertiary lymphoid structures was the most differentially expressed gene compared to healthy adipose tissue, showing a 6.74 $\log_2$ fold-increase in expression ($p<0.0001$). (Supplemental Table 4, statistics not shown).

The above analysis confirms that DDLS tumors can be classified into at least two distinct immune-inflammatory phenotypes, therefore further immune analysis and differential expression analysis was performed on each DDLS phenotype separately. First, we evaluated immune cell types present within inflamed and non-inflamed DDLS tumors. Cell types were classified based on the expression levels of predefined genes previously shown to be characteristic of a cell population. In inflamed tumors, cell types that were detected at statistically significant levels (p-value <0.05) include cytotoxic cells (*GZMB, PRF1, GZMH, KLRB1, GZMA, CTSW*), macrophages (*CD84, CD163, CD68*),

T cells (*SH2D1A, CD3D, CD3E*), mast cells (*TPSAB1, MS4A2*), neutrophils (*CSF3R, S100A12*) and CD8 T cells (*CD8A, CD8B*) (Supplemental Figure 12B). Notably, exhausted CD8 T cells (T cells characterized by *LAG3* expression) were not detected in inflamed tumors (Supplemental Figure 12B). Cytotoxic cells, macrophages, T cells and CD8 T cell scores were higher in inflamed tumors compared to healthy adipose controls, however, did not reach statistical significance. In non-inflamed tumors, only dendritic cells were detected (Supplemental Figure 12C).

Differential expression analysis of inflamed and non-inflamed tumors compared to healthy adipose tissue revealed shared genes in both upregulated and downregulated immune-inflamed profiles, as shown in Figure 3C and 3D. Five significantly upregulated genes are shared between both immune phenotypes; *FN1, CDK1, BIRC5, TTK* and *PBK* (Figure 3.3C). In contrast, twenty downregulated genes were shared between the two immune sub-types of DDLS, and are involved in adhesion and loss of adipocyte function (Figure 3.3D).

Altogether, this data shows that DDLS can have two distinct immune phenotypes that demonstrate different levels of immune cell infiltration and expression of immune related genes.

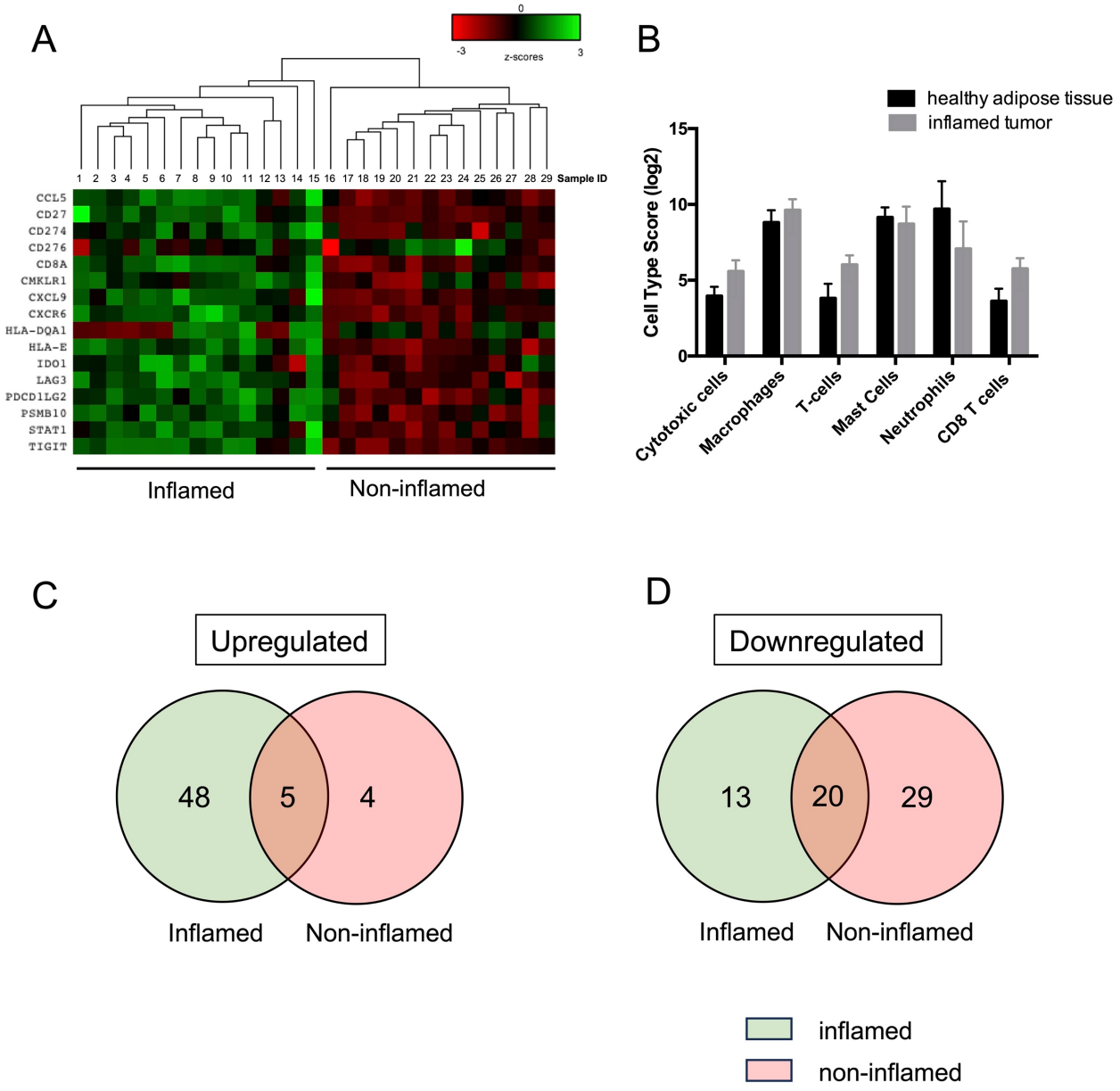
A
0
-3
z-scores
3
1 2 3 4 5 6 7 8 9 10 11 12 13 14 15 16 17 18 19 20 21 22 23 24 25 26 27 28 29 Sample ID
CCL5
CD27
CD274
CD276
CD8A
CMKLR1
CXCL9
CXCR6
HLA-DQA1
HLA-E
IDO1
LAG3
PDCD1LG2
PSMB10
STAT1
TIGIT
Inflamed
Non-inflamed
B
healthy adipose tissue
inflamed tumor
Cell Type Score (log2)
15
10
5
0
Cytotoxic cells
Macrophages
T-cells
Mast Cells
Neutrophils
CD8 T cells
C
Upregulated
48
5
4
Inflamed
Non-inflamed
D
Downregulated
13
20
29
Inflamed
Non-inflamed
inflamed
non-inflamed

Figure 3.3 Immune profiling of DDLS reveals two distinct tumor immune microenvironments **(A)** Heatmap of mRNA normalized counts of tumor immune-related genes in DDLS tumors. Data was z-score transformed, scaled to give all gene equal variance, and heat-map generated by hierarchical clustering using Euclidean distance and average linkage method. Clustering reveals two inflammation signatures, separating samples into 15 inflamed and 14 non-inflamed tumors. **(B)** Cell type scores of immune cells detected in inflamed DDLS tumor. No statistically significant differences were identified. Venn diagrams showing overlap of significantly differentially expressed genes **(C)** upregulated and **(D)** downregulated by inflamed and non-inflamed tumors. Significance calculated using the Benjamini-Yekutieli procedure, a p-value <0.005 threshold was set for significant differences in gene expression.

3.2.5 Cancer testis antigens are transcriptionally expressed in DDLS

The development of targeted immunotherapy for DDLS relies on the identification and characterization of targetable tumor antigens. The 770 gene Nanostring Immune Profiling Panel includes probes to detect mRNA gene expression of 30 CTAs. We next took advantage of this feature to detect CTA expression in DDLS samples. Out of 30 CTAs included, 23 were detectably expressed at the mRNA level in DDLS (Figure 4A). From the results in Figure 4A, it emerges that the three most frequently observed antigens are TTK protein kinase (TTK), Lymphokine-activated killer T-cell-originated protein kinase (PBK) and Sperm Autoantigenic Protein 17 (SPA17), detected in over 80% of DDLS tumors. Looking further at average mRNA expression levels for these antigens reveals that *TTK, PBK* and *SPA17* are also the most highly expressed in DDLS compared to other CTAs (Supplemental Figure 13A). These antigens were therefore selected for further analysis and validation. We next compared the mRNA expression of these antigens in DDLS relative to healthy adipose tissue (Figure 3.4B). The antigens *PBK* and *TTK* showed a significant increase in mRNA expression compared to healthy adipose tissue controls (Figure 3.4B). Interestingly, we found that *TTK* and *PBK* were often co-expressed and observed a weak (r^2=0.4547) but highly statistically significant (p-value < 0.0001) correlation between their expression levels (Supplemental Figure 13B). While *SPA17* was expressed at the highest levels in DDLS, it was also expressed at high levels in healthy adipose controls.

We further sought to delineate *TTK* and *PBK* expression in DDLS tumors of different immunological profiles, across inflamed and non-inflamed classifications as outlined in Figure 3A. Both inflamed and non-inflamed tumors showed significant increases in expression of *TTK* and *PBK* compared to healthy adipose tissue controls (Figure 3.4C). Consistent with Figure 4B, *SPA17* expression was not significantly different compared to healthy adipose controls in both inflamed and non-inflamed tumors (Figure 3.4C).

Overall, analysis of mRNA expression of 30 CTAs revealed three candidate antigens, *TTK*, *PBK* and *SPA17* that are expressed in the majority of inflamed and non-inflamed DDLS tumors,

however, only TTK and PBK demonstrate increased expression compared to healthy adipose tissue controls, an important consideration when selecting an immunotherapeutic target for DDLS treatment.

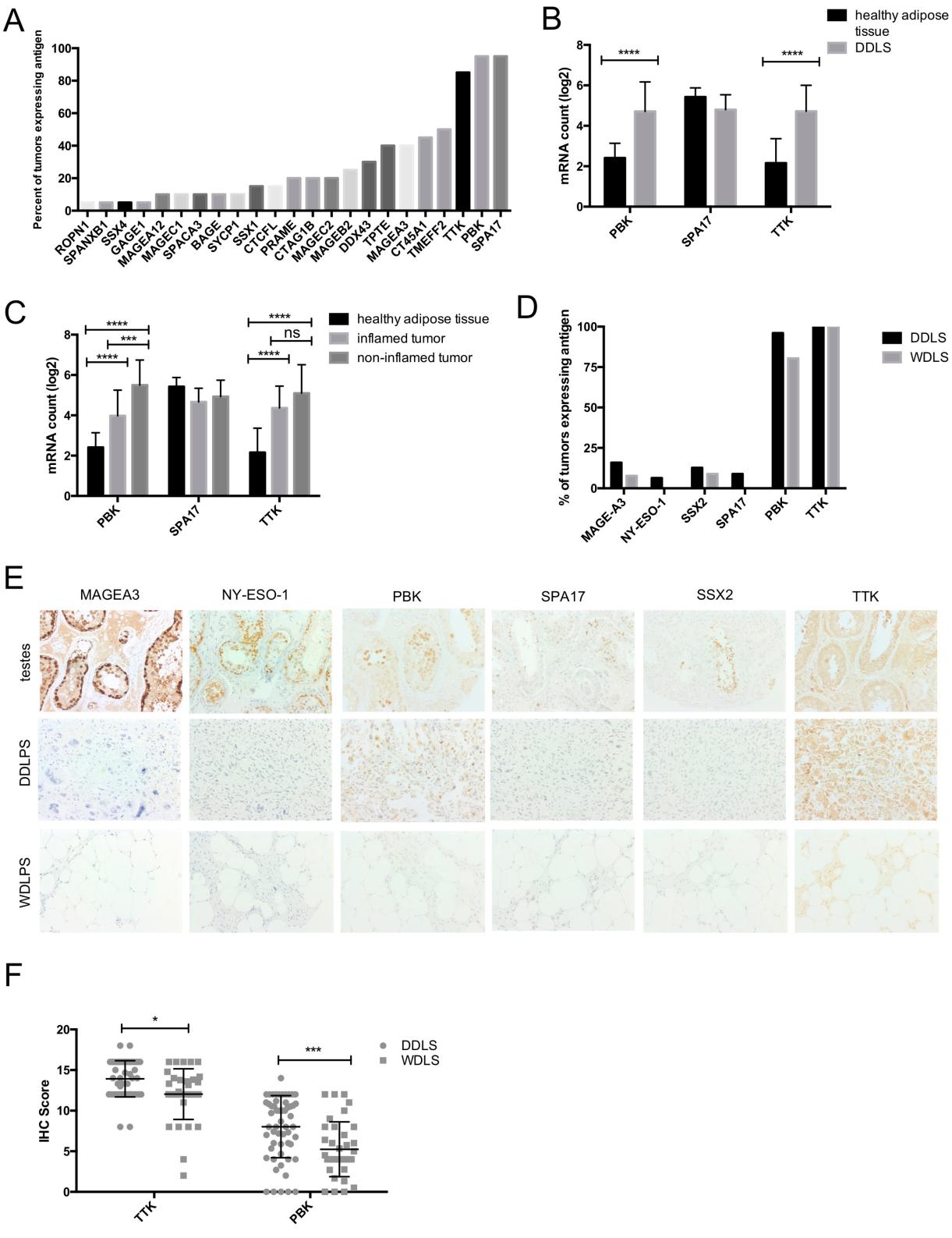
A
Percent of tumors expressing antigen
ROPN1
SPANXB1
SSX4
GAGE1
MAGEA12
MAGEC1
SPACA3
BAGE
SYCP1
SSX1
CTCFL
PRAME
CTAG1B
MAGEC2
MAGEB2
DDX43
TPTE
MAGEA3
CT45A1
TMEFF2
TTK
PBK
SPA17
B
healthy adipose tissue
DDLS
mRNA count (log2)
****
****
PBK
SPA17
TTK
C
healthy adipose tissue
inflamed tumor
non-inflamed tumor
mRNA count (log2)
****
***
****
****
ns
****
PBK
SPA17
TTK
D
DDLS
WDLS
% of tumors expressing antigen
MAGE-A3
NY-ESO-1
SSX2
SPA17
PBK
TTK
E
MAGEA3
NY-ESO-1
PBK
SPA17
SSX2
TTK
testes
DDLPS
WDLPS
F
IHC Score
*
***
DDLS
WDLS
TTK
PBK

Figure 3.4 Analysis of mRNA and protein expression of cancer-testis antigens in liposarcoma allows for identification of targetable antigens (A) Percentage of tumors expressing CTA mRNA **(B)** mRNA expression of antigens in healthy adipose tissue and DDLS **(C)** mRNA expression patterns of TTK, PBK and SPA17 in healthy adipose tissue, inflamed and non-inflamed tumors. **(D)** Percent of tumor specimens expressing CTAs determined by IHC. **(E)** representative staining of human testis (positive control), DDLS and WDLS for CTAs MAGE-A3, NY-ESO-1, PBK and SSX2. **(F)** IHC scores of PBK and TTK expression, IHC score is determined by staining intensity and percentage of positive cells. Significance calculated using 2way ANOVA Sidak's multiple comparisons test. **** = p-value < 0.0001, *** = p-value <0.001

3.2.6 Cancer testis antigens proteins are expressed in DDLS and WDLS

T-cell based immunotherapies targeting antigens exert their anti-tumor function following antigen specific T-cell engagement with MHC-antigen complexes presented at the surface of tumor cells. Antigens must be expressed at the protein level to be loaded onto MHC molecules, therefore, analysis of protein expression of potential target antigens in tumors is critical. Furthermore, 10% of DDLS cases arise from WDLS, and often present as a biphasic neoplasm containing WDLS components[187], therefore, it is important to confirm antigen expression in both WDLS and DDLS when developing an antigen-based immunotherapy for this sarcoma subtype. We performed immunohistochemistry (IHC) on DDLS and WDLS to confirm protein expression of TTK, PBK and SPA17, as well as other well-known immunogenic cancer testis antigens such as NY-ESO-1(included in Nanostring panel as *CTAG1B*), SSX2 and MAGE-A3 that are currently being evaluated as targets in several cancer immunotherapies (ClinicalTrials.gov: NCT04908111, NCT03462316, NCT03093350).

IHC staining was observed with varying frequency for all antigens in both WDLS and DDLS (Figure 3.4D,E). However, TTK and PBK were by far the most frequently expressed (Figure 3.4D). TTK was expressed in 100% of DDLS (52/52) and WDLS (36/36) samples. PBK was found to be expressed in 96% (52/54) of DDLS samples and 80.4% (33/41) of WDLS samples (Figure 3.4D). The next most expressed antigen was MAGEA3 which was observed in 15.87% (10/63) of DDLS and 7.67% (3/45); followed by SSX2 in 12.7% (8/63) of DDLS and 8.88% (4/45) of WDLS; then NY-ESO-1 in 6.35% (4/62) of DDLS and not detected in WDLS. Finally, SPA17 was detected at the protein level only in 5.5% (3/54) of DDLS, in sharp contrast with transcriptional data (Figure 3.4A) and was not detected in WDLS. Looking further at overall IHC scoring intensity for the two most frequently observed antigens, DDLS tumors showed significantly higher expression of both TTK and PBK compared to WDLS (Figure 3.4F). Further to this, testes, healthy adipose tissue, bone marrow, colon, dermis, fibrous tissue, kidney, lymph node, skeletal muscle, small bowel and smooth muscle were

stained for PBK and TKK to assess protein expression in normal tissues. Expression of PBK was only observed in male testes and colon (Figure 3.4E, Supplemental Figure 14A), whereas TTK was expressed in all normal tissues tested (Supplemental Figure 14A, B).

3.3 Discussion

DDLS is a rare sarcoma subtype with poor prognosis and limited novel therapeutics in clinical development. Cancer immunotherapy has emerged as an alternative to conventional treatment options and employs different platforms to stimulate the immune system to reject tumors. A strong understanding of the immune mechanisms at play within the tumor as well as the characterization of targets are essential for the design for successful immunotherapy. However, current knowledge of targetable antigens and immune profiling in DDLS is very limited. Gene expression analysis studies of DDLS have focused on the differences between liposarcoma subtypes, and genomic complexity between DDLS and control fat, but have not focused on immune mechanisms. [223,224] Immunological studies to date have contained small sample sizes and characterize a limited number of immune targets, including CD8+ T cells, CD4+ T cells, B cells and expression of immune inhibitory molecules.[225,226] Finally, no consistent and reliable tumor antigen has been identified in DDLS, existing studies have determined low to absent expression of the CTAs PRAME, NY-ESO-1, and MAGE-A4 in DDLS. [227–230]

The goal of this study was to investigate the expression of immune related genes as well as to identify CTAs unique to DDLS that would direct future studies on effective immunotherapeutic treatment for this sarcoma subtype. In this study, analysis of expression patterns characteristic of DDLS tumors was performed leveraging the nCounter Nanostring platform. We assessed differentially expressed genes between DDLS tumors and healthy adipose tissue, identified distinct inflamed and non-inflamed profiles for DDLS, and identified a potentially promising antigen to drive future development of target immunotherapies for DDLS.

Differential expression analysis of DDLS compared to healthy adipose controls revealed several downregulated genes that have previously been identified to be implicated in adipocyte function or with immune cells present within adipose tissue. The observed significant downregulation of cytokines *CCL14*, *CXCL2* and *CCL2* is likely due to comparing expression profiles of DDLS tumors to

subcutaneous healthy adipose controls, where chemokine expression by adipocytes has been observed and linked to obesity-inflammation. [231,232] Other downregulated genes include *SAA1*, an obesity-related gene; *PPARG*, a master regulator of adipogenesis and lipid storage, and finally, *DUSP6* that plays a role in adipocyte differentiation. [233–235] Together, these gene expression patterns point to a loss of adipocyte function upon adipocyte dedifferentiation and the development of DDLS.

Within the context of the adhesion pathways, the dysregulation of certain adhesion molecules, including the downregulation of *MCAM*, *ITGA1*, *IMCAM2* and *ITGB4*, and the upregulation of *FN1, COL3A*1 and *ALCAM* may play pivotal roles in promoting DDLS tumor cell dissemination and facilitating the establishment of metastatic disease.[236] The significant upregulation of fibronectin and collagen should not be overlooked, as they serve as critical scaffolds for tumor invasion and metastasis.[237–239] Moreover, collagen contributes to formation of a physical barrier within the ECM which can impede T-cell infiltration - an association that has been shown in several studies.[240,241] In our study, we observed significantly increased expression of ALCAM in tumors from patients with metastasis present compared to those without metastasis. This finding implies that elevated expression of ALCAM potentially plays a role in driving the process of metastasis in DDLS. However, the role of ALCAM in sarcoma remains relatively unexplored, and our results contrast with those of Yang *et al*. [242]This study showed a significant correlation between high ALCAM expression and the absence of metastasis in Ewing's sarcoma patients. Such discrepancies raise questions about the selective context-dependent functions of ALCAM in various tumor types. Indeed, *in vitro* studies have shown that the knock-down of ALCAM reduces cell motility, indicating its involvement in metastasis.[243–245] Nevertheless, it is crucial to recognize the interactions between ALCAM and its various ligands in the tumor microenvironment that influence the overall contribution of ALCAM to the metastatic process and may vary between different tumor types.

Other members that play a role in cell-cell adhesion include integrins. While some differential expression of integrins was observed and may be the result of comparing DDLS to adipose tissue

known to express integrins, the overall expression patterns of integrins suggest their relevance in DDLS.[246–249] Specifically, the integrin heterodimer A1B1 has been associated with vascularization [250,251] aligning with findings from a study by Petitprez *et al.* that demonstrated a highly vascularized phenotype of approximately 20% of DDLS, predominantly marked by the expression of endothelial-cell-related genes.[26] Furthermore, we observed a correlation of expression of integrin subunits AL/B2, AM/B2, AX/B2, which are expressed on leukocytes, and suggest the presence of tumor immune cell infiltration.[252] Despite these potential associations, integrin biology in mesenchymal tumors is largely unexplored. One study explored ITGA6 protein expression in well-differentiated liposarcoma and normal fat tissue and found 90% of ITGA6 subunit expression in WDLS. In our study, *ITGA6* subunit was expressed in 100% of samples at an mRNA level. More studies are needed to determine if integrins are significant drivers of tumor progression in DDLS.

Several studies have shown that the response of various sarcoma subtypes to immunotherapy is not in direct correlation with tumor histology, but rather with the complex immune mechanisms at play within tumors, therefore an understanding of the immune cells and mechanisms of immune suppression that are active within DDLS tumors can help rationalize the design of immunotherapy regimens.[26,222,253,254] Immune cell profiling of DDLS tumors compared to fat revealed large tumor heterogeneity in the type of infiltrating leukocytes, as previously described.[255,224] Clustering of DDLS samples based on expression levels of selected tumor inflammation signature genes revealed two distinct immune phenotypes that were termed inflamed and non-inflamed. Inflamed tumors represent approximately 50% of our DDLS samples, and demonstrate increased levels of cytotoxic cells, macrophages, T-cells, mast cells, neutrophils and CD8 T cells. Importantly, T-cells present within the TME suggest that DDLS may be permissive to T cell infiltration upon generation of a large pool tumor-specific T cells after administration of an immunotherapy. One consideration when assessing tumor infiltration lymphocytes is pre-operative treatment, however, few patients in this current study received

neoadjuvant therapy, and no associations between inflammatory status and preoperative chemotherapy or radiation could be made.

One significantly upregulated gene observed in inflamed DDLS particularly was IDO1, which is induced by pro-inflammatory cytokines and controls immune response by conversion of local tryptophan to the immunosuppressive metabolite kynurenine.[256] Given the biological importance of IDO1 in cancer immune escape, several IDO1 inhibitors have advanced into clinical trials as monotherapies or in combination with conventional therapies for cancer treatment, and are summarized by Tang *et al*.[257] A Phase II study of an IDO1 inhibitor (epacadostat) in combination with pembrolizumab for treatment of advanced metastatic sarcoma is currently recruiting (NCT03414229). Similarly, our study provides rationale for targeting IDO1 in inflamed DDLS subtypes.

In this study, we focused on characterizing CTAs, a class of antigens that are considered to be promising immunotherapeutic targets due to their restricted expression to germline cells, overexpression in cancer, and their immunogenic nature. CTAs that have emerged as target candidates include MAGE-A3, NY-ESO-1 and SSX2, with several clinical trials evaluating immunotherapies targeting these antigens underway or completed (NCT02111850, NCT02285816, NCT01343043, NCT03192462).[258–260] However, our findings indicate that these common antigens (MAGE-A3, NY-ESO-1 and SSX2) are not frequently expressed in DDLS, making them suboptimal candidate antigens for immunotherapy of DDLS. The CTAs PBK and TTK were identified to be uniformly expressed in DDLS by IHC, and also significantly overexpressed compared to healthy adipose tissue by Nanostring. Additionally, we identified positively correlated patterns of PBK and TTK expression, suggesting targeting both antigens. Importantly, the success of an antigen as an immunotherapeutic target relies on its upregulation in cancer as compared to normal tissue. Evaluation of TTK and PBK expression by IHC staining revealed extensive expression in healthy tissues such as colon, bone marrow, lymph node, skeletal muscle and small bowel, while PBK was only found to be expressed in male testes (Supplemental Figure 11B). The high expression of PBK observed in human testes tissues is negligible

when considering a PBK targeted immunotherapy as germ-line cells do not express HLA complexes, and therefore PBK specific T cells would not be able to form a TCR-HLA complexes and exert their cytotoxic activity.[261] The expression of TTK in healthy tissues may lead to negative side effects upon administration of an TTK targeting immunotherapy, thereby making PBK a potentially safer target in our study.

In addition to limited expression in normal tissue, PBK was found to be expressed in approximately 80% of WDLS samples. This is beneficial in the context of a PBK targeted therapy as DDLS is defined as a malignant neoplasm that transitions from WDLS, where both components are often present. PBK expression based on subject variables, such as tumor location or tumor type (primary, recurrence, or metastatic disease) could not be effectively assessed as the majority of samples included were primary disease. Overall, due to its potential contributor as an oncogenic driver, and its comparatively low expression in normal tissues, we propose PBK as a novel target antigen to develop vaccination-based immunotherapy for DDLS. To the best of our knowledge, immunotherapies targeting PBK have not yet reached the clinic. The presence of PBK specific CD8+ T cells in DDLS patient PBMCs or TILS can determine if PBK is a potent antigenic target for immunotherapy and is a subject of further investigations.

In conclusion, this study revealed the existence of two distinct inflammatory phenotypes within DDLS tumors. Novel approaches that induce a broad and strong immune response against non-inflamed tumors will facilitate the development of efficient immunotherapies for DDLS. Furthermore, we identified PBK as a novel specific immunogenic target antigen in DDLS both in inflamed and non-inflamed tumors.

3.4 Materials and Methods

3.4.1 Quality assessment of FFPE tissue specimens and RNA isolation

All tumor samples were obtained by surgical resection. Hematoxylin/eosin (HE) stained FFPE tumor sections were evaluated by a pathologist and selected based on quantity of DDLS and quality of tissue within section. FFPE blocks were cut at 10 uM onto positively charged slides in RNA-free environment. Total RNA was extracted from 2-5 slides per case of DDLS, and 20 slides per case of normal fat using RecoverAll™ Total Nucleic Acid Isolation Kit for FFPE (ThermoFisher Scientific, AM1975) following manufacturer's protocol. RNA was quantified by Qubit Assay and purity was determined by Nanodrop spectrophotometer. DDLS and normal fat RNA was diluted in RNA-free Ribo-free water at a concentration of 60 ng/ul and 20 ng/ul, respectively. Gene expression analysis was conducted by Nanostring nCounter platform using the PanCancer Immune Profiling Panel consists of 770 genes related to 14 different immune cell types, common checkpoint inhibitors, CT antigens, and genes covering both the adaptive and innate immune response. 300 ng of DDLS RNA or 100 ng of normal fat RNA in 5 uL was mixed with capture and reporter probes and hybridized for 18 hours at 65C. Samples were scanned on a nCounter Digital Analyzer. 29 DDLS, 10 healthy normal adipose tissue controls were run on the nCounter Nanostring platform and passed quality control analysis performed by Nanostring Advanced analysis platform.

3.4.2 Nanostring Analysis

Normalization, differential gene expression analysis, and pathway analysis was performed using nSolver Advanced Analysis Software 2.0 (NanoString Technologies).

Differential expression analysis: For analysis of differentially expressed genes, a threshold Benajmin-Yekutieli adjusted p-value of <0.005 was selected and differentially expressed genes that fell within this threshold were further analyzed. Differentially expressed genes were grouped into immune response categories determined by nSolver Advanced Analysis Software 2.0.

Pathway analysis: To identify active pathways within DDLS, each sample's gene expression profile can be condensed into a set of pathway scores. Pathway scores are determined by nSolver Advanced Analysis Software 2.0 and are fit using the principal component of each gene set's data and are oriented such that increasing scores correspond to increasing expression of genes included within the pathway. Statistical analysis was performed by GraphPad Prism 6.0. Statistical significance between pathway scores of DDLS and healthy adipose controls and of expression of each individual gene within selected pathways was calculated by 2-way ANOVA tests using Sidaks multiple comparisons. Significance is based on a p-value <0.05

Cell type score: Immune cell profiling was performed using the genes sets on nSolver 4.0. Cell type scores are determined by Advanced Analysis Software 2.0 using expression data of genes previously shown to be characteristic of a cell population. Statistical significance of cell type scores between DDLs and healthy adipose controls was calculated by 2-way ANOVA tests using Sidaks multiple comparisons using GraphPad Prism 6.0. Significance is based on a p-value <0.05.

Immune phenotyping of DDLS: Classification of DDLS tumor into inflamed or non-inflamed phenotypes was performed based on expression of selected tumor inflammation signature (TIS) genes (CCL5, CD27, CD274, CD8A, CMKLR1, CXCL9, CXCR6, HLA-DQA1, HLA-E, IDO1, LAG3, PDCDILG2, PSMB10, STAT1, TIGIT) previously defined by Ayers et al.[262] Hierarchical clustering of samples based on expression of TIS genes was performed to classify tumors and inflamed and non-inflamed.[27] Normalized mRNA counts were z-score transformed, scaled to give all genes equal variance. A heat-map was generated by hierarchical clustering using Euclidean distance and average linkage methods by nSolver 4.0.

Antigen expression: Antigen expression in DDLS was based on the detection of probes specific to each antigen and are considered to be positive when these counts are more than double the median counts of negative controls probes, as determined by Advanced Analysis Software 2.0.

3.4.3 TMA Production

HE stained FFPE tumor sections were evaluated by a pathologist for adequate representation of DDLS, WDLS or normal tissue within sample, tissue quality, and level of necrosis, and appropriate tumor areas for TMA construction were identified. The tissue microarrays were created using 63 DDLS samples, 54 WDLS samples with healthy matched patient tissue, selected tissue areas from FFPE blocks were punched manually using by Veridian Tissue Arrayer using a 1mm punch needle and manually deployed into recipient paraffin wax blocks. Between 1-6 FFPE blocks were provided per each tumor, two cores were randomly selected from each FFPE block to ensure adequate representation of the whole tumor in TMA. For controls, matched normal tissue, in addition to kidney, spleen, testis and colon were included in recipient blocks. TMAs were sectioned (4um) at the Louise Pelletier Histology Core, University of Ottawa (RRID:SCR_021737).

3.4.4 Immunohistochemistry

Immunohistochemical staining for CTA was performed on TMAs using MAGE-A3 (1:500, Santa Cruz Biotechnology, Dallas, TX), SSX2 (1:200, Origene, Rockville, MD), and NY- ESO-1(1:200, Santa Cruz Biotechnology, Dallas, TX), PBK (1:2000, Thermo Scientific, Walthman, MA) and TTK (1:1000, Thermo Scientific, Walthman, MA), SPA17 (1:200, Thermo Scientific, Walthman, MA). Slides were deparaffinized and rehydrated through graded CitriSolv and alcohol solutions. Antigen retrieval was performed by heat-induced epitope retrieval, in which slides were heated in sodium citrate buffer (pH 6.0) in a microwave for 10 minutes and cooled down to RT for 30 minutes. Slides were quenched in 3% H_2O_2 for 10 minutes to block endogenous peroxidase activity. After rinsing with PBS, slides were incubated for 10 minutes in DAKO protein block serum-free to inhibit non-specific staining during the immunohistochemical detection of antigens. Slides were rinsed in PBS and treated with primary antibodies at 4°C overnight. ImmPRESS® HRP Anti-Mouse IgG (Peroxidase) Polymer Detection Kit is applied to slides and incubated for 30 minutes at room

temperature. Staining was visualized with DAB (5-minute development). Slides were counterstained in Harris Modified hematoxylin and dehydrated through graded ethanol and CitriSolv solutions. Testis tissue was used as a positive control for all cancer testes antigens staining.

3.4.5 IHC scoring and statistical analysis.

Immunohistochemical staining was graded by a pathologist. The staining intensity is graded as 0 (no staining), 1 (weak), 2 (moderate), or 3 (strong). The percentage of positive cells is graded as 0 (negative), 1 (1-25 %), 2 (26–50 %), 3 (51–75 %), or 4 (76-100 %). The final IHC score is calculated by the multiplication of staining intensity and percentage of positive cells. The final IHC score is the mean of values recorded for each individual case. Statistical analysis was performed by GraphPad Prism 6.0. Statistical significance of antigen expression between DDLS and WDLS was calculated by 2-way ANOVA tests using Sidaks multiple comparisons. Significance is based on a p-value <0.05.

Chapter 4 - Developing a heterologous prime-boost immunotherapy targeting endogenous murine sarcoma tumor antigens

4.1 Introduction

Evaluating novel immunotherapies targeting clinically relevant antigens in pre-clinical studies is critical for optimizing therapeutic regimens, identifying potential treatment side effects, and providing valuable insights into the immunological mechanisms generated by immunization. In this regard, the use if appropriate immune-competent mouse models is essential to accurately model the complex interactions between the immune system and cancer cells. Therefore, we aimed to evaluate our prime-boost immunotherapy by targeting an endogenous murine sarcoma antigen. Employing an endogenous target antigen, rather than a model exogenous antigen such as ovalbumin, allows us to study potential mechanisms of peripheral immune tolerance that may inhibit the immune response against self-antigens, and to develop vaccination strategies geared towards overcoming immune tolerance. Several murine tumour-specific antigens have been discovered, such as P1A in murine lymphomas TRP-2, MUC1 and DTC in B16 murine melanoma, gp70 in CT26WT, and have successfully been used as vaccine targets in pre-clinical studies.[263–268] However, the rarity of sarcoma poses a significant challenge to identifying appropriate antigens for pre-clinical studies. Indeed, the use of xenograft models can help evaluate certain types of therapies; but the lack of immune competence in these mouse models makes them less suitable for studying immunotherapies. The research aim described in this chapter is divided into two objectives. First, to validate an antigen to use for pre-clinical sarcoma research; and second, to evaluate a prime-boost immunotherapy targeting an endogenous antigen in pre-clinical models.

In this study we validated two tumor antigens in K7M2 osteosarcoma and WEHI-164 fibrosarcoma models using *in vivo* and *in vitro* assays. The first candidate target antigen is the endogenous AH1 immunodominant H-2L^d restricted peptide, derived from the murine leukemia virus (MuLV) envelope

gp70. Gp70 was first identified by McWilliams *et al.* as a tumor-associated antigen in the BALB/c-derived colon carcinoma CT26; this antigen can elicit robust CTL responses in tumour-bearing mice.[269] Gp70 expression has been further traced by others in additional BALB/c derived cell lines by qPCR, including K7M2 osteosarcoma.[270] Therefore, we hypothesize the gp70 could be used as a target sarcoma antigen in murine studies. The second potential target antigen emerged in our study of human DDLS (Chapter 3), where we discovered that the CTA PBK was highly expressed in human DDLS. Importantly, Kreiter *et al.* showed that PBK is expressed in BALB/c mice, and identified a mutated PBK sequence as a neo-antigen in B16F10 tumors (of C57BL/6 origin)[271] which was subsequently used as a target in a poly-epitope cDNA vaccine designed for B16F10 melanoma.[272] Based on our observations in human DDLS, and previous murine studies performed in B16F10, we hypothesized that PBK could be an effective target antigen in murine sarcoma studies. Therefore, our objective was to validate the immunogenicity of gp70 and PBK in murine sarcoma cell lines for downstream application as immunotherapeutic targets.

As a second objective, we aimed to employ these antigens as targets of our DEC205 prime and OV boost immunotherapy (presented in Chapter 2). Challenges in producing aDEC205 conjugated to tumor antigens prompted us to explore alternative priming approaches. This included assessing the efficacy of reduced DEC205 dosing, exploring alternative DC targeting antibodies including single chain aDEC205 and anti-DCIR, and the viral vector Modified vaccinia Ankara (MVA).

MVA is a highly attenuated and non-replicative vaccinia virus capable of infecting mammalian cells and undergoing DNA replication without generating infective viral particles. Due to its attenuated properties, infection with recombinant MVA generates an immune response predominantly targeted towards the encoded protein as opposed to the MVA vector.[273,274] Due to the polarization of the immune response, antigens encoded by MVA are more likely to induce cytotoxic T cells compared to other unattenuated vaccine strains.

MVAs unique safety profile and ability to induce a robust immune response against encoded antigens have propelled it to clinical testing. MVA has proven to be effective as a vector in heterologous prime-boost vaccination against cancer and infectious diseases, as demonstrated in both in pre-clinical and clinical studies (ClinicalTrials.gov: NCT05617040, NCT04491955, NCT04990479).[275–280] Examples of efficient use of MVA that reached clinical testing include the prophylactic prime-boost vaccine regimen employing Ad26.ZEBOV prime, followed by MVA-BN-filo, for vaccination against Ebola virus disease (ClinicalTrials.gov: NCT02376400).[281] In this phase I trial, various MVA and Ad26 prime/boost vector combinations were assessed, with the Ad26/MVA group demonstrating the highest T cell responses against Ebola virus .[281] In summary, the body of evidence supports MVA's efficacy as a boost vector when administered subsequent to DNA or adenovirus-based vaccines, and is optimal for generating strong and enduring CD8+ T cell responses. [282–285] However, MVA's potential in the context of prime-boost vaccination strategies, particularly in conjunction with oncolytic viruses, remains unexplored. Therefore, we evaluated the immunogenicity of alternative prime-boost vaccination regimens using VSVΔ51 and MVA encoding a target tumor antigen.

Overall, the research described in this chapter aimed to overcome the challenges of pre-clinical models of mouse sarcoma and to establish a novel immunotherapy targeting clinically relevant antigens to treat sarcoma.

4.2 Results

4.2.1 Characterization of the murine sarcomas K7M2 and WEHI-164

Tumor immune profiling offers valuable insights for the selection of appropriate pre-clinical models and for the design of effective immunotherapeutic strategies. Tumor infiltration of immune cells, MHC expression by tumor cells, and the expression of immune inhibitory molecules are all critical factors that impact the success of immunotherapy and should be characterized. For example, a pre-clinical model that displays high MHC expression and robust tumor immune infiltration is an optimal candidate for the evaluation of immunotherapy that relies on the induction and effector activity of immune cells. However, the immunological landscape of murine sarcoma tumors remains poorly characterized. Before the evaluation of the efficacy of our therapy in pre-clinical sarcoma models, we conducted immune profiling of candidate sarcoma tumors.

Our research methodology comprised of flow cytometry and immunohistochemistry (IHC) to conduct immune profiling of WEHI-164 and K7M2 tumors. Flow cytometry is a valuable tool for immune cell profiling and distinguishing various populations of immune cells, and IHC enables visualization of immune cell location and density within the tumor. Tumors were established in BALB/c mice by subcutaneous injection of $1x10^6$ K7M2 or WEHI-164 cells. They were isolated when they reached an average size of 5 mm x 5 mm - the size at which treatment will be initiated in future experiments. Tumours were fixed for IHC, and staining for CD3 revealed the presence of T cells within both K7M2 and WEHI-164 tumors, suggesting tumor infiltration of T cells upon administration of immunotherapy. (Figure 4.1A)

We initially observed highly variable tumor growth rates with K7M2 injected subcutaneously in PBS, leading us to test using Geltrex™ to establish more uniform tumors in future experiments. Geltrex matrix is a basement membrane extract containing laminin, collagen IV, entactin, and heparin sulfate proteoglycans that can support the growth of cells. Subcutaneous implantation of tumor cells

with Geltrex results in better tumor take rates and more uniform tumor growth (Supplemental Figure 15). We immune profiled K7M2, K7M2 with Geltrex (K7M2+Geltrex), and WEHI-164 tumors by flow cytometry. The percentage of CD4+ T cells, Tregs, CD8+ T cells, activated CD8+ T cells, NK cells, macrophages, dendritic cells, and B-cells were evaluated (flow gating strategy shown in Supplemental Figure 16 and 17).

We observed immune cell infiltration in both K7M2 and K7M2+Geltrex tumors, with NK cells comprising approximately 25% of all infiltrating immune cells, followed by about 20% macrophages, 13% CD4 T cells and 9% CD8 T cells. Interestingly, in K7M2 tumors, about 65% of CD8+ T cells showed activation (CD69+CD25+), as opposed to 85% in K7M2+Geltrex tumors. In both models, 50% of CD4+ T cells were categorized as Tregs (CD25+CD127-). Notably, in both models, approximately 80% of activated CD8+ T cells expressed PD1+, suggesting potential benefit from anti-PD1 therapy (Supplemental Figure 16). Furthermore, K7M2+Geltrex showed higher DC infiltration than K7M2 tumors, and no detectable B cell infiltration (Figure 4.1B, C).

Flow cytometry analysis revealed immune cell infiltration in all WEHI-164 tumors. The majority of immune infiltrate comprised of NK cells, accounting for approximately 30% of CD45+ cells within the tumor microenvironment. CD8+ T cells accounted for approximately 10% of immune cells, with approximately 30% of CD8+ T cells showing an activated phenotype (CD25+CD69+). Notably, a significant proportion of activated CD8+ T cells (90%) expressed PD-1 (Supplemental Figure 12). Additionally, CD4+ T cells constituted approximately 15% of immune cells, with regulatory T cells (CD25+CD127-) making up almost 40% of the CD4+ T cell population. Moreover, we identified the presence of dendritic cells, B cells, and macrophages within WEHI-164 tumors. (Figure 4.1D)

Assessing the expression of MHC complexes on tumor cells is crucial for determining their ability to be recognized by T cells. Therefore, we evaluated the expression of H-2L^d and H-2K^d MHC-I haplotypes on K7M2 and WEHI-164 cell lines using flow cytometry. We found that both H-2L^d and

H-2K^d haplotypes are expressed in both tumor types, with H-2K^d being expressed at higher levels than H-2L^d (Figure 4.1E.) Notably, K7M2 exhibited higher overall MHC-I expression compared to WEHI-164. To further investigate the suitability of our preclinical models for OV therapy, we infected tumor cores from K7M2 and WEHI-164 tumors with VSVΔ51-GFP *in vitro*. 24 hours post-infection, we observed GFP expression in VSVΔ51 infected cores, indicating susceptibility to OV infection in both tumor types (Figure 4.1F).

Overall, our findings of immune cell tumor infiltration, MHC-I expression, and susceptibility to OV infection suggest that both K7M2 and WEHI-164 tumors are suitable pre-clinical models for evaluating immunotherapy. Additionally, the use of Geltrex can result in more uniform tumor growth without compromising immune infiltration.

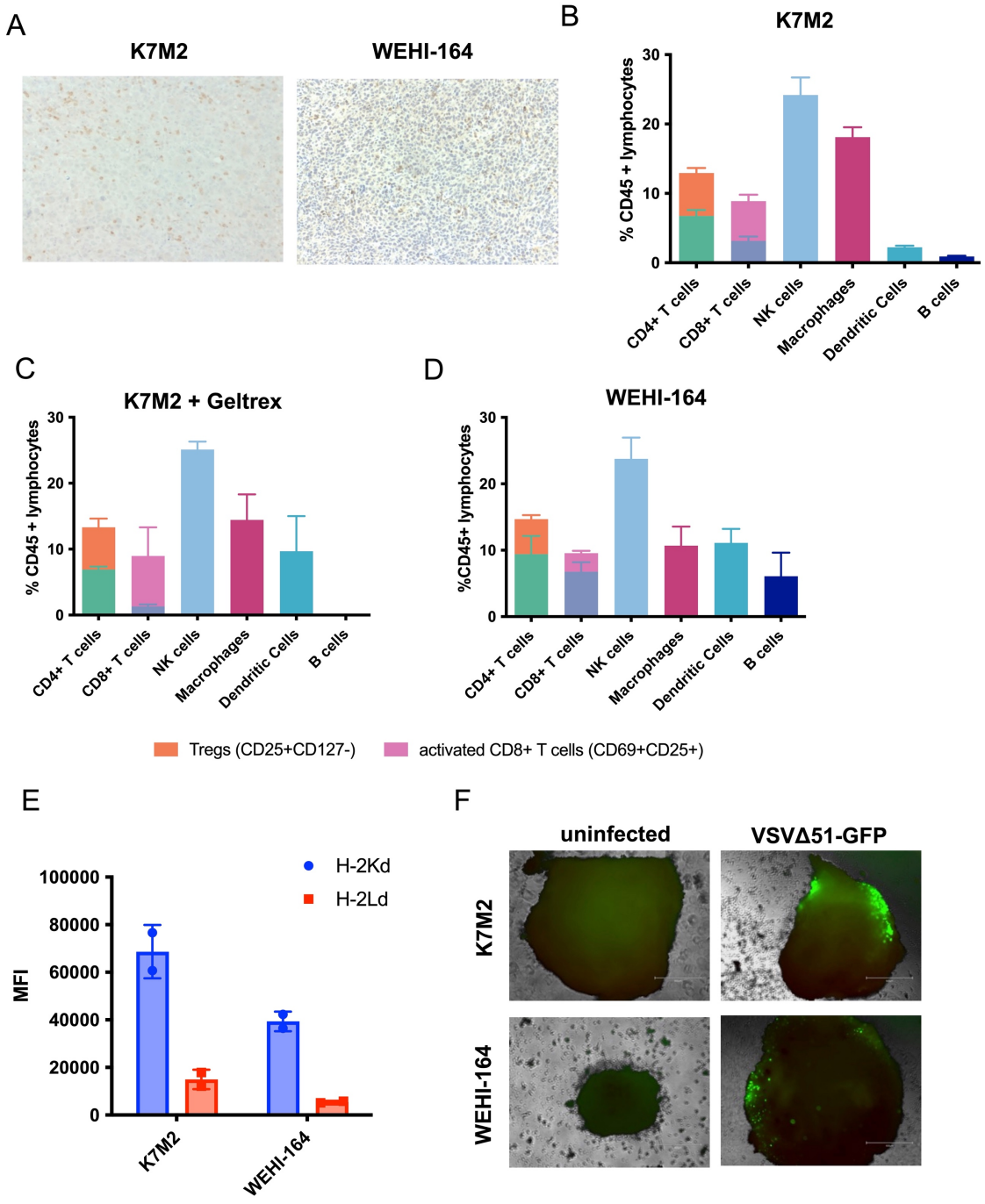
A
K7M2
WEHI-164
B
K7M2
% CD45 + lymphocytes
30
20
10
0
CD4+ T cells
CD8+ T cells
NK cells
Macrophages
Dendritic Cells
B cells
C
K7M2 + Geltrex
% CD45 + lymphocytes
D
WEHI-164
%CD45+ lymphocytes
Tregs (CD25+CD127-)
activated CD8+ T cells (CD69+CD25+)
E
H-2Kd
H-2Ld
MFI
100000
80000
60000
40000
20000
0
K7M2
WEHI-164
F
uninfected
VSVΔ51-GFP
K7M2
WEHI-164

Figure 4.1 Characterization of murine sarcoma tumors. K7M2 and WEHI-164 tumors were established by subcutaneous injection of $1x10^6$ cells, tumors were harvested when they reached 5x5 mm for immune profiling. (A) IHC staining for CD3+ in K7M2 and WEHI-164 tumors. Immune profiling of tumour infiltrating lymphocytes by flow cytometry in **(B)** K7M2, **(C)** K7M2 + Geltrex and **(D)** WEHI-164 tumors. Graphs shows the percentage of each cell type gated from CD45+ lymphocytes. Cell types are determined by expression of immune cell markers; CD4+ (CD45+CD3+CD4+), T regs (CD45+CD3+CD4+, CD25+CD127-), CD8 (CD45+CD3+CD8+), activated CD8+ ((CD45+CD3+CD8+CD69+CD25+), NK cells (CD45+CD3+CD49b+), macrophages (CD45+CD11b+F4/80+), dendritic cells (CD45+CD11c+) and B cells (CD45+CD19+) **(E)** MHC-I expression on K7M2 and WEHI-164. Graph shows mean fluorescent intensity (MFI) of H-$2K^d$ and H-$2L^d$ determined by flow cytometry **(F)** VSVΔ51-GFP infection of K7M2 and WEHI-164 tumor cores. 2x2mm tumor cores were obtained and infected with $1x10^4$ PFU of virus and incubated for 24 hours. Tumor infection was visualized under an EVOS microscope, images show GFP expression 24 hours post-infection.

4.2.2 Validation of AH1 as a potential target antigen in murine sarcoma tumors.

A minimal number of endogenous murine tumor antigens that can be used as efficient targets to test immunotherapies in pre-clinical models have been identified; one potential antigen is the gp70 derived AH1. To validate the suitability of AH1 as a target antigen, we confirmed expression and immunogenicity of this antigen in the murine sarcoma cell lines selected. We investigated anti-AH1 responses following immunization with a K7M2 autologous vaccine, a strategy previously used in our lab to successfully identify anti-AH1 responses in a CT26WT model.[53] Briefly, this vaccination consists of an immunization with irradiated K7M2 injected intraperitoneally (i.p.) as prime, followed 7 days later by an infected cell vaccine (irradiated K7M2 infected with VSVΔ51-GFP) i.p. as a boost (Figure 4.2A).

The antigen-specific immune response following immunization was evaluated by a cytotoxic T lymphocyte assay. Briefly, AH1 (SPSYVYHQF) peptide pulsed target cells were transferred to previously immunized mice, 16 hours after transfer of cells, mice were sacrificed and splenocytes were evaluated by flow cytometry for cytolytic CD8+ T cell activity. The absence of target cell lysis in K7M2 immunized mice suggests that there was no AH1 peptide specific T cell response (Figure 4.2B,C). Contrastingly, the CT26WT immunized positive control demonstrated approximately 50% killing of target cells (Figure 4.2C,D). Overall, we found that this vaccination strategy using K7M2 did not generate an AH1 peptide specific CD8+ T cell response, suggesting that AH1 is not immunogenic in K7M2.

The failure to generate an AH1-specific immune response in K7M2 based immunization led us to explore alternative cell lines for our sarcoma model. Notably, a study by Probst *et al.* demonstrated gp70 expression in the murine fibrosarcoma cell line WEHI-164.[286] Additionally, the presence of AH1 specific CD8+ T cells in WEHI-164 cured mice (treated with F8-TNF and doxorubicin) suggest that AH1 is an immunogenic peptide that contributes to tumor rejection.[286] We confirmed immunogenicity of the AH1 antigen in WEHI-164 by the autologous immunization (ICV) strategy described above.

The *in vivo* CTL assay demonstrated approximately 20% target cell lysis in WEHI-164 ICV groups, and ICS showed a significant increase in IFNγ production upon *in vitro* re-stimulation of CD8+ T cells with the AH1 peptide compared to CT26WT control ($p<0.0001$) (Figure 4.2D,E).

Finally, we obtained Ad5 and MG1 viruses encoding AH1. To determine if a prime-boost vaccination against AH1 can protect against tumor growth, naïve BALB/c mice were prophylactically immunized with an Ad5-AH1 prime and MG1-AH1 boost, and subsequently challenged with subcutaneous injections of K7M2 and WEHI-164 (Figure 4.3A). Prophylactic vaccination against AH1 protected against tumor growth in both sarcoma models. Notably, mice that received WEHI-164 were tumor-free at day 30. K7M2 tumors demonstrated tumor growth, although much slower compared to PBS control (Figure 4.3B,C).

Overall, these findings demonstrate that AH1 represents a potential target for immunotherapy in pre-clinical mouse models of sarcoma. Specifically, immunization against the AH1 epitope conferred protection against tumor growth following subcutaneous challenge with K7M2 and WEHI-164 cell lines. However, i*n vivo* cytotoxic T lymphocyte assays following K7M2 ICV immunization revealed that AH1 was not highly immunogenic within the context of an infected cell vaccine. This could be attributed to the potential presence of other immunodominant epitopes within the K7M2 ICV vaccine the skew the immune response away from AH1.

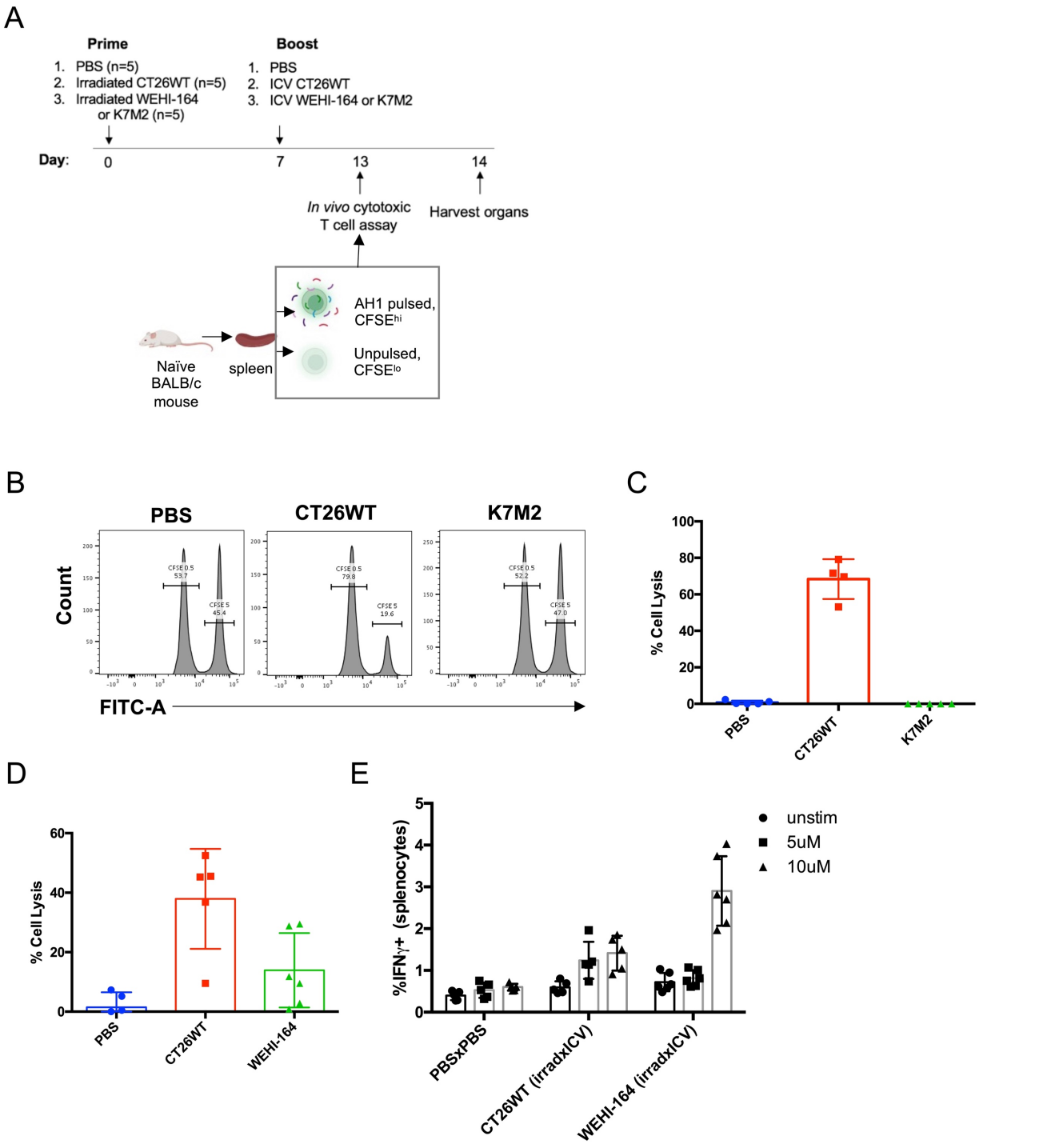
A
Prime
1. PBS (n=5)
2. Irradiated CT26WT (n=5)
3. Irradiated WEHI-164 or K7M2 (n=5)
Boost
1. PBS
2. ICV CT26WT
3. ICV WEHI-164 or K7M2
Day: 0 7 13 14
In vivo cytotoxic T cell assay
Harvest organs
AH1 pulsed, CFSEhi
Unpulsed, CFSElo
Naïve BALB/c mouse
spleen
B
PBS
CT26WT
K7M2
Count
FITC-A
C
% Cell Lysis
PBS
CT26WT
K7M2
D
% Cell Lysis
PBS
CT26WT
WEHI-164
E
%IFNγ+ (splenocytes)
unstim
5uM
10uM
PBSxPBS
CT26WT (irradxICV)
WEHI-164 (irradxICV)

Figure 4.2 *In vivo* cytotoxic T cell assays show that WEHI-164 ICV immunization generates an AH1 specific T-cell response.(A) Schematic representation of immunization schedule. Naïve BALB/c mice were immunized with irradiated tumor cells at day 0 followed by a boost with VSVΔ51-GFP infected irradiated tumor cells at day 7. Six days post-boost, immunized mice were transferred $CFSE^{HI}$ (5uM) cells loaded with AH1 peptide, and $CFSE^{LO}$ (0.5 uM) cells without peptide at 1:1 ratio intravenously. 16 hours after transfer of cells, splenocytes from immunized mice were harvested to quantify proportion of $CFSE^{HI}$ and $CFSE^{LO}$ cells by flow cytometry. **(B)** Representative histograms showing the percentage of $CFSE^{LO}$ and pulsed $CFSE^{HI}$ cells. **(C, D)** Graphs showing the percentage of AH1 pulsed specific cell killing compared to control groups. **(E)** Results of intracellular cytokine staining of immunized mice. Graph shows the percentage of AH1- specific T cells producing IFNγ in the spleen in response to AH1 stimulation in vitro.

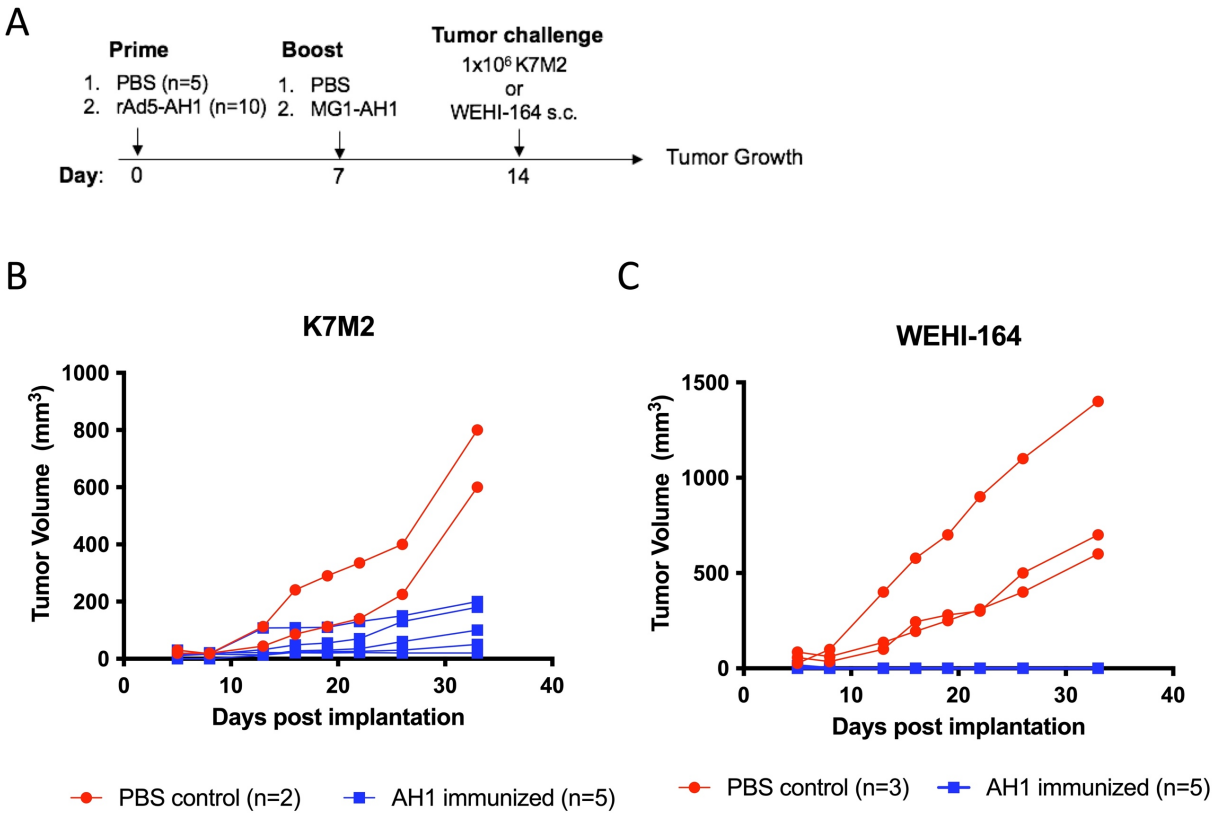
A
Prime
1. PBS (n=5)
2. rAd5-AH1 (n=10)
Boost
1. PBS
2. MG1-AH1
Tumor challenge
1x10^6 K7M2
or
WEHI-164 s.c.
Day: 0
7
14
Tumor Growth
B
K7M2
Tumor Volume (mm3)
Days post implantation
PBS control (n=2)
AH1 immunized (n=5)
C
WEHI-164
Tumor Volume (mm3)
Days post implantation
PBS control (n=3)
AH1 immunized (n=5)

Figure 4.3 AH1 targeted prophylactic prime-boost protects against tumor challenge. (A) Schematic representation of immunization schedule. Mice were immunized with a prime of 10^8 PFU rAd5-AH1 or PBS, and boosted at day 7 with 10^8 PFU MG1-AH1 or PBS. Mice were challenged subcutaneously with $1x10^6$ K7M2 or WEHI-164 cells 7 days post boost. **(B, C)** K7M2 and WEHI-164 tumor volume was measured over time.

4.2.3 Generation of AH1 encoding prime and boost vectors

Immunization against an entire protein elicits broader and more robust anti-tumor immune responses by simultaneously activating CD4+ T cell, CD8+ T cell and B cell responses. Contrastingly, vaccination with a peptide may only include single epitopes to induce either CD8+ or CD4+ T cell responses. Therefore, we aimed to target the full gp70 protein antigen using the aDEC205 prime and VSVΔ51 boost.

To generate anti-DEC205 antibodies conjugated to the target antigen, we replace the ovalbumin sequence in pcDNA-DEC205-OVA (pDEC205) with the full gp70 sequence amplified from K7M2 using NotI and XhoI restriction sites. Insertion of the epitope was confirmed by sequencing. aDEC205 antibodies are produced in-house by transient co-transfection of HEK293T cells with the pDEC205 plasmid carrying the antigen, and pDEC-Kappa (plasmid containing the light chain), followed by isolation of full-length fusion protein from the supernatant by protein G Sepharose bead column purification. The successful isolation of antibodies is confirmed by western blot by probing for IgG. Evaluation of purified antibody under reducing conditions demonstrated the presence of three bands; a 25KDa corresponding to the light kappa chain, one of approximately 53 KDa that corresponds to the heavy chain that is not conjugated with protein, and one at 80 kDa corresponding to heavy chain conjugated with gp70 (Figure 4.4A). Analysis of the gp70 amino acid sequence revealed the presence of a signal peptide at position 33 within N-terminal region, indicating a potential cleavage site. Cleavage at this position resulted in an antibody conjugated to a portion of the N terminal region of the gp70 protein, lacking the immunodominant AH1 peptide.

To avoid this issue, we designed and purchased a codon-optimized pDEC205 encoding the immunodominant epitope of gp70; AH1, containing a HIS-tag to confirm the presence of conjugated protein during downstream antibody production. Following several attempts at antibody production, no antibody was isolated despite the successful production of positive controls. We hypothesized that the antibody was not secreted from transfected cells in culture, and as the AH1 epitope is derived from

a glycoprotein it may be anchored in the lipid bilayer of the cell membrane - preventing antibody secretion. To test if the antibody was being translated but not secreted, 293T cells were transfected with either light chain or heavy chain plasmids and lysed 48 hours later. The cell lysate was probed for IgG by WB. However, the heavy chain of DEC205 conjugated to AH1 was not observed, while a light chain band was detected (Figure 4.4B). We reasoned that the codon-optimized pDEC205-AH1 construct was not translated post-transfection and next focused on cloning AH1 into the original anti-DEC205 heavy chain backbone.

To verify the translation and secretion of the newly cloned anti-DEC205-AH1, cell lysate and supernatant were collected from transfected cells and probed for anti-IgG by Western Blot. aDE205-AH1 was absent in the culture supernatant but present in the cell lysate, suggesting that this antibody is not being secreted (Figure 4.4D).

VSVΔ51-AH1 was cloned by insertion of the epitope between the G and L proteins of the VSVΔ51 using XhoI and NheI restriction sites and produced as previously described.[287] A multi-step growth curve showed that VSVΔ51-AH1 retained viral kinetics of parental VSV-GFP (Figure 4.4E).

While VSVΔ51-AH1 was successfully rescued, overall, DEC205 conjugated to the full gp70 protein or the AH1 epitope could not be produced, forcing us to test additional options which are discussed in Appendix I.

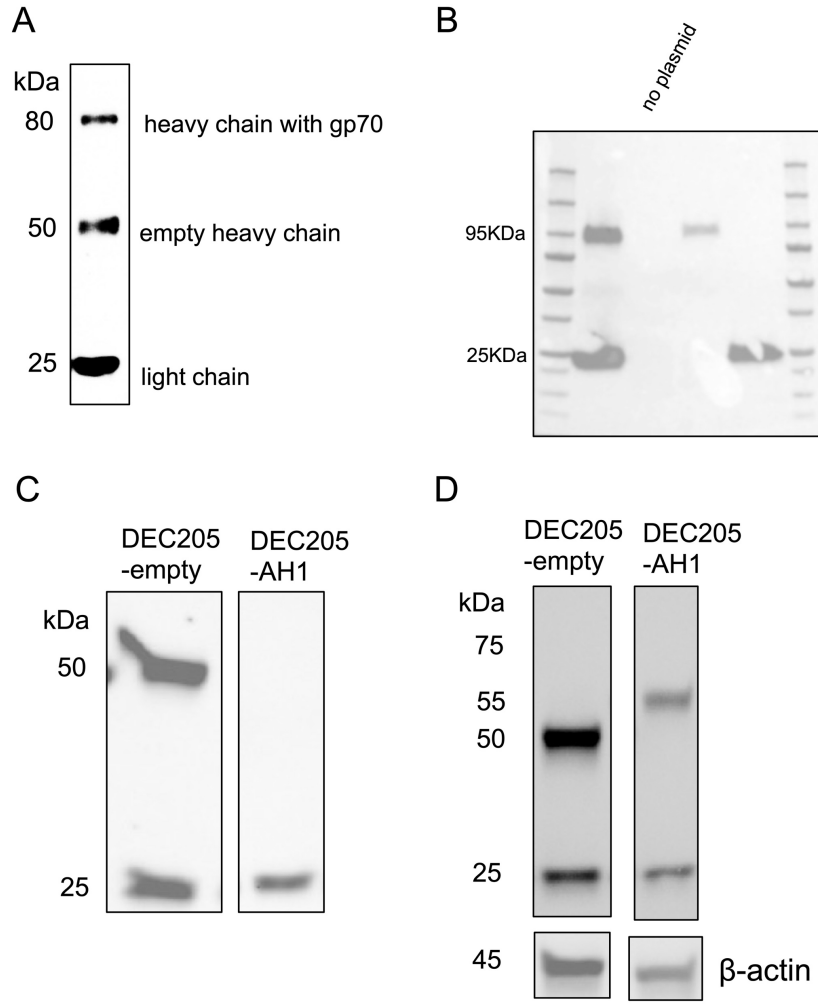
A
kDa
80
heavy chain with gp70
50
empty heavy chain
25
light chain
B
no plasmid
pDEC205-AH1
(heavy)
95KDa
25KDa
C
DEC205
-empty
DEC205
-AH1
kDa
50
25
D
DEC205
-empty
DEC205
-AH1
kDa
75
55
50
25
45
β-actin
E
Virus titer (log10)
10
9
8
7
6
5
4
1
12
16
24
36
48
Time post infection
VSV-GFP
VSV-AH1
ns

Figure 4.4 Production of prime and boost vectors encoding AH1. aDEC205 antibodies were generated by transfection of HEK293T cells in vitro, and subsequent purification of the antibody. The final antibody product was reduced by β-mercaptoethanol and verified by immunoblotting for the heavy and light chains. **(A)** aDEC205-gp70 shows a heavy chain conjugated to gp70 at 80 kDa, an empty heavy chain at 50kDa and light chain at 25kDa **(B)** 293T cells were transfected with several plasmids and lysed to extract protein 3 days later. The cell lysate was reduced by β-mercaptoethanol and verified by immunoblotting for the heavy and light chains. Purified aDEC205-OVA was used as a positive control. Light and heavy chains of antibody are detected in aDEC205-OVA, pDEC205-OVA and pDEC205-kappa lanes, no antibody is detected in pDEC205-AH1 lanes. Antibody was evaluated 48 hours post transfection in **(C)** supernatant and in transfected **(D)** cell lysate. The supernatant of transfected cells shows presence of light chain at 25kDa and DEC205-empty heavy chain at 50 kDa and the absence of heavy chain of DEC205-AH1. Transfected cell lysates show the presence of DEC205-empty, and -AH1 heavy chains at 50 kDa and 55 kDa, respectively, and a light chain at 25 kDa. **(E)** VSV-AH1 retained viral kinetics in multi-step growth curve compared to VSV-GFP. Vero cells were infected with an MOI 0.01, supernatants were collected at several time points post infection (1, 12, 16, 24, 36, 48h) and tittered by plaque assay.

4.2.4 Identification of PBK as a potential target antigen in murine sarcoma tumors

The poor immunogenicity of AH1 in K7M2, coupled with the challenges in the production of DEC205-AH1 antibodies motivated us to explore a new murine sarcoma antigen. After discovering high expression of the CTA PBK in human DDLS, which was also identified as a tumor antigen in B16F10 tumors and used a vaccine target for B16F10 melanoma in mice, we hypothesized that PBK could serve as a promising target antigen in murine studies.[272] We conducted Western blot analysis on four murine sarcoma cell lines, which confirmed PBK protein expression (Figure 4.5A). To further validate this antigen, we performed IHC staining on K7M2 and WEHI-164 tumors which revealed widespread PBK expression in both models (Figure 4.5B).

Having confirmed PBK expression in murine sarcoma, we next cloned and produced the prime and boost vectors. Sequencing of PBK by PCR amplification from WEHI-164 and K7M2 cells confirmed that this antigen did not harbor any mutations compared to the PBK sequence derived from healthy BALB/C tissue (as determined by NCBI), and PBK derived from WEHI-164 and K7M2 were identical. An ideal therapeutic cancer vaccine would contain antigens that are presented by MHC-I and MHC-II for activation of CD8+ T cells and CD4+ T cells, which synergize to promote antitumor immunity. Therefore, a truncated version of PBK sequence (with the nuclear localization signal removed) containing several CD4+ and CD8+ epitopes was isolated by PCR from the K7M2 sarcoma cell line and cloned into prime and boost vectors.

Prior to undertaking large-scale purification of aDEC205-PBK antibody, we wanted to verify its translation and subsequent secretion. We co-transfected HEK293T cells with light chain and heavy chain plasmids for 48 hours and collected cell lysate and supernatant, which were then probed for mouse IgG and PBK by WB. The presence of a band at 75 kDA confirms the proper translation of PBK and successful conjugation to the DEC205 antibody (Figure 4.5E). When probing for IgG, we observed that DEC205-PBK is present in cell lysates but absent in the cell supernatant, indicating that the heavy chain portion of the antibody conjugated to PBK was not being secreted (Figure 4.5C, D). To determine

the cause of this issue, we conducted immunofluorescent staining and imaging to visualize the location of DEC205 antibodies within transfected HEK293T cells (Figure 4.5F). Staining for IgG revealed that DEC205-PBK appears to be forming large protein aggregates within transfected cells, this effect is less pronounced in DEC205-OVA. Overall, this data shows that the fusion protein conjugated to DEC205 can substantially affect the final antibody yield.

Due to difficulties in the cloning and production of anti-DEC205 antibodies conjugated to antigens, we produced an alternative vector for antigen delivery. Given its extensive use as a vaccination platform, we opted to test MVA-PBK as an alternative priming vector in our prime-boost therapy targeting the PBK antigen in murine sarcoma. To this end, MVA-PBK was produced, and transgene expression was confirmed by Western Blot probing for PBK on MVA-PBK infected DF1 cell lysates (Figure 4.5G).

PBK was inserted into the VSVΔ51 backbone between the G and L genes by restriction enzyme cloning and subsequently plaque purified, as previously described.[287] Transgene expression was confirmed by VSVΔ51-PBK infection of Vero cells, and a subsequent Western Blot probing for PBK on cell lysate (Figure 4.5H). A multi-step growth curve showed that VSVΔ51-PBK retained viral kinetics of parental VSVΔ51-GFP, and in fact grew to slightly higher titers as early as 26h. (Figure 4.5I)

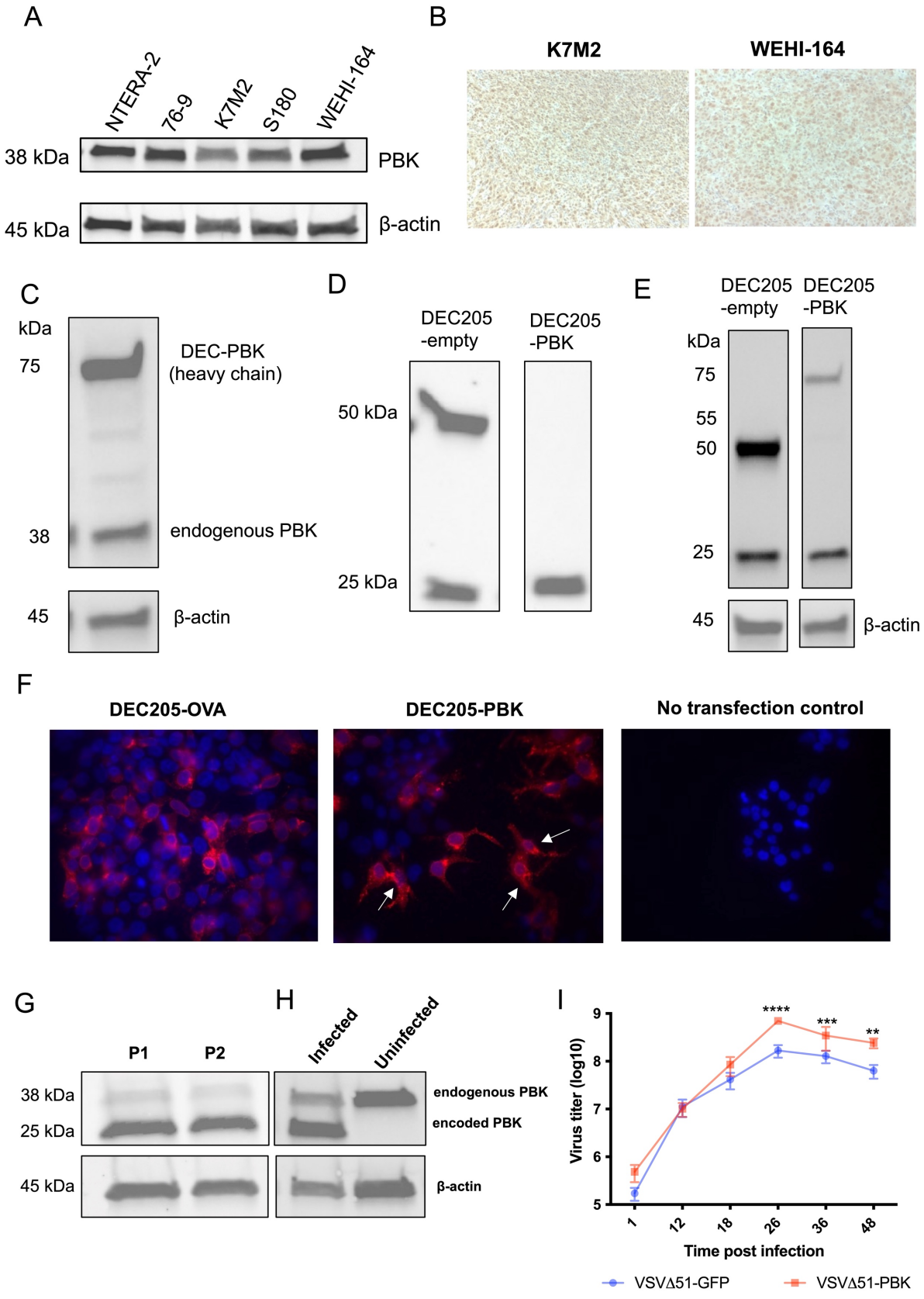
A
NTERA-2
76-9
K7M2
S180
WEHI-164
38 kDa
PBK
45 kDa
β-actin
B
K7M2
WEHI-164
C
kDa
75
DEC-PBK
(heavy chain)
38
endogenous PBK
45
β-actin
D
DEC205
-empty
DEC205
-PBK
50 kDa
25 kDa
E
DEC205
-empty
DEC205
-PBK
kDa
75
55
50
25
45
β-actin
F
DEC205-OVA
DEC205-PBK
No transfection control
G
P1
P2
38 kDa
25 kDa
45 kDa
H
Infected
Uninfected
endogenous PBK
encoded PBK
β-actin
I
Virus titer (log10)
9
8
7
6
5
****
***
**
1
12
18
26
36
48
Time post infection
VSVΔ51-GFP
VSVΔ51-PBK

Figure 4.5 Validation of PBK as a target and generation of PBK encoding prime and boost vectors. (A) Western blot of murine sarcoma cell lines probing for anti-PBK. **(B)** Immunohistochemistry on K7M2 and WEHI-164 tumors probing for anti-PBK. **(C)** The transfected cell lysate was probed with anti-PBK and shows the heavy chain of DEC205 conjugated to PBK at 75 kDa, and the presence of endogenous PBK. The presence of antibodies was evaluated 48 hours post-transfection in **(D)** supernatant and in **(E)** transfected cell lysates by western blot, samples were run in reducing conditions and probed for anti-IgG. β-actin was used as a loading control for cell lysate samples. Supernatant shows the presence of a light chain at 25kDa and DEC205-empty heavy chain at 50 kDa, and the absence of the heavy chain of DEC205-PBK. Transfected cell lysates show presence of DEC205-empty, and –PBK heavy chains at 50 kDa and 75 kDa, respectively, and a light chain at 25 kDa. **(F)** HEK293T cells were seeded on coverslips and transfected with 0.5μg of pDEC205-OVA and pDEC205-PBK for 48 hours then cells were fixed with 2% PFA, permeabilized and labelled with anti-IgG secondary antibody (red) and Hoechst counterstain for nuclei (blue); white arrows depict protein aggregates. Western blot on cell lysate from **(G)** MVA-PBK passage 1 (P1) or passage 2 (P2) infected DF-1 cells or **(H)** VSVΔ51-PBK infected or uninfected Vero cells. Cell lysate was run on gel and probed with anti-PBK (1:1000). **(I)** Multi step growth curve comparing VSV-PBK to VSV-GFP. Vero cells were infected with MOI 0.01 of virus, and cell supernatant was collected 1, 12, 18, 26, 36, and 48 hours post infection and tittered. 2-way ANOVA.

4.2.5 Optimization of peptides for *in vitro* analysis of viral and PBK specific responses

Studies evaluating immunization against PBK require the analysis of the cellular PBK antigen specific response. However, there are no commercially available tools such as tetramers or PBK peptides. Therefore, we used the IEDB T cell epitope prediction tool to predict MHC-I CD8+ T cell PBK epitopes for downstream experiments. Four predicted PBK peptides were evaluated for future *in vitro* assays. Additionally, we tested two previously identified MVA peptides.[25,26] Naïve BALB/c mice were immunized with VSVΔ51-PBK followed by MVA-PBK at day 7 and day 14. Splenocytes were isolated at day 21 and evaluated for antigen specific responses by IFNγ ELISPOT. Analysis of ELISPOT reveals that the H-2L^d restricted epitope PBK$_{11-20}$ and H-2K^d restricted epitope PBK$_{72-80}$ give the highest IFN-γ signal following peptide stimulation (Supplemental Figure 18). PBK$_{11-20}$ and PBK$_{72-80}$ was subsequently used for *in vitro* assays to evaluate the PBK-specific immune response. Additionally, MVA peptides generated a strong IFN-γ-response following stimulation.

4.2.6 Immunization with viruses encoding PBK generates antigen specific cellular and humoral immunity

Having successfully produced prime and boost vectors expressing the PBK antigen, the next step was determining if immunization with MVA-PBK and VSVΔ51-PBK generates antigen specific cellular and humoral immunity. We tested alternative prime-boost vaccination regimens employing VSVΔ51-PBK or MVA-PBK.

Naïve BALB/c mice were immunized with different prime-boost combinations, consisting of either 10^8 PFU of VSVΔ51-PBK (i.v.), or 10^7 PFU MVA-PBK (i.m.) administered bilaterally and compared to PBS control (i.v.) (Figure 8A). At days 7, 21 and 34 post prime immunization, splenocytes were isolated from immunized mice and stimulated *ex vivo* with PBK peptides. We assessed the antigen specific immune response against H-2K^d-restricted $PBK_{72\text{-}80}$ and H-2L^d-restricted $PBK_{11\text{-}20}$ peptides by IFN-γ ELISPOT assay and by intracellular cytokine staining.

At day 7 post prime, the MVA-PBK prime generated significantly higher IFN-γ spot forming units (SFU) in response to stimulation with PBK peptides compared to PBS and VSVΔ51-PBK groups. VSVΔ51-PBK immunization also generated a higher number of IFN-γ SFU in response to PBK peptide stimulation. However, they did not reach statistical significance compared to PBS (Figure 4.6A, B).

At Day 21, seven days after the administration of boost immunization, the VSVΔ51/MVA group demonstrated a significant increase in IFN-γ SFU in both PBK conditions compared to PBS mice. The MVA/VSV Δ51 boosted group showed significantly higher IFN-γ SFU in unstimulated and DMSO conditions compared to PBS control and VSVΔ51/MVA mice (Figure 4.6A,B). IFN-γ SFU did not significantly increase in response to stimulation with PBK peptides compared to unstimulated and DMSO conditions. This non-specific activation of immune cells may be the result of immunization with a viral vector; since the immune response was assessed seven days post boost (around the peak of the adaptive immune response) the baseline activation and IFN-γ production of splenocytes is expected to be high as the immune response may be directed against the viral vector in addition to encoded

antigen. This effect is not observed in MVA-PBK boosted mice - MVA is a highly attenuated vector, and immune responses are predominantly directed against antigen load versus the viral vector.

Following the primary expansion of antigen specific immunity, T cells undergo a contraction phase and form a pool of adaptive memory T cells. Immunological memory allows the immune system to respond more rapidly and effectively when exposed to previously encountered antigens. Therefore, we evaluated the immune response to PBK antigen at day 34, twenty days post-boost. We confirmed the establishment of memory CD8+ T cells by flow cytometry (Supplemental Figure 19). MVA/ VSVΔ51 mice demonstrated significantly higher IFN-γ SFU in response to stimulation with PBK peptides compared to PBS mice and VSVΔ51/MVA mice. VSVΔ51/MVA mice demonstrated a higher number of IFN-γ SFU than PBS in PBK stimulated conditions; however, this did not reach statistical significance (Figure 4.6A,B).

To assess the CD8+ T cell response to antigen, we performed intracellular cytokine staining of splenocytes stimulated *ex vivo* with PBK peptides and control conditions. At day 7, after prime, VSVΔ51-PBK generated a significantly higher IFN-γ response in splenocytes stimulated with PBK_{72-80} compared to MVA-PBK and PBS immunized groups (Figure 4.6F). At day 21, both groups immunized with the PBK encoding viruses generated a significantly higher percentage of IFN-γ + CD8+ T cells when stimulated with PBK_{11-20} and PBK_{72-80} (Figure 4.6F). At day 34, the VSVΔ51/MVA group demonstrated significantly higher percentage of IFN-γ CD8+ T cells compared to PBS in response to stimulation with PBK. The MVA/VSVΔ51 group did not show an increase in IFN-γ production in response to PBK peptides (Figure 4.6F). We further assessed PD1+ expression on CD8+ T cells responding to antigen stimulation by flow cytometry on day 21 (Figure 4.6E) and 34 (Figure 4.6F). Both groups immunized with PBK encoding viruses showed a significant increase in the percentage of PD1+ CD8+ T cells compared to the PBS group. At day 34, there was an overall decrease in the percentage of PD1+ IFNγ+ CD8+ T cells (gating strategy shown in Supplemental Figure 16).

Finally, to assess the humoral response to PBK, serum isolated from immunized mice was incubated with PBK expressing cells (K7M2) *ex vivo*, and IgG binding to K7M2 target cells was assessed by flow cytometry. At day 21, MVA/VSVΔ51 group had a significantly higher percentage of IgG positive cells compared to PBS and VSVΔ51/MVA (Figure 4.6G).

Overall, both MVA/ VSVΔ51 and VSVΔ51/MVA prime and boost combinations generate a PBK specific cellular and humoral response and T-cell memory that responds to secondary antigen encounters.

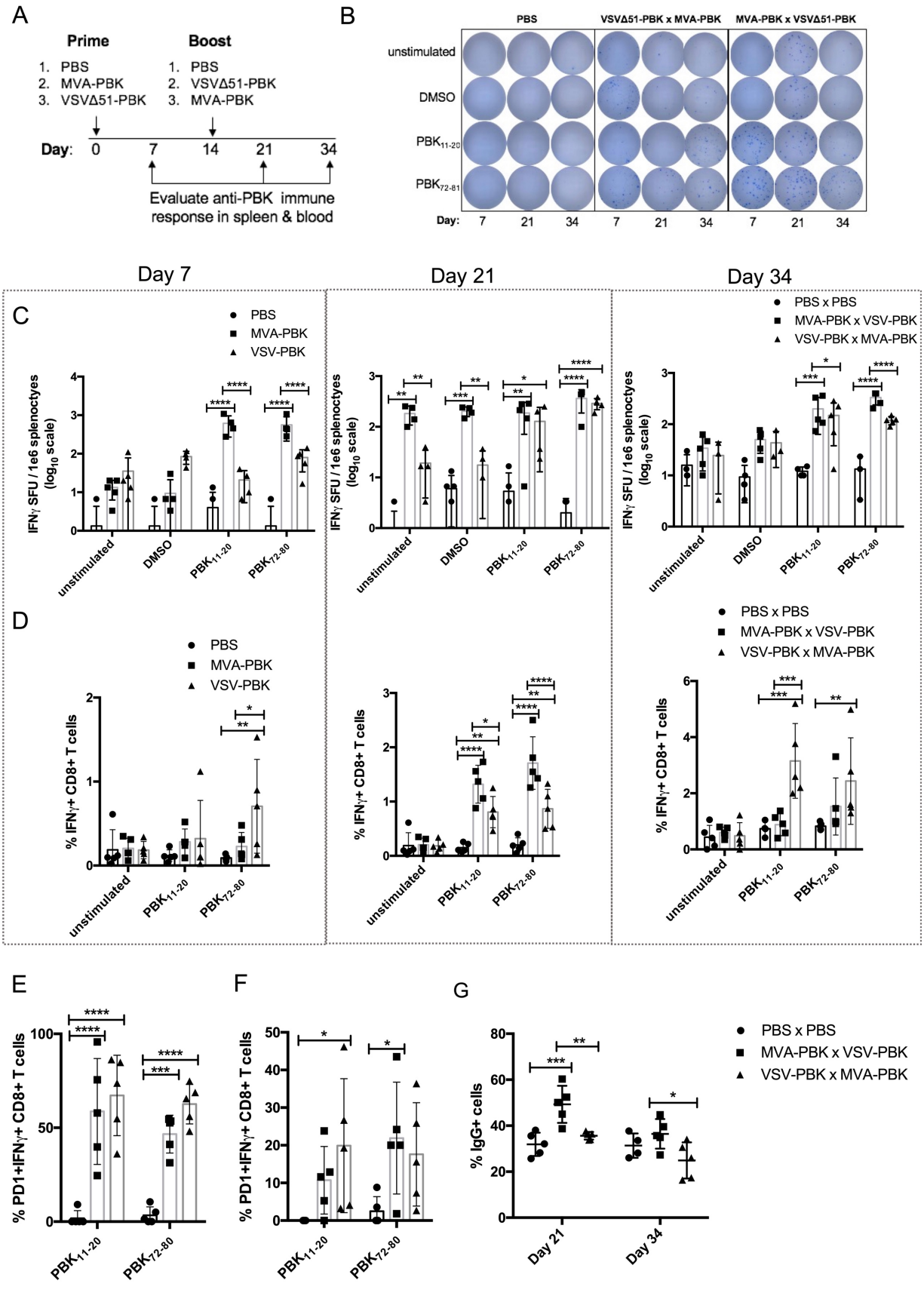
A
Prime
Boost
1. PBS
2. MVA-PBK
3. VSVΔ51-PBK
1. PBS
2. VSVΔ51-PBK
3. MVA-PBK
Day: 0 7 14 21 34
Evaluate anti-PBK immune response in spleen & blood
B
PBS
VSVΔ51-PBK x MVA-PBK
MVA-PBK x VSVΔ51-PBK
unstimulated
DMSO
PBK11-20
PBK72-81
Day: 7 21 34 7 21 34 7 21 34
Day 7
Day 21
Day 34
C
PBS
MVA-PBK
VSV-PBK
PBS x PBS
MVA-PBK x VSV-PBK
VSV-PBK x MVA-PBK
IFNγ SFU / 1e6 splenoctyes (log10 scale)
unstimulated
DMSO
PBK11-20
PBK72-80
D
% IFNγ+ CD8+ T cells
E
% PD1+IFNγ+ CD8+ T cells
F
% PD1+IFNγ+ CD8+ T cells
G
% IgG+ cells
Day 21
Day 34

Figure 4.6 Induction of cellular and humoral PBK-specific immune responses following immunization with MVA-PBK and VSV-PBK. (A) Schematic representation of immunization schedule. Naïve BALB/c mice received prime immunization at day 0, and boost immunization at day 14. Mice were administered PBS (50 uL i.v.), 10^7 PFU MVA-PBK i.m. (50 uL, i.m. bilateral), or 10^8 PFU VSVΔ51-PBK (50 uL, i.v.) Immune analysis was performed at day 7, day 21, and day 34. **(B)** Representative plates from ELISPOT assay. Splenocytes isolated from immunized mice were co-cultured with either media, DMSO, PBK_{11-20}, PBK_{72-81} peptides for 24 hours. **(C)** Graph of IFNγ spot forming units (SFU) per $1x10^6$ splenocytes (log 10 scale) at day 7, day 21 and day 34. n=5 per condition. **(D)** Percentage of IFNγ + CD8+ T cells determined by flow cytometry. $1x10^6$ splenocytes were isolated from immunized mice and co-cultured with media, PBK_{11-20} or PBK_{72-81} overnight and stained for IFNγ at days 7, day 21 and day 34. Percentage of PD1+ CD8+ T cells at **(E)** day 21 and **(F)** day 34. **(G)** Serum binding assay. Percentage of IgG+ K7M2 cells, serum isolated from immunized mice was incubated with K7M2 cells and probed for IgG. IgG binding was detected by flow cytometry. Mean +- SD. 2-way ANOVA. $P < 0.0001$ = ****, $p<0.001$ = ***, $p<0.01$ = **, $p <0.05$ = *

4.2.7 Immunization with combination of prime and boost vectors confers protection against K7M2 sarcoma.

Previous results demonstrated that prime-boost immunization using both combinations of VSVΔ51-PBK and MVA-PBK generates a PBK specific response. Our next objective was to determine whether this immune response could confer protection against murine sarcoma cell lines expressing the PBK antigen in a prophylactic setting. To achieve this, naïve BALB/c mice were immunized with alternative prime-boost combinations, consisting of either 10^8 PFU of VSVΔ51-PBK (i.v.) or 10^7 PFU MVA-PBK administered (i.m.) bilaterally and compared to PBS control (i.v.). As the PBK-specific immune response did not show significant differences between prime-boost combinations, we assessed both prime-boost combinations of viruses to determine whether one provided enhanced protection. Mice were challenged with a subcutaneous (s.c.) injection of either $1x10^6$ K7M2 or WEHI-164 cells seven days post-boost (Figure 4.7A). As the adaptive immune response generated by immunization peaks around seven days post-boost, we hypothesized that there would be clonally expanded PBK-specific T cells post-immunization, which would confer protection against tumor challenge. Furthermore, we assessed the activation of circulating CD8+ T cells on days 7, 13 and 21 post-prime, before tumor challenge.

T cell activation was determined by the expression of CD44 and CD62L on CD8+ T cells detected by flow cytometry. Both prime and boost combinations generated a significantly higher percentage of activated CD8 T cells (CD44+CD62L-) when compared to PBS. MVA/VSVΔ51 boost generated a higher percentage of activated CD8+ T cells compared to VSVΔ51/MVA, but this difference did not reach statistical significance (Figure 4.7B).

Mice immunized with prime-boost demonstrate a slower rate of K7M2 tumor growth compared to PBS immunized mice (Figure 4.7C). Furthermore, VSVΔ51/MVA immunization significantly contributed to the overall survival of K7M2-challenged mice, conferring survival advantage to 80% (4/5) of mice, compared to 40% in MVA/VSVΔ51 and 0% in PBS groups (Figure 4.7E). Contrastingly,

prime-boost vaccination did not confer protection to WEHI-164 challenged mice, and mice receiving PBS demonstrated the slowest tumor growth (Figure 4.7D). The PBS group showed the highest overall survival, and significantly better survival compared to VSVΔ51/MVA (Figure 4.7F).

Overall, prophylactic prime-boost vaccination targeting PBK contributes to tumor control in mice challenged with K7M2 sarcoma but not WEHI-164.

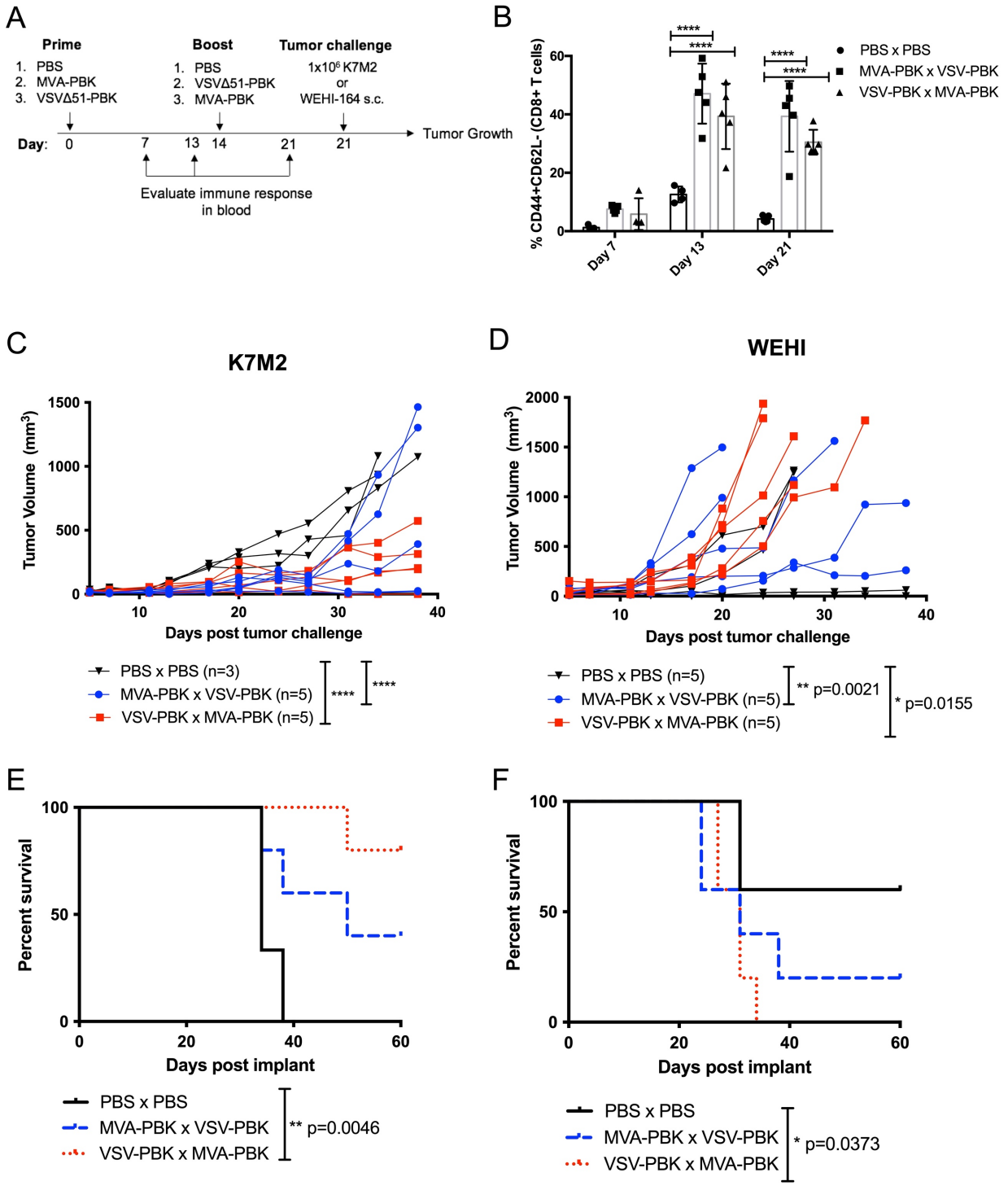
A
Prime
1. PBS
2. MVA-PBK
3. VSVΔ51-PBK
Boost
1. PBS
2. VSVΔ51-PBK
3. MVA-PBK
Tumor challenge
1x10^6 K7M2
or
WEHI-164 s.c.
Day: 0 7 13 14 21 21
Tumor Growth
Evaluate immune response in blood
B
% CD44+CD62L- (CD8+ T cells)
Day 7
Day 13
Day 21
PBS x PBS
MVA-PBK x VSV-PBK
VSV-PBK x MVA-PBK
C
K7M2
Tumor Volume (mm3)
Days post tumor challenge
PBS x PBS (n=3)
MVA-PBK x VSV-PBK (n=5)
VSV-PBK x MVA-PBK (n=5)
D
WEHI
Tumor Volume (mm3)
Days post tumor challenge
PBS x PBS (n=5)
MVA-PBK x VSV-PBK (n=5)
VSV-PBK x MVA-PBK (n=5)
** p=0.0021
* p=0.0155
E
Percent survival
Days post implant
PBS x PBS
MVA-PBK x VSV-PBK
VSV-PBK x MVA-PBK
** p=0.0046
F
Percent survival
Days post implant
PBS x PBS
MVA-PBK x VSV-PBK
VSV-PBK x MVA-PBK
* p=0.0373

Figure 4.7 Evaluation of prime and boost combinations in prophylactic settings (A) Schematic representation of immunization schedule. Naïve BALB/c mice received prime immunization at day 0 and boost immunization at day 14. Mice were administered PBS (50 uL i.v.), 10^7 PFU MVA-PBK (50 uL, i.m. bilateral), or 10^8 PFU VSVΔ51-PBK (50 uL, i.v.). Mice were challenged 7 days post-boost with $1x10^6$ K7M2 or WEHI-164 cells administered s.c. **(B)** Activation of immune cells was assessed by flow cytometry a Day 7, 13 and 21. Graphs show the percentage of CD8+ T cells that are CD44+ and CD62L-. Mean ± SD **(C, D)** Tumor growth (2-way ANOVA, **** $p<0.0001$. Significance calculated at day 34 for K7M2 and Day 20 for WEHI-164) **(E, F)** Percent overall mouse survival. Log-rank mantel-cox test.

4.2.8 Prophylactic prime-boost immunization against PBK but not GFP confers protection against K7M2 tumor challenge

To resolve conflicting results observed in WEHI-164 tumors, we aimed to discern the relative contribution of the anti-viral immune response (innate or adaptive) versus the PBK-specific response in conferring tumor control. To achieve this, we employed VSVΔ51 and MVA viruses encoding GFP as a control.

Naïve BALB/c mice were immunized with an MVA prime (10^7 PFU, intramuscularly) and VSVΔ51 boost (10^8 PFU, i.v.) encoding PBK or GFP, or PBS control (i.v.) and subsequently challenged subcutaneously with $1x10^6$ K7M2 or WEHI-164 cells (Figure 4.8A). We monitored mice for tumor growth and survival and evaluated circulating lymphocytes by flow cytometry to characterize changes in peripheral immunity between vaccination groups, and to identify immune populations potentially contributing to therapeutic benefits. This strategy enables us to assess whether protection is predominantly driven by an antigen-specific response or an unspecific anti-viral immune response (to viral vectors) contributing to tumor control.

Mice immunized with MVA/VSVΔ51-PBK boost demonstrated significantly lower K7M2 tumor volume at day 54 compared to PBS and GFP virus control groups (Figure 4.10B). PBK vaccinated mice demonstrated 60% overall survival, compared to 0% in GFP virus control group and PBS control group (Figure 4.8D). In mice challenged with WEHI-164, immunization against PBK did not contribute to tumor control or improve overall survival compared to GFP and PBS control groups (Figure 4.8C,E).

Circulating immune cells were evaluated in the blood at days 7, 13 and 21 post-prime. The percentage of CD3+ T cells in MVA-GFP group was significantly lower compared to PBS and MVA-PBK groups. The percentage of CD4+ T cells was significantly lower in virus vaccinated groups compared to PBS control group, and the percentage of CD8+ T cells was significantly higher in virus vaccinated groups compared to the PBS groups on day 7 (Figure 4.9 A,B,C). A significant decrease in

CD4:CD8 T cell ratio is observed between both virus vaccinated and PBS groups (Figure 4.11D). A decrease in CD4:CD8 T cell ratio has been previously associated with a favourable response to peptide vaccination.[27] However, no significant changes in CD4:CD8 T cell ratio was observed at day 13 or day 21.

Next, the activation of CD8+ T cells was assessed based on the expression of CD44 and CD62L. At day 7, MVA-PBK vaccinated mice showed a significant increase in the percentage of activated CD8+ T cells (CD44+CD62L-) compared to PBS and MVA-GFP groups (Figure 4.9E). This data suggests that the PBK antigen is highly immunogenic and leads to clonal expansion of PBK specific T cells, generating a high percentage of activated CD8+ T cells when delivered via the MVA viral vector. At day 21, both groups receiving the boost virus show a significantly higher percentage of activated CD8+ T cells compared to PBS, suggesting that T cells are activated in response to VSV virus irrespective of encoded antigen (Figure 4.9E). Analysis of circulating dendritic cells (CD11c+CD3-) showed a significantly higher percentage of DCs in MVA-GFP group compared to both MVA-PBK and PBS groups at day 7, no differences were observed at other time points. MVA-PBK group had the highest percentage of circulating B cells (CD19+CD3-) compared to controls at day 7, but the lowest percentage on day 21 (Figure 4.9F). Finally, we assessed the generation of antigen specific antibodies via serum isolated from immunized mice. Serum was incubated with K7M2 cells and probed with a secondary antibody against IgG. The percentage of IgG+ K7M2 cells was determined by flow cytometry. At all time-points, the MVA/VSVΔ51-PBK group demonstrated a significantly higher percentage of IgG positive cells compared to control groups, indicating the generation of PBK specific IgG (Figure 4.9H).

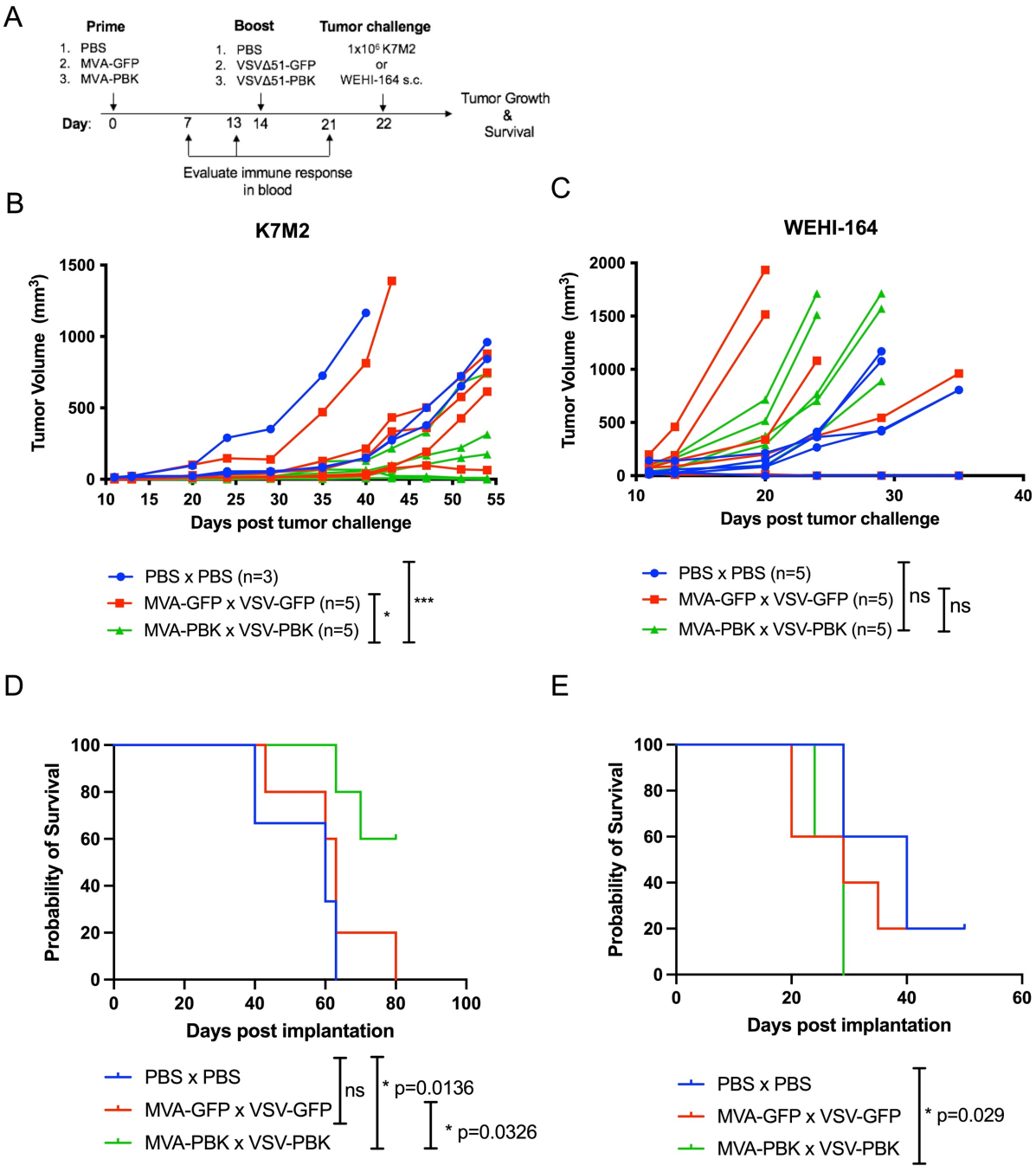
A
Prime
1. PBS
2. MVA-GFP
3. MVA-PBK
Boost
1. PBS
2. VSVΔ51-GFP
3. VSVΔ51-PBK
Tumor challenge
1x10⁶ K7M2
or
WEHI-164 s.c.
Day: 0 7 13 14 21 22
Tumor Growth & Survival
Evaluate immune response in blood
B
K7M2
Tumor Volume (mm³)
Days post tumor challenge
PBS x PBS (n=3)
MVA-GFP x VSV-GFP (n=5)
MVA-PBK x VSV-PBK (n=5)
*
***
C
WEHI-164
Tumor Volume (mm³)
Days post tumor challenge
PBS x PBS (n=5)
MVA-GFP x VSV-GFP (n=5)
MVA-PBK x VSV-PBK (n=5)
ns
ns
D
Probability of Survival
Days post implantation
PBS x PBS
MVA-GFP x VSV-GFP
MVA-PBK x VSV-PBK
ns
* p=0.0136
* p=0.0326
E
Probability of Survival
Days post implantation
PBS x PBS
MVA-GFP x VSV-GFP
MVA-PBK x VSV-PBK
* p=0.029

Figure 4.8 Prophylactic prime-boost immunization targeting PBK but not GFP confers protection against K7M2 tumor challenge. (A) Schematic representation of immunization schedule. Naïve BALB/c mice received prime immunization at day 0 and boost immunization at day14. Mice were administered PBS (50 uL i.v.), 10^7 PFU MVA-PBK or -GFP i.m. (50 uL, i.m. bilateral), or 10^8 PFU VSVΔ51-PBK or -GFP (50 uL, i.v.). Mice were challenged 7 days post-boost with $1x10^6$ K7M2 or WEHI-164 cells administered s.c.. **(B, C)** Graph of tumor volume over time. (Significance calculated by 2-way ANOVA at D54 for K7M2. $P < 0.0001$ = ****, $p<0.001$ = ***, $p<0.01$ = **, $p <0.05$ = * **(D,E)** Overall mouse survival was observed. Log-rank mantel-cox test.

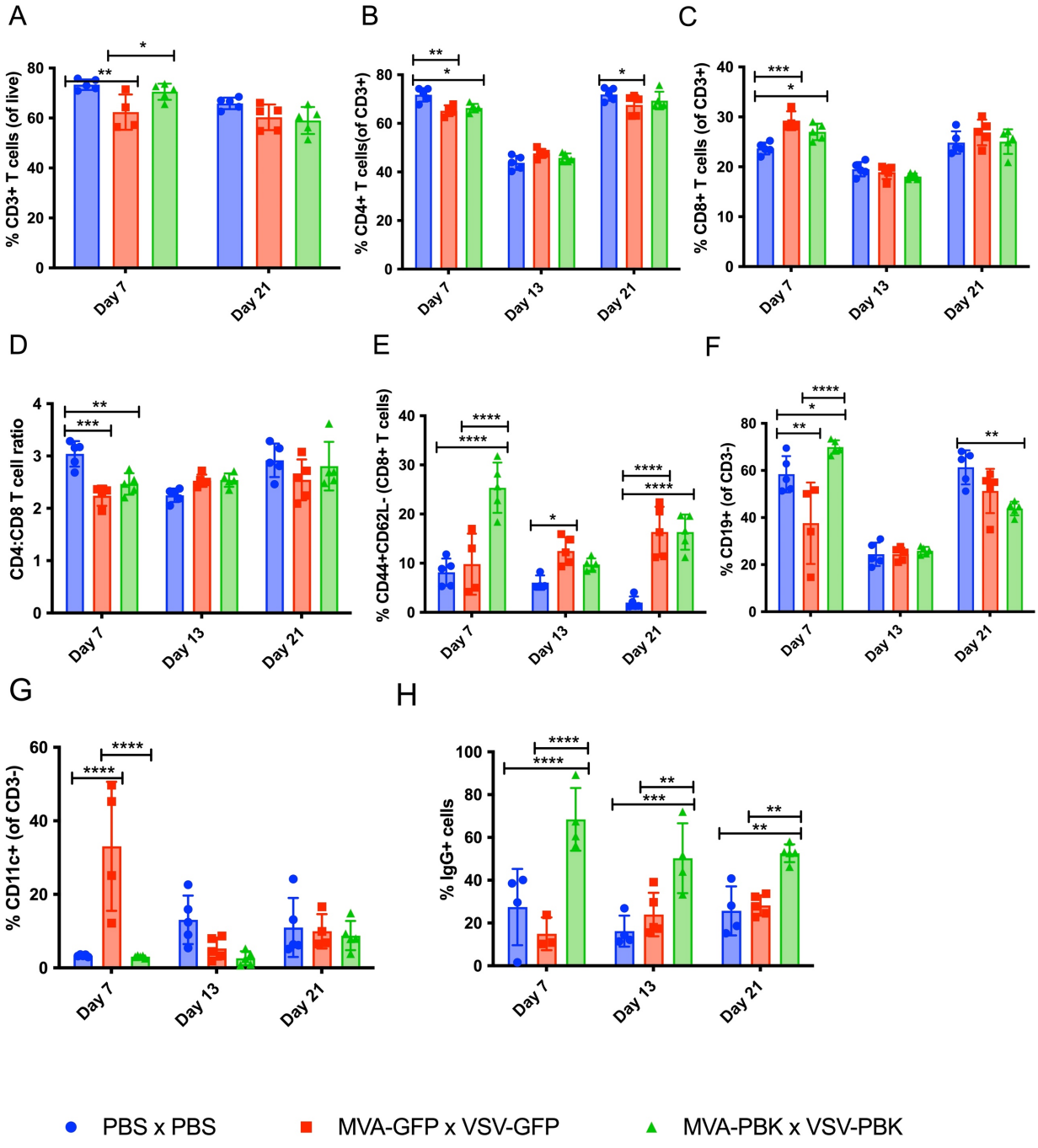
A
% CD3+ T cells (of live)
Day 7
Day 21
B
% CD4+ T cells(of CD3+)
Day 7
Day 13
Day 21
C
% CD8+ T cells (of CD3+)
Day 7
Day 13
Day 21
D
CD4:CD8 T cell ratio
Day 7
Day 13
Day 21
E
% CD44+CD62L- (CD8+ T cells)
Day 7
Day 13
Day 21
F
% CD19+ (of CD3-)
Day 7
Day 13
Day 21
G
% CD11c+ (of CD3-)
Day 7
Day 13
Day 21
H
% IgG+ cells
Day 7
Day 13
Day 21
PBS x PBS
MVA-GFP x VSV-GFP
MVA-PBK x VSV-PBK

Figure 4.9 Immune analysis of circulating immune cells following prime-boost immunization. (A-G) Immune analysis was performed at days 7, 13 and 21. Saphenous bleeds were performed to assess circulating lymphocytes, **(H)** and to assess levels of antigen specific IgG by flow cytometry. Serum was diluted 1:100 and incubated with $5x10^5$ K7M2 cells, IgG was probed for by secondary antibody and detected by flow cytometry. Mean ± SD. 2-way ANOVA. $P < 0.0001$ = ****, $p<0.001$ = ***, $p<0.01$ = **, $p <0.05$ = *

4.2.9 Addressing the efficiency of prophylactic immunization and WEHI-164 tumor challenge

Our previous results have shown that prophylactic vaccination targeting the PBK antigen is insufficient to protect against WEHI-164 tumor growth when challenged 7 days post-boost. A variety of factors can contribute to these results, including a potent anti-viral response that may outweigh the PBK response required to target WEHI-164 cells effectively. To rule out the possibility that innate or adaptive anti-viral cellular responses are confounding factors that provide a growth advantage to tumors, we employed our prime-boost vaccination strategy followed by tumor challenge 14 days post-boost (Figure 4.10A). At this time point, all innate anti-viral responses have subsided, and the adaptive immune response has contracted and formed antigen specific memory population. Theoretically, the administration of WEHI-164 at this time point should stimulate the clonal expansion of T cells specific to PBK and other tumor antigens, without the influence of anti-viral responses upon tumor challenge.

Prophylactic immunization with MVA-PBK and VSVΔ51-PBK did not significantly slow WEHI-164 tumor growth or confer a survival advantage to challenged mice. Tumor growth was delayed in 2/5 mice compared to control groups. However, this did not reach statistical significance. Furthermore, prophylactic vaccination with GFP viruses provided protection against WEHI-164 tumor growth in 2/5 mice (Figure 4.10B, C).

We analyzed the circulating immune cells after several time points post-boost to identify potential differences in proportions of immune cell types that may be affecting WEHI-164 tumor growth. Analysis of circulating CD3+ shows no significant differences between groups at day 15 or 22; at day 29, the PBK vaccinated group showed a significantly lower percentage of CD3+ T cells compared to control groups (Figure 4.11A). A significant difference in the percentage of CD4+ and CD8+ T cells is observed at day 22 in both virus vaccinated groups, which is predictive of response to vaccination (Figure 4.11B, F). Activated CD8+ T cells are significantly increased in virus vaccinated groups at days 15 and 22 (Figure 4.11C). No significant differences in central memory CD8+ T cells or B cells were observed between groups and any time points (Figure 4.11D, J). Notably, no differences

in immune cells, other than the percentage of circulating CD3+ T cells, are observed at day 29 between groups. These results suggest that a different vaccination strategy or a different vaccine target may be needed to target WEHI-164 tumor growth effectively, further studies will be required to identify the most effective vaccine approach for this murine sarcoma.

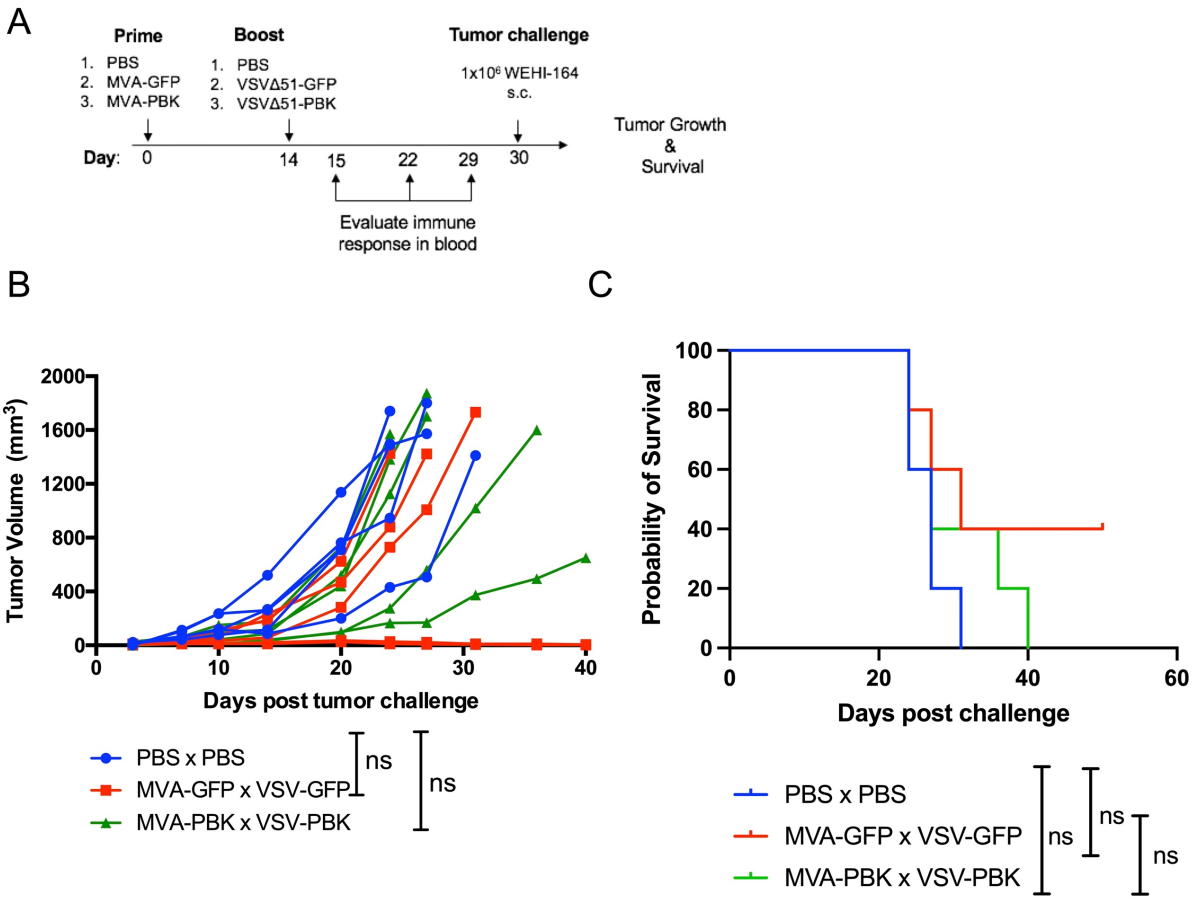
A
Prime
1. PBS
2. MVA-GFP
3. MVA-PBK
Boost
1. PBS
2. VSVΔ51-GFP
3. VSVΔ51-PBK
Tumor challenge
1x10⁶ WEHI-164
s.c.
Day: 0 14 15 22 29 30
Tumor Growth
&
Survival
Evaluate immune
response in blood
B
Tumor Volume (mm³)
2000
1600
1200
800
400
0
0 10 20 30 40
Days post tumor challenge
PBS x PBS
MVA-GFP x VSV-GFP
MVA-PBK x VSV-PBK
ns
ns
C
Probability of Survival
100
80
60
40
20
0
0 20 40 60
Days post challenge
PBS x PBS
MVA-GFP x VSV-GFP
MVA-PBK x VSV-PBK
ns
ns
ns

Figure 4.10 Prophylactic immunization with PBK targeting prime-boost does not confer protection against WEHI-164 tumor challenge. (A) Schematic representation of immunization schedule. Naïve BALB/c mice received prime immunization at day 0, and boost immunization at day14. Mice were administered PBS (50 uL i.v.), 10^7 PFU MVA-PBK or -GFP i.m. (50 uL, i.m. bilateral), or 10^8 PFU VSVΔ51-PBK or -GFP (50 uL, i.v.). Mice were challenged 14 days post-boost with $1x10^6$ K7M2 or WEHI-164 cells administered s.c.. **(B)** Graph of tumor volume over time. Significance calculated by 2-way ANOVA. **(C)** Overall mouse survival was observed. Log-rank mantel-cox test.

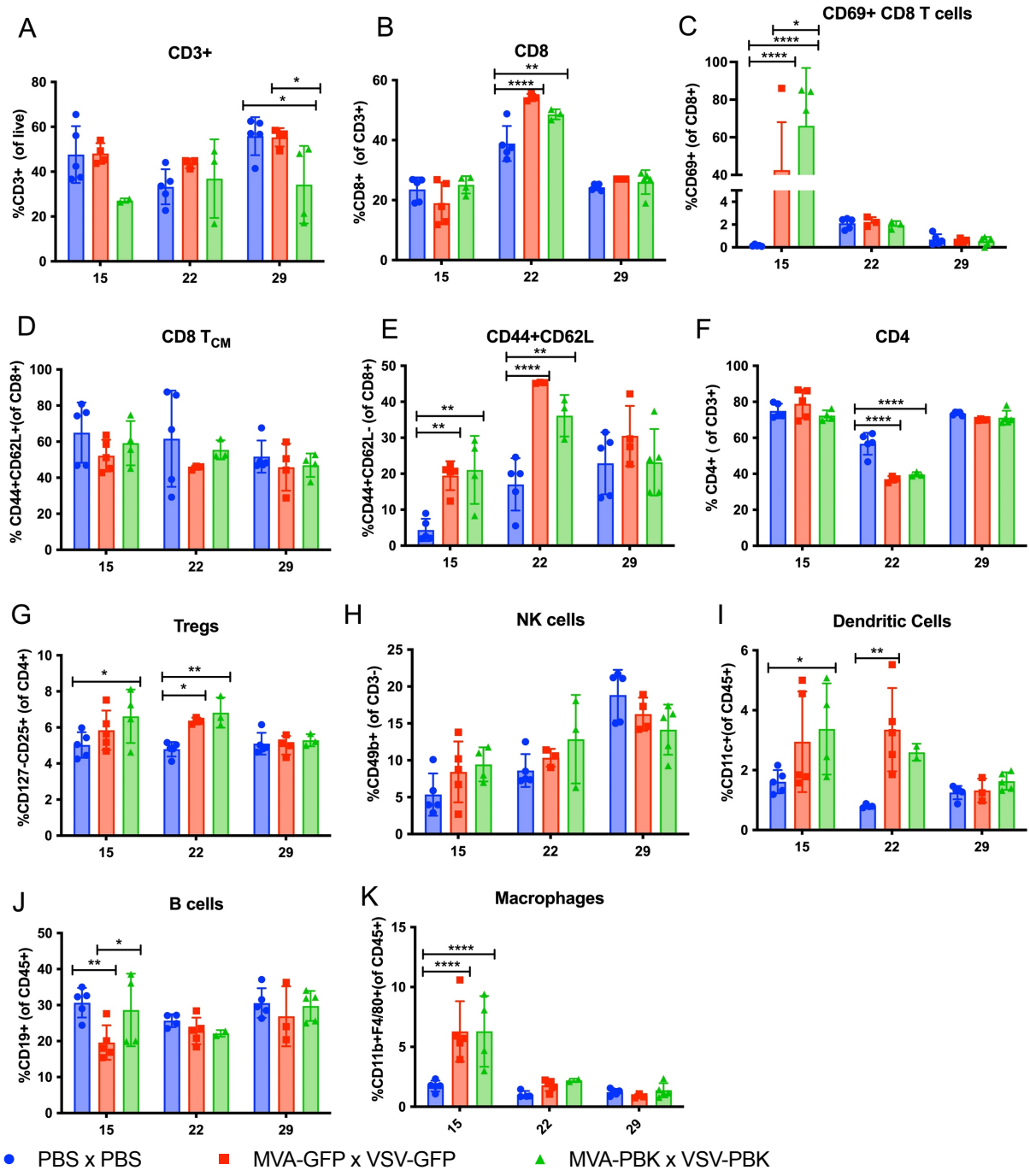
A
CD3+
%CD3+ (of live)
B
CD8
%CD8+ (of CD3+)
C
CD69+ CD8 T cells
%CD69+ (of CD8+)
D
CD8 T$_{CM}$
% CD44+CD62L+(of CD8+)
E
CD44+CD62L
%CD44+CD62L- (of CD8+)
F
CD4
% CD4+ (of CD3+)
G
Tregs
%CD127-CD25+ (of CD4+)
H
NK cells
%CD49b+ (of CD3-)
I
Dendritic Cells
%CD11c+(of CD45+)
J
B cells
%CD19+ (of CD45+)
K
Macrophages
%CD11b+F4/80+(of CD45+)
15
22
29
PBS x PBS
MVA-GFP x VSV-GFP
MVA-PBK x VSV-PBK

Figure 4.11 Immune profiling of circulating immune cells after boost. Immune analysis was performed at days 15, 22 and 29 by flow cytometry. Significance calculated by 2-way ANOVA. P < 0.0001 = ****, p<0.001 = ***, p<0.01 = **, p <0.05 = *

4.2.10 A preliminary evaluation of therapeutic prime-boost vaccination reveals that VSVΔ51/MVA generates a stronger antigen specific response compared to MVA/VSVΔ51 vaccination in K7M2 tumor bearing mice

The next study aimed to evaluate the prime-boost as a therapeutic strategy for K7M2 tumors. Mice were implanted with $1x10^6$ K7M2 cells s.c. and treated with prime and boost immunization when tumors reached 100 mm^3 (Figure 4.12A). Challenges with poor tumor-take rates were encountered, despite this limitation, we evaluated the antigen-specific immune response in mice that reach the experimental end-point (tumor size of approximately 1500 mm^3) (Figure 4.12B). Specifically, splenocytes were stimulated with PBK and AH1 peptides and IFN-γ production was measured by ELISPOT. AH1 is a K7M2 tumor antigen that is not directly targeted by this therapy, however, assessment of an immune response against this peptide will inform if this vaccination strategy leads to antigen spreading.

Interestingly, it was observed that mice that received the VSVΔ51/MVA-PBK had a more robust antigen-specific response to antigen compared to the reverse vaccination order. This was also observed in mice that received VSVΔ51-GFP as a prime (Figure 4.12C). Our findings suggest that immunization with VSVΔ51 as prime (encoding either GFP or PBK), leads to antigen spreading and enhances the immune response against K7M2. Thus, a prime-boost approach using VSVΔ51 followed by MVA may be an effective strategy for enhancing the immune response against K7M2 tumours.

A

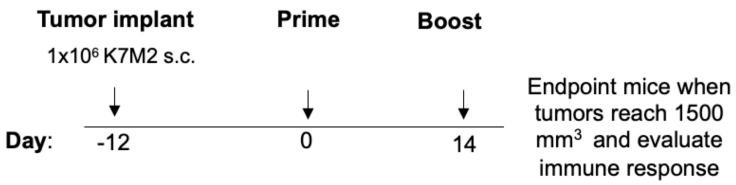
Tumor implant
1x10⁶ K7M2 s.c.
Prime
Boost
Day:
-12
0
14
Endpoint mice when tumors reach 1500 mm³ and evaluate immune response

B

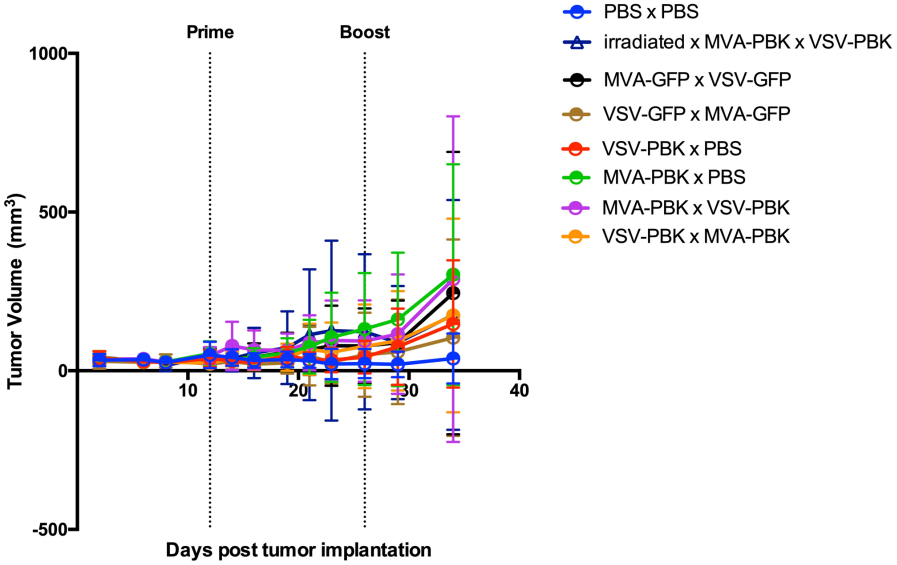
Prime
Boost
1000
500
0
-500
10
20
30
40
Tumor Volume (mm³)
Days post tumor implantation
PBS x PBS
irradiated x MVA-PBK x VSV-PBK
MVA-GFP x VSV-GFP
VSV-GFP x MVA-GFP
VSV-PBK x PBS
MVA-PBK x PBS
MVA-PBK x VSV-PBK
VSV-PBK x MVA-PBK

C

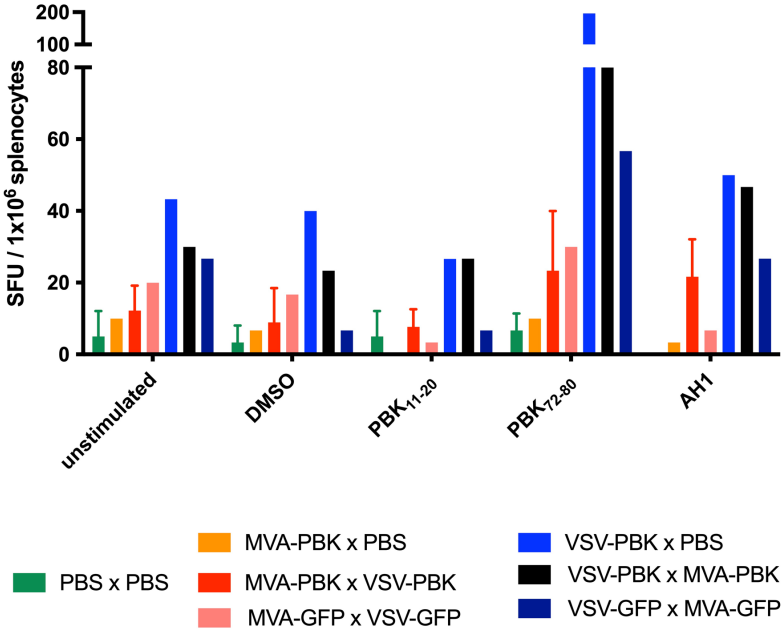
200
100
80
60
40
20
0
SFU / 1x10⁶ splenocytes
unstimulated
DMSO
PBK11-20
PBK72-80
AH1
PBS x PBS
MVA-PBK x PBS
MVA-PBK x VSV-PBK
MVA-GFP x VSV-GFP
VSV-PBK x PBS
VSV-PBK x MVA-PBK
VSV-GFP x MVA-GFP

Figure 4.12 Preliminary survival experiment reveals that VSV prime and MVA boost generates a broader immune response. (A) Schematic representation of immunization schedule. BALB/c mice received a s.c. injections of $1x10^6$ K7M2 cells, when tumors reached an average size of 100 m^3, mice were administered prime immunization of PBS, 10^8 PFU VSV-PBK or -GFP i.v., followed 14 days later by a boost immunization of PBS, 10^7 PFU MVA-PBK or -GFP i.m.. **(B)** Graph showing tumor volume over time. **(C)** IFNγ ELISPOT assay was performed on splenocytes isolated from mice that reached endpoint at day 54 post-implant. $2.5x10^5$ splenocytes were cultured for 24 hours in the presence of culture media (unstimulated), DMSO (vehicle), or 10 uM of PBK_{11-20}, PBK_{72-80} or AH1 peptides. IFNγ spots were imaged and quantified using an automatic plate-scanner.

4.2.11 Therapeutic efficacy of PBK targeted immunotherapy in K7M2 osteosarcoma

Finally, we evaluated if VSVΔ51-PBK prime and MVA-PBK boost confers therapeutic benefit to K7M2 tumor-bearing mice. Naïve BALB/c mice were implanted subcutaneously with $1x10^6$ K7M2 cells. When tumors reached an average size of 100 m^3, mice were administered a prime of 10^8 PFU VSVΔ51 encoding -GFP or -PBK, or PBS (i.v.), followed 14 days later with a boost of MVA encoding -PBK or -GFP, or PBS (i.m.). Mice were weighed throughout therapy to identify a treatment reaction and were monitored for tumor progression. Additionally, mice were bled at days -29, -7, 7, 13, 21 and 26 to evaluate humoral responses, and at days 7, 14, 21 to assess the cellular immune response. Mice were end-pointed at day 26, and antigen specific immune responses were evaluated in the spleen (Figure 4.13A).

Monitoring of mouse weights showed that the prime-boost therapy was well tolerated, with a slight decrease in weight observed following VSVΔ51 treatments, however, animals recovered within 3 days. A decrease in weight was not observed following the administration of MVA boost (Figure 4.13B). Tumor growth was monitored over time, a significant difference in tumor size was observed at day 26 between PBS and VSVΔ51/MVA. No significant difference in tumor progression was observed between PBK vaccinated group and control groups (Figure 4.13C). Altogether, VSVΔ51-PBK prime and MVA-PBK boost did not provide therapeutic benefit to K7M2 tumor bearing mice.

Humoral and cellular immune responses were evaluated throughout the treatment. Tumor specific antibodies were assessed from serum, serum was diluted 1:100 and incubated with $5x10^5$ K7M2 cells, bound antibody was detected using a secondary antibody against IgG and evaluated by flow cytometry. Prior to tumor implant, K7M2 specific IgG were not detected. Post tumor-implant, the percentage of IgG positive K7M2 cells varied between mice, ranging from 5% - 40% binding. Notably, seven days after administration of prime immunization, mice receiving VSVΔ51-PBK or VSVΔ51-GFP showed a decrease in the percentage of IgG positive K7M2 cells compared to before prime injections, suggesting a reduction in tumor specific antibody titers post-prime, while PBS mice

continued to show an increase in the percentage of IgG binding to K7M2. (Figure 4.13D) This data suggests that VSVΔ51 infection can blunt the generation of tumor specific IgG. Previous studies have shown that VSV directly infects splenic B cells, this permissive infection may lead to infection-induced elimination of antigen-specific B cell clones, reducing the tumor specific IgG in serum.[28,29] At day 13, K7M2 specific serum IgG rises again in PBS and GFP control groups, however, the percentage of K7M2 specific IgG continues to drop in 3/4 PBK immunized mice. Following MVA boost, the percentage of IgG bound K7M2 cells increases in VSVΔ51/MVA-PBK group. (Figure 4.13D)

Mice were end-pointed 26 days post-prime, and antigen specific immune responses were assessed. Splenocytes were harvested and stimulated *ex vivo* with PBK peptides (PBK_{11-20} and PBK_{72-80}) or with the gp70 immunodominant epitope AH1. The antigen specific immune response was evaluated by ELISPOT and ICS assays by probing for IFN-γ. VSVΔ51/MVA-PBK group showed significantly higher production of IFN-γ SFU in response to PBK_{11-20} and PBK_{72-80} compared to PBS control group. No significant increase in IFN-γ was observed between groups when stimulated with the AH1 peptide (Figure 4.13E). Intracellular cytokine staining showed that VSVΔ51/MVA-PBK group had higher (but not significant) production of IFN-γ compared to control groups in unstimulated conditions (Figure 4.13F). This suggests that baseline activation of CD8+ T cells is higher in the PBK immunized group compared to controls. We further assessed the percentage PD1 expression of IFN-γ + CD8+ T cells that responded to PBK_{11-20} and $PBK_{72-80.}$ When stimulated with PBK_{11-20}, a significant increase in the percentage of PD1+ IFN-γ producing CD8+ T cells was observed in PBK group compared to the PBS control. (Figure 4.13G; gating strategy shown in Supplemental Figure 20)

Overall, this study revealed that a VSVΔ51-PBK prime followed by an MVA-PBK boost generates an antigen specific cellular and humoral immune response in K7M2 tumor bearing mice, however, this does not lead to therapeutic benefit in this model.

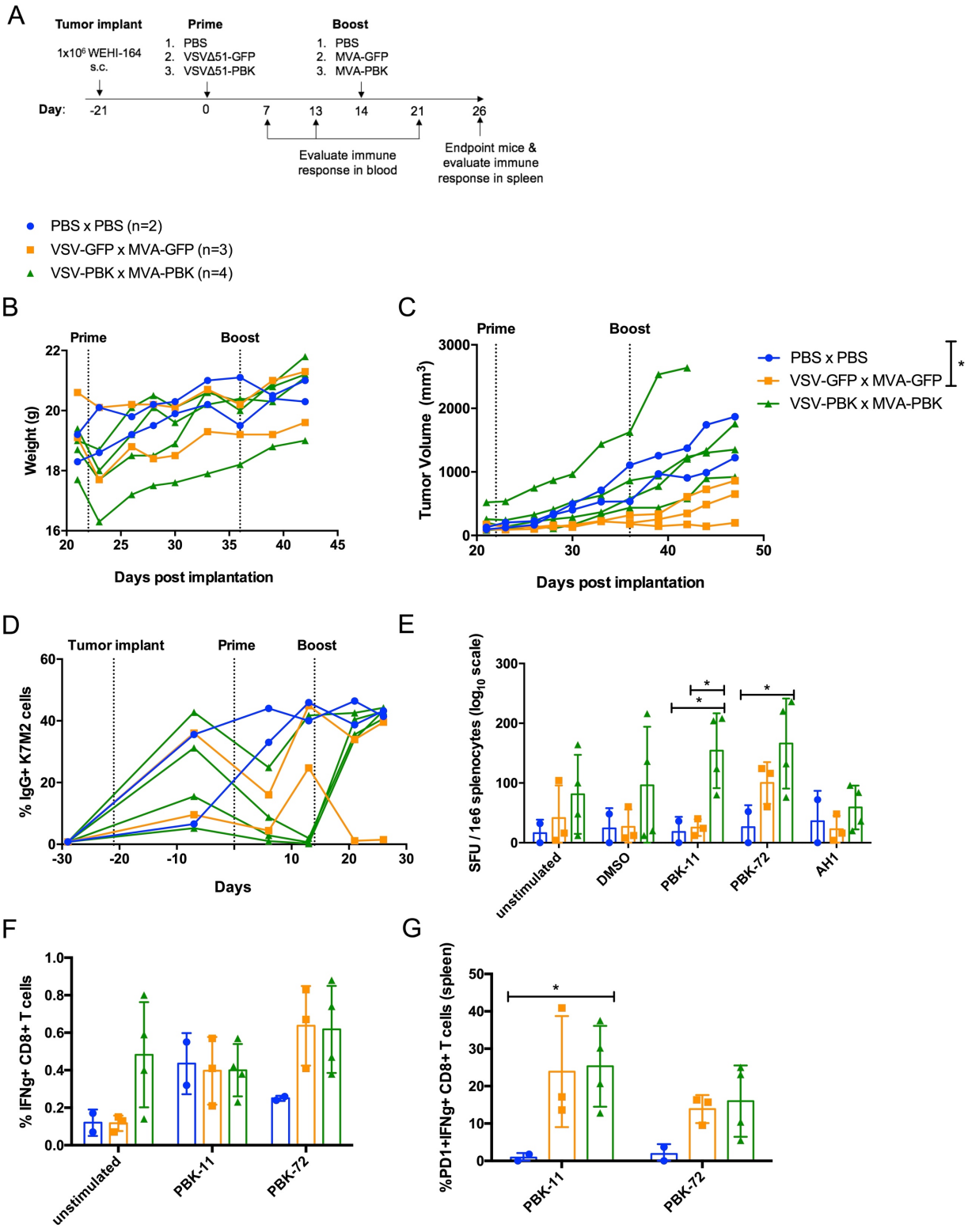
A
Tumor implant
1x10⁶ WEHI-164
s.c.
Prime
1. PBS
2. VSVΔ51-GFP
3. VSVΔ51-PBK
Boost
1. PBS
2. MVA-GFP
3. MVA-PBK
Day: -21 0 7 13 14 21 26
Evaluate immune response in blood
Endpoint mice & evaluate immune response in spleen
PBS x PBS (n=2)
VSV-GFP x MVA-GFP (n=3)
VSV-PBK x MVA-PBK (n=4)
B
Prime
Boost
Weight (g)
Days post implantation
C
Prime
Boost
Tumor Volume (mm³)
PBS x PBS
VSV-GFP x MVA-GFP
VSV-PBK x MVA-PBK
*
Days post implantation
D
Tumor implant
Prime
Boost
% IgG+ K7M2 cells
Days
E
SFU / 1e6 splenocytes (log10 scale)
unstimulated
DMSO
PBK-11
PBK-72
AH1
F
% IFNg+ CD8+ T cells
unstimulated
PBK-11
PBK-72
G
%PD1+IFNg+ CD8+ T cells (spleen)
PBK-11
PBK-72

Figure 4.13 Therapeutic Efficacy of a VSV-PBK prime and MVA-PBK boost vaccine. (A) Schematic representation of immunization schedule. BALB/c mice received a s.c. injections of $1x10^6$ K7M2 cells, when tumors reached an average size of 100 m^3, mice were administered prime immunization of PBS, 10^8 PFU VSV-PBK or -GFP i.v., followed 14 days later by a boost immunization of PBS, 10^7 PFU MVA-PBK or -GFP i.m.. **(B)** Mouse weights and **(C)** tumor size were monitored. **(D)** Percentage of K7M2 specific IgG was evaluated in serum at days, -29, -7, 7, 13, 21 and 26. Serum was diluted 1:100 and incubated with $5x10^5$ K7M2 cells, IgG was probed for by secondary antibody and detected by flow cytometry. **(E)** IFNγ ELISPOT assay was performed to quantify antigen specific responses at day 26. $5x10^5$ splenocytes were cultured for 24 hours in the presence of culture media (unstimulated), DMSO (vehicle), or 10 uM of PBK_{11-20}, PBK_{72-80} or AH1 peptides. IFNγ spots were imaged and quantified using an automatic plate-scanner. **(F)** intracellular cytokine staining was performed to quantify antigen specific CD8+ T cell response. $1x10^6$ splenocytes were stimulated with culture media (unstimulated), DMSO (vehicle), or 10 uM of PBK_{11-20} or PBK_{72-80} peptides. The percentage of IFNγ + CD8+ T cells was evaluated by flow cytometry. **(G)** IFNγ+ CD8+ T cells were further evaluated for PD1 expression by flow cytometry. Mean ±SD. 2-way ANOVA. $p < 0.05$ = *

4.3 Discussion

In this chapter, we conducted the validation of tumor antigens, and subsequently employed them as targets in a prime-boost immunotherapy. For the first time, this study identified the endogenous tumor antigen PBK in the sarcoma cell lines K7M2 and WEHI-164 and assessed the immunogenicity and therapeutic efficacy of a novel PBK targeted prime-boost immunotherapy.

4.3.1 Murine sarcoma antigens

The development of antigen-targeted immunotherapies has been limited by the need for immunogenic endogenous murine tumor antigens. We assessed the immunogenicity of two murine antigens AH1 and PBK, and found that AH1 is immunogenic in K7M2 and WEHI-164. Additionally, we demonstrated the expression of PBK across several murine sarcoma cell lines and showed that a PBK-specific antigen response can protect against K7M2 tumor growth. Furthermore, PBK has been shown to have oncogenic properties in many human cancer subtypes and is relatively highly expressed in most cancers compared to normal healthy tissue, highlighting its potential as a relevant antigen to target.[288] To the best of our knowledge, there has been no reported use of PBK as an immunotherapeutic target in clinical settings. Although one pre-clinical study has reported PBK as an antigenic target in B16 melanoma, this study used a H-2K^{d} restricted PBK epitope in a poly-epitope vaccine and did not specifically investigate the immunogenicity or effectiveness of PBK targeting alone. In contrast, we employed a truncated PBK protein as an antigen, conserving the most immunodominant epitopes while removing a nuclear localization signal. This approach enables the induction of a CD8+ and CD4+ T cell responses, in turn generating a much broader antigen specific response. Altogether, these findings provide new antigenic targets to employ in pre-clinical studies that will drive the development of novel immunotherapies.

4.3.2 DEC205 antibodies

The objective of this study was to employ newly identified antigens in a DEC205 prime and ORV boost immunotherapy; however, a key limitation was the generation of DC-targeting antibodies. To overcome this issue, we evaluated the efficacy of reduced dosing of DEC205, and of single chain DEC205 (Appendix I) - both methods were shown to be alternative options to DEC205-OVA vaccine strategy demonstrated in Chapter 2 when boosted with VSVΔ51.

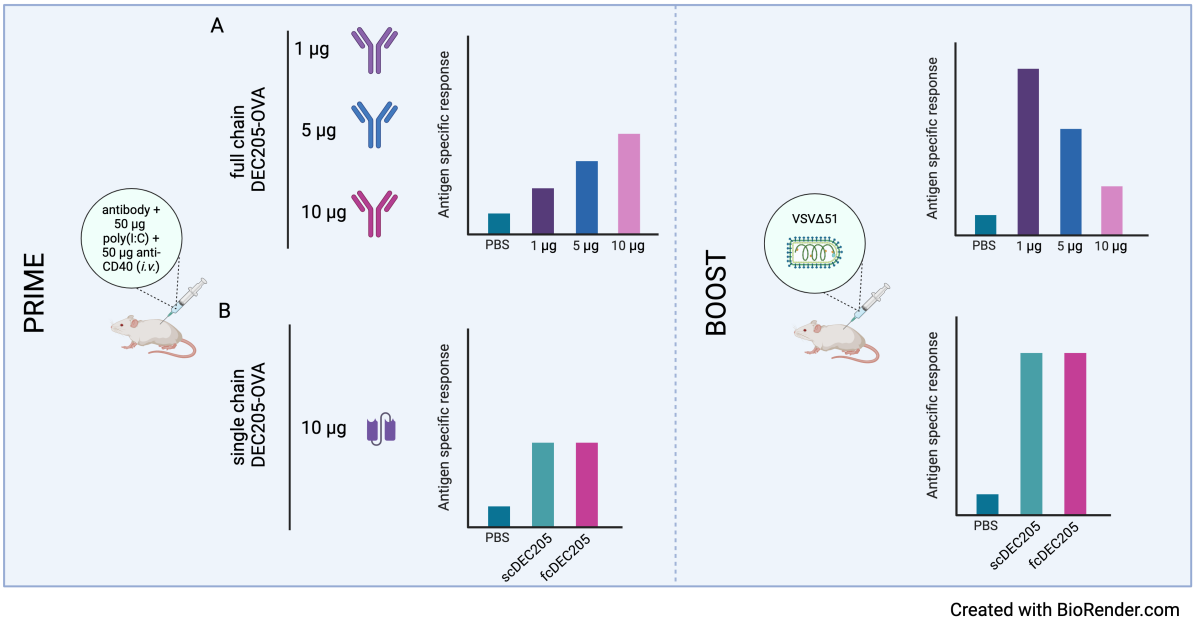

Figure 4.14 Summary of DEC205 targeting approaches evaluated in Chapter 3. (A) Dose escalation study. Antigen specific responses were evaluated following administration of 1ug, 5 ug and 10 ug of full chain DEC205-OVA as well as following VSV51 boost. Antigen specific responses were strongest in the 10ug group following prime, and highest in group receiving 1 ug following boost. **(B)** Single chain (sc) vs full chain (fc) DEC205. Antigen specific responses were evaluated after administration of 10ug of full chain or single chain OVA. Antigen specific responses were equivalent following prime and boost.

Despite our efforts to produce antibodies conjugated to target antigens, we demonstrated low or no yield of DEC205 antibodies conjugated to AH1 or PBK, or of DCIR-OVA (Appendix I) compared to DEC205-OVA and DEC205-empty. Indeed, we observed antibody clusters or aggregates within cells transfected with DEC205-OVA and DEC205-PBK, which may have contributed to the overall low antibody yield. To address this limitation, methods that can predict protein folding and

potential protein-protein interactions within the cell would be highly valuable in determining the efficacy of secretion of a given DEC205-antigen conjugate. Such programs would enable more rapid redirection to alternative antigens, leading to an overall acceleration of DEC205 antibody development. Nevertheless, DEC205 remains a promising vaccine vector, as evidenced by its ability to generate strong antigen-specific responses in clinical trials.[118]

4.3.3 MVA as a prime and boost vector

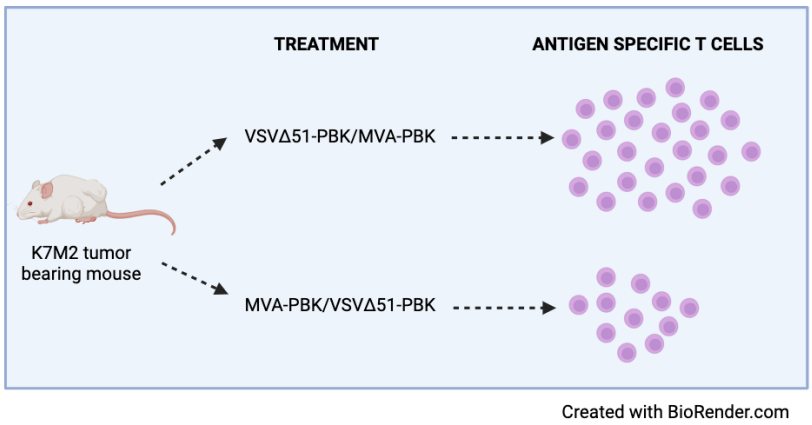

Figure 4.15 Schematic overview of immune response following prime-boost vaccination. Evaluation of PBK specific T cell responses after treatment of K7M2 tumor bearing BALB/c mice with prime/boost combination revealed that VSVΔ51/MVA-PBK generates a larger antigen specific T cell response.

In this study, we presented for the first time the effective combination of MVA and an oncolytic rhabdovirus in a prime-boost immunotherapy for the treatment of cancer. While MVA has been extensively explored as a vaccine vector for efficient antigen delivery, its use as a standalone therapy or in combination with other vectors has not yet been approved for cancer treatment. We hypothesize that the oncolytic properties of VSVΔ51 and its antigen delivery capabilities significantly enhance the antitumor response in ways that prime-boost vaccination approaches employing combinations of MVA with non-oncolytic adenovirus or DNA vaccines cannot achieve.

Although MVA is typically used as an effective boosting vector, our results demonstrate that both prime-boost combinations of MVA and VSVΔ51 generate similar magnitudes of antigen specific responses in naïve mice, and slow tumor growth when administered prophylactically to K7M2

challenge. However, we observed differences in the magnitude of the immune response when evaluating alternate prime-boost combinations in K7M2 tumor-bearing mice; our data show that VSVΔ51/MVA generates a more robust antigen response than MVA/ VSVΔ51. One explanation for this observation is that MVA, when used as a prime, may not break tumor immune tolerance, rendering boosting with VSVΔ51 less effective. Additionally, our data suggest that priming with VSVΔ51 generates a more robust response to additional tumor antigens (gp70) compared to MVA; this is rational since OVs can enhance anti-tumor immunity and release novel antigen through oncolysis, whereas MVA does not share these oncolytic properties. However, once VSVΔ51 is used as a boost, this antigen spreading effect is lost, possibly because of the development of immune resistance mechanisms between the prime and boost immunization.

Despite generating an antigen specific response, our evaluation of VSVΔ51/MVA in K7M2 tumor-bearing mice did not demonstrate therapeutic efficacy. Future studies evaluating different dosing schedules may be considered. We do not predict that increasing the boosting dose of MVA will generate a more substantial immune response. In human trials, the dose administered intramuscularly is between $1x10^8$ to $4x10^8$ infectious units (ClinicalTrials.gov: NCT0224087, NCT04491955, NCT04711356), whereas our study employed $1x10^7$ in mice, (approximately 100x the dose per kg used in human studies). Administration of a subsequent MVA boost may be of benefit, and this approach is being evaluated in a clinical trial of a heterologous prime-boost Ebola virus vaccine employing two doses of MVA as a boost.[17] Furthermore, evidence of immune checkpoint expression in K7M2 tumors (Supplemental Figure 4D), in addition to our data showing increased expression of PD1 on antigen-specific T cells (Figure 4.8F, 4.15G), provides a rationale for combination of ICB with prime-boost therapy.[289] The efficacy of combining OVs with CPI has been clearly demonstrated in pre-clinical studies,[290] and evaluation of this combination regimen is currently ongoing in over 15 clinical trials.[291] Notably, VSV expressing human IFN-β and sodium iodide symporter in combination with pembrolizumab is being evaluated in Phase I trials for solid tumors (ClinicalTrials.gov:

NCT02923466) or non-small-cell lung carcinoma (ClinicalTrials.gov: NCT03647163), no data has yet been published.

4.3.4 Impact of tumor histopathology and mutational burden on immunotherapy outcome

The results of our study highlight the heterogeneity of responses to immunotherapy among different sarcoma models. While we demonstrated that targeting PBK prophylactically provides protection against K7M2, we did not observe similar efficacy against WEHI-164. Several factors may contribute to this outcome. Firstly, the WEHI-164 cell line is a 3-methylcholanthrene (MCA) induced fibrosarcoma; MCA-induced sarcomas exhibit a high mutational burden.[292] Although tumor mutational burden (TMB) has been established as a predictive biomarker for pembrolizumab immunotherapy in solid tumors, this may not apply to prime-boost immunotherapy driven by the generation of an immune response against a single tumor antigen. Additionally, an increased number of neoantigens due to high mutational burden may lead to antigen immunodominance that may affect the outcome of therapy.[293] Immunodominance is the phenomenon where only a selection of T cell epitopes capable of eliciting an immune response will generate an immune response – several mechanisms of immunodominance have been described.[294] In the context of a highly mutated tumor, an abundance of epitopes creates competition for epitope binding to MHC-I, leading to an immune response against dominant epitopes that bind to MHC with the highest stability. This has been shown in a model of adenocarcinoma, where CD8+ T cell expansion is predominantly driven by antigens that most stably bind to MHC.[295] Mass spectrometry-based identification of MHC-associated peptides is used to detect the peptide landscape of tumors, this approach could be employed for the identification of immunogenic peptides presented by WEHI-164 to determine whether PBK is an immunodominant antigen in this cell line.

Another potential explanation for the different responses observed between WEHI-164 and K7M2 cell lines has been outlined in a study by Wedekind *et al.*[289] This study investigated the efficacy of combination oncovirotherapy and immune checkpoint inhibition in osteosarcoma models F420 and

K7M2, which demonstrated similar permissiveness to OV infection and levels of PD-L1 expression. Interestingly, while the F420 models did not respond to therapy, the K7M2 osteosarcoma showed prolonged survival in response to treatment. Comparison of RNAseq data of these two tumor models revealed no significant differences in mutational burden and in predicted MHC-I epitopes. Instead, the study identified three murine endogenous retrovirus genes, including gp70, that are highly overexpressed in K7M2 but not F420, suggesting that retroviral proteins are targets of anti-tumor immunity. RNA sequencing of WEHI-164 would delineate whether endogenous retrovirus genes are highly expressed. A final consideration is that the therapy outcome will largely be dictated by tissue histology, irrespective of the antigen expression level.

4.3.6 Characterization of pre-existing antigen specific responses in cancer patients

Cancer immunotherapy relies on the activation of naïve or boosting pre-existing tumor- specific cytotoxic CD8+ T cells in patients, achieved by various vaccination strategies. Profiling of existing antigen-specific T cells within patient peripheral blood mononuclear cells (PBMCs) serves as a predictive measure of a patient's ability to elicit an antigen-specific response following administration of an antigen targeted immunotherapy. This approach has been performed by several groups who detected MAGE-A3 T cells in the PBMCs of cancer patients using tetramer staining.[296,297] Within the scope of or study, our objective was to investigate PBK-specific T cell responses in sarcoma patients. Given the lack of commercially available PBK tetramers, we evaluated antigen specific responses by ELISPOT and flow cytometry following PBMC stimulation with an overlapping pool of PBK peptides. We identified four patient tumors that demonstrated PBK expression and for which we possessed high quality PBCMs, and evaluated PBK specific responses. Unfortunately, our methodology did not yield observable outcomes (data not shown). It is important to note that the absence of detectable signals using our methodologies does not imply their absence altogether. Further refinement of these methods is imperative, given the limited availability of rare and invaluable samples, and will be an indicator of the potential of a PBK targeted immunotherapy.

4.3.5 Concluding Remarks

Throughout this study, we systematically evaluated various prime and boost vector combinations and introduced a novel immunogenic murine sarcoma antigen that holds promise as a target for pre-clinical studies. Our results demonstrate that, while promising in some contexts, fusion antibody approaches targeting DEC205 or other DC receptors (e.g. DCIR; Appendix I) can suffer from major production issues that are not yet easily predictable or overcome. In such contexts, reducing the dose of the full-chain DEC205 antibody or utilizing a single-chain DEC205 in combination with an oncolytic rhabdovirus boost, can provide strategies to generate robust antigen-specific T-cell immune responses regardless. While oncolytic rhabdoviruses are viable boosting candidates for prime-boost immunotherapy regimens, we extensively explored the use of modified vaccinia Ankara (MVA) as an alternative. Our studies established its effectiveness as a potent boost when combined with VSVΔ51 as a prime. Finally, we successfully employed a novel sarcoma tumor antigen as a target of our prime-boost immunotherapy. Within the limitations of mouse models, our findings indicate that prophylactic PBK targeted prime-boost vaccination can generate a humoral and cellular antigen specific response, and effectively slow the growth of at least some tumors, as exemplified by K7M2.

4.4 Materials and Methods

4.4.1 Cell lines

K7M2 (ATCC cat CRL-2836), S180 (ATCC cat TIB-66), CT26WT (ATCC cat CRL-2638) and NTERA-2 (ATCC cat CRL-1973) were cultured in Dulbecco's Modified Eagle's Medium (DMEM) supplemented with 10% fetal bovine serum (FBS) and 5% penicillin/streptomycin. WEHI-164 (ATCC cat CRL-1751) were cultured in RMPI-1640 Medium supplemented with 10% FBS and 5% penicillin/streptomycin. 76-9 cells were kindly gifted by Dr. Martin Holcik (University of Ottawa) and were cultured in Roswell Park Memorial Institute (Hyclone) supplemented with 15% fetal bovine serum, 5% penicillin/streptomycin, 1M HEPES buffer, and 50uM β-mercaptoethanol. Human embryonic kidney cells (HEK) 293T cells used for antibody production were kindly donated by the Oncolytic Virus Manufacturing Facility (OVMF, Ottawa, Canada). HEK293T cells were cultured in DMEM supplemented with 10% ultra-low IgG FBS, 5% penicillin/streptomycin, and 5% L-glutamine. All cells were incubated at 37C in a 5% CO2 humidified incubator. Cells were regularly tested for mycoplasma contamination by Hoechts staining.

4.4.2 Mice

Six- to eight-week-old BALB/c mice were purchased from Charles River. All animals were handled in strict accordance with good animal practice and approved by an appropriate committee in collaboration with the Office of Animal Ethics and Compliance.

4.4.3 Peptides

The following peptides were custom synthesized JPT Peptide Technologies (>90% purity): MVA-E3$_{140}$ (VGPSNSPTF), MVA-C6$_{74}$ (SFIRSLQNI), PBK$_{188}$ (YYAALGTRPSI), PBK$_{72}$ (KYLHQEKKL), PBK$_{53}$ (SPFLAAVIL), PBK$_{11}$ (HPNIIGYHAF). VSV-N (MPYLIDFGL) and OVA derived SIINFEKL were custom synthesized by CanPeptide (>98% purity). The H-2L^{d} restricted gp70 derived AH1 peptide (SPSYVYHQF) was purchased from MBL International (cat SPM521).

4.4.4 Cloning antigens into DEC205-antibody

The pcDNA plasmids expressing the heavy chain anti-DEC205-OVA, heavy chain anti-DEC205-empty, light chain DEC- kappa sequences were provided by Dr. Silvia Boscardin (University of Sao Paulo). Anti-DEC-205-AHI was generated by PCR amplification from K7M2 using nested primers: forward 1: CTCGAGGAGTTCGGTAGGTTCATGCTTAATCTTACCACTGATTACTGTGTAC, forward 2: GGGTTTGCTAGCGACATGGCCAAGAAGGAGACAGTCTGGAGGCTCGAGGAGTTCGGTAGGTTC, and reverse: GGGTTTGCGGCCGCTTAGCCGAGCAAGAGAGCGAGTGTGAGGGAGACAGGTTCCCGTTT Anti-DEC205-PBK was generated by PCR amplification of PBK from K7M2 using the following primers nested primers; forward 1: CTGGAGGCTCGAGGAGTTCGGTAGGTTCATGAAGCTAAGATTTAAA, forward 2: GGGTTTGCTAGCGACATGGCCAAGAAGGAGACAGTCTGGAGGCTCGAGGAG and reverse: GGGTTTGCGGCCGCAATGACCTTTCTGGTAGGATTCATCCAGCTCT. PCR amplicons were digested using NheI and NotI restriction enzymes and inserted into pcDNA-DEC205-OVA after removing the OVA sequence by restriction digest. Positive clones were screened by colony PCR, restriction digestion mapping, and verified by sequencing.

4.4.5 Full chain and single chain DEC205 antibody production

The pcDNA plasmids expressing the heavy-chain aDEC205-OVA, aDEC205-empty, aDEC205-AH1, aDEC205-PBK, single-chain aDEC205-OVA and light-chain DEC205-kapa sequences were individually transformed in competent DH5-a, and DNA was purified using the QIAGEN Plasmid Maxi Kit (cat 12165). Antibodies were purified as previously described.[184] Briefly, 90% of confluent HEK293T cells in 150mm tissue culture dishes were co-transfected with the light chain and heavy chain plasmids. Six days post-transfection, culture supernatant was collected, and the

antibody was isolated by immunoprecipitation using Protein G Sepharose 4 Fast Flow (Cytiva, cat 17-0618-01) Single chain DEC205-OVA antibody was isolated from culture supernatant using rProtein A Sepharose Fast Flow beads (GE Healthcare, cat 17-1279-01)

4.4.6 VSVΔ51 cloning

The AH1 epitope was PCR amplified from pcDNA expressing aDEC-205-AH1 using the following primers, forward primer: GATATCACGCTCGAGCCACCATGCTTAATCT, reverse primer: AGAATCTGGCTAGCTTAGCCGAGCAAGAGAGCGA. The PBK epitope was PCR amplified from K7M2 using the following primers, forward primer: GTGCTCGAGATGGAAGGAATTAATAATTTCAAGAC, reverse primer: GTGGCTAGCTTAATGCTTTGAGCTTAGACCACAAC. The PCR amplicons were digested by XhoI and NheI and cloned into the multiple cloning site (MCS) of pBSSK-VSVΔ51-GFP after removing GFP. Positive clones were screened by colony PCR, restriction digestion mapping and verified by sequencing.

4.4.7 Oncolytic rhabdovirus rescue and purification

Recombinant VSVΔ51-AH1 and VSVΔ51-PBK were rescued and purified using previously described methods.[185] 50-70% confluent 293T cells were infected with an MOI 0.05 of T7 Vaccinia virus for 1.5 hours; after infection, the media was replaced and cells were transfected with the following plasmids; 1μg VSV-N, 0.25 μg VSV-L, 1.25 μg VSV-P, and 2μg VSV-antigen in Optimem and lipofectamine 2000. After 48 hours, the supernatant was filtered through a 0.2 uM filter unit and transferred to a new plate of Vero cells. Once cytopathic effects were observed, cell supernatant was collected and filtered. To plaque purify virus, Vero cells were infected with filtered supernatant for 1 hour, the virus was removed from cells and cells were overlaid with a 1:1 mixture of 1% agarose: 2x high glucose DMEM. Once plaques formed, isolated plaques were picked and used to infect Vero cells as described. The final plaque purified virus was grown on Vero cells in a T175 roller bottle, and purified on 5-50% Optiprep gradient. The final virus titer was quantified using plaque assay.

4.4.8 Plaque assay for VSVΔ51 titers

Vero cells were seeded in 12 well plates at a density of 2.5 x 10^5 cells in 1 mL. 24 hours later, a 10-fold serial dilution of the virus was performed, and each dilution was plated in duplicate. 500 uL of virus dilutions 5 to10 were plated and incubated for 60 minutes. After 60 minutes, the virus was aspirated from wells and infected Vero cells were overlaid 1:1 mixture of 1% agarose: 2x high glucose DMEM. To quantify titer, plaques were fixed, stained with Coomassie Blue, and counted. The final titer was determined by averaging titers for each dilution where plaques were countable.

4.4.10 Mouse immunizations and tumor models

Tumor models: K7M2 and WEHI-164 tumors were established in 8-week-old female BALB/c mice by s.c. Injection of 1x106 cells in 100uL of PBS, or in a 1:1 ratio of 50 uL cells and 50uL Geltrex™ LDEV-Free Reduced Growth Factor Basement Membrane Matrix (ThermoFisher, cat A1413201). Tumor growth was monitored and measured using a digital caliper.

Irradiated and Infected cell vaccine (ICV): For the irradiated cell vaccine administered as a prime CT26WT, K7M2 or WEHI-164 cells were harvested and 3x10^7 cells in 300 uL of PBS were g-irradiated for 60Gy. After irradiation, one volume of PBS was added to the cells. Mice were administered 5x10^6 cells in 100uL intraperitoneally (i.p.). For the infected cell vaccine as a boost, cells were irradiated as described above and infected with an MOI 10 of VSVΔ51-GFP in one volume of PBS. Cells were left rotating at 37°C for 2 hours. Mice were administered 5x10^6 cells in 100 uL I.p. The boosting dose of ICV was administered 14 days post-prime.

Anti-DEC205-OVA prime, VSVΔ51-OVA boost immunization: 1, 5 or 10μg aDEC205 was injected in combination with 50μg poly (I:C) (InVivoGen, cat tlrl-pic) and 50μg anti-CD40 ligand (Leinco, clone FGK45 cat C2825) in 100 uL PBS i.v. VSVΔ51-OVA (10^8 PFU) was administered I.v. in 50 uL of PBS.

MVA-PBK/VSVΔ51-PBK prime-boost: MVA-PBK (10^7 PFU) in 100uL of PBS was administered by bilateral intramuscular (I.m.) injection. 50uL of the solution was injected into each hind leg. VSVΔ51-PBK (10^8 PFU) was administered I.v. in 50 uL of PBS.

4.4.11 Multi-Step Growth Curve

A multi-step growth curve was performed to compare the viral kinetics of newly purified VSVΔ51 viruses compared to VSVΔ51-GFP. $5x10^5$ Vero cells in a 6-well plate were infected with an MOI of 0.01 per well. Cell supernatant was collected at ours 0, 12, 24, 36, 48 and 72 post-infection. Samples were spun down to remove any cell debris, and tittered by plaque assay.

4.4.12 ImmunoBlotting

For verification of antibody production, 50uL of the sample was run on a Mini-PROTEAN TGX Stain-Free Gel (Bio Rad, cat 4568084) under reducing conditions using β-mercaptoethanol. Protein was transferred to a nitrocellulose membrane using a Trans-Blot Turbo Transfer System (BioRad cat 1704150). The membrane was blocked with 5% BSA in 0.1% TBS-Tween20 (T) and probed with goat anti-mouse peroxidase-conjugated antibody (1:2000). To detect PBK expression, 50uL of cell lysate was run on a gel in reducing conditions using dithiothreitol (DTT). Protein was transferred to a nitrocellulose membrane using a Trans-Blot Turbo Transfer System (BioRad cat 1704150); the membrane was blocked with 5% BSA in 0.1 % TBS-T and probed with anti-PBK primary antibody (ThermoFisher Scientific, cat PA5-79786) overnight at 4°C. The membrane was washed with TBS-T and a goat anti-mouse peroxidase-conjugated antibody (1:2000) was added as the secondary antibody. Bands were visualized using the Clarity™ Western ECL Substrate (BioRad, cat 170-5061) and imaged using the BioRad ChemiDoc Imaging System.

4.4.13 Tissue processing

Antigen-specific T-cell responses were measured in the spleen. Spleens were excised from immunized mice in sterile conditions. Splenocytes were filtered through a 100uM cell strainer, and red

blood cells were lysed using ACK lysis buffer. Cells were stained with Trypan blue and counted using a hematocytometer. To assess tumor immune infiltrate, tumors were isolated from sacrificed mice in sterile conditions. Tumors were dissociated using the Tumor Dissociation Kit-mouse (Miltenyi, cat 130-096-730) according to the manufacturer's instructions. To assess circulating immune cells, blood was collected by saphenous bleed using glass capillary tubes and centrifuged in a hematocrit centrifuge. The buffy coat was collected, and red blood cells were lysed with ACK buffer when required. Cells were washed with FACs buffer and stained for flow cytometry. Mouse serum was isolated from blood collected by saphenous bleed using Microvette® 200 Z-gel tubes (Sarstedt cat 20.1291). Approximately 100 uL of blood was collected, and tubes were centrifuged for 20 minutes at 14,000 RPM. Serum was collected and stored at –80C.

4.4.14 In vivo CTL assay

In vivo CTL assays were performed following immunization. Naïve BALB/c mice were sacrificed, and their spleens were excised in sterile conditions. Splenocytes were collected and stained with either 0.5 uM ($CFSE_{LO}$) or 5 uM ($CFSE_{HI}$) of CFSE. $CFSE_{HI}$ cells were pulsed with 5um of peptide. $CFSE_{HI}$ and $CFSE_{LO}$ cells were mixed in a 1:1 ratio, and a total of $2x10^7$ cells in 100 uL of PBS were transferred intravenously via the tail vein to immunized mice. Mice were euthanized 18 hours post transfer of CFSE labelled cells, and spleens were excised and splenocytes isolated. The proportion of $CFSE_{LO}$ to $CFSE_{HI}$ cells was determined by flow cytometry.

4.4.15 Peptide stimulation for Intracellular cytokine staining (ICS)

Antigen-specific T-cell responses were measured by ICS. $1x10^6$ splenocytes were stimulated with 10 uM of each peptide for 24 hours. BD Golgi Plug Protein Transport Inhibitor (0.2uL per sample) (BD BioSCiences, cat 51-2301KZ) was added to the stimulation for the final 6 hours. As a positive control, a Cell Activation Cocktail (without Brefeldin A) (BioLegend, cat 423301), diluted 1:500 was

added to cells for the final 6 hours of stimulation. After stimulation, the cells were washed and stained for flow cytometry.

4.4.16 Enzyme-linked ImmunoSpot (ELISPOT)

ELISPOT was performed using Mouse IFNγ Single-Color ELISPOT (Cellular Technology Limited, mIFNγp-2M) according to the manufacturer's instructions. Briefly, $2.5x10^5$ splenocytes diluted in 200 uL CTL-Test medium and were cultured overnight at 37°C in the presence of peptide. For peptide stimulation, 10uM of peptide was added to splenocytes and cultured for 24 hours. Cell Stimulation Cocktail (BioLegend, cat 423301) was added as a positive control for 6 hours. The plate was developed following the manufacturer's instructions, and spots were counted using a CTL Immunospot ® Analyzer.

4.4.17 Flow Cytometry

Tetramer staining: Cells were stained with 3uL of H-$2K^b$-SIINFEKL pentamer-APC (Proimmune) in 50 uL of FACS buffer and incubated for 10 minutes at room temperature in the dark. Cells were washed twice with FACS buffer and stained with fixable viability dye for 30 minutes at 4°C. Cells were washed with FACS buffer and incubated with anti-CD16/32 in FACS for 5 minutes at 4°C. Next, cells were stained with anti-CD8-PE-CF594 and anti-CD3-AF700 for 30 minutes at 4°C. For further memory phenotyping, cells were stained with anti-CD62L-FITC and anti-CD128-PeCy7.

Serum antibody binding assay: $2.5x10^5$ K7M2 cells were incubated with mouse sera diluted 1:100 for 60 minutes. Bound antibody was detected using anti-IgG-APC as secondary antibodies followed by flow cytometry.

For all other staining:

Following tissue processing, single cell suspensions were stained with fixable viability stain 510 (BD Horizon, 564406) in PBS for 15 minutes at room temperature. Cells were washed with 0.5% BSA in PBS (FACS buffer) and incubated with anti-CD16/32 (BD Biosciences, cat 553142) in FACs for 5

minutes at 4°C. Following a wash, cells were stained for 30 minutes, at 4°C covered from light, using the following protocols:

MHC-II staining of WEHI-164 and K7M2: $5x10^5$ K7M2 and WEHI-164 were stained with anti-H-$2L^d$ and anti-H-$2K^d$.

ICS: $1x10^6$ Cells were stained for cell surface markers for 30 minutes at 4°C. Cells were washed twice with FACs buffer. Next, cells were permeabilized using the mouse Cytofix/Cytoperm Plus kit (BD Biosciences, cat 555028) as per the manufacturer's instructions. Following permeabilization, cells were incubated in antibodies to detect intracellular cytokines for 30 minutes at 4°C. The following antibody panels were used: anti-CD3-APC-Cy7 (BD Biosciences, cat 560590), anti-CD4-V450 (BD Horizon, cat 560468), anti-CD8-FITC (BD Pharmingen, cat 553031), anti-CD69-BV605 (BD Horizon, cat 563290) anti-IFNγ-APC (Invitrogen, cat 17-7311-82); **OR** anti-CD3-AF700 (BD Pharmingen, cat 557984), anti-CD8-PE-CF594 (BD Horizon, cat 562283), anti-IFNγ-BV650 (BD Biosciences, cat 563854), anti-TNFα-AF647 (BD Pharmingen, cat 557730) ; OR anti-CD3-AF700 (BD Pharmingen, cat 557984), anti-CD8-PE-CF594 (BD Horizon, cat 562283), anti-CD25-PE (Invitrogen, 12-0251-82), anti-CD69-BV605 (BD Horizon, cat 563290), anti-PD1-BV785 (BioLegend, 135225), anti-IFNγ-BV421 (BD Horizon, 563376), anti-TNFα-AF647 (BD Pharmingen, cat 557730).

Tumor Immune Profiling of TILs: $1x10^6$ cells were stained with anti-CD45-BV786 (BD Horizon, cat 564225), anti-CD3-AF700 (BD Pharmingen, cat 557984), anti-CD4-V450 (BD Horizon, cat 560468), anti-CD8-PerCpCy5.5 (BD Pharmingen, cat 551162), anti-CD25-PE (Invitrogen, 12-0251-82), anti-CD127-PeCy7 (BD Pharmingen, cat 552543), anti-CD44-BV711 (BioLegend, cat 103057), anti-CD62L-FITC (BD Pharmingen, cat 561917), anti-NKp46-APC (BioLegend, cat 137608), anti-PD1-APC-Cy7 (BioLegend, cat 135223), anti-CD69-BV605 BV605 (BD Horizon, cat 563290).

Tumor Immune Profiling of DCs, macrophages and B cells: $1x10^6$ cells were stained with anti-CD45-BV786 (BD Horizon, cat 564225), anti-CD11b-APC-Cy7 (BioLegend, cat 101226), anti-CD11c-PE (BD Pharmingen, cat 553802), anti-F4/80-AF647 (BD Pharmingen, cat 565853), anti-CD86-APCR700

(BD Horizon, cat 565479), anti-IA/IE(MHC-II)-BV605 (BD Horizon, cat 563413), anti-CD19-FITC (BD Biosciences, cat 553785), anti-CD138-BV711 (BioLegend, cat 142519), anti-PD-L1-PECy7 (BioLegend, cat 124313)

Circulating T cells: Cells isolated from 75uL of blood were stained with anti-CD45-BV786 (BD Horizon, cat 564225), anti-CD3-AF700 (BD Pharmingen, cat 557984), anti-CD4-V450 anti-CD4-V450 (BD Horizon, cat 560468), anti-CD8-PerCpCy5.5 (BD Pharmingen, cat 551162), anti-CD25-PE (Invitrogen, 12-0251-82), anti-CD127-PeCy7 (BD Pharmingen, cat 552543), anti-CD44-BV711 (BioLegend, cat 103057), anti-CD62L-FITC (BD Pharmingen, cat 561917), anti-CD49b-APC (BioLegend, cat 108909) anti-PD1-APC-Cy7 (BioLegend, cat 135223), anti-CD69-BV605 (BD Horizon, cat 563290)

Circulating DCs, macrophages, and B cells: Cells isolated from 75uL of blood were stained with anti-CD45-BV786 (BD Horizon, cat 564225), anti-CD11b-APC-Cy7 (BioLegend, cat 101226), anti-CD11c-PE (BD Pharmingen, cat 553802), anti-F4/80-AF647 (BD Pharmingen, cat 565853), anti-CD86-APCR700 (BD Horizon, cat 565479), anti-IA/IE(MHC-II)-BV605 (BD Horizon, cat 563413), anti-CD19-FITC (BD Biosciences, cat 553785)

After staining, cells were washed with FACs buffer and fixed in 1% paraformaldehyde. Cells were acquired on Becton Dickinson (BD) flow cytometry (Fortessa), and analysis was performed using FlowJo software v10.

4.4.18 Immunofluorescent Staining

HEK293T cells were seeded on coverslips and transfected with 0.5 μg of pDEC205-OVA and pDEC205-PBK. Cells were permeabilized with Triton-X 100, labelled with anti-IgG secondary antibody, and counterstained with Hoechst stain to detect nuclei.

4.4.19 Statistics

Statistical analysis was performed by GraphPad Prism 9.0. Statistical significance was calculated using one-way ANOVA, or two-way ANOVA. The significance of overall survival studies was calculated using the log-rank (Mantel-Cox) test. Significance is based on a p-value <0.05. Error bars represent standard deviation of the mean.

Chapter 5 – Concluding Remarks

5.1 General Discussion

Sarcoma is a rare tumor with limited treatment options that would benefit from development of novel therapies. From our studies, we propose that a prime-boost vaccination approach can be an effective treatment for sarcoma. In Chapter 2, we conducted a proof-of-concept study evaluating a novel prime-boost combination of aDEC205 prime and an oncolytic rhabdovirus boost targeting the model antigen ovalbumin. Our findings showed that this prime-boost combination generates a robust antigen-specific cellular and humoral immune response. Notably, this response is comparable to the ongoing standard of Ad5 and MG1, which is currently being evaluated in clinical trials. This study established that our novel therapeutic prime-boost approach not only serves as a compelling alternative to Ad5, but it also offers a distinct advantage over the use of Ad5 as a delivery vector. These results pave the way for the further development of this treatment strategy in general, and suggest the possibility of its application for developing sarcoma treatments.

The successful translation of our prime-boost therapy to sarcoma patients relies on the identification of human sarcoma antigens and a comprehensive understanding of the tumor immune microenvironment. Given the heterogeneity of sarcomas, Chapter 3 of this study focused specifically on dedifferentiated liposarcoma, a highly aggressive sarcoma subtype with low survival rates. Through mRNA profiling and immunohistochemistry analysis, we successfully identified PBK as a DDLS tumor antigen. Clinically, PBK has been extensively investigated as an unfavorable prognostic marker in various cancer types, including, but not limited to, breast cancer, prostate cancer, gastric cancer and lung cancer .[298–300] The inhibition of PBK is hypothesized to hold therapeutic potential for patients with PBK expression, offering a promising avenue for targeted therapy. Consequently, potent PBK inhibitors have been identified and studied. However, it is important to note that PBK expression has also been implicated in critical roles during spermatogenesis,[301] suggesting that it may not be the most

suitable target of inhibitors that are systematically administered or that lack tumor specificity. Considering that the testes are devoid of MHC expression, it is worth exploring PBK as a target of immunotherapy strategies. Notably, a study by Lee *et al*. shows that PBK expression is correlated with an increased accumulation of CD8+ T cells, CD4+ T cells, NK cells and M1 macrophages in colon cancer that presented a cytotoxic and inflammatory immune signature, and propose that patients with high PBK expression will response favorably to immunotherapy.[209]

In addition to antigen discovery, immune profiling revealed two distinct immune phenotypes with DDLS tumors; "inflamed" and "non-inflamed." This finding holds implications for both the evaluation of immunotherapies and the development of novel treatments for DDLS. Prior research has consistently demonstrated varying outcomes of immunotherapies based on tumor inflammation. In the context of our immunotherapy that focuses on oncolytic virotherapy, it is important to consider that one of the key mechanisms of action of OVs is their ability to convert a "cold" tumor into a "hot" tumor. This effect plays a vital role in enhancing tumor immunogenicity and promoting an immune response against tumor cells. However, baseline inflamed tumors which are characterised by active immunological pathways may exhibit reduced permissiveness to OV infections. Together, this suggests that OV therapy holds promise as a viable therapy for "cold" tumors, although this is still an area of active research and the specific impacts of OVs on "cold" versus "hot" tumors is context-dependent. However, regardless of inflammation status, we discovered the PBK antigen that was expressed in almost all DDLS samples, emphasizing the need for an approach that effectively treats both inflamed and non-inflamed tumors.

Chapter 4 of this study aimed to assess the efficacy of our prime-boost therapy in murine models, with a specific focus on targeting endogenous tumour antigens. Throughout our investigation, we encountered challenges related to DEC205 antibody production; in an effort to overcome this issue, we aimed to evaluate alternative DC targeting antibodies such as scDEC205 and aDCIR, as well as reduced dosing of aDEC205 (Appendix I). Although reduced dosing of aDEC205 generated a sufficient

antigen-specific response, both scDEC205 and aDCIR faced similar production challenges as aDEC205 (Appendix I). Despite these limitations, it is essential to acknowledge that aDEC205 holds significant potential as a highly effective vaccine vector, provided these limitations are addressed. In addition to DC targeting antibodies, we explored MVA as an alternative antigen delivery vector. We show for the first time, the effective combination of VSVΔ51 prime and MVA boost that generates cellular and humoral antigen specific responses.

The identification of the PBK antigen, expressed across various murine sarcoma types, presents a novel and promising target antigen for evaluating therapies in pre-clinical models. The targeting of this shared antigen opens possibilities for clinical translation of potential therapies, facilitating the development of treatments applicable to a broader patient population. We encourage further investigation of PBK expression in other murine cancer cell lines, as its potential impact could extend beyond murine sarcomas. Despite the limited efficacy of our prime-boost combination within a therapeutic context, combinations with other immunotherapies, such as checkpoint inhibitors or drugs targeting disease-specific factors such as CDK4 inhibitors, warrant further exploration. Overall, immunizing against the PBK antigen generated strong antigen specific responses, suggesting future studies can adapt the novel PBK antigen and explore alternative immunization vectors in combination with other therapies.

In addition, this study highlighted the challenges encountered in the development of an immunotherapy for a rare cancer type. A limitation in our sarcoma murine studies was the absence of well-characterized sarcoma cell lines. This is a significant drawback considering the large heterogeneity observed among sarcomas; this was particularly evident between K7M2 osteosarcoma and WEHI-164 fibrosarcoma. To advance the field, there is a pressing need for well-characterized murine sarcoma cell lines, including a model of DDLS, which was notably absent in our study.

5.2 Conclusion

Immunotherapy has emerged as the pivotal frontier for cancer therapy. While several immunotherapeutic approaches have shown promise for specific malignancies, the progress in developing and applying these therapies for sarcoma has been relatively slow. This study outlines a foundational framework for developing an immunotherapeutic approach tailored to DDLS. We have evaluated diverse vaccine platforms, including DC targeting antibodies, oncolytic viruses (OVs), and viral vectors, within a prime-boost context, successfully eliciting an antigen-specific response. These findings introduce novel prime-boost combinations for cancer immunotherapy. The growing body of research emphasizes that a single immunotherapeutic strategy may fall short in effectively treating heterogeneous malignancies. This underscores the importance of investigating combinatorial approaches, integrating OVS, immune checkpoint inhibitors (ICIs), CAR-T cells, small molecules, and more. This study lays a strong foundation for further research in this promising field.

This study has made contributions to the field of dedifferentiated liposarcoma research—a rare and understudied sarcoma. Our efforts have provided essential insights into the immunological phenotypes and molecular pathways at play in DDLS. Additionally, we have identified immunogenic tumor antigens suitable for assessing antigen-targeted immunotherapies in pre-clinical studies. This expands the limited repertoire of known murine antigens and offers a potential target for clinical vaccine development.

In conclusion, this study established a solid foundation for the development of an antigen targeted prime-boost immunotherapy for sarcoma. It makes significant contributions to the field by identifying a novel antigen, evaluating various antigen delivery vectors, and demonstrating the efficacy of innovative prime/boost combinations.

References

1. Release notice - Canadian Cancer Statistics 2021. *Health Promotion and Chronic Disease Prevention in Canada*. 2021;41(11):399-399. doi:10.24095/hpcdp.41.11.09
2. Hanahan D, Weinberg RA. Review Hallmarks of Cancer : The Next Generation. *Cell*. 2011;144(5):646-674. doi:10.1016/j.cell.2011.02.013
3. Hanahan D. Hallmarks of Cancer: New Dimensions. *Cancer Discov*. 2022;12(1):31-46. doi:10.1158/2159-8290.CD-21-1059
4. *Canadian Cancer Statistics: A 2022 Special Report on Cancer Prevalence*. Accessed May 8, 2023. https://cdn.cancer.ca/-/media/files/research/cancer-statistics/2022-statistics/2022-special-report/2022_prevalence_report_final_en.pdf?rev=7755f9f350e845d58e268a59e3be608e&hash=3F3F30CADD8CAF0049636B5A41EDBB13&_gl=1*3edxkb*_ga*OTM3NDcwNjQxLjE2ODM1NzM4ODI.
5. Statistics Canada. Table 13-10-0111-01 Number and rates of new cases of primary cancer, by cancer type, age group and sex.
6. Üren A, Toretsky JA. Ewing's sarcoma oncoprotein EWS–FLI1: the perfect target without a therapeutic agent. *Future Oncology*. 2005;1(4):521-528. doi:10.2217/14796694.1.4.521
7. Kawaguchi S, Tsukahara T, Ida K, et al. SYT-SSX breakpoint peptide vaccines in patients with synovial sarcoma: A study from the Japanese Musculoskeletal Oncology Group 19. *Cancer Sci*. Published online 2012. doi:10.1111/j.1349-7006.2012.02370.x
8. Kawaguchi S, Wada T, Ida K, et al. Phase I vaccination trial of SYT-SSX junction peptide in patients with disseminated synovial sarcoma. *J Transl Med*. 2005;3(1):1. doi:10.1186/1479-5876-3-1
9. Suminoe A, Matsuzaki A, Hattori H, Koga Y, Hara T. Immunotherapy with autologous dendritic cells and tumor antigens for children with refractory malignant solid tumors. *Pediatr Transplant*. 2009;13(6):746-753. doi:10.1111/j.1399-3046.2008.01066.x
10. Hsu JY, Seligson ND, Hays JL, Miles WO, Chen JL. Clinical Utility of CDK4/6 Inhibitors in Sarcoma: Successes and Future Challenges. *JCO Precis Oncol*. 2022;(6). doi:10.1200/PO.21.00211
11. Voskoboinik I, Whisstock JC, Trapani JA. Perforin and granzymes: function, dysfunction and human pathology. *Nat Rev Immunol*. 2015;15(6):388-400. doi:10.1038/nri3839
12. Wolf NK, Kissiov DU, Raulet DH. Roles of natural killer cells in immunity to cancer, and applications to immunotherapy. *Nat Rev Immunol*. 2023;23(2):90-105. doi:10.1038/s41577-022-00732-1
13. Butcher MJ, Zhu J. Recent advances in understanding the Th1/Th2 effector choice. *Fac Rev*. 2021;10. doi:10.12703/r/10-30
14. Smith KM, Pottage L, Thomas ER, et al. Th1 and Th2 CD4+ T Cells Provide Help for B Cell Clonal Expansion and Antibody Synthesis in a Similar Manner In Vivo. *The Journal of Immunology*. 2000;165(6):3136-3144. doi:10.4049/jimmunol.165.6.3136
15. MANTOVANI A, SICA A, SOZZANI S, ALLAVENA P, VECCHI A, LOCATI M. The chemokine system in diverse forms of macrophage activation and polarization. *Trends Immunol*. 2004;25(12):677-686. doi:10.1016/j.it.2004.09.015
16. Mantovani A, Marchesi F, Malesci A, Laghi L, Allavena P. Tumour-associated macrophages as treatment targets in oncology. *Nat Rev Clin Oncol*. 2017;14(7):399-416. doi:10.1038/nrclinonc.2016.217
17. Li K, Shi H, Zhang B, et al. Myeloid-derived suppressor cells as immunosuppressive regulators and therapeutic targets in cancer. *Signal Transduct Target Ther*. 2021;6(1):362. doi:10.1038/s41392-021-00670-9

18. Sharpe AH, Pauken KE. The diverse functions of the PD1 inhibitory pathway. *Nat Rev Immunol*. 2018;18(3):153-167. doi:10.1038/nri.2017.108
19. Walker LSK. Treg and CTLA-4: Two intertwining pathways to immune tolerance. *J Autoimmun*. 2013;45:49-57. doi:10.1016/j.jaut.2013.06.006
20. Anderson AC, Joller N, Kuchroo VK. Lag-3, Tim-3, and TIGIT: Co-inhibitory Receptors with Specialized Functions in Immune Regulation. *Immunity*. 2016;44(5):989-1004. doi:10.1016/j.immuni.2016.05.001
21. Galon J, Pagès F, Marincola FM, et al. The immune score as a new possible approach for the classification of cancer. *J Transl Med*. 2012;10(1):1. doi:10.1186/1479-5876-10-1
22. Angell HK, Bruni D, Barrett JC, Herbst R, Galon J. The Immunoscore: Colon Cancer and Beyond. *Clinical Cancer Research*. 2020;26(2):332-339. doi:10.1158/1078-0432.CCR-18-1851
23. Roelands J, Kuppen P, Vermeulen L, et al. Immunogenomic Classification of Colorectal Cancer and Therapeutic Implications. *Int J Mol Sci*. 2017;18(10):2229. doi:10.3390/ijms18102229
24. Deng L, Long F, Wang T, et al. Identification of an Immune Classification and Prognostic Genes for Lung Adenocarcinoma Based on Immune Cell Signatures. *Front Med (Lausanne)*. 2022;9. doi:10.3389/fmed.2022.855387
25. Wang T, Li T, Li B, et al. Immunogenomic Landscape in Breast Cancer Reveals Immunotherapeutically Relevant Gene Signatures. *Front Immunol*. 2022;13. doi:10.3389/fimmu.2022.805184
26. Petitprez F, de Reyniès A, Keung EZ, et al. B cells are associated with survival and immunotherapy response in sarcoma. *Nature*. 2020;577(7791):556-560. doi:10.1038/s41586-019-1906-8
27. Danaher P, Warren S, Lu R, et al. Pan-cancer adaptive immune resistance as defined by the Tumor Inflammation Signature (TIS): results from The Cancer Genome Atlas (TCGA). *J Immunother Cancer*. 2018;6(1):63. doi:10.1186/s40425-018-0367-1
28. Zhang L, Conejo-Garcia JR, Katsaros D, et al. Intratumoral T Cells, Recurrence, and Survival in Epithelial Ovarian Cancer. *New England Journal of Medicine*. 2003;348(3):203-213. doi:10.1056/NEJMoa020177
29. Hussein MR. Analysis of the mononuclear inflammatory cell infiltrate in the normal breast, benign proliferative breast disease, in situ and infiltrating ductal breast carcinomas: preliminary observations. *J Clin Pathol*. 2006;59(9):972-977. doi:10.1136/jcp.2005.031252
30. Reiman JM, Kmieciak M, Manjili MH, Knutson KL. Tumor immunoediting and immunosculpting pathways to cancer progression. *Semin Cancer Biol*. 2007;17(4):275-287. doi:10.1016/j.semcancer.2007.06.009
31. Chang CC, Ogino T, Mullins DW, et al. Defective Human Leukocyte Antigen Class I-associated Antigen Presentation Caused by a Novel β2-Microglobulin Loss-of-function in Melanoma Cells. *Journal of Biological Chemistry*. 2006;281(27):18763-18773. doi:10.1074/jbc.M511525200
32. So T, Takenoyama M, Mizukami M, et al. Haplotype Loss of HLA Class I Antigen as an Escape Mechanism from Immune Attack in Lung Cancer. *Cancer Res*. 2005;65(13):5945-5952. doi:10.1158/0008-5472.CAN-04-3787
33. Norell H, Carlsten M, Ohlum T, et al. Frequent Loss of HLA-A2 Expression in Metastasizing Ovarian Carcinomas Associated with Genomic Haplotype Loss and HLA-A2-Restricted HER-2/ neu -Specific Immunity. *Cancer Res*. 2006;66(12):6387-6394. doi:10.1158/0008-5472.CAN-06-0029
34. Romero JM, Aptsiauri N, Vazquez F, et al. Analysis of the expression of HLA class I, proinflammatory cytokines and chemokines in primary tumors from patients with localized

and metastatic renal cell carcinoma. *Tissue Antigens*. 2006;68(4):303-310. doi:10.1111/j.1399-0039.2006.00673.x
35. Cabrera T, Collado A, Fernandez MA, et al. High frequency of altered HLA class I phenotypes in invasive colorectal carcinomas. *Tissue Antigens*. 1998;52(2):114-123. doi:10.1111/j.1399-0039.1998.tb02274.x
36. Taube JM, Anders RA, Young GD, et al. Colocalization of Inflammatory Response with B7-H1 Expression in Human Melanocytic Lesions Supports an Adaptive Resistance Mechanism of Immune Escape. *Sci Transl Med*. 2012;4(127). doi:10.1126/scitranslmed.3003689
37. Lv M, Wang K, Huang X jun. Myeloid-derived suppressor cells in hematological malignancies: friends or foes. *J Hematol Oncol*. 2019;12(1):105. doi:10.1186/s13045-019-0797-3
38. Courau T, Nehar-Belaid D, Florez L, et al. TGF-β and VEGF cooperatively control the immunotolerant tumor environment and the efficacy of cancer immunotherapies. *JCI Insight*. 2016;1(9):e85974-e85974. doi:10.1172/jci.insight.85974
39. Zajac P, Oertli D, Marti W, et al. Phase I/II Clinical Trial of a Nonreplicative Vaccinia Virus Expressing Multiple HLA-A0201-Restricted Tumor-Associated Epitopes and Costimulatory Molecules in Metastatic Melanoma Patients. *Hum Gene Ther*. 2003;14(16):1497-1510. doi:10.1089/104303403322495016
40. Kantoff PW, Schuetz TJ, Blumenstein BA, et al. Overall Survival Analysis of a Phase II Randomized Controlled Trial of a Poxviral-Based PSA-Targeted Immunotherapy in Metastatic Castration-Resistant Prostate Cancer. *Journal of Clinical Oncology*. 2010;28(7):1099-1105. doi:10.1200/JCO.2009.25.0597
41. Gulley JL, Arlen PM, Madan RA, et al. Immunologic and prognostic factors associated with overall survival employing a poxviral-based PSA vaccine in metastatic castrate-resistant prostate cancer. *Cancer Immunology, Immunotherapy*. 2010;59(5):663-674. doi:10.1007/s00262-009-0782-8
42. Quoix E, Lena H, Losonczy G, et al. TG4010 immunotherapy and first-line chemotherapy for advanced non-small-cell lung cancer (TIME): results from the phase 2b part of a randomised, double-blind, placebo-controlled, phase 2b/3 trial. *Lancet Oncol*. 2016;17(2):212-223. doi:10.1016/S1470-2045(15)00483-0
43. Adamina M, Rosenthal R, Weber WP, et al. Intranodal Immunization With a Vaccinia Virus Encoding Multiple Antigenic Epitopes and Costimulatory Molecules in Metastatic Melanoma. *Molecular Therapy*. 2010;18(3):651-659. doi:10.1038/mt.2009.275
44. Lubaroff DM, Williams RD, Vaena D, et al. Abstract 2692: An ongoing Phase II trial of an adenovirus/PSA vaccine for prostate cancer. *Cancer Res*. 2012;72(8_Supplement):2692-2692. doi:10.1158/1538-7445.AM2012-2692
45. PASQUINUCCI G. POSSIBLE EFFECT OF MEASLES ON LEUKqMIA. *The Lancet*. 1971;297(7690):136. doi:10.1016/S0140-6736(71)90869-5
46. Gross S. MEASLES AND LEUKÆMIA. *The Lancet*. 1971;297(7695):397-398. doi:10.1016/S0140-6736(71)92232-X
47. Bluming AvrumZ, Ziegler JohnL. REGRESSION OF BURKITT'S LYMPHOMA IN ASSOCIATION WITH MEASLES INFECTION. *The Lancet*. 1971;298(7715):105-106. doi:10.1016/S0140-6736(71)92086-1
48. De Pace N. Sulla scomparsa di un enorme cancro vegetante del collo dell'utero senza cura chirurgica. Published online 1912.
49. Atherton MJ, Stephenson KB, Tzelepis F, et al. Transforming the prostatic tumor microenvironment with oncolytic virotherapy. *Oncoimmunology*. 2018;7(7). doi:10.1080/2162402X.2018.1445459

50. Breitbach CJ, De Silva NS, Falls TJ, et al. Targeting Tumor Vasculature With an Oncolytic Virus. *Molecular Therapy*. 2011;19(5):886-894. doi:10.1038/mt.2011.26
51. Breitbach CJ, Arulanandam R, De Silva N, et al. Oncolytic Vaccinia Virus Disrupts Tumor-Associated Vasculature in Humans. *Cancer Res*. 2013;73(4):1265-1275. doi:10.1158/0008-5472.CAN-12-2687
52. Arulanandam R, Batenchuk C, Angarita FA, et al. VEGF-Mediated Induction of PRD1-BF1/Blimp1 Expression Sensitizes Tumor Vasculature to Oncolytic Virus Infection. *Cancer Cell*. 2015;28(2):210-224. doi:10.1016/j.ccell.2015.06.009
53. Alluqmani N, Jirovec A, Taha Z, et al. Vanadyl sulfate-enhanced oncolytic virus immunotherapy mediates the antitumor immune response by upregulating the secretion of pro-inflammatory cytokines and chemokines. *Front Immunol*. 2022;13. doi:10.3389/fimmu.2022.1032356
54. Saha D, Martuza RL, Rabkin SD. Macrophage Polarization Contributes to Glioblastoma Eradication by Combination Immunovirotherapy and Immune Checkpoint Blockade. *Cancer Cell*. 2017;32(2):253-267.e5. doi:10.1016/j.ccell.2017.07.006
55. Roth JC, Cassady KA, Cody JJ, et al. Evaluation of the Safety and Biodistribution of M032, an Attenuated Herpes Simplex Virus Type 1 Expressing hIL-12, After Intracerebral Administration to Aotus Nonhuman Primates. *Hum Gene Ther Clin Dev*. 2014;25(1):16-27. doi:10.1089/humc.2013.201
56. Veinalde R, Grossardt C, Hartmann L, et al. Oncolytic measles virus encoding interleukin-12 mediates potent antitumor effects through T cell activation. *Oncoimmunology*. 2017;6(4):e1285992. doi:10.1080/2162402X.2017.1285992
57. Pol JG, Zhang L, Bridle BW, et al. Maraba virus as a potent oncolytic vaccine vector. *Mol Ther*. 2014;22(2):420-429. doi:10.1038/mt.2013.249
58. Pol JG, Acuna SA, Yadollahi B, Tang N, Stephenson KB, Atherton MJ. Preclinical evaluation of a MAGE-A3 vaccination utilizing the oncolytic Maraba virus currently in first-in-human trials. *Oncoimmunology*. 2019;8(1):1-15. doi:10.1080/2162402X.2018.1512329
59. Grandi P, Fernandez J, Szentirmai O, et al. Targeting HSV-1 virions for specific binding to epidermal growth factor receptor-vIII-bearing tumor cells. *Cancer Gene Ther*. 2010;17(9):655-663. doi:10.1038/cgt.2010.22
60. Kopecky SA, Willingham MC, Lyles DS. Matrix Protein and Another Viral Component Contribute to Induction of Apoptosis in Cells Infected with Vesicular Stomatitis Virus. *J Virol*. 2001;75(24):12169 LP - 12181. doi:10.1128/JVI.75.24.12169-12181.2001
61. Cai Z, Lv H, Cao W, et al. Targeting strategies of adenovirus-mediated gene therapy and virotherapy for prostate cancer. *Mol Med Rep*. 2017;16(5):6443-6458. doi:10.3892/mmr.2017.7487
62. Finkelshtein D, Werman A, Novick D, Barak S, Rubinstein M. LDL receptor and its family members serve as the cellular receptors for vesicular stomatitis virus. *Proceedings of the National Academy of Sciences*. 2013;110(18):7306-7311. doi:10.1073/pnas.1214441110
63. Nikolic J, Belot L, Raux H, Legrand P, Gaudin Y, A. Albertini A. Structural basis for the recognition of LDL-receptor family members by VSV glycoprotein. *Nat Commun*. 2018;9(1):1029. doi:10.1038/s41467-018-03432-4
64. Sun X, Roth SL, Bialecki MA, Whittaker GR. Internalization and fusion mechanism of vesicular stomatitis virus and related rhabdoviruses. *Future Virol*. 2010;5(1):85-96. doi:10.2217/fvl.09.72
65. Holzwarth G, Bhandari A, Tommervik L, Macosko JC, Ornelles DA, Lyles DS. Vesicular stomatitis virus nucleocapsids diffuse through cytoplasm by hopping from trap to trap in random directions. *Sci Rep*. 2020;10(1):10643. doi:10.1038/s41598-020-66942-6

66. Clarke DK, Hendry RM, Singh V, et al. Live virus vaccines based on a vesicular stomatitis virus (VSV) backbone: Standardized template with key considerations for a risk/benefit assessment. *Vaccine*. 2016;34(51):6597-6609. doi:10.1016/j.vaccine.2016.06.071
67. Hoff NA, Bratcher A, Kelly JD, et al. Immunogenicity of rVSVΔG-ZEBOV-GP Ebola vaccination in exposed and potentially exposed persons in the Democratic Republic of the Congo. *Proceedings of the National Academy of Sciences*. 2022;119(6). doi:10.1073/pnas.2118895119
68. Henao-Restrepo AM, Camacho A, Longini IM, et al. Efficacy and effectiveness of an rVSV-vectored vaccine in preventing Ebola virus disease: final results from the Guinea ring vaccination, open-label, cluster-randomised trial (Ebola Ça Suffit!). *The Lancet*. 2017;389(10068):505-518. doi:10.1016/S0140-6736(16)32621-6
69. Bridle BW, Boudreau JE, Lichty BD, et al. Vesicular Stomatitis Virus as a Novel Cancer Vaccine Vector to Prime Antitumor Immunity Amenable to Rapid Boosting With Adenovirus. *Molecular Therapy*. 2009;17(10):1814-1821. doi:10.1038/mt.2009.154
70. Das K, Belnoue E, Rossi M, et al. A modular self-adjuvanting cancer vaccine combined with an oncolytic vaccine induces potent antitumor immunity. *Nat Commun*. 2021;12(1):5195. doi:10.1038/s41467-021-25506-6
71. Ahmed M, Puckett S, Lyles DS. Susceptibility of breast cancer cells to an oncolytic matrix (M) protein mutant of vesicular stomatitis virus. *Cancer Gene Ther*. 2010;17(12):883-892. doi:10.1038/cgt.2010.46
72. Le Boeuf F, Niknejad N, Wang J, et al. Sensitivity of cervical carcinoma cells to vesicular stomatitis virus-induced oncolysis: Potential role of human papilloma virus infection. *Int J Cancer*. 2012;131(3):E204-E215. doi:10.1002/ijc.27404
73. Wollmann G, Rogulin V, Simon I, Rose JK, van den Pol AN. Some Attenuated Variants of Vesicular Stomatitis Virus Show Enhanced Oncolytic Activity against Human Glioblastoma Cells relative to Normal Brain Cells. *J Virol*. 2010;84(3):1563-1573. doi:10.1128/JVI.02040-09
74. Wollmann G, Davis JN, Bosenberg MW, van den Pol AN. Vesicular Stomatitis Virus Variants Selectively Infect and Kill Human Melanomas but Not Normal Melanocytes. *J Virol*. 2013;87(12):6644-6659. doi:10.1128/JVI.03311-12
75. Kubo T, Shimose S, Matsuo T, et al. Oncolytic vesicular stomatitis virus administered by isolated limb perfusion suppresses osteosarcoma growth. *Journal of Orthopaedic Research*. 2011;29(5):795-800. doi:10.1002/jor.21307
76. Johnson JE, Nasar F, Coleman JW, et al. Neurovirulence properties of recombinant vesicular stomatitis virus vectors in non-human primates. *Virology*. 2007;360(1):36-49. doi:10.1016/j.virol.2006.10.026
77. Hill C, Carlisle R. Achieving systemic delivery of oncolytic viruses. *Expert Opin Drug Deliv*. 2019;16(6):607-620. doi:10.1080/17425247.2019.1617269
78. Breitbach CJ, Burke J, Jonker D, et al. Intravenous delivery of a multi-mechanistic cancer-targeted oncolytic poxvirus in humans. *Nature*. Published online 2011. doi:10.1038/nature10358
79. Ahmed M, McKenzie MO, Puckett S, Hojnacki M, Poliquin L, Lyles DS. Ability of the Matrix Protein of Vesicular Stomatitis Virus To Suppress Beta Interferon Gene Expression Is Genetically Correlated with the Inhibition of Host RNA and Protein Synthesis. *J Virol*. 2003;77(8):4646-4657. doi:10.1128/JVI.77.8.4646-4657.2003
80. Marquis KA, Becker RL, Weiss AN, Morris MC, Ferran MC. The VSV matrix protein inhibits NF-κB and the interferon response independently in mouse L929 cells. *Virology*. 2020;548:117-123. doi:10.1016/j.virol.2020.06.013

81. Wollmann G, Davis JN, Bosenberg MW, van den Pol AN. Vesicular Stomatitis Virus Variants Selectively Infect and Kill Human Melanomas but Not Normal Melanocytes. *J Virol*. 2013;87(12):6644-6659. doi:10.1128/JVI.03311-12
82. Ahmed M, Cramer SD, Lyles DS. Sensitivity of prostate tumors to wild type and M protein mutant vesicular stomatitis viruses. *Virology*. 2004;330(1):34-49. doi:10.1016/j.virol.2004.08.039
83. Stojdl DF, Lichty BD, TenOever BR, et al. VSV strains with defects in their ability to shutdown innate immunity are potent systemic anti-cancer agents. *Cancer Cell*. 2003;4(4):263-275. doi:10.1016/S1535-6108(03)00241-1
84. Duntsch CD, Zhou Q, Jayakar HR, et al. Recombinant vesicular stomatitis virus vectors as oncolytic agents in the treatment of high-grade gliomas in an organotypic brain tissue slice—glioma coculture model. *J Neurosurg*. 2004;100(6):1049-1059. doi:10.3171/jns.2004.100.6.1049
85. Diaz RM, Galivo F, Kottke T, et al. Oncolytic Immunovirotherapy for Melanoma Using Vesicular Stomatitis Virus. *Cancer Res*. 2007;67(6):2840-2848. doi:10.1158/0008-5472.CAN-06-3974
86. Bridle BW, Stephenson KB, Boudreau JE, et al. Potentiating Cancer Immunotherapy Using an Oncolytic Virus. *Molecular Therapy*. 2010;18(8):1430-1439. doi:10.1038/mt.2010.98
87. Bridle BW, Boudreau JE, Lichty BD, et al. Vesicular Stomatitis Virus as a Novel Cancer Vaccine Vector to Prime Antitumor Immunity Amenable to Rapid Boosting With Adenovirus. *Molecular Therapy*. 2009;17(10):1814-1821. doi:10.1038/mt.2009.154
88. Alajez NM, Mocanu JD, Shi W, et al. Efficacy of Systemically Administered Mutant Vesicular Stomatitis Virus (VSVΔ51) Combined with Radiation for Nasopharyngeal Carcinoma. *Clinical Cancer Research*. 2008;14(15):4891-4897. doi:10.1158/1078-0432.CCR-07-4134
89. Balathasan L, Tang VA, Yadollahi B, et al. Activating Peripheral Innate Immunity Enables Safe and Effective Oncolytic Virotherapy in the Brain. *Mol Ther Oncolytics*. 2017;7:45-56. doi:10.1016/j.omto.2017.09.004
90. Bourgeois-Daigneault MC, Roy DG, Falls T, et al. Oncolytic vesicular stomatitis virus expressing interferon-σ has enhanced therapeutic activity. *Mol Ther Oncolytics*. 2016;3:16001. doi:10.1038/mto.2016.1
91. Alluqmani N, Jirovec A, Taha Z, et al. Vanadyl sulfate-enhanced oncolytic virus immunotherapy mediates the antitumor immune response by upregulating the secretion of pro-inflammatory cytokines and chemokines. *Front Immunol*. 2022;13. doi:10.3389/fimmu.2022.1032356
92. Bastin DJ, Montroy J, Kennedy MA, et al. Safety and efficacy of autologous cell vaccines in solid tumors: a systematic review and meta-analysis of randomized control trials. *Sci Rep*. 2023;13(1):3347. doi:10.1038/s41598-023-29630-9
93. Lemay CG, Rintoul JL, Kus A, et al. Harnessing Oncolytic Virus-mediated Antitumor Immunity in an Infected Cell Vaccine. *Molecular Therapy*. 2012;20(9):1791-1799. doi:10.1038/mt.2012.128
94. Niavarani SR, Lawson C, Boudaud M, Simard C, Tai LH. Oncolytic vesicular stomatitis virus–based cellular vaccine improves triple-negative breast cancer outcome by enhancing natural killer and CD8 + T-cell functionality. *J Immunother Cancer*. 2020;8(1):e000465. doi:10.1136/jitc-2019-000465
95. Brun J, McManus D, Lefebvre C, et al. Identification of Genetically Modified Maraba Virus as an Oncolytic Rhabdovirus. *Molecular Therapy*. 2010;18(8):1440-1449. doi:10.1038/mt.2010.103

96. Le Boeuf F, Selman M, Son HH, et al. Oncolytic Maraba Virus MG1 as a Treatment for Sarcoma. *Int J Cancer*. 2017;141(6):1257-1264. doi:10.1002/ijc.30813
97. McAuliffe J, Chan HF, Noblecourt L, et al. Heterologous prime-boost vaccination targeting MAGE-type antigens promotes tumor T-cell infiltration and improves checkpoint blockade therapy. *J Immunother Cancer*. 2021;9(9):e003218. doi:10.1136/jitc-2021-003218
98. Heery CR, Ibrahim NK, Arlen PM, et al. Docetaxel Alone or in Combination With a Therapeutic Cancer Vaccine (PANVAC) in Patients With Metastatic Breast Cancer. *JAMA Oncol*. 2015;1(8):1087. doi:10.1001/jamaoncol.2015.2736
99. Pollack SM. The potential of the CMB305 vaccine regimen to target NY-ESO-1 and improve outcomes for synovial sarcoma and myxoid/round cell liposarcoma patients. *Expert Rev Vaccines*. 2018;17(2):107-114. doi:10.1080/14760584.2018.1419068
100. Shrimpton RE, Butler M, Morel AS, Eren E, Hue SS, Ritter MA. CD205 (DEC-205): A recognition receptor for apoptotic and necrotic self. *Mol Immunol*. 2009;46(6):1229-1239. doi:10.1016/j.molimm.2008.11.016
101. Cao L, Chang H, Shi X, Peng C, He Y. Keratin mediates the recognition of apoptotic and necrotic cells through dendritic cell receptor DEC205/CD205. *Proceedings of the National Academy of Sciences*. 2016;113(47):13438-13443. doi:10.1073/pnas.1609331113
102. Lahoud MH, Ahmet F, Zhang JG, et al. DEC-205 is a cell surface receptor for CpG oligonucleotides. *Proceedings of the National Academy of Sciences*. 2012;109(40):16270-16275. doi:10.1073/pnas.1208796109
103. Jiang W, Swiggard WJ, Heufler C, et al. The receptor DEC-205 expressed by dendritic cells and thymic epithelial cells is involved in antigen processing. *Nature*. 1995;375(6527):151-155. doi:10.1038/375151a0
104. Gully BS, Venugopal H, Fulcher AJ, et al. The cryo-EM structure of the endocytic receptor DEC-205. *Journal of Biological Chemistry*. 2021;296:100127. doi:10.1074/jbc.RA120.016451
105. Witmer-Pack MD, Swiggard WJ, Mirza A, Inaba K, Steinman RM. Tissue Distribution of the DEC-205 Protein That Is Detected by the Monoclonal Antibody NLDC-145. *Cell Immunol*. 1995;163(1):157-162. doi:10.1006/cimm.1995.1110
106. Kato M, Mcdonald KJ, Khan S, et al. Expression of human DEC-205 (CD205) multilectin receptor on leukocytes. 2006;18(6):857-869. doi:10.1093/intimm/dxl022
107. Kato M, Neil TK, Fearnley DB, McLellan AD, Vuckovic S, Hart DNJ. Expression of multilectin receptors and comparative FITC–dextran uptake by human dendritic cells. *Int Immunol*. 2000;12(11):1511-1519. doi:10.1093/intimm/12.11.1511
108. Mahnke K, Guo M, Lee S, et al. The Dendritic Cell Receptor for Endocytosis, Dec-205, Can Recycle and Enhance Antigen Presentation via Major Histocompatibility Complex Class II–Positive Lysosomal Compartments. *Journal of Cell Biology*. 2000;151(3):673-684. doi:10.1083/jcb.151.3.673
109. Bonifaz LC, Bonnyay DP, Charalambous A, et al. In Vivo Targeting of Antigens to Maturing Dendritic Cells via the DEC-205 Receptor Improves T Cell Vaccination. *The Journal of Experimental Medicine J Exp Med*. 2004;038151000(6):815-824. doi:10.1084/jem.20032220
110. Bozzacco L, Trumpfheller C, Siegal FP, et al. DEC-205 receptor on dendritic cells mediates presentation of HIV gag protein to CD8 + T cells in a spectrum of human MHC I haplotypes. *Proceedings of the National Academy of Sciences*. 2007;104(4):1289-1294. doi:10.1073/pnas.0610383104
111. BIRKHOLZ Michael; KELLNER, Christian; GROSS, Stefanie; FEY, Georg; SCHULER-TURNER, Beatrice; SCHULER, Gerold; SCHAFT, Niels; DÖRIE, Jan KS. Targeting of DEC-205 on human dendritic Cells results in efficient MHC class II-restricted antigen presentation. *Blood Journal*. 2010;116(13):2277-2285. doi:10.1182/blood-2010-02-268425.The

112. Ahmed EH, Brooks E, Sloan S, et al. Targeted Delivery of BZLF1 to DEC205 Drives EBV-Protective Immunity in a Spontaneous Model of EBV-Driven Lymphoproliferative Disease. *Vaccines (Basel)*. 2021;9(6):555. doi:10.3390/vaccines9060555
113. Flynn BJ, Kastenmüller K, Wille-Reece U, et al. Immunization with HIV Gag targeted to dendritic cells followed by recombinant New York vaccinia virus induces robust T-cell immunity in nonhuman primates. *Proceedings of the National Academy of Sciences*. 2011;108(17):7131-7136. doi:10.1073/pnas.1103869108
114. Bozzacco L, Trumpfheller C, Siegal FP, et al. DEC-205 receptor on dendritic cells mediates presentation of HIV gag protein to CD8 + T cells in a spectrum of human MHC I haplotypes. *Proceedings of the National Academy of Sciences*. 2007;104(4):1289-1294. doi:10.1073/pnas.0610383104
115. Silva MO, Almeida BS, Sales NS, et al. Antigen Delivery to DEC205 + Dendritic Cells Induces Immunological Memory and Protective Therapeutic Effects against HPV-Associated Tumors at Different Anatomical Sites. *Int J Biol Sci*. 2021;17(11):2944-2956. doi:10.7150/ijbs.57038
116. Birkholz K, Schwenkert M, Kellner C, et al. Targeting of DEC-205 on human dendritic cells results in efficient MHC class II–restricted antigen presentation. *Blood*. 2010;116(13):2277-2285. doi:10.1182/blood-2010-02-268425
117. Griffiths EA, Srivastava P, Matsuzaki J, et al. NY-ESO-1 Vaccination in Combination with Decitabine Induces Antigen-Specific T-lymphocyte Responses in Patients with Myelodysplastic Syndrome. *Clinical Cancer Research*. 2018;24(5):1019 LP - 1029. doi:10.1158/1078-0432.CCR-17-1792
118. Bhardwaj N, Friedlander PA, Pavlick AC, et al. Flt3 ligand augments immune responses to anti-DEC-205-NY-ESO-1 vaccine through expansion of dendritic cell subsets. *Nat Cancer*. 2020;1(12):1204-1217. doi:10.1038/s43018-020-00143-y
119. Stern JNH, Keskin DB, Kato Z, et al. Promoting tolerance to proteolipid protein-induced experimental autoimmune encephalomyelitis through targeting dendritic cells. *Proceedings of the National Academy of Sciences*. 2010;107(40):17280-17285. doi:10.1073/pnas.1010263107
120. Spiering R, Margry B, Keijzer C, et al. DEC205+ Dendritic Cell–Targeted Tolerogenic Vaccination Promotes Immune Tolerance in Experimental Autoimmune Arthritis. *The Journal of Immunology*. 2015;194(10):4804-4813. doi:10.4049/jimmunol.1400986
121. Mukherjee G, Geliebter A, Babad J, et al. DEC-205-mediated antigen targeting to steady-state dendritic cells induces deletion of diabetogenic CD8+ T cells independently of PD-1 and PD-L1. *Int Immunol*. 2013;25(11):651-660. doi:10.1093/intimm/dxt031
122. Quintarelli C, Dotti G, Hasan ST, et al. High-avidity cytotoxic T lymphocytes specific for a new PRAME-derived peptide can target leukemic and leukemic-precursor cells. *Blood*. 2011;117(12):3353-3362. doi:10.1182/blood-2010-08-300376
123. van der Bruggen P, Traversari C, Chomez P, et al. A Gene Encoding an Antigen Recognized by Cytolytic T Lymphocytes on a Human Melanoma. *Science (1979)*. 1991;254(5038):1643-1647. doi:10.1126/science.1840703
124. Chen YT, Scanlan MJ, Sahin U, et al. A testicular antigen aberrantly expressed in human cancers detected by autologous antibody screening. *Proceedings of the National Academy of Sciences*. 1997;94(5):1914-1918. doi:10.1073/pnas.94.5.1914
125. Gotter J, Brors B, Hergenhahn M, Kyewski B. Medullary epithelial cells of the human thymus express a highly diverse selection of tissue-specific genes colocalized in chromosomal clusters. *J Exp Med*. 2004;199(2):155-166. doi:10.1084/jem.20031677
126. Nagata Y, Gnjatic S, Wada H, et al. Monitoring CD8 T cell responses to NY-ESO-1 : Correlation of humoral and cellular immune responses. Published online 2000:1-6.

127. Bricard G, Bouzourene H, Martinet O, et al. Naturally Acquired MAGE-A10- and SSX-2-Specific CD8 + T Cell Responses in Patients with Hepatocellular Carcinoma. Published online 2019. doi:10.4049/jimmunol.174.3.1709
128. van der Bruggen P, Traversari C, Chomez P, et al. A Gene Encoding an Antigen Recognized by Cytolytic T Lymphocytes on a Human Melanoma. *Science (1979)*. 1991;254(5038):1643-1647. doi:10.1126/science.1840703
129. Lee SY, Obata Y, Yoshida M, et al. Immunomic analysis of human sarcoma. *Proceedings of the National Academy of Sciences*. 2003;100(5):2651-2656. doi:10.1073/pnas.0437972100
130. Tyagi P, Mirakhur B. MAGRIT: The Largest-Ever Phase III Lung Cancer Trial Aims to Establish a Novel Tumor-Specific Approach to Therapy. *Clin Lung Cancer*. 2009;10(5):371-374. doi:10.3816/CLC.2009.n.052
131. Movva S, Wen W, Chen W, et al. Multi-platform profiling of over 2000 sarcomas : Identification of biomarkers and novel therapeutic targets. 2000;6(14).
132. Kim R, Kulkarni P, Hannenhalli S. Derepression of Cancer/Testis Antigens in cancer is associated with distinct patterns of DNA Hypomethylation. *BMC Cancer*. 2013;13(1):144. doi:10.1186/1471-2407-13-144
133. Conley AP, Wang WL, Livingston JA, et al. MAGE-A3 Is a Clinically Relevant Target in Undifferentiated Pleomorphic Sarcoma/Myxofibrosarcoma. *Cancers (Basel)*. 2019;11(5):677. doi:10.3390/cancers11050677
134. Lai JP, Robbins PF, Raffeld M, et al. NY-ESO-1 expression in synovial sarcoma and other mesenchymal tumors: significance for NY-ESO-1-based targeted therapy and differential diagnosis. *Modern Pathology*. 2012;25(6):854-858. doi:10.1038/modpathol.2012.31
135. Jungbluth AA, Antonescu CR, Busam KJ, et al. Monophasic and biphasic synovial sarcomas abundantly express cancer/testis antigen ny-eso-1 but not mage-a1 or ct7. *Int J Cancer*. 2001;94(2):252-256. doi:10.1002/ijc.1451
136. Nüssing S, Trapani JA, Parish IA. Revisiting T Cell Tolerance as a Checkpoint Target for Cancer Immunotherapy. *Front Immunol*. 2020;11. doi:10.3389/fimmu.2020.589641
137. Pedersen SR, Sørensen MR, Buus S, Christensen JP, Thomsen AR. Comparison of Vaccine-Induced Effector CD8 T Cell Responses Directed against Self- and Non–Self-Tumor Antigens: Implications for Cancer Immunotherapy. *The Journal of Immunology*. 2013;191(7):3955-3967. doi:10.4049/jimmunol.1300555
138. Strausberg RL. Tumor microenvironments, the immune system and cancer survival. *Genome Biol*. 2005;6(3):211. doi:10.1186/gb-2005-6-3-211
139. Russell SJ, Peng KW, Bell JC. Oncolytic virotherapy. *Nat Biotechnol*. 2012;30(7):658-670. doi:10.1038/nbt.2287
140. Ilkow CS, Swift SL, Bell JC, Diallo JS. From Scourge to Cure: Tumour-Selective Viral Pathogenesis as a New Strategy against Cancer. *PLoS Pathog*. 2014;10(1):e1003836. doi:10.1371/journal.ppat.1003836
141. Gujar S, Bell J, Diallo JS. SnapShot: Cancer Immunotherapy with Oncolytic Viruses. *Cell*. 2019;176(5):1240-1240.e1. doi:10.1016/j.cell.2019.01.051
142. Russell SJ, Peng KW. Measles Virus for Cancer Therapy. In: *Measles*. Springer Berlin Heidelberg; :213-241. doi:10.1007/978-3-540-70617-5_11
143. Miyamoto S, Inoue H, Nakamura T, et al. Coxsackievirus B3 Is an Oncolytic Virus with Immunostimulatory Properties That Is Active against Lung Adenocarcinoma. *Cancer Res*. 2012;72(10):2609-2621. doi:10.1158/0008-5472.CAN-11-3185
144. Chiocca EA, Rabkin SD. Oncolytic Viruses and Their Application to Cancer Immunotherapy. *Cancer Immunol Res*. 2014;2(4):295-300. doi:10.1158/2326-6066.CIR-14-0015
145. Brun J, McManus D, Lefebvre C, et al. Identification of genetically modified Maraba virus as an oncolytic rhabdovirus. *Mol Ther*. 2010;18(8):1440-1449. doi:10.1038/mt.2010.103

146. Lichty BD, Breitbach CJ, Stojdl DF, Bell JC. Going viral with cancer immunotherapy. *Nat Rev Cancer*. 2014;14(8):559-567. doi:10.1038/nrc3770
147. Zamarin D, Ricca JM, Sadekova S, et al. PD-L1 in tumor microenvironment mediates resistance to oncolytic immunotherapy. *Journal of Clinical Investigation*. 2018;128(4):1413-1428. doi:10.1172/JCI98047
148. Selman M, Rousso C, Bergeron A, et al. Multi-modal Potentiation of Oncolytic Virotherapy by Vanadium Compounds. *Molecular Therapy*. 2018;26(1):56-69. doi:10.1016/j.ymthe.2017.10.014
149. Lu S. Heterologous prime–boost vaccination. *Curr Opin Immunol*. 2009;21(3):346-351. doi:10.1016/j.coi.2009.05.016
150. Pol JG, Zhang L, Bridle BW, et al. Maraba Virus as a Potent Oncolytic Vaccine Vector. *Molecular Therapy*. 2014;22(2):420-429. doi:10.1038/mt.2013.249
151. Bridle BW, Nguyen A, Salem O, et al. Privileged Antigen Presentation in Splenic B Cell Follicles Maximizes T Cell Responses in Prime-Boost Vaccination. *The Journal of Immunology*. 2016;196(11):4587 LP - 4595. doi:10.4049/jimmunol.1600106
152. Sekaly RP. The failed HIV Merck vaccine study: a step back or a launching point for future vaccine development? *Journal of Experimental Medicine*. 2008;205(1):7-12. doi:10.1084/jem.20072681
153. Barnes E, Folgori A, Capone S, et al. Novel Adenovirus-Based Vaccines Induce Broad and Sustained T Cell Responses to HCV in Man. *Sci Transl Med*. 2012;4(115). doi:10.1126/scitranslmed.3003155
154. Mast TC, Kierstead L, Gupta SB, et al. International epidemiology of human pre-existing adenovirus (Ad) type-5, type-6, type-26 and type-36 neutralizing antibodies: Correlates of high Ad5 titers and implications for potential HIV vaccine trials. *Vaccine*. 2010;28(4):950-957. doi:10.1016/j.vaccine.2009.10.145
155. Nwanegbo E, Vardas E, Gao W, et al. Prevalence of Neutralizing Antibodies to Adenoviral Serotypes 5 and 35 in the Adult Populations of The Gambia , South Africa , and the United States. 2004;11(2):351-357. doi:10.1128/CDLI.11.2.351
156. Saxena M, Van TTH, Baird FJ, Coloe PJ, Smooker PM. Pre-existing immunity against vaccine vectors – friend or foe? *Microbiology (N Y)*. 2013;159(Pt_1):1-11. doi:10.1099/mic.0.049601-0
157. Trombetta ES, Mellman I. CELL BIOLOGY OF ANTIGEN PROCESSING IN VITRO AND IN VIVO. *Annu Rev Immunol*. 2005;23(1):975-1028. doi:10.1146/annurev.immunol.22.012703.104538
158. Bonifaz L, Bonnyay D, Mahnke K, Rivera M, Nussenzweig MC, Steinman RM. Efficient Targeting of Protein Antigen to the Dendritic Cell Receptor DEC-205 in the Steady State Leads to Antigen Presentation on Major Histocompatibility Complex Class I Products and Peripheral CD8+ T Cell Tolerance. *Journal of Experimental Medicine*. 2002;196(12):1627-1638. doi:10.1084/jem.20021598
159. Moriya K, Wakabayashi A, Shimizu M, Tamura H, Dan K, Takahashi H. Induction of tumor-specific acquired immunity against already established tumors by selective stimulation of innate DEC-205+ dendritic cells. *Cancer Immunology, Immunotherapy*. 2010;59(7):1083-1095. doi:10.1007/s00262-010-0835-z
160. Yang TC, Dayball K, Wan YH, Bramson J. Detailed analysis of the CD8+ T-cell response following adenovirus vaccination. *J Virol*. 2003;77(24):13407-13411. doi:10.1128/jvi.77.24.13407-13411.2003
161. Dudziak D, Kamphorst AO, Heidkamp GF, et al. Differential Antigen Processing by Dendritic Cell Subsets in Vivo. *Science (1979)*. 2007;315(5808):107-111. doi:10.1126/science.1136080

162. Mukherjee G, Geliebter A, Babad J, et al. DEC-205-mediated antigen targeting to steady-state dendritic cells induces deletion of diabetogenic CD8+ T cells independently of PD-1 and PD-L1. *Int Immunol*. 2013;25(11):651-660. doi:10.1093/intimm/dxt031
163. Zhang P, Andorko JI, Jewell CM. Impact of dose, route, and composition on the immunogenicity of immune polyelectrolyte multilayers delivered on gold templates. *Biotechnol Bioeng*. 2017;114(2):423-431. doi:10.1002/bit.26083
164. Scott AM, Allison JP, Wolchok JD. Monoclonal antibodies in cancer therapy. *Cancer Immun*. 2012;12:14.
165. Liu M, Wang X, Wang L, et al. Targeting the IDO1 pathway in cancer: from bench to bedside. *J Hematol Oncol*. 2018;11(1):100. doi:10.1186/s13045-018-0644-y
166. Zhao Y, Adjei AA. The clinical development of MEK inhibitors. *Nat Rev Clin Oncol*. 2014;11(7):385-400. doi:10.1038/nrclinonc.2014.83
167. Liang K, Liu Q, Li P, Luo H, Wang H, Kong Q. Genetically engineered Salmonella Typhimurium: Recent advances in cancer therapy. *Cancer Lett*. 2019;448:168-181. doi:10.1016/j.canlet.2019.01.037
168. Miliotou AN, Papadopoulou LC. CAR T-cell Therapy: A New Era in Cancer Immunotherapy. *Curr Pharm Biotechnol*. 2018;19(1):5-18. doi:10.2174/1389201019666180418095526
169. Zamarin D, Holmgaard RB, Subudhi SK, et al. Localized Oncolytic Virotherapy Overcomes Systemic Tumor Resistance to Immune Checkpoint Blockade Immunotherapy. *Sci Transl Med*. 2014;6(226). doi:10.1126/scitranslmed.3008095
170. Phan M, Watson MF, Alain T, Diallo JS. Oncolytic Viruses on Drugs: Achieving Higher Therapeutic Efficacy. *ACS Infect Dis*. 2018;4(10):1448-1467. doi:10.1021/acsinfecdis.8b00144
171. Brun J, McManus D, Lefebvre C, et al. Identification of Genetically Modified Maraba Virus as an Oncolytic Rhabdovirus. *Molecular Therapy*. 2010;18(8):1440-1449. doi:10.1038/mt.2010.103
172. Miller G, Pillarisetty VG, Shah AB, Lahrs S, DeMatteo RP. Murine Flt3 Ligand Expands Distinct Dendritic Cells with Both Tolerogenic and Immunogenic Properties. *The Journal of Immunology*. 2003;170(7):3554-3564. doi:10.4049/jimmunol.170.7.3554
173. Nair A, Jacob S. A simple practice guide for dose conversion between animals and human. *J Basic Clin Pharm*. 2016;7(2):27. doi:10.4103/0976-0105.177703
174. Tacken PJ, de Vries IJM, Torensma R, Figdor CG. Dendritic-cell immunotherapy: from ex vivo loading to in vivo targeting. *Nat Rev Immunol*. 2007;7(10):790-802. doi:10.1038/nri2173
175. Nestle FO, Alijagic S, Gilliet M, et al. Vaccination of melanoma patients with peptide- or tumorlysate-pulsed dendritic cells. *Nat Med*. 1998;4(3):328-332. doi:10.1038/nm0398-328
176. Hsu FJ, Benike C, Fagnoni F, et al. Vaccination of patients with B–cell lymphoma using autologous antigen–pulsed dendritic cells. *Nat Med*. 1996;2(1):52-58. doi:10.1038/nm0196-52
177. Lesterhuis WJ, Aarntzen EHJG, De Vries IJM, et al. Dendritic cell vaccines in melanoma: From promise to proof? *Crit Rev Oncol Hematol*. 2008;66(2):118-134. doi:10.1016/j.critrevonc.2007.12.007
178. Caminschi I, Maraskovsky E, Heath WR. Targeting Dendritic Cells in vivo for Cancer Therapy. *Front Immunol*. 2012;3. doi:10.3389/fimmu.2012.00013
179. Wen PY, Reardon DA, Armstrong TS, et al. A Randomized Double-Blind Placebo-Controlled Phase II Trial of Dendritic Cell Vaccine ICT-107 in Newly Diagnosed Patients with Glioblastoma. *Clinical Cancer Research*. 2019;25(19):5799-5807. doi:10.1158/1078-0432.CCR-19-0261
180. Vonderheide RH, Flaherty KT, Khalil M, et al. Clinical Activity and Immune Modulation in Cancer Patients Treated With CP-870,893, a Novel CD40 Agonist Monoclonal Antibody. *Journal of Clinical Oncology*. 2007;25(7):876-883. doi:10.1200/JCO.2006.08.3311

181. Bowen WS, Svrivastava AK, Batra L, Barsoumian H, Shirwan H. Current challenges for cancer vaccine adjuvant development. *Expert Rev Vaccines*. 2018;17(3):207-215. doi:10.1080/14760584.2018.1434000
182. Anandasabapathy N, Feder R, Mollah S, et al. Classical Flt3L-dependent dendritic cells control immunity to protein vaccine. *Journal of Experimental Medicine*. 2014;211(9):1875-1891. doi:10.1084/jem.20131397
183. Bhardwaj N, Pavlick AC, Ernstoff MS, et al. A Phase II Randomized Study of CDX-1401, a Dendritic Cell Targeting NY-ESO-1 Vaccine, in Patients with Malignant Melanoma Pre-Treated with Recombinant CDX-301, a Recombinant Human Flt3 Ligand. *Journal of Clinical Oncology*. 2016;34(15_suppl):9589-9589. doi:10.1200/JCO.2016.34.15_suppl.9589
184. Henriques HR, Rampazo E V., Gonçalves AJS, et al. Targeting the Non-structural Protein 1 from Dengue Virus to a Dendritic Cell Population Confers Protective Immunity to Lethal Virus Challenge. *PLoS Negl Trop Dis*. 2013;7(7):e2330. doi:10.1371/journal.pntd.0002330
185. Diallo JS, Vähä-Koskela M, Le Boeuf F, Bell J. Propagation, Purification, and In Vivo Testing of Oncolytic Vesicular Stomatitis Virus Strains. In: ; 2012:127-140. doi:10.1007/978-1-61779-340-0_10
186. Thway K. Well-differentiated liposarcoma and dedifferentiated liposarcoma: An updated review. *Semin Diagn Pathol*. 2019;36(2):112-121. doi:https://doi.org/10.1053/j.semdp.2019.02.006
187. Nishio J, Nakayama S, Nabeshima K, Yamamoto T. Biology and Management of Dedifferentiated Liposarcoma: State of the Art and Perspectives. *J Clin Med*. 2021;10(15). doi:10.3390/jcm10153230
188. Park JO, Qin LX, Prete FP, Antonescu C, Brennan MF, Singer S. Predicting outcome by growth rate of locally recurrent retroperitoneal liposarcoma: the one centimeter per month rule. *Ann Surg*. 2009;250(6):977-982. doi:10.1097/sla.0b013e3181b2468b
189. Crago AM, Singer S. Clinical and molecular approaches to well differentiated and dedifferentiated liposarcoma. *Curr Opin Oncol*. 2011;23(4):373-378. doi:10.1097/CCO.0b013e32834796e6
190. Singer S, Antonescu CR, Riedel E, Brennan MF. Histologic subtype and margin of resection predict pattern of recurrence and survival for retroperitoneal liposarcoma. *Ann Surg*. 2003;238(3):358-371. doi:10.1097/01.sla.0000086542.11899.38
191. Tirumani SH, Tirumani H, Jagannathan JP, et al. Metastasis in dedifferentiated liposarcoma: Predictors and outcome in 148 patients. *European Journal of Surgical Oncology (EJSO)*. 2015;41(7):899-904. doi:10.1016/j.ejso.2015.01.012
192. Thirasastr P, Somaiah N. Overview of systemic therapy options in liposarcoma, with a focus on the activity of selinexor, a selective inhibitor of nuclear export in dedifferentiated liposarcoma. *Ther Adv Med Oncol*. 2022;14:17588359221081072. doi:10.1177/17588359221081073
193. Knebel C, Lenze U, Pohlig F, et al. Prognostic factors and outcome of Liposarcoma patients: a retrospective evaluation over 15 years. *BMC Cancer*. 2017;17(1):410. doi:10.1186/s12885-017-3398-y
194. Dalal KM, Antonescu CR, Singer S. *Diagnosis and Management of Lipomatous Tumors*. Vol 97. John Wiley & Sons, Ltd; 2008. doi:https://doi.org/10.1002/jso.20975
195. Tawbi HA, Burgess M, Bolejack V, et al. Pembrolizumab in advanced soft-tissue sarcoma and bone sarcoma (SARC028): a multicentre, two-cohort, single-arm, open-label, phase 2 trial. *Lancet Oncol*. 2017;18(11):1493-1501. doi:10.1016/S1470-2045(17)30624-1
196. Robbins PF, Kassim SH, Tran TLN, et al. A Pilot Trial Using Lymphocytes Genetically Engineered with an NY-ESO-1–Reactive T-cell Receptor: Long-term Follow-up and

Correlates with Response. *Clinical Cancer Research*. 2015;21(5):1019-1027. doi:10.1158/1078-0432.CCR-14-2708
197. Somaiah N, Chawla SP, Block MS, et al. Immune response, safety, and survival impact from CMB305 in NY-ESO-1+ recurrent soft tissue sarcomas (STS). *Journal of Clinical Oncology*. 2017;35(15_suppl):11006. doi:10.1200/JCO.2017.35.15_suppl.11006
198. Somaiah N, Chawla SP, Block MS, et al. A Phase 1b Study Evaluating the Safety, Tolerability, and Immunogenicity of CMB305, a Lentiviral-Based Prime-Boost Vaccine Regimen, in Patients with Locally Advanced, Relapsed, or Metastatic Cancer Expressing NY-ESO-1. *Oncoimmunology*. 2020;9(1):1847846. doi:10.1080/2162402X.2020.1847846
199. D'Angelo SP, Mahoney MR, Van Tine BA, et al. Nivolumab with or without ipilimumab treatment for metastatic sarcoma (Alliance A091401): two open-label, non-comparative, randomised, phase 2 trials. *Lancet Oncol*. 2018;19(3):416-426. doi:10.1016/S1470-2045(18)30006-8
200. Chen JL, Mahoney MR, George S, et al. A multicenter phase II study of nivolumab +/- ipilimumab for patients with metastatic sarcoma (Alliance A091401): Results of expansion cohorts. *Journal of Clinical Oncology*. 2020;38(15_suppl):11511-11511. doi:10.1200/JCO.2020.38.15_suppl.11511
201. Keung EZ, Lazar AJ, Torres KE, et al. Phase II study of neoadjuvant checkpoint blockade in patients with surgically resectable undifferentiated pleomorphic sarcoma and dedifferentiated liposarcoma. *BMC Cancer*. 2018;18(1):913. doi:10.1186/s12885-018-4829-0
202. Carvajal RD, Agulnik M, Ryan CW, et al. Trivalent ganglioside vaccine and immunologic adjuvant versus adjuvant alone in metastatic sarcoma patients rendered disease-free by surgery: A randomized phase 2 trial. *Journal of Clinical Oncology*. 2014;32(15_suppl):10520-10520. doi:10.1200/jco.2014.32.15_suppl.10520
203. Kawaguchi S, Tsukahara T, Ida K, et al. SYT-SSX breakpoint peptide vaccines in patients with synovial sarcoma: A study from the Japanese Musculoskeletal Oncology Group. *Cancer Sci*. 2012;103(9):1625-1630. doi:10.1111/j.1349-7006.2012.02370.x
204. Burgess MA, Bolejack V, Schuetze S, et al. Clinical activity of pembrolizumab (P) in undifferentiated pleomorphic sarcoma (UPS) and dedifferentiated/pleomorphic liposarcoma (LPS): Final results of SARC028 expansion cohorts. *Journal of Clinical Oncology*. 2019;37(15_suppl):11015. doi:10.1200/JCO.2019.37.15_suppl.11015
205. D'Angelo SP, Melchiori L, Merchant MS, et al. Antitumor Activity Associated with Prolonged Persistence of Adoptively Transferred NY-ESO-1 c259T Cells in Synovial Sarcoma. *Cancer Discov*. 2018;8(8):944-957. doi:10.1158/2159-8290.CD-17-1417
206. Ramachandran I, Lowther DE, Dryer-Minnerly R, et al. Systemic and local immunity following adoptive transfer of NY-ESO-1 SPEAR T cells in synovial sarcoma. *J Immunother Cancer*. 2019;7(1):276. doi:10.1186/s40425-019-0762-2
207. Janku F. Tumor heterogeneity in the clinic: is it a real problem? *Ther Adv Med Oncol*. 2013;6(2):43-51. doi:10.1177/1758834013517414
208. Tu Z, Peng J, Long X, et al. Sperm Autoantigenic Protein 17 Predicts the Prognosis and the Immunotherapy Response of Cancers: A Pan-Cancer Analysis. *Front Immunol*. 2022;13. doi:10.3389/fimmu.2022.844736
209. Lee DH, Jeong YJ, Won JY, Sim HI, Park Y, Jin HS. PBK/TOPK Is a Favorable Prognostic Biomarker Correlated with Antitumor Immunity in Colon Cancers. *Biomedicines*. 2022;10(2):299. doi:10.3390/biomedicines10020299
210. Nilsson S, Kaniowska D, Brakebusch C, Fässler R, Johansson S. Threonine 788 in integrin subunit β1 regulates integrin activation. *Exp Cell Res*. 2006;312(6):844-853. doi:10.1016/j.yexcr.2005.12.001

211. Liu J, DeYoung SM, Zhang M, Zhang M, Cheng A, Saltiel AR. Changes in integrin expression during adipocyte differentiation. *Cell Metab*. 2005;2(3):165-177. doi:10.1016/j.cmet.2005.08.006
212. Ruiz-Ojeda FJ, Wang J, Bäcker T, et al. Active integrins regulate white adipose tissue insulin sensitivity and brown fat thermogenesis. *Mol Metab*. 2021;45:101147. doi:10.1016/j.molmet.2020.101147
213. Bouvard D, Brakebusch C, Gustafsson E, et al. Functional Consequences of Integrin Gene Mutations in Mice. *Circ Res*. 2001;89(3):211-223. doi:10.1161/hh1501.094874
214. Münsterberg J, Loreth D, Brylka L, et al. ALCAM contributes to brain metastasis formation in non-small-cell lung cancer through interaction with the vascular endothelium. *Neuro Oncol*. 2020;22(7):955-966. doi:10.1093/neuonc/noaa028
215. Wu Z, Wu Z, Li J, et al. MCAM is a novel metastasis marker and regulates spreading, apoptosis and invasion of ovarian cancer cells. *Tumor Biology*. 2012;33(5):1619-1628. doi:10.1007/s13277-012-0417-0
216. Zhang D, Bi J, Liang Q, et al. VCAM1 Promotes Tumor Cell Invasion and Metastasis by Inducing EMT and Transendothelial Migration in Colorectal Cancer. *Front Oncol*. 2020;10. doi:10.3389/fonc.2020.01066
217. Finlin BS, Confides AL, Zhu B, et al. Adipose Tissue Mast Cells Promote Human Adipose Beiging in Response to Cold. *Sci Rep*. 2019;9(1):8658. doi:10.1038/s41598-019-45136-9
218. Divoux A, Moutel S, Poitou C, et al. Mast Cells in Human Adipose Tissue: Link with Morbid Obesity, Inflammatory Status, and Diabetes. *J Clin Endocrinol Metab*. 2012;97(9):E1677-E1685. doi:10.1210/jc.2012-1532
219. Ishijima Y, Ohmori S, Ohneda K. Mast cell deficiency results in the accumulation of preadipocytes in adipose tissue in both obese and non-obese mice. *FEBS Open Bio*. 2014;4(1):18-24. doi:10.1016/j.fob.2013.11.004
220. Tanaka A, Nomura Y, Matsuda A, Ohmori K, Matsuda H. Mast cells function as an alternative modulator of adipogenesis through 15-deoxy-delta-12, 14-prostaglandin J $_2$. *American Journal of Physiology-Cell Physiology*. 2011;301(6):C1360-C1367. doi:10.1152/ajpcell.00514.2010
221. Shi MA, Shi GP. Different Roles of Mast Cells in Obesity and Diabetes: Lessons from Experimental Animals and Humans. *Front Immunol*. 2012;3. doi:10.3389/fimmu.2012.00007
222. Danaher P, Warren S, Lu R, et al. Pan-cancer adaptive immune resistance as defined by the Tumor Inflammation Signature (TIS): Results from The Cancer Genome Atlas (TCGA). *J Immunother Cancer*. 2018;6(1):1-17. doi:10.1186/s40425-018-0367-1
223. Singer S, Socci ND, Ambrosini G, et al. Gene Expression Profiling of Liposarcoma Identifies Distinct Biological Types/Subtypes and Potential Therapeutic Targets in Well-Differentiated and Dedifferentiated Liposarcoma. *Cancer Res*. 2007;67(14):6626 LP - 6636. doi:10.1158/0008-5472.CAN-07-0584
224. Pollack SM, He Q, Yearley JH, et al. T-cell infiltration and clonality correlate with programmed cell death protein 1 and programmed death-ligand 1 expression in patients with soft tissue sarcomas. *Cancer*. 2017;123(17):3291-3304. doi:10.1002/cncr.30726
225. Tseng WW, Malu S, Zhang M, et al. Analysis of the Intratumoral Adaptive Immune Response in Well Differentiated and Dedifferentiated Retroperitoneal Liposarcoma. Ferguson PC, ed. *Sarcoma*. 2015;2015:547460. doi:10.1155/2015/547460
226. Yan L, Wang Z, Cui C, et al. Comprehensive immune characterization and T-cell receptor repertoire heterogeneity of retroperitoneal liposarcoma. *Cancer Sci*. 2019;110(10):3038-3048. doi:https://doi.org/10.1111/cas.14161
227. Hemminger JA, Toland AE, Scharschmidt TJ, Mayerson JL, Guttridge DC, Iwenofu OH. Expression of cancer-testis antigens MAGEA1, MAGEA3, ACRBP, PRAME, SSX2, and

CTAG2 in myxoid and round cell liposarcoma. *Mod Pathol*. 2014;27(9):1238-1245. doi:10.1038/modpathol.2013.244
228. Kakimoto T, Matsumine A, Kageyama S, et al. Immunohistochemical expression and clinicopathological assessment of the cancer testis antigens NY-ESO-1 and MAGE-A4 in high-grade soft-tissue sarcoma. *Oncol Lett*. Published online February 14, 2019. doi:10.3892/ol.2019.10044
229. Shurell E, Vergara-Lluri ME, Li Y, et al. Comprehensive adipocytic and neurogenic tissue microarray analysis of NY-ESO-1 expression - a promising immunotherapy target in malignant peripheral nerve sheath tumor and liposarcoma. *Oncotarget*. 2016;7(45):72860-72867. doi:10.18632/oncotarget.12096
230. Iura K, Kohashi K, Hotokebuchi Y, et al. Cancer-testis antigens PRAME and NY-ESO-1 correlate with tumour grade and poor prognosis in myxoid liposarcoma. *J Pathol Clin Res*. 2015;1(3):144-159. doi:https://doi.org/10.1002/cjp2.16
231. Wolf RM, Jaffe AE, Steele KE, et al. Cytokine, Chemokine, and Cytokine Receptor Changes Are Associated With Metabolic Improvements After Bariatric Surgery. *J Clin Endocrinol Metab*. 2019;104(3):947-956. doi:10.1210/jc.2018-02245
232. Tourniaire F, Romier-Crouzet B, Lee JH, et al. Chemokine Expression in Inflamed Adipose Tissue Is Mainly Mediated by NF-κB. *PLoS One*. 2013;8(6):e66515. https://doi.org/10.1371/journal.pone.0066515
233. Wang Y, Cao F, Wang Y, Yu G, Jia BL. Silencing of SAA1 inhibits palmitate- or high-fat diet induced insulin resistance through suppression of the NF-κB pathway. *Molecular Medicine*. 2019;25(1):17. doi:10.1186/s10020-019-0075-4
234. Ma X, Wang D, Zhao W, Xu L. Deciphering the Roles of PPARγ in Adipocytes via Dynamic Change of Transcription Complex . *Frontiers in Endocrinology* . 2018;9. https://www.frontiersin.org/article/10.3389/fendo.2018.00473
235. Pfuhlmann K, Pfluger PT, Schriever SC, Müller TD, Tschöp MH, Stemmer K. Dual specificity phosphatase 6 deficiency is associated with impaired systemic glucose tolerance and reversible weight retardation in mice. *PLoS One*. 2017;12(9):e0183488. https://doi.org/10.1371/journal.pone.0183488
236. Janiszewska M, Primi MC, Izard T. Cell adhesion in cancer: Beyond the migration of single cells. *Journal of Biological Chemistry*. 2020;295(8):2495-2505. doi:10.1074/jbc.REV119.007759
237. Zeng ZZ, Jia Y, Hahn NJ, Markwart SM, Rockwood KF, Livant DL. Role of focal adhesion kinase and phosphatidylinositol 3'-kinase in integrin fibronectin receptor-mediated, matrix metalloproteinase-1-dependent invasion by metastatic prostate cancer cells. *Cancer Res*. 2006;66(16):8091-8099. doi:10.1158/0008-5472.CAN-05-4400
238. Erdogan B, Ao M, White LM, et al. Cancer-associated fibroblasts promote directional cancer cell migration by aligning fibronectin. *J Cell Biol*. 2017;216(11):3799-3816. doi:10.1083/jcb.201704053
239. Attieh Y, Clark AG, Grass C, et al. Cancer-associated fibroblasts lead tumor invasion through integrin-β3-dependent fibronectin assembly. *J Cell Biol*. 2017;216(11):3509-3520. doi:10.1083/jcb.201702033
240. Provenzano PP, Inman DR, Eliceiri KW, et al. Collagen density promotes mammary tumor initiation and progression. *BMC Med*. 2008;6:11. doi:10.1186/1741-7015-6-11
241. Jiang H, Hegde S, DeNardo DG. Tumor-associated fibrosis as a regulator of tumor immunity and response to immunotherapy. *Cancer Immunol Immunother*. 2017;66(8):1037-1048. doi:10.1007/s00262-017-2003-1

242. Yang Y, Ma Y, Gao H, et al. A novel HDGF-ALCAM axis promotes the metastasis of Ewing sarcoma via regulating the GTPases signaling pathway. *Oncogene*. 2021;40(4):731-745. doi:10.1038/s41388-020-01485-8
243. Devis L, Moiola CP, Masia N, et al. Activated leukocyte cell adhesion molecule (ALCAM) is a marker of recurrence and promotes cell migration, invasion, and metastasis in early-stage endometrioid endometrial cancer. *J Pathol*. 2017;241(4):475-487. doi:10.1002/path.4851
244. Hansen AG, Arnold SA, Jiang M, et al. ALCAM/CD166 is a TGF-β-responsive marker and functional regulator of prostate cancer metastasis to bone. *Cancer Res*. 2014;74(5):1404-1415. doi:10.1158/0008-5472.CAN-13-1296
245. Hein S, Müller V, Köhler N, et al. Biologic role of activated leukocyte cell adhesion molecule overexpression in breast cancer cell lines and clinical tumor tissue. *Breast Cancer Res Treat*. 2011;129(2):347-360. doi:10.1007/s10549-010-1219-y
246. Ruiz-Ojeda FJ, Wang J, Bäcker T, et al. Active integrins regulate white adipose tissue insulin sensitivity and brown fat thermogenesis. *Mol Metab*. 2021;45:101147. doi:10.1016/j.molmet.2020.101147
247. Nilsson S, Kaniowska D, Brakebusch C, Fässler R, Johansson S. Threonine 788 in integrin subunit beta1 regulates integrin activation. *Exp Cell Res*. 2006;312(6):844-853. doi:10.1016/j.yexcr.2005.12.001
248. Liu J, DeYoung SM, Zhang M, Zhang M, Cheng A, Saltiel AR. Changes in integrin expression during adipocyte differentiation. *Cell Metab*. 2005;2(3):165-177. doi:10.1016/j.cmet.2005.08.006
249. Ruiz-Ojeda FJ, Wang J, Bäcker T, et al. Active integrins regulate white adipose tissue insulin sensitivity and brown fat thermogenesis. *Mol Metab*. 2021;45:101147. doi:10.1016/j.molmet.2020.101147
250. Pozzi A, LeVine WF, Gardner HA. Low plasma levels of matrix metalloproteinase 9 permit increased tumor angiogenesis. *Oncogene*. 2002;21(2):272-281. doi:10.1038/sj.onc.1205045
251. Pozzi A, Moberg PE, Miles LA, Wagner S, Soloway P, Gardner HA. Elevated matrix metalloprotease and angiostatin levels in integrin α1 knockout mice cause reduced tumor vascularization. *Proceedings of the National Academy of Sciences*. 2000;97(5):2202-2207. doi:10.1073/pnas.040378497
252. Bednarczyk M, Stege H, Grabbe S, Bros M. β2 Integrins-Multi-Functional Leukocyte Receptors in Health and Disease. *Int J Mol Sci*. 2020;21(4). doi:10.3390/ijms21041402
253. Italiano A, Bessede A, Pulido M, et al. Pembrolizumab in soft-tissue sarcomas with tertiary lymphoid structures: a phase 2 PEMBROSARC trial cohort. *Nat Med*. 2022;28(6):1199-1206. doi:10.1038/s41591-022-01821-3
254. Keung EZ, Burgess M, Salazar R, et al. Correlative Analyses of the SARC028 Trial Reveal an Association Between Sarcoma-Associated Immune Infiltrate and Response to Pembrolizumab. *Clinical Cancer Research*. 2020;26(6):1258-1266. doi:10.1158/1078-0432.CCR-19-1824
255. Schroeder BA, LaFranzo NA, LaFleur BJ, et al. CD4+ T cell and M2 macrophage infiltration predict dedifferentiated liposarcoma patient outcomes. *J Immunother Cancer*. 2021;9(8):e002812. doi:10.1136/jitc-2021-002812
256. van Baren N, Van den Eynde BJ. Tryptophan-Degrading Enzymes in Tumoral Immune Resistance. *Front Immunol*. 2015;6. doi:10.3389/fimmu.2015.00034
257. Tang K, Wu YH, Song Y, Yu B. Indoleamine 2,3-dioxygenase 1 (IDO1) inhibitors in clinical trials for cancer immunotherapy. *J Hematol Oncol*. 2021;14(1):68. doi:10.1186/s13045-021-01080-8
258. Robbins PF, Morgan RA, Feldman SA, et al. Tumor Regression in Patients With Metastatic Synovial Cell Sarcoma and Melanoma Using Genetically Engineered Lymphocytes Reactive

With NY-ESO-1. *Journal of Clinical Oncology*. 2011;29(7):917-924. doi:10.1200/JCO.2010.32.2537
259. D'Angelo S, Demetri G, Tine B Van, et al. 298 Final analysis of the phase 1 trial of NY-ESO-1–specific T-cell receptor (TCR) T-cell therapy (letetresgene autoleucel; GSK3377794) in patients with advanced synovial sarcoma (SS). *J Immunother Cancer*. 2020;8(Suppl 3):A182 LP-A183. doi:10.1136/jitc-2020-SITC2020.0298
260. Smaglo BG, Musher BL, Vasileiou S, et al. A phase I trial targeting advanced or metastatic pancreatic cancer using a combination of standard chemotherapy and adoptively transferred nonengineered, multiantigen specific T cells in the first-line setting (TACTOPS). *Journal of Clinical Oncology*. 2020;38(15_suppl):4622. doi:10.1200/JCO.2020.38.15_suppl.4622
261. Fijak M, Meinhardt A. The testis in immune privilege. *Immunol Rev*. 2006;213(1):66-81. doi:10.1111/j.1600-065X.2006.00438.x
262. Ayers M, Lunceford J, Nebozhyn M, et al. IFN-γ–related mRNA profile predicts clinical response to PD-1 blockade. *J Clin Invest*. 2017;127(8):2930-2940. doi:10.1172/JCI91190
263. Xu G, Smith T, Grey F, Hill AB. Cytomegalovirus-based cancer vaccines expressing TRP2 induce rejection of melanoma in mice. *Biochem Biophys Res Commun*. 2013;437(2):287-291. doi:10.1016/j.bbrc.2013.06.068
264. Yamano T, Kaneda Y, Huang S, Hiramatsu SH, Hoon DSB. Enhancement of Immunity by a DNA Melanoma Vaccine against TRP2 with CCL21 as an Adjuvant. *Molecular Therapy*. 2006;13(1):194-202. doi:10.1016/j.ymthe.2005.05.018
265. Fang J, Hu B, Li S, Zhang C, Liu Y, Wang P. A multi-antigen vaccine in combination with an immunotoxin targeting tumor-associated fibroblast for treating murine melanoma. *Mol Ther Oncolytics*. 2016;3:16007. doi:10.1038/mto.2016.7
266. Gao T, Cen Q, Lei H. A review on development of MUC1-based cancer vaccine. *Biomedicine & Pharmacotherapy*. 2020;132:110888. doi:10.1016/j.biopha.2020.110888
267. Pol JG, Atherton MJ, Stephenson KB, et al. Enhanced immunotherapeutic profile of oncolytic virus-based cancer vaccination using cyclophosphamide preconditioning. *J Immunother Cancer*. 2020;8(2):e000981. doi:10.1136/jitc-2020-000981
268. Huang AY, Gulden PH, Woods AS, et al. The immunodominant major histocompatibility complex class I-restricted antigen of a murine colon tumor derives from an endogenous retroviral gene product. *Proceedings of the National Academy of Sciences*. 1996;93(18):9730-9735. doi:10.1073/pnas.93.18.9730
269. McWilliams JA, Sullivan RT, Jordan KR, et al. Age-dependent tolerance to an endogenous tumor-associated antigen. *Vaccine*. 2008;26(15):1863-1873. doi:10.1016/j.vaccine.2008.01.052
270. Scrimieri F, Askew D, Corn DJ, et al. Murine leukemia virus envelope gp70 is a shared biomarker for the high-sensitivity quantification of murine tumor burden. *Oncoimmunology*. 2013;2(11):e26889. doi:10.4161/onci.26889
271. Kreiter S, Vormehr M, van de Roemer N, et al. Mutant MHC class II epitopes drive therapeutic immune responses to cancer. *Nature*. 2015;520(7549):692-696. doi:10.1038/nature14426
272. Lopes A, Feola S, Ligot S, et al. Oncolytic adenovirus drives specific immune response generated by a poly-epitope pDNA vaccine encoding melanoma neoantigens into the tumor site. *J Immunother Cancer*. 2019;7(1):174. doi:10.1186/s40425-019-0644-7
273. Guo ZS, Lu B, Guo Z, et al. Vaccinia virus-mediated cancer immunotherapy: cancer vaccines and oncolytics. *J Immunother Cancer*. 2019;7(1):6. doi:10.1186/s40425-018-0495-7
274. Acres B, Bonnefoy JY. Clinical development of MVA-based therapeutic cancer vaccines. *Expert Rev Vaccines*. 2008;7(7):889-893. doi:10.1586/14760584.7.7.889

275. Alharbi NK, Padron-Regalado E, Thompson CP, et al. ChAdOx1 and MVA based vaccine candidates against MERS-CoV elicit neutralising antibodies and cellular immune responses in mice. *Vaccine*. 2017;35(30):3780-3788. doi:10.1016/j.vaccine.2017.05.032
276. Guo Q, Wang L, Xu P, et al. Heterologous prime-boost immunization co-targeting dual antigens inhibit tumor growth and relapse. *Oncoimmunology*. 2020;9(1). doi:10.1080/2162402X.2020.1841392
277. Reyes-Sandoval A, Berthoud T, Alder N, et al. Prime-Boost Immunization with Adenoviral and Modified Vaccinia Virus Ankara Vectors Enhances the Durability and Polyfunctionality of Protective Malaria CD8 + T-Cell Responses. *Infect Immun*. 2010;78(1):145-153. doi:10.1128/IAI.00740-09
278. McConkey SJ, Reece WHH, Moorthy VS, et al. Enhanced T-cell immunogenicity of plasmid DNA vaccines boosted by recombinant modified vaccinia virus Ankara in humans. *Nat Med*. 2003;9(6):729-735. doi:10.1038/nm881
279. Tapia MD, Sow SO, Lyke KE, et al. Use of ChAd3-EBO-Z Ebola virus vaccine in Malian and US adults, and boosting of Malian adults with MVA-BN-Filo: a phase 1, single-blind, randomised trial, a phase 1b, open-label and double-blind, dose-escalation trial, and a nested, randomised, double-bli. *Lancet Infect Dis*. 2016;16(1):31-42. doi:10.1016/S1473-3099(15)00362-X
280. Venkatraman N, Ndiaye BP, Bowyer G, et al. Safety and Immunogenicity of a Heterologous Prime-Boost Ebola Virus Vaccine Regimen in Healthy Adults in the United Kingdom and Senegal. *J Infect Dis*. 2019;219(8):1187-1197. doi:10.1093/infdis/jiy639
281. Anywaine Z, Whitworth H, Kaleebu P, et al. Safety and Immunogenicity of a 2-Dose Heterologous Vaccination Regimen With Ad26.ZEBOV and MVA-BN-Filo Ebola Vaccines: 12-Month Data From a Phase 1 Randomized Clinical Trial in Uganda and Tanzania. *J Infect Dis*. 2019;220(1):46-56. doi:10.1093/infdis/jiz070
282. Rollier CS, Hill AVS, Reyes-Sandoval A. Influence of adenovirus and MVA vaccines on the breadth and hierarchy of T cell responses. *Vaccine*. 2016;34(38):4470-4474. doi:10.1016/j.vaccine.2016.07.050
283. Valentin A, McKinnon K, Li J, et al. Comparative analysis of SIV-specific cellular immune responses induced by different vaccine platforms in rhesus macaques. *Clinical Immunology*. 2014;155(1):91-107. doi:10.1016/j.clim.2014.09.005
284. Sun Y, Santra S, Buzby AP, Mascola JR, Nabel GJ, Letvin NL. Recombinant vector-induced HIV/SIV-specific CD4+ T lymphocyte responses in rhesus monkeys. *Virology*. 2010;406(1):48-55. doi:10.1016/j.virol.2010.07.004
285. Reyes-Sandoval A, Berthoud T, Alder N, et al. Prime-Boost Immunization with Adenoviral and Modified Vaccinia Virus Ankara Vectors Enhances the Durability and Polyfunctionality of Protective Malaria CD8 $^{+}$ T-Cell Responses. *Infect Immun*. 2010;78(1):145-153. doi:10.1128/IAI.00740-09
286. Probst P, Kopp J, Oxenius A, et al. Sarcoma Eradication by Doxorubicin and Targeted TNF Relies upon CD8 þ T-cell Recognition of a Retroviral Antigen. 2017;77(8):3644-3655. doi:10.1158/0008-5472.CAN-16-2946
287. Bourgeois-Daigneault MC, Roy DG, Falls T, et al. Oncolytic vesicular stomatitis virus expressing interferon-σ has enhanced therapeutic activity. *Mol Ther Oncolytics*. 2016;3:16001. doi:10.1038/mto.2016.1
288. Wen H, Chen Z, Li M, et al. An Integrative Pan-Cancer Analysis of PBK in Human Tumors. *Front Mol Biosci*. 2021;8. doi:10.3389/fmolb.2021.755911
289. Wedekind MF, Miller KE, Chen CY, et al. Endogenous retrovirus envelope as a tumor-associated immunotherapeutic target in murine osteosarcoma. *iScience*. 2021;24(7):102759. doi:10.1016/j.isci.2021.102759

290. Tang S, Shi L, Luker BT, et al. Modulation of the tumor microenvironment by armed vesicular stomatitis virus in a syngeneic pancreatic cancer model. *Virol J*. 2022;19(1):32. doi:10.1186/s12985-022-01757-7
291. Hwang JK, Hong J, Yun CO. Oncolytic Viruses and Immune Checkpoint Inhibitors: Preclinical Developments to Clinical Trials. *Int J Mol Sci*. 2020;21(22):8627. doi:10.3390/ijms21228627
292. Lee CL, Mowery YM, Daniel AR, et al. Mutational landscape in genetically engineered, carcinogen-induced, and radiation-induced mouse sarcoma. *JCI Insight*. 2019;4(13). doi:10.1172/jci.insight.128698
293. Strickler JH, Hanks BA, Khasraw M. Tumor Mutational Burden as a Predictor of Immunotherapy Response: Is More Always Better? *Clinical Cancer Research*. 2021;27(5):1236-1241. doi:10.1158/1078-0432.CCR-20-3054
294. SA F. Immunodominance with Hosts. In: *Immunology and Evolution of Infectious Disease.* ; :Chapter 6. https://www.ncbi.nlm.nih.gov/books/NBK2386/
295. Burger ML, Cruz AM, Crossland GE, et al. Antigen dominance hierarchies shape TCF1+ progenitor CD8 T cell phenotypes in tumors. *Cell*. 2021;184(19):4996-5014.e26. doi:https://doi.org/10.1016/j.cell.2021.08.020
296. Pearce H, Hutton P, Chaudhri S, et al. Spontaneous CD4(+) and CD8(+) T-cell responses directed against cancer testis antigens are present in the peripheral blood of testicular cancer patients. *Eur J Immunol*. 2017;47(7):1232-1242. doi:10.1002/eji.201646898
297. Tsuji T, Altorki NK, Ritter G, Old LJ, Gnjatic S. Characterization of Preexisting MAGE-A3-Specific CD4+ T Cells in Cancer Patients and Healthy Individuals and Their Activation by Protein Vaccination. *The Journal of Immunology*. 2009;183(7):4800-4808. doi:10.4049/jimmunol.0900903
298. Qiao L, Ba J, Xie J, et al. Overexpression of PBK/TOPK relates to poor prognosis of patients with breast cancer: a retrospective analysis. *World J Surg Oncol*. 2022;20(1):316. doi:10.1186/s12957-022-02769-x
299. Zhang Y, Yang X, Wang R, Zhang X. Prognostic Value of PDZ-Binding Kinase/T-LAK Cell-Originated Protein Kinase (PBK/TOPK) in Patients with Cancer. *J Cancer*. 2019;10(1):131-137. doi:10.7150/jca.28216
300. Xu M, Xu S. PBK/TOPK overexpression and survival in solid tumors. *Medicine*. 2019;98(10):e14766. doi:10.1097/MD.0000000000014766
301. Zhao S. PDZ-binding kinase participates in spermatogenesis. *Int J Biochem Cell Biol*. 2001;33(6):631-636. doi:10.1016/S1357-2725(01)00005-X
302. Ngu LN, Nji NN, Ambada GE, et al. In vivo targeting of protein antigens to dendritic cells using anti-DEC-205 single chain antibody improves HIV Gag specific CD4 þ T cell responses protecting from airway challenge with recombinant vaccinia-gag virus. Published online 2017:1-13. doi:10.1002/iid3.151
303. Neubert K, Lehmann CHK, Heger L, et al. Antigen Delivery to $CD11c^{+}CD8^{-}$ Dendritic Cells Induces Protective Immune Responses against Experimental Melanoma in Mice In Vivo. *The Journal of Immunology*. 2014;192(12):5830 LP - 5838. doi:10.4049/jimmunol.1300975
304. Meyer-wentrup F, Cambi A, Joosten B, et al. DCIR is endocytosed into human dendritic cells and inhibits TLR8-mediated cytokine production system as pattern-recognition and antigen-uptake. Published online 2008. doi:10.1189/jlb.0608352

Contributions of Collaborators

Dr. Silvia Boscardin (University of Sao Paulo) provided aDEC205-OVA and aDEC205-empty encoding plasmids.

Dr. Robin Parks (The Ottawa Hospital Research Institute) provided all adenoviruses used in Chapter 2.

Dr. Nikolas Martin (The Ottawa Hospital Research Institute) assisted in the cloning of MVA-PBK, and produced the virus used in Chapter 4.

Dr. Fanny Tzelepis and Dr. Harsimrat Birdi were crucial for performing, analysis and experimental assistance for the experiments in Figures 2-1 to 2-9, and Appendix II Supplemental Figures 1-3

Andrew Chem assisted with all *in vivo* experiments for Chapters 2 and 4 and the production of VSV used in Chapter 4.

Dr. Bibianna Purgina and Dr. Ashley Flaman (The Ottawa Hospital) selected FFPE blocks and conducted the scoring of immunohistochemical staining for Chapter 3.

Appendix I. Supplemental Results

Supplemental Result 1. Dose optimization of DEC205-OVA for prime-boost vaccination regimen.

A persistent challenge encountered during the production of DEC205 antibodies was the limited yield or even absence of antibody secretion into the supernatant. To address this issue and to prepare for potential low yields of future constructs, we sought to evaluate the feasibility of using a reduced dose of anti-DEC205 for priming. By utilizing a reduced dose, we anticipate a substantial reduction in both the time and cost associated with antibody production.

We assessed if a reduced dose of aDEC205-OVA can generate a robust SIINFEKL-specific T cell response in the context of our prime-boost immunization. Naïve BALB/C mice were primed (i.v.) with either 1, 5, or 10 ug of aDEC205-OVA in combination with 50 ug poly(I:C) and 50 ug anti-CD40, and boosted (i.v.) 9 days later with 10^8 PFUs of VSV-OVA. SIINFEKL-specific antigen responses were evaluated in blood at day 4 and day 6 by staining with $H2K^b$-SIINFEKL pentamer. (Figure 5A) Antigen specific T cells were not detected 4 days post prime. However, a significantly higher percentage of SIINFEKL-specific CD8+ T cells were detected in mice receiving 10 ug of aDEC205-OVA compared to 1 ug at D6. (Figure I.1B, C) At day 23 after a boost, splenocytes from immunized mice were restimulated with SIINFEKL peptide *ex vivo* and followed by intracellular cytokine staining (ICS) for IFNγ and TNFα. IFN γ +TNFα + CD8+ T cells were significantly increased in the 1ug dose compared to the 10 μg dose. (Figure I.1D) This difference may be due to contaminants in our antibody preparation that come from our antibody purification protocol. Together, these results indicate that priming with a reduced dose of aDEC205-OVA generates a smaller number of antigen specific T cells after prime (from 6% in 10 ug group to 4% in 1 μg group); however, after boost immunization, the 1μg group demonstrates a more robust cytokine response to antigen stimulation. This suggests that the dose of aDEC205-OVA can be reduced while maintaining the anti-SIINFEKL T cell response.

Altogether, reducing the dose of DEC205 prime when combined with a VSVΔ51 boost will generate robust antigen-specific immune responses, and can be used as an alternative to a 10μg dose of DEC205.

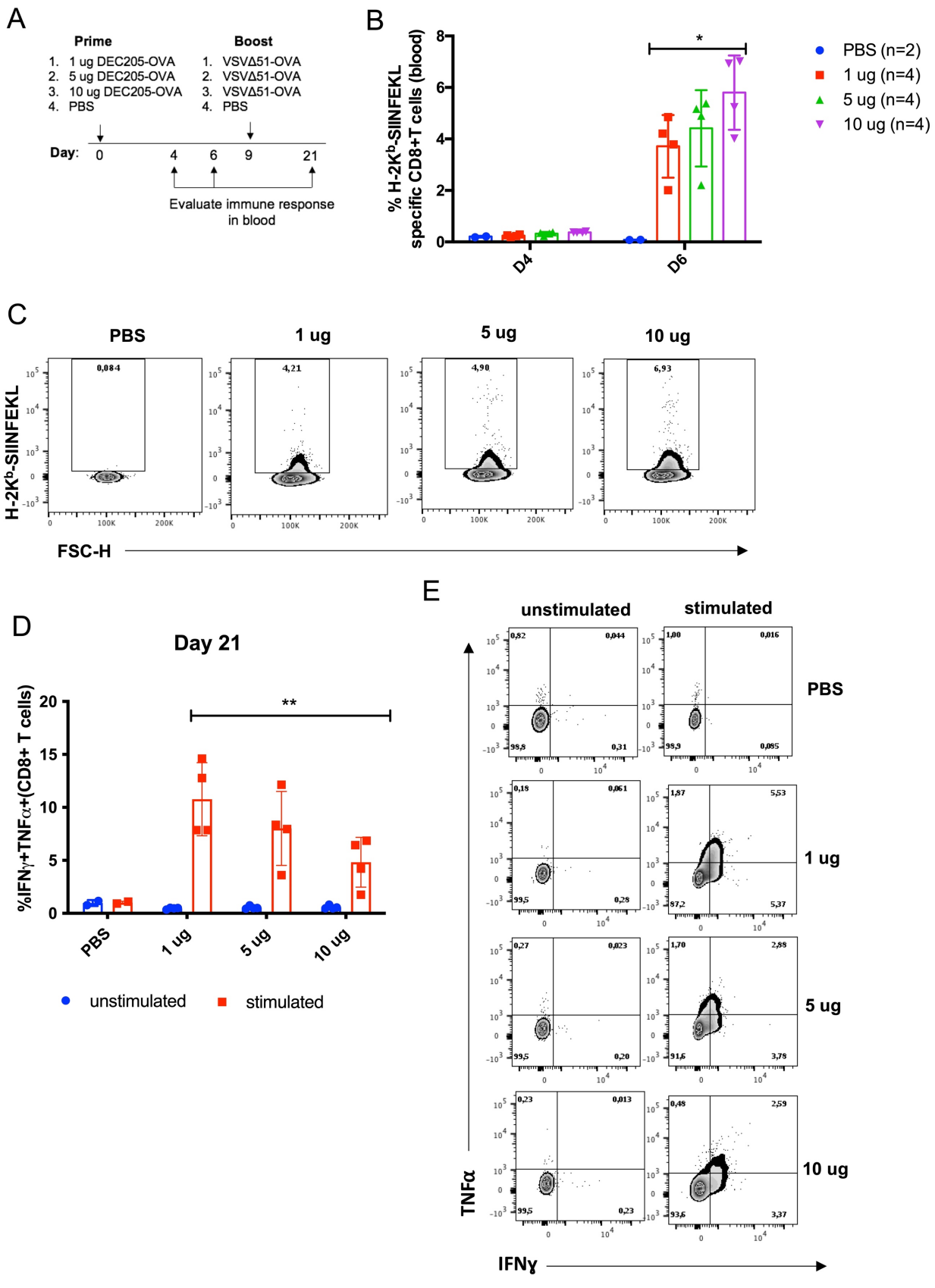
A
Prime
1. 1 ug DEC205-OVA
2. 5 ug DEC205-OVA
3. 10 ug DEC205-OVA
4. PBS
Boost
1. VSVΔ51-OVA
2. VSVΔ51-OVA
3. VSVΔ51-OVA
4. PBS
Day: 0 4 6 9 21
Evaluate immune response in blood
B
% H-2Kb-SIINFEKL specific CD8+T cells (blood)
D4
D6
PBS (n=2)
1 ug (n=4)
5 ug (n=4)
10 ug (n=4)
C
PBS
1 ug
5 ug
10 ug
H-2Kb-SIINFEKL
FSC-H
D
Day 21
%IFNγ+TNFα+(CD8+ T cells)
unstimulated
stimulated
E
unstimulated
stimulated
PBS
1 ug
5 ug
10 ug
TNFα
IFNγ

Supplemental Figure 1. Comparing SIINFEKL-specific T cell response at several time points after administration of full chain or single chain anti-DEC205-OVA prime (A) Naïve BALB/C mice were primed (i.v.) with either 1, 5, or 10 μg of DEC205-OVA in combination with 50 μg poly(I:C) and 50 μg anti-CD40, and boosted (i.v.) 9 days later with 10^8 PFUs of VSVΔ51-OVA. **(B)** SIINFEKL-specific antigen responses were evaluated in blood at day 4 and **(C)** day 6 by staining with $H2K^b$-SIINFEKL pentamer **(D, E)** The percentage of SIINFEKL-specific T cells producing IFNγ and TNFα in the spleen were also evaluated by ICS and flow cytometry at day 21. Mean ± SD. 2-way ANOVA. $p < 0.05$ = *, $p < 0.01$ = **. N=4 for experimental groups, n=2 for PBS control group.

Supplemental Result 2. Comparison of single chain DEC205 and full chain DEC205 antibodies employed in prime-boost immunotherapy

An interesting alternative to reducing the dose of aDEC205 is to use a single chain version of aDEC205, which offers several advantages over full chain aDEC205 (fcDEC205), including the absence of the Fc domain, which eliminates unwanted interactions with Fc receptors that may interfere with DC targeting and the generation of immunity against the Fc portion of the antibody. Additionally, single chain DEC205 is less costly to produce and yields higher antibody concentrations than the full chain variant. Lastly, a study by Ngu *et al*. showed that administration of a scDEC205 results in a shorter duration of antigen presentation by dendritic cells (7 days) compared to full aDEC205 (15 days), in turn promoting the earlier formation of a central memory T cell (T_{CM}) population.[302]

The immunization schedule we optimized in Chapter 2 consists of a prime of 10μg aDEC205-OVA in combination with 50μg poly: IC and 50μg anti-CD40 (*i.v.*), and boost 9 to 14 days later with 10^8 pfu of VSVΔ51-OVA (*i.v.*). Earlier contraction of the effector CTL population and establishment of the central memory pool of T cells after administration of scDEC205 would theoretically allow for an earlier boosting schedule. These findings suggest that the use of single chain DEC205 offers a promising alternative immunization strategy.

To evaluate if scDEC205-OVA is equivalent to fcDEC205-OVA as a priming vector, we compared the ability of scDEC205-OVA and fcDE205-OVA to generate an antigen specific response and to establish a T_{CM} population. We administered 10μg fcDEC205-OVA or scDEC205-OVA, both in combination with 50μg polyI: C and 50μg anti-CD40 (*i.v.*) and boosted 9 days later with 10^8 pfu of VSVΔ51-OVA (*i.v.*) (Figure I.2A). SIINFEKL-specific T cells were evaluated by flow cytometry. H-2K^b-SIINFEKL pentamer staining showed statistically similar percentages of SIINFEKL-specific CD8+ T cells at all time points tested, and both groups showed a significant increase over PBS control at days 8, 12, 14, 16 and 27. (Figure I.2B,C).

Antigen-specific memory T cells were evaluated at day 8 post prime and day 27 post prime immunization. To identify antigen-specific memory T cells, cells were stained for CD8a, H-2K^{b}-SIINFEKL pentamer, and phenotypic markers of T cell differentiation; CD62L and CD127. Pentamer staining allows for the isolation of antigen-specific T cells; additionally, staining for CD62L and CD127 allows for phenotyping of antigen-specific CD8+ T cells as effector (CD62L-CD127-), T_{CM} (CD62L+CD127+) or effector memory T cells (CD62L-CD127+), and intermediate T cells that are differentiating from naïve to effector (CD62L+CD127-). At day 8 post-prime immunization, the percentage of antigen-specific effector T cells, effector memory T cells, and central memory T cells was approximately 70%, 19% and 4% in the scDEC205 group, and 65%, 28%, 2% in the fcDEC205 group. (Figure I.2D) While the scDEC205-OVA and fcDE205-OVA groups demonstrated no significant difference in the formation of antigen-specific T cell memory pool, fcDEC205-OVA induced a higher percentage of memory T cells (30%) compared to scDEC205 (23%). This contrasts with the findings of Ngu *et al*., which showed that scDEC205 leads to faster contraction of antigen-specific effector cells and generation of antigen-specific memory pool of T cells.[302] One important consideration is that these immune populations were evaluated in the blood. However, T-cell memory subtypes are home to different tissues. T_{CM} are mainly found in lymphoid organs, whereas T_{EM} can be found in the blood where they can rapidly localize to inflamed peripheral tissue, and thus frequencies of cell populations evaluated only in the blood will underestimate the total frequency of some T cell types. At day 27 (post-boost), no significant differences were observed in the percentages of antigen-specific effector and memory T cells between groups, indicating that the immune response generated after the boost results in the same T cell populations, regardless of the antibody used for priming (Figure I.2E,F) Overall, no difference in antigen specific T cell responses after prime and boost was observed between scDE205-OVA and fcDE205-OVA, therefore we hypothesize that scDEC205 could be used in place of fcDEC205 in future studies.

Altogether, using scDEC205 as prime in combination with a VSVΔ51 boost generates robust immune response and can be an attractive alternative approach to overcome challenges with full aDEC205 production should they arise.

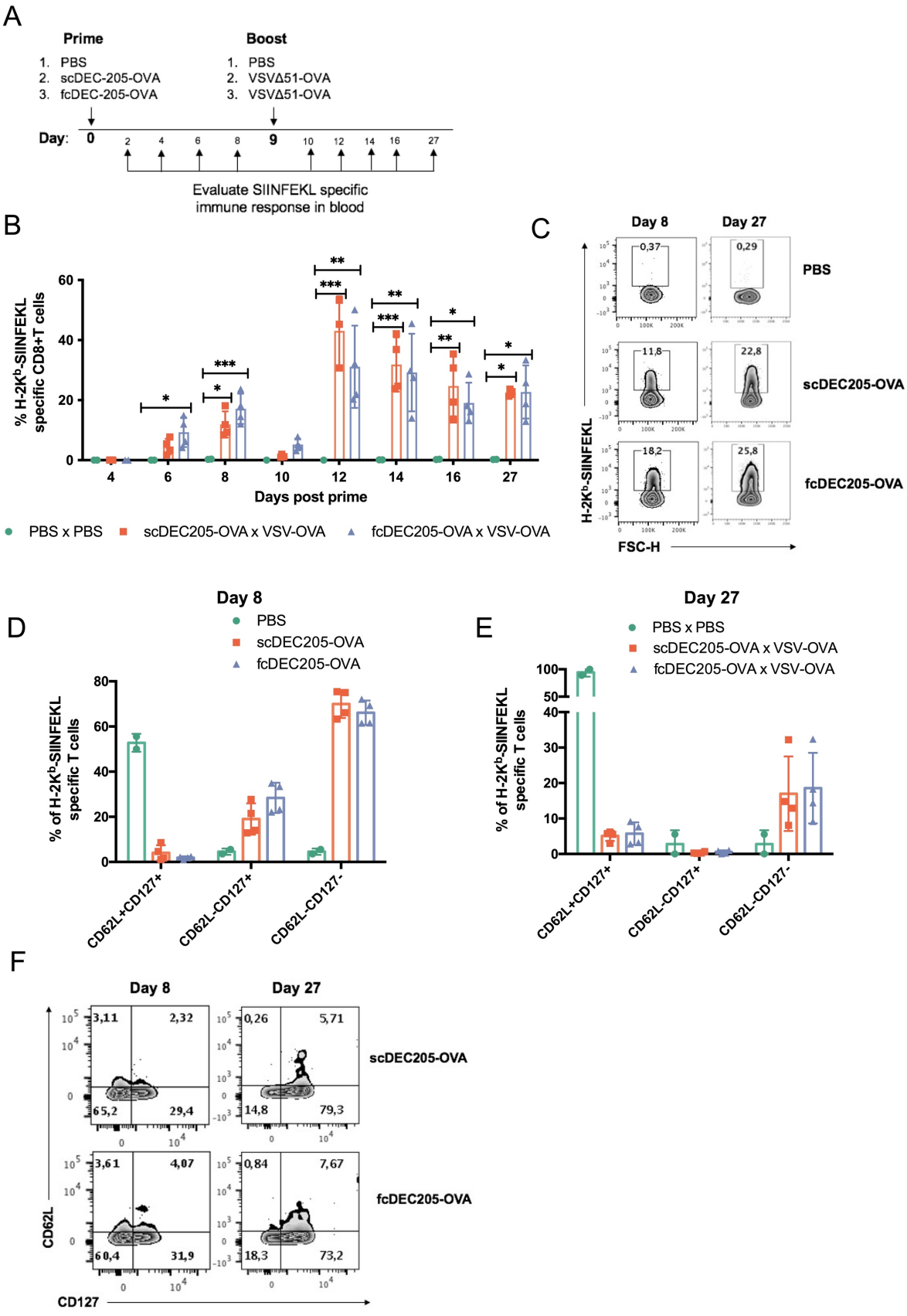
A
Prime
1. PBS
2. scDEC-205-OVA
3. fcDEC-205-OVA
Boost
1. PBS
2. VSVΔ51-OVA
3. VSVΔ51-OVA
Day: 0 2 4 6 8 9 10 12 14 16 27
Evaluate SIINFEKL specific immune response in blood
B
% H-2Kb-SIINFEKL specific CD8+T cells
Days post prime
PBS x PBS
scDEC205-OVA x VSV-OVA
fcDEC205-OVA x VSV-OVA
C
Day 8
Day 27
PBS
scDEC205-OVA
fcDEC205-OVA
H-2Kb-SIINFEKL
FSC-H
0,37
0,29
11,8
22,8
18,2
25,8
D
Day 8
PBS
scDEC205-OVA
fcDEC205-OVA
% of H-2Kb-SIINFEKL specific T cells
CD62L+CD127+
CD62L-CD127+
CD62L-CD127-
E
Day 27
PBS x PBS
scDEC205-OVA x VSV-OVA
fcDEC205-OVA x VSV-OVA
% of H-2Kb-SIINFEKL specific T cells
CD62L+CD127+
CD62L-CD127+
CD62L-CD127-
F
Day 8
Day 27
scDEC205-OVA
fcDEC205-OVA
CD62L
CD127
3,11
2,32
65,2
29,4
0,26
5,71
14,8
79,3
3,61
4,07
60,4
31,9
0,84
7,67
18,3
73,2

Supplemental Figure 2. Comparing SIINFEKL-specific T cell response at several time points after administration of full chain or single chain anti-DEC205-OVA. (A) Naïve C57BL/6 mice were immunized with PBS(n=4), single chain (n=8) or full chain DEC205-OVA (n=8) + 50 μg polyI:C + 50μg anti-CD40 at day 0, followed by a boost with 10^8 pfu VSV-OVA i.v. or PBS. Two PBS mice and four immunized mice from each group were bled at each time point. **(B,C)** The percentage of SIINFEKL-specific CD8+ T cells in the blood was determined by H2-K^b-SIINFEKL pentamer staining every 2 days after administration of prime. **(D, E, F)** Memory phenotype of antigen specific CD8+ T cells was determined by flow on day 8 and day 27 post-prime by staining for CD62L and CD127. CD8+ T cells are described as effector (CD62L-CD127-), T_{CM} (CD62L+CD127+) or effector memory T cells (T_{EM})(CD62L-CD127+), and intermediate T cells that are differentiating from naïve to effector (CD62L+CD127-). Mean ± SD. 2-way ANOVA. $p < 0.05$ = *, $p < 0.01$ = ** $p < 0.001$ = ***

Supplemental Result 3. aDCIR as an alternative vector to aDEC205

Another endocytic receptor that may serve as a candidate for DC-directed antibody-mediated antigen delivery is the DCIR receptor expressed on dendritic cells. Analogous to aDEC205, targeted antigen delivery to DCIR via a recombinant DCIR antibody results in antigen presentation by MHC-I and MHC-II.[303,304] As such, we aimed to compare aDCIR and aDEC205 priming capabilities by evaluating the anti-OVA immune response generated by immunizing mice with aDCIR-OVA or aDEC205-OVA. Anti-DCIR-OVA was produced by co-transfection of HEK293T cells with two plasmids: pDCIR-OVA (plasmid containing the murine heavy chain in frame) and pDCIR-Kappa (plasmid containing the light chain) followed by antibody purification from the culture supernatant. After two attempts of antibody purification, very small quantities of antibody were produced. Probing for IgG by Western blot (WB) at each step of antibody purification revealed that the antibody was present throughout the purification process (Figure I.3). However, the final antibody concentration was 0.05 mg/mL, and although this was detected by western blot, this yield needs to be higher and more concentrated for *in vivo* applications.

While the DCIR receptor shows potential as an endocytic receptor the DC-directed antibody-mediated antigen delivery, further optimization is necessary to achieve higher and more concentrated antibody yields for efficient *in vivo* applications.

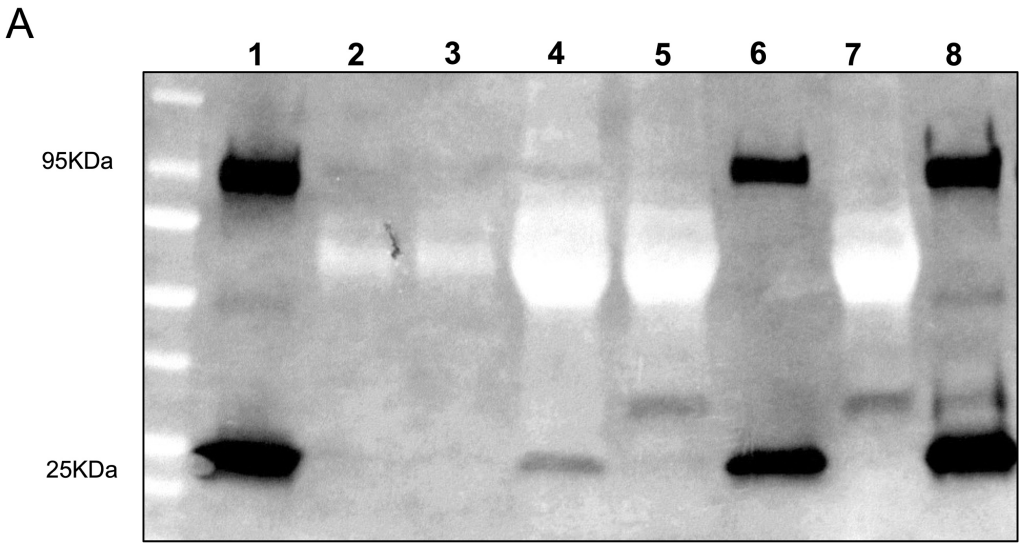

1. DEC-OVA control
2. Supernatant on day 7
3. Filtered supernatant
4. After 1st dialysis
5. Supernatant after 1st round of protein G beads
6. After 2nd round of dialysis
7. Supernatant after 2nd round of protein G beads
8. DCIR-OVA after 1st elution

Supplemental Figure 3. Production of aDCIR-OVA (A) aDCIR-OVA and aDEC205-OVA positive control were generated by transfection of 293T cells in vitro, and subsequent antibody purification. Antibody was reduced by β-mercaptoethanol and verified by immunoblotting for the heavy and light chains. aDCIR-OVA and aDEC205-OVA shows the heavy chain linked with OVA at 95kDa; indicating presence of OVA antigen, and a light chain at 25kDa

Supplemental Result 4. Validating K7M2 cell lines for future experiments

The poor take rate observed in Chapter 4.2.11 prompted us to explore parameters that may have affected tumor growth of implanted K7M2 cells. Among those we analyzed the growth kinetics of K7M2 cells used for this experiment (K7M2 V2) compared to the original stock of K7M2 cells (K7M2 V1), and found that K7M2 V1 exhibited higher proliferation compared to K7M2 V2. We also assessed MHC-1 and PD-L1 expression on K7M2 V1, K7M2 V2, S180 and WEHI-164 cells by flow cytometry. Increased MHC expression by tumor cells can lead to faster tumor clearance by enhancing the presentation of tumor antigens to T cells, thereby generating a stronger immune response against the tumor. Furthermore, increased expression of the inhibitory molecule PD-L1 on tumor cells can favor tumor growth by decreasing the activity of tumor-specific T cells, causing T cell exhaustion and immune evasion.

To evaluate MHC-I expression, we probed for H-2K^{d} and H-2L^{d}. K7M2 V2 showed lower overall expression of MHC-I compared to K7M2 V1. (Figure I.4C) Evaluation of PD-L1 expression showed that K7M2 V1 express higher levels of PD-L1 compared to K7M2 V2, suggesting that K7M2 V1 cells can evade the anti-tumor immune response in turn leading to tumor growth, whereas K7M2 V2 express lower levels of PD-L1, leaving them more susceptible to T-cell mediated killing. (Figure I.4D)

Both PD-L1 and MHC expression play important but different roles in regulating the immune response to tumors, and their relative importance may depend on the specific context of the tumor microenvironment. It is difficult to say whether PD-L1 expression outweighs MHC-I expression. Still, we hypothesize that PD-L1 expression on K7M2 V1 prevented T cell-mediated killing of tumor cells, despite high levels of MHC-I expression. Altogether, this data suggests that K7M2 V1, which was used in initial experiments had a growth advantage due to a higher rate of proliferation and higher PD-L1 expression compared to K7M2 V2, and provides a rationale for the poor tumor take rates and slow tumor growth of K7M2 V2 tumors.

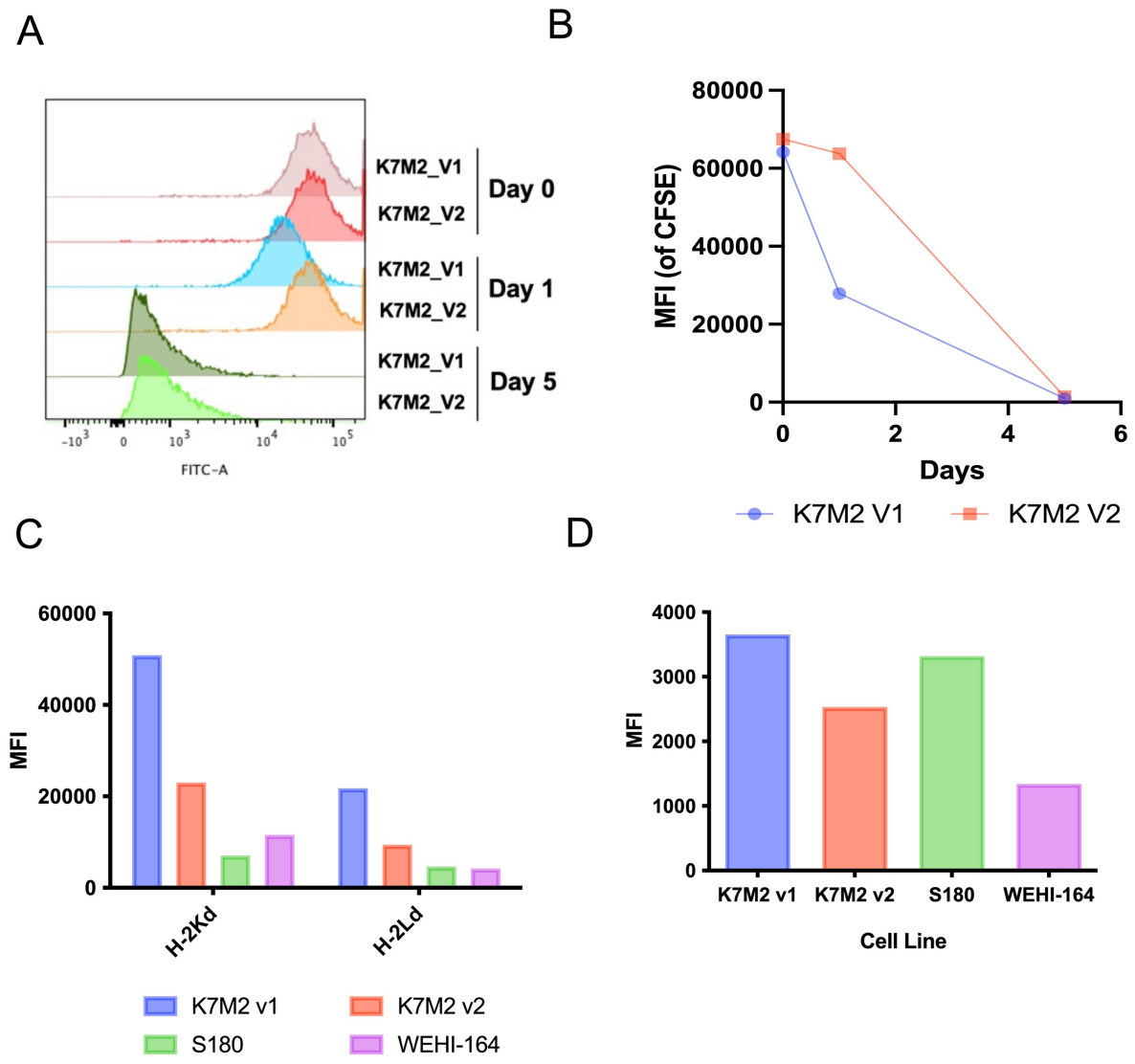

Supplemental Figure 4. CFSE proliferation assay, MHC-I, and PD-L1 expression was compared between K7M2 after only three passages (K7M2 V1) cells used in survival experiments (K7M2 V2), and other sarcoma cell lines (S180 and WEHI-164) A.B. Cells were labelled with CFSE, brightness of CFSE was assessed at D0, D1 and D5 by flow cytometry. Reduction of the brightness of CFSE is indicative of cell proliferation. **C.** Expression of the MHC-I haplotypes H-2K^{d} and H-2L^{d} were assessed by flow cytometry. **D.** PD-L1 expression on sarcoma cell lines was assessed by flow cytometry

Appendix II. Supplemental Figures and Tables

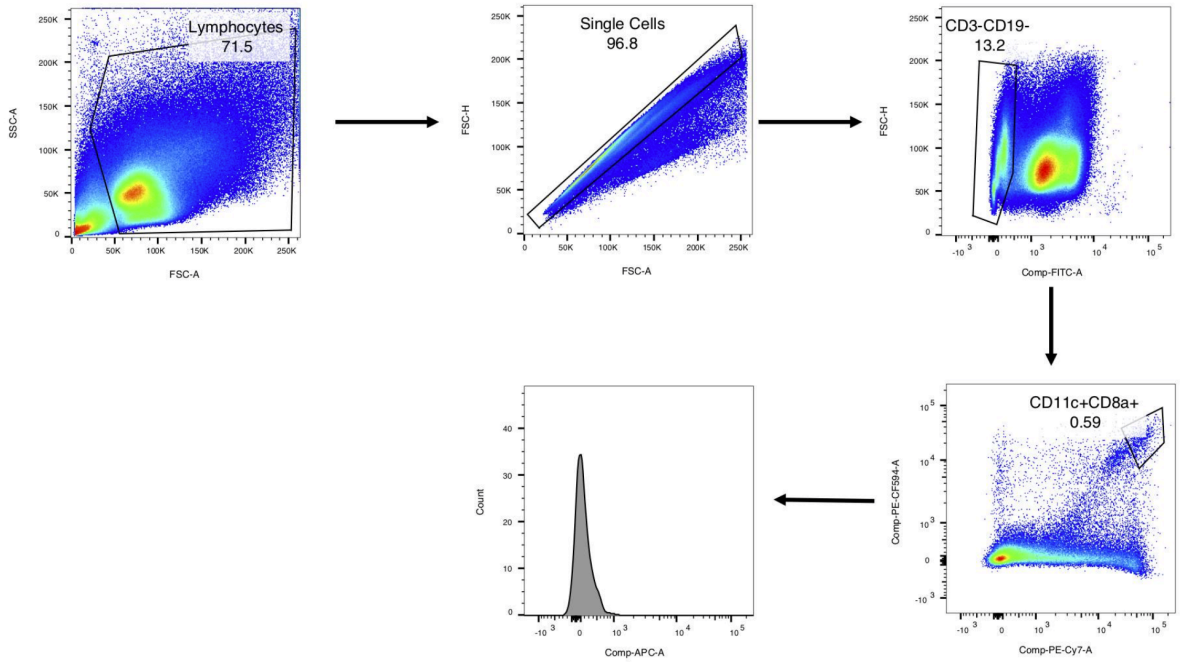

Supplemental Figure 5. Gating strategy of binding assay to determine the binding efficacy of aDEC205-OVA to CD11c+CD8+ DCs.

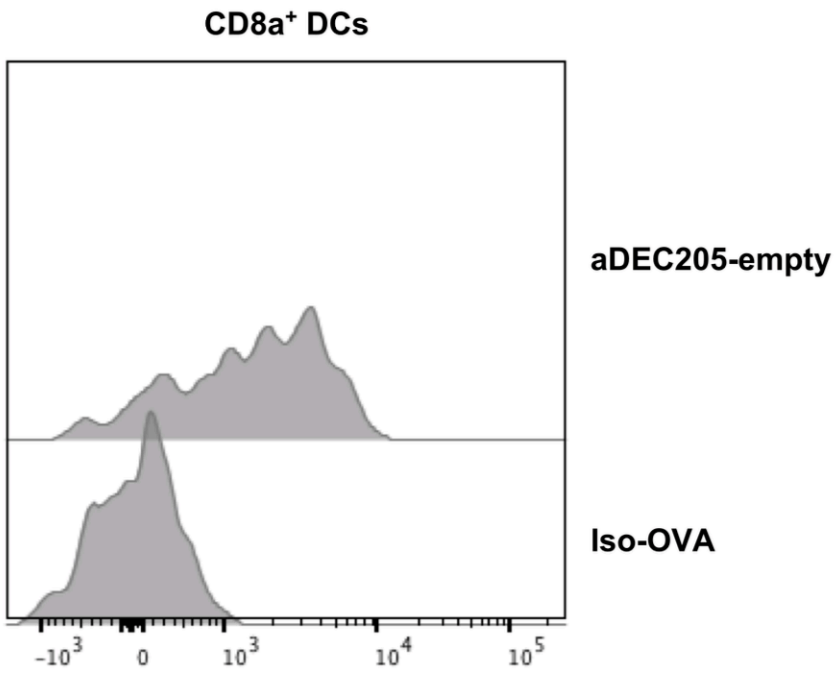

Supplemental Figure 6. A binding assay was performed to verify effective binding of aDEC205-empty to the DEC205 receptor on CD11c+CD8+ dendritic cells (DCs) isolated from murine splenocytes. aDEC205-empty is probed with an anti-IgG1-APC antibody and detected by flow cytometry. The histogram overlay depicts high binding of aDEC205-empty to CD11c+CD8+ DCs at a concentration of 10μg/mL compared to isotype control.

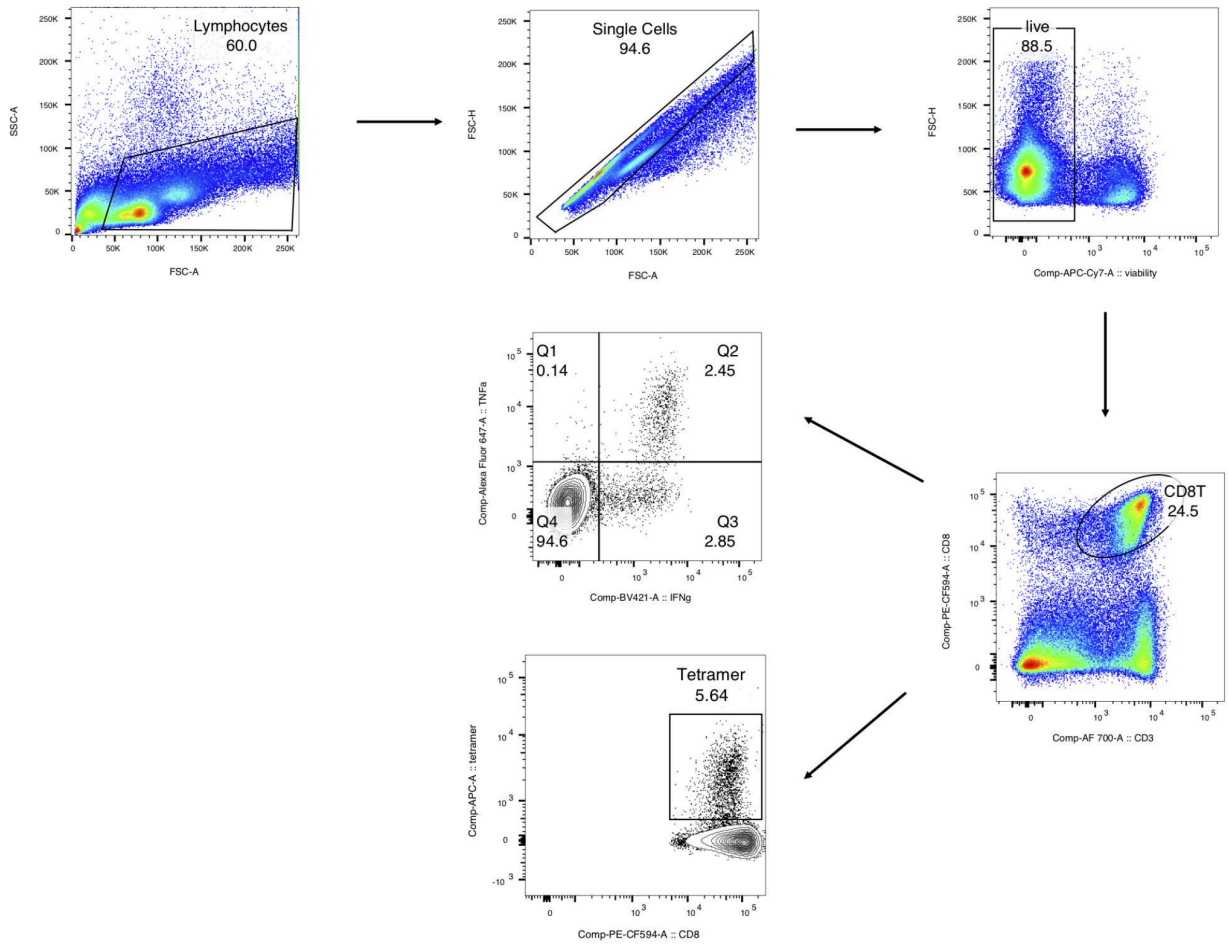

Supplemental Figure 7. Gating strategy to determine percentage of CD8+CD3+ T cells producing IFNγ and TNFα and positive H2-Kb-SIINFEKL pentamer staining.

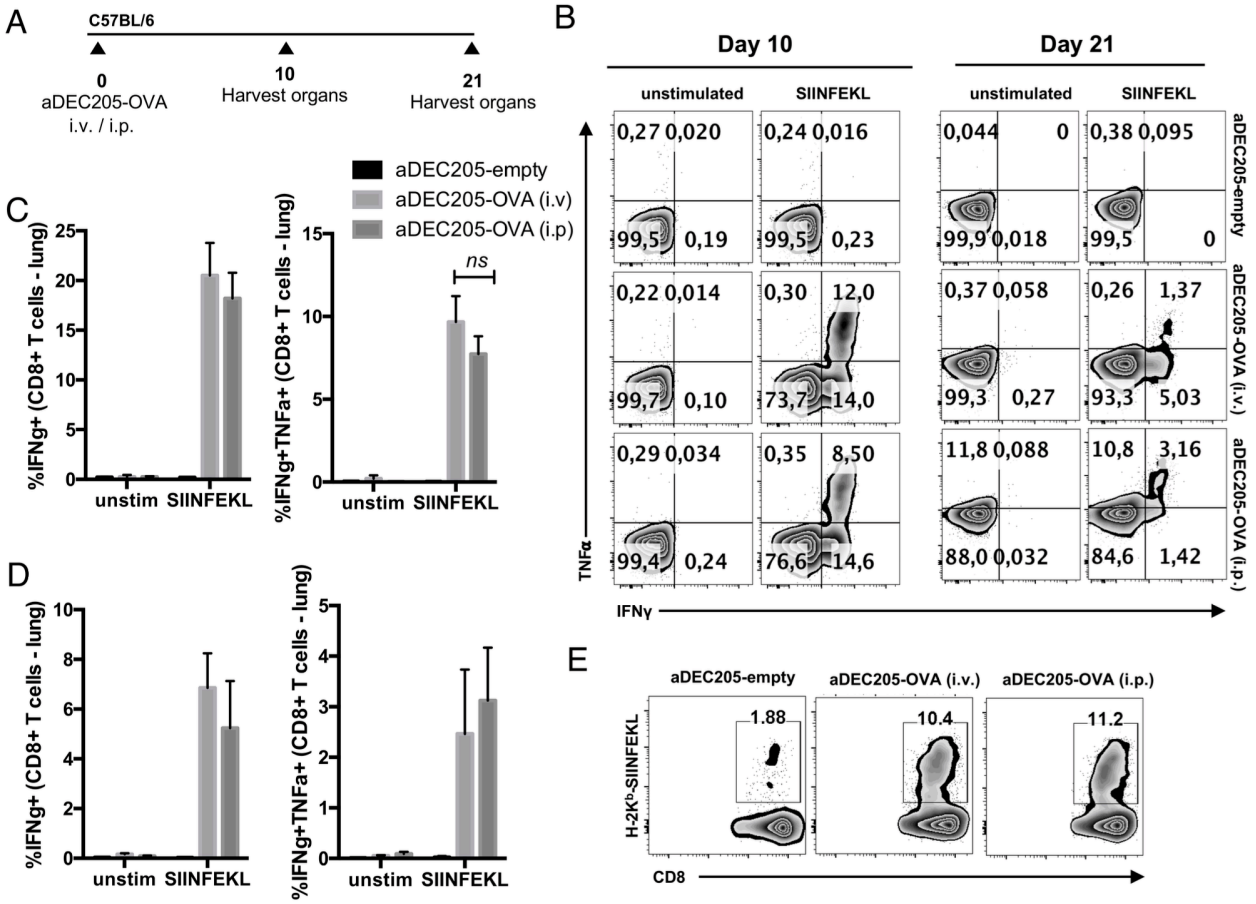

Supplemental Figure 8. aDEC205-OVA administered i.v. or i.p. elicits OVA specific T cells in the lungs of immunized mice. (A) Naïve C57BL/6 mice were primed with 10µg of aDEC205-OVA or aDEC205-empty + 50µg poly:IC + 50µg anti-CD40 i.v. or i.p. The percentage of SIINFEKL-specific T cells producing IFNγ and TNFα in the lungs (**B, C** (D10), **D** (D21)) was evaluated by flow cytometry. Quantification of SIINFEKL specific T cells by pentamer staining (H-2K^b- SIINFEKL) was also assessed in the € lungs by flow cytometry at day 21 post injection. *P*-value considered nonsignificant (NS) when >0.05 (two-way ANOVA).

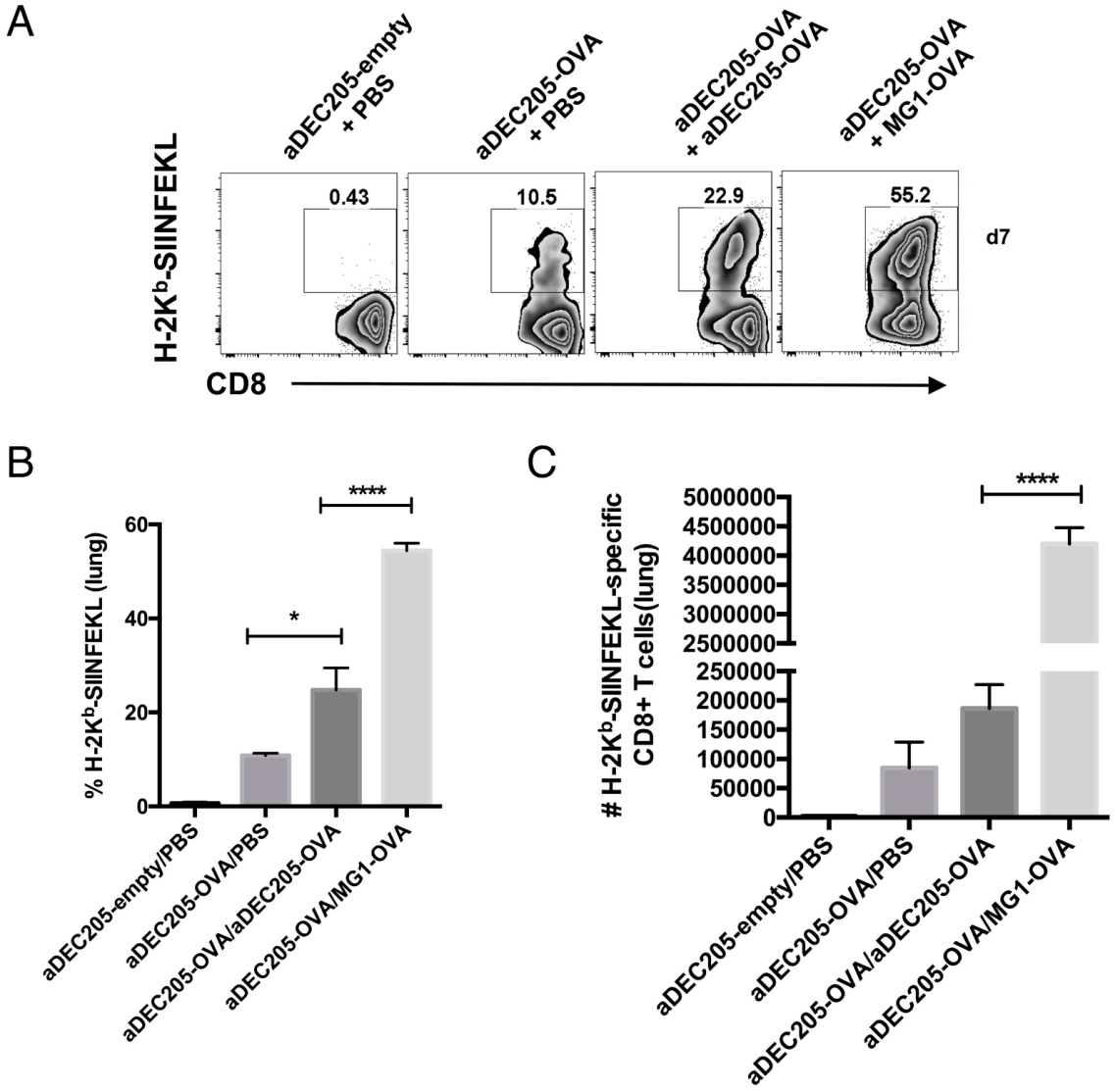

Supplemental Figure 9. Induction of potent cellular OVA-specific CD8+ T cells in the lungs of mice immunized with aDEC205-OVA prime and MG1-OVA boost. C57BL/6 mice were immunized i.v with 10µg of aDEC205-OVA or aDEC205-empty+50µg poly:IC+50µg anti-CD40 at day 0 (D0). Fourteen days later, mice were immunized with a boosting dose of either, PBS, 10µg aDEC205- OVA i.v +50µg poly:IC+ 50µg anti-CD40 or 10^8 pfu of MG1-OVA. Lungs were harvested 7 days following boost to evaluate cellular immune response to prime-boost regimens. (**A,B**) The percentage and **(C)** total number of SIINFEKL-specific CD8+ T cells was determined by H-2K^b-SIINFEKL pentamer staining. *, $p<0.05$; **** $p<0.0001$ (one-way ANOVA).

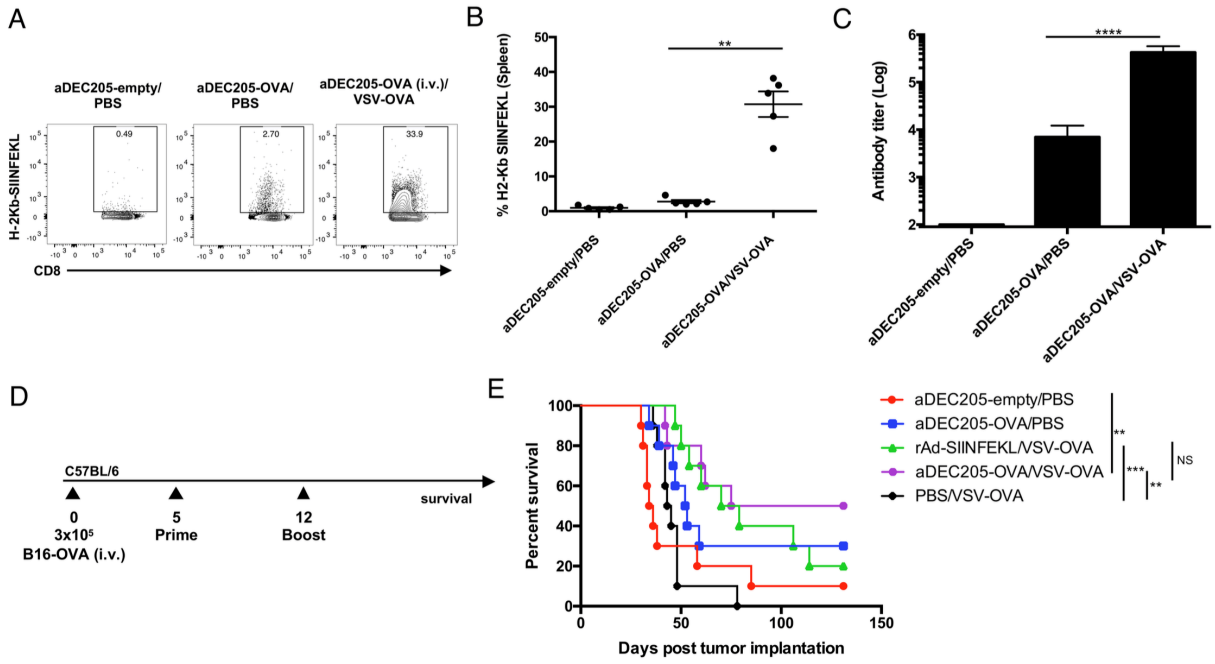

Supplemental Figure 10. Evaluation of the boosting capacity of VSV-OVA and survival in tumour bearing mice. (**A, B)** C57BL/6 mice were immunized i.v. with 10µg of aDEC205-OVA or aDEC205-empty+ 50µg poly:IC+50µg anti-CD40 at D0. At day 14 mice received a boosting dose of 10^8 VSV-OVA or PBS. Spleens were harvested on day 21 and assessed for the percentage of OVA-specific CD8+ T cells determined by H-2K^b-SIINFEKL pentamer staining. **(C)** The titers of anti-OVA antibodies in the sera of mice were determined by ELISA to evaluate the humoral immune response to aDEC205-OVA prime-boost regimen day 7. **(D)** C57BL/6 mice were given i.v. injections of $3x10^5$ B16-OVA tumour cells. After 5 days, mice were given i.m. injection of rAd5 or i.v. injections of aDEC205-OVA or aDEC205-empty. 7 days post prime, all mice were injected VSV-OVA *i.v.*. **(E)** Mice were monitored for survival 140 days post B16-OVA implantation. $^{**}p < 0.005$, $^{****}p < 0.0005$

Supplemental Table 1. Individual clinical characteristics of patient FFPE samples used in nCounter Nanostring analysis

	Immune Phenotype	Gender	Age	Site	Tumor size (cm3)	Primary/recurrence/metastasis	Treatment	Metastasis present at time of resection, site	Outcome (last visit)
1	inflamed	F	70	retroperitoneal	20	primary	NA	NA	NA
2	inflamed	M	77	retroperitoneal	NA	primary	NA	NA	NA
3	inflamed	M	85	right chest wall	11	primary	Adjuvant XRT	No	deceased
4	inflamed	M	68	spermatic cord	NA	primary	NA	NA	NA
5	inflamed	M	80	left leg	15	primary	Surgery	No	deceased
6	inflamed	M	61	right leg	14.5	recurrence	NA	NA	NA
7	inflamed	F	58	left medial thigh	31	primary	Surgery	NA	NA
8	inflamed	F	54	left thigh	6	primary	Surgery	Yes, lungs and local recurrence	deceased
9	inflamed	M	75	retroperitoneal	25	primary	Neoadjuvant XRT	NA	NA
10	inflamed	M	71	right chest wall	5.4	primary	Surgery + Adjuvant XRT	No	disease free (2019)
11	inflamed	M	54	left thigh	29.6	primary	Surgery + Adjuvant XRT	No	disease free (2020)
12	inflamed	M	43	retroperitoneal	18.5	primary	Neoadjuvant XRT + Surgery	Yes, lung	disease free (2020)

13	inflamed	M	61	left medial calf	N/A	primary	Surgery	Yes, lungs	disease free (2019)
14	inflamed	M	71	retroperitoneal	19.7	primary	Surgery	Yes, lymph nodes	NA
15	inflamed	F	86	right thigh	35	primary	Surgery	No	deceased
16	non-inflamed	M	60	left chest wall	4.4	primary	Neoadjuvant XRT + Surgery	No	disease free (2020)
17	non-inflamed	F	57	left anterior thigh	10.6	recurrence	NA	NA	NA
18	non-inflamed	F	71	retroperitoneal	34	primary	NA	NA	NA
19	non-inflamed	M	47	chest wall	14.8	primary	Neoadjuvant XRT	NA	NA
20	non-inflamed	M	53	retroperitoneal	40	primary	NA	NA	NA
21	non-inflamed	F	88	left shoulder	NA	recurrence	Surgery	No	disease free (2020)
22	non-inflamed	M	43	left arm	1.7	recurrence	Surgery	NA	Lost to F/U
23	non-inflamed	F	73	right upper arm	NA	primary	Surgery + Adjuvant XRT	No	deceased, not from disease
24	non-inflamed	F	73	left popliteal fossa	7	primary	Adjuvant XRT	Yes, lungs	disease free (2019)
25	non-inflamed	M	65	retroperitoneal	31.5	primary	Surgery	No	Lost to F/U

26	non-inflamed	F	45	right popliteal fossa	4	primary	Neoadjuvant XRT	No	disease free
27	non-inflamed	NA	NA	NA	NA	NA	NA	NA	NA
28	non-inflamed	M	50	retroperitoneal	16.5	primary	Surgery + Adjuvant XRT + CTX	No	disease free (2018)
29	non-inflamed	F	75	left medial thigh	NA	primary	NA	NA	NA

NA = information not available, XRT = radiation therapy, CTX = chemotherapy

Supplemental Table 2. Differentially expressed genes in DDLS compared to healthy adipose control

Gene	Log2 Fold Change	Adjusted Benjamini-Yekutieli p-value
SAA1	-8.29	1.18E-06
CCL21	-4.22	0.00377
S100B	-4.18	3.14E-05
CD36	-4.05	1.18E-06
FOS	-3.67	1.00E-07
CXCL2	-3.5	1.50E-05
MCAM	-3.41	1.63E-12
IL18RAP	-3.35	1.18E-06
C6	-3.13	0.0018
CSF3R	-3.13	0.00394
PTGS2	-3.1	0.00158
CCL14	-3.09	4.95E-06
EGR1	-3.05	3.52E-06
ITGB4	-2.82	0.000679
CFD	-2.79	0.00215
CCL2	-2.7	0.00151
PPARG	-2.62	6.36E-05
CDH5	-2.15	1.44E-06
NLRP3	-2.07	8.92E-06
PLA2G6	-1.85	1.24E-06
ITGA	-1.71	1.13E-05
ANXA1	-1.69	5.79E-06
NOTCH1	-1.66	1.00E-07
DUSP6	-1.65	5.48E-05
PRKCD	-1.61	0.000121
STAT5B	-1.6	7.74E-06
BCL6	-1.57	0.00104
ICAM2	-1.51	0.000605
NFKBIA	-1.47	7.19E-05
CD46	-1.32	1.95E-06
BCL2	-1.19	7.19E-05
DOCK9	-1.14	0.000679
MAPK3	-0.958	0.000679
JAK2	-0.857	0.00193
TNFRSF1A	-0.659	0.00478
EP300	-0.582	0.000141
BAX	0.936	0.00158
ISG15	1.3	0.00277

GZMA	2.33	0.00343
FN1	2.44	7.19E-05
NUP107	2.86	0.0032
CDK1	2.92	3.52E-06
CD8A	2.93	0.0038
IDO1	3.07	0.00309
FCGR1A	3.1	0.00394
CXCL10	3.63	0.00104
CCR5	3.77	0.00168
BIRC5	3.86	2.19E-06
NEFL	4.23	0.000103
TTK	4.44	1.18E-06
PBK	5.17	4.41E-07

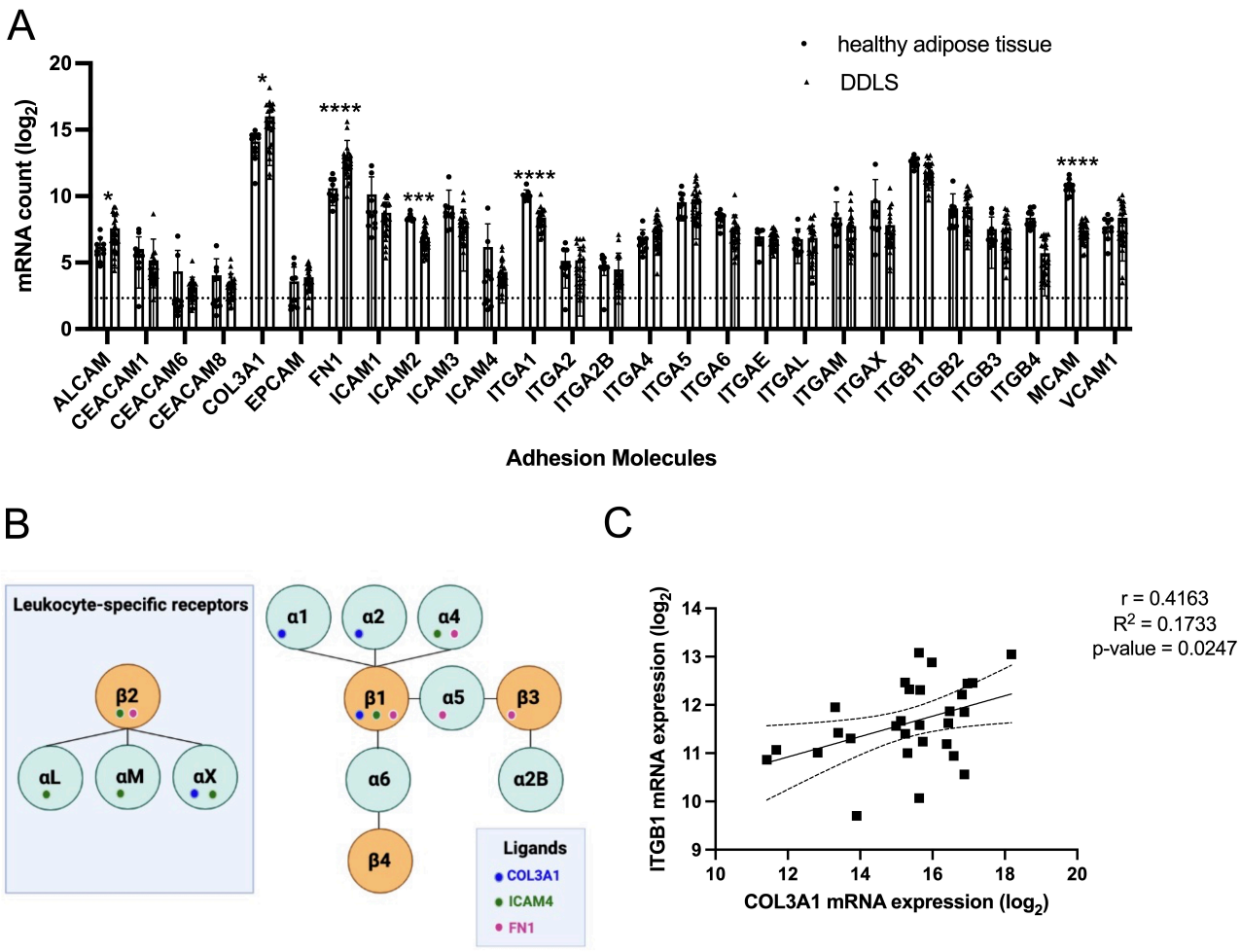

Supplemental Figure 11. (A) Log2 mRNA counts of adhesion molecules in healthy adipose tissue and in DDLS. Significance of differential expression between groups is calculated using the Benjamini-Yekutieli procedure. *= *p*-value<0.05, ** = *p*-value <0.01, *** = *p*-value<0.001, ****= *p*-value < 0.0001 **(B)** Schematic representation of integrin heterodimer pairs and their ligands included in correlation analysis. **(C)** Correlation of expression of ITGB1 integrin and COL3A1 ligand shows a moderate (r=0.4163), statistically significant (p-value= < 0.05) correlation of expression.

Supplemental Table 3. Correlation of co-expression of integrin alpha and beta heterodimers

	ITGA1	ITGA2	ITGA2B	ITGA4	ITGA5	ITGA6	ITGAL	ITGAM	ITGAX
ITGB1	r=0.4345 R^2= 0.1888 P=0.0185 *	r=0.02280 R^2= 0.00052 P=0.9065 NS	-	r=0.3999 R^2= 0.1599 P=0.0316 *	r=0.2649 R^2= 0.0702 P=-0.1649 NS	r=-0.04652 R^2= 0.002164 P=0.8106 NS	-	-	-
ITGB2	r=0.03219 R^2= 0.001 P=0.8683 NS	-	-	-	-	-	r=0.6511 R^2= 0.4240 P=0.0001 ***	r=0.71 R^2= 0.5041 P<0.0001 ****	r=0.7304 R^2= 0.5334 P<0.0001 ****
ITGB3	-	-	r=-0.1102 R^2= 0.01213 P=0.5695 NS	-	r=0.3175 R^2= 0.1008 P=0.0933 NS	-	-	-	-
ITGB4	-	-	-	-		r=0.5364 R^2= 0.2877 P=0.0027 **	-	-	-

- correlation of expression analysis not performed, NS = not significant

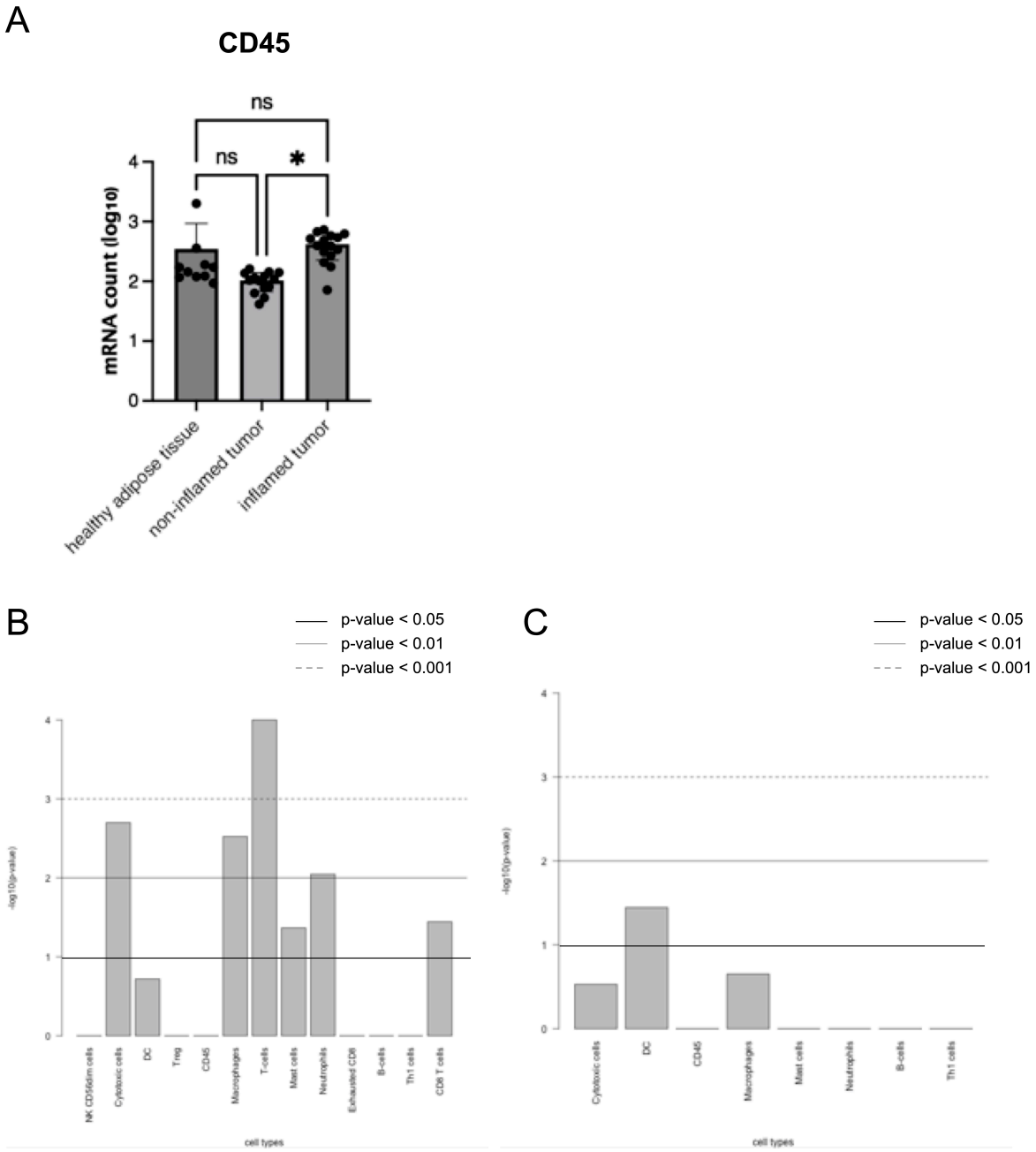

Supplemental Figure 12. **(A)** Barplot of CD45 mRNA counts in healthy adipose tissue, non-inflamed tumors, an inflamed tumors. Ordinary one way Anova, *= *p*-value < 0.05 Quality control plot exploring the validity of each cell types measurements based on detection of all pre-determined markers associated with each cell type. Barplot of p-values (-log10 transformed) across cell types in **(B)** inflamed and **(C)** non-inflamed tumors. Bars above the black line indicate cell types that were confidently detected at statistically significant levels (p-value of 0.05).

Supplemental Table 4. Table of upregulated and downregulated genes relative to healthy adipose tissue in inflamed and non-inflamed tumors, and those that are shared between both tumor phenotypes.

	Inflamed	Non-inflamed	Shared
Upregulated genes	*TRAF2, HLA-A, CD47, PSMB8, BAX, TAPBP, HLA-G, TAP1, IKBKE, HLA-B, OAS3, CSF1R, ITGA4, TAP2, HLA-DMB, CD84, C2, IL32, PSMB9, ISG15, LY96, MICB, CD74, CYBB, IL18, HLA-DRB3, HLA-DPB1, HLA-DRA, ITK, LCK, HLA-DPA1, GZMK, LY86, CCL5, IL2RB, GZMA, CD3E, IL7R, CD3D, TIGIT, CD8A, IDO1, SLAMF7, CD27, CXCL10, CXCL9, CCL17, CXCL13*	*GTF3C1, NCAM1, NUP107, NEFL*	*FN1, CDK1, BIRC5, TTK, PBK*
Downregulated genes	*C6, CFD, CX3CL1, DOCK9, DUSP6, EWSR1, ITGA1, ITGB4, LTF, MAPK3, NFATC1, PRKCD, PTGS2*	*BCL2L1, BST2, CCL2, CD59, CHIT1, CSF2RB, CSF3R, FOS, HCK, HLA-DMA, HLA-E, ICAM3, IL18RAP, IL1R2, ITGA1, ITGAX, ITGB4, JAK1, JAK2, LILRB3, NCF4, NFKBIA, PECAM1, PRKCD, SELL, TNFRSF14, TNFRSF1A, TNFSF12, TXNIP*	*ANXA1, BCL2, CCL14, CD36, CD46, CDH5, CXCL2, EGR1, EP300, FOS, ICAM2, MCAM, NLRP3, NOTCH1, PLA2G6, PPARG, PPBP, S100B, SAA1, STAT5B*

A

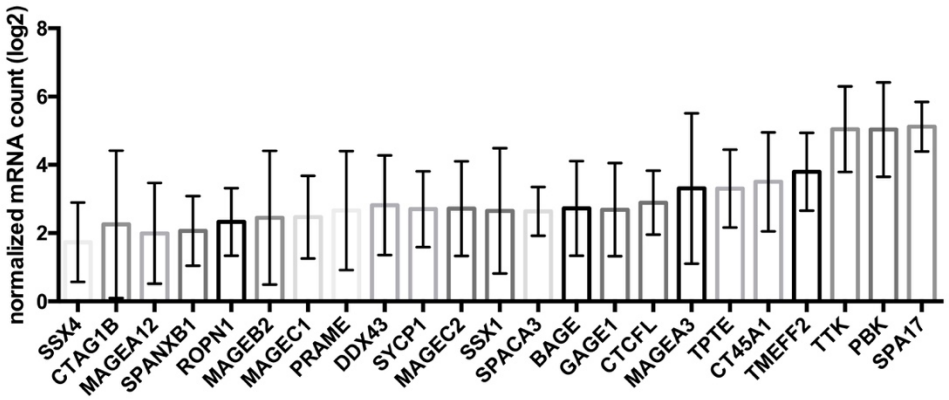

B

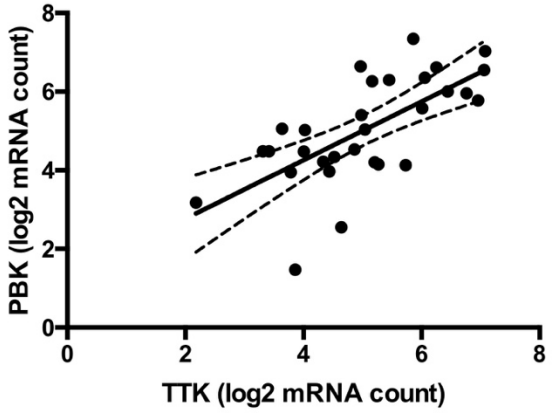

Supplemental Figure 13. (A) log2 normalized mRNA counts of CTAs in positive DDLS samples. **(B)** correlation of expression of PBK and TTK CTAs. log2 mRNA of PBK over log2 mRNA count of TTK shows a weak (r^2=0.4547) but statistically significant (p-value= < 0.0001) correlation of expression.

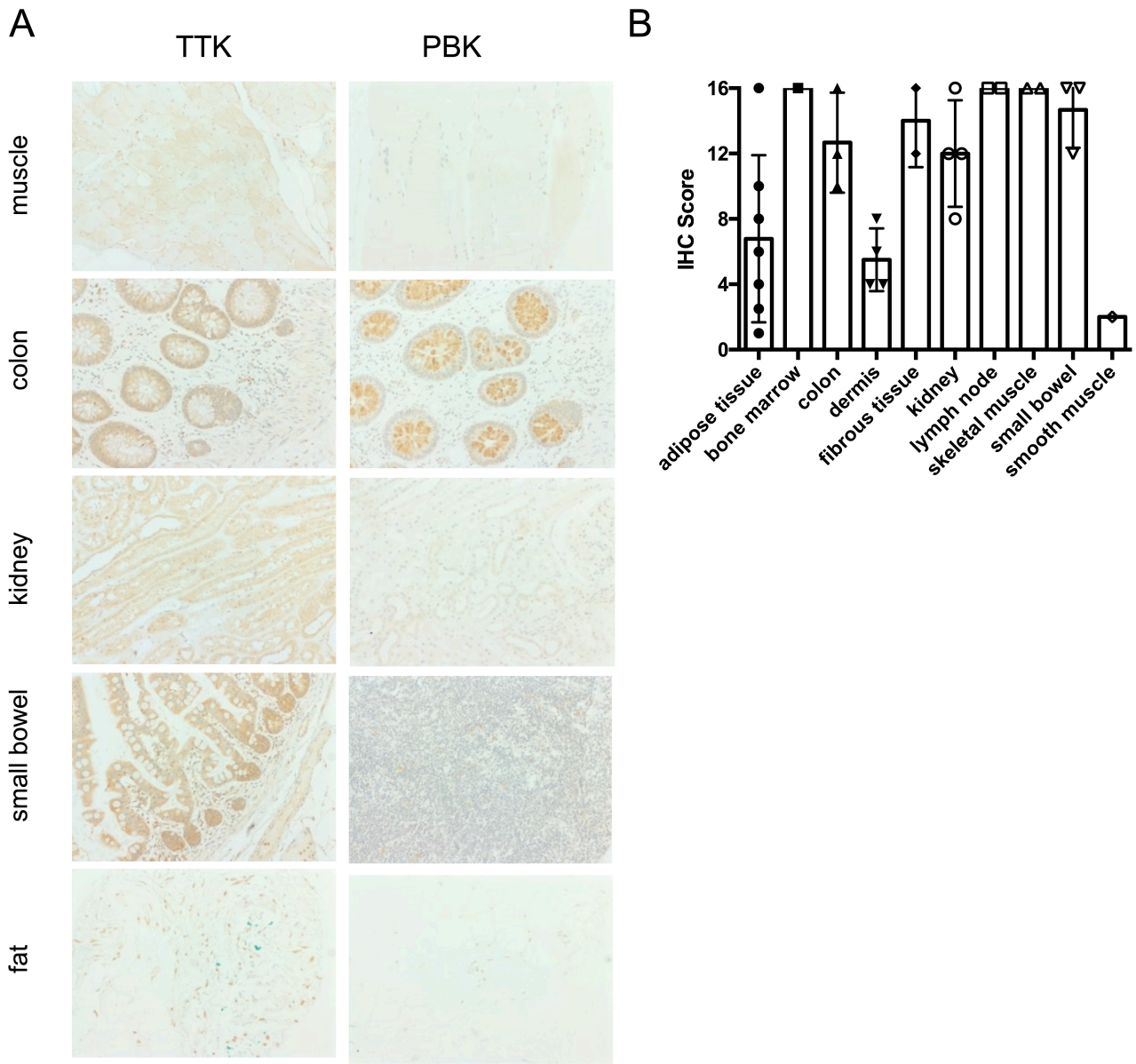

Supplemental Figure 14. (A) Representative images of positive IHC staining of TTK and PBK in in healthy tissues (**B)** IHC score of TTK expression in healthy tissues.

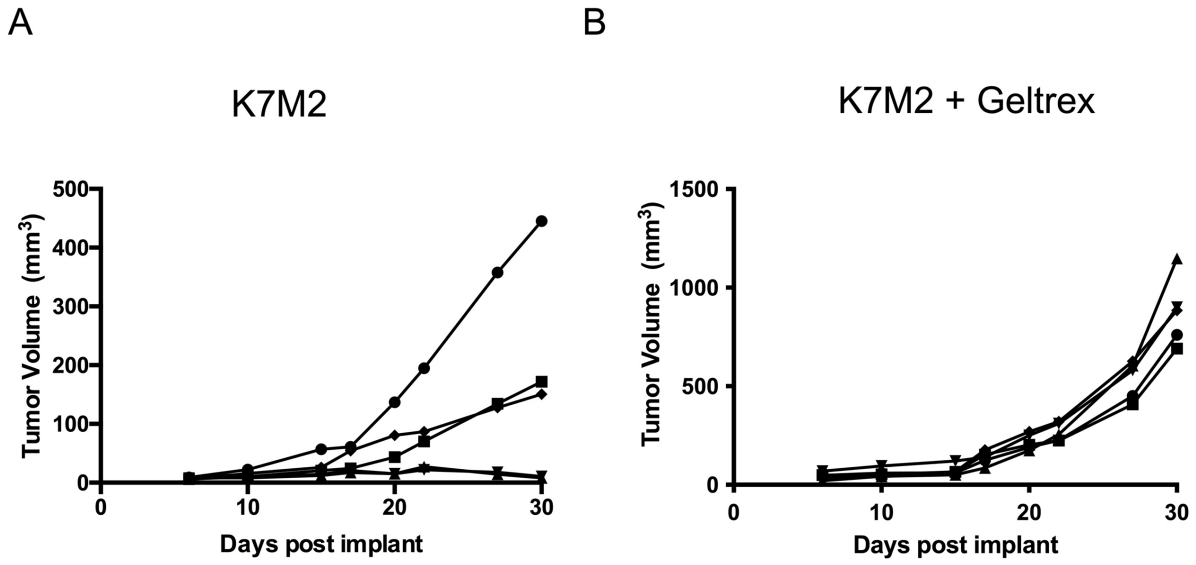

Supplementary Figure 15. Comparison of **(A)** K7M2 and **(B)** K7M2 + Geltrex tumor growth. Tumors were established by subcutaneous injection of $1x10^6$ K7M2 cells in PBS or in Geltrex, tumor growth was monitored over time.

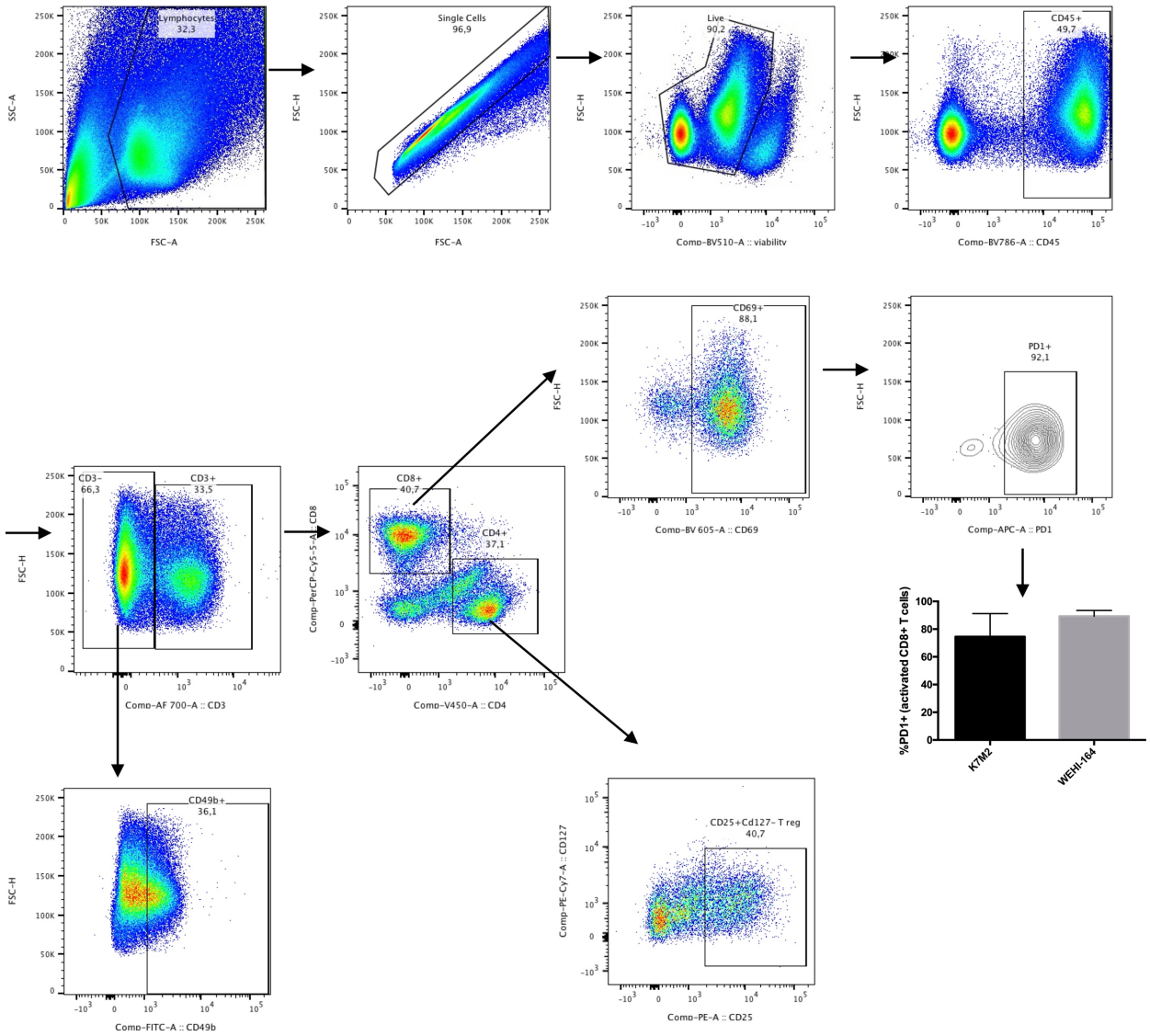

Supplemental Figure 16. Gating strategy for identification of intra-tumoral CD4+ T cells, Tregs, CD8+ T cells, activated CD8+ T cells, NK cells and PD1+ activated intra-tumoral CD8+ T cells.

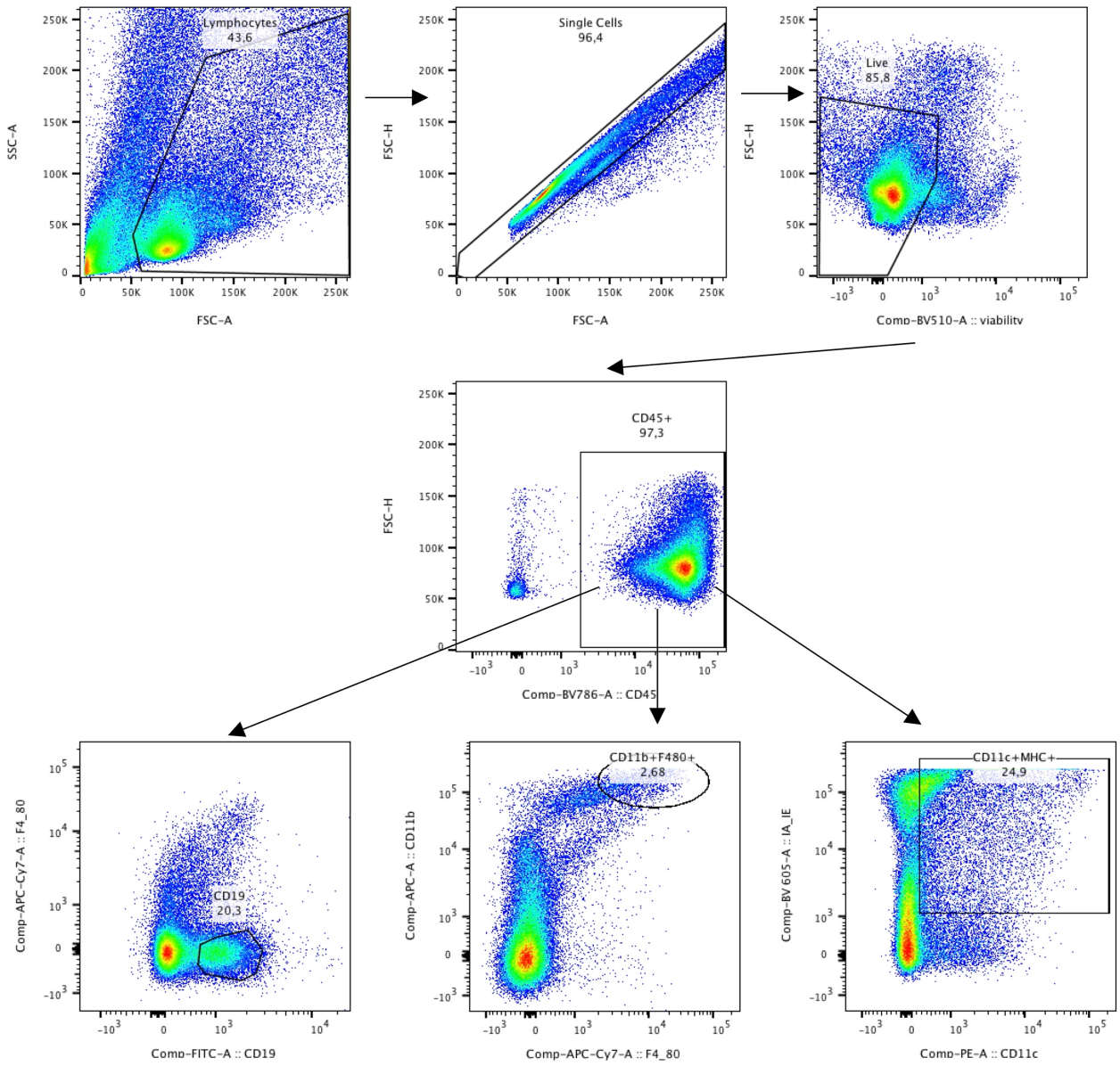

Supplemental Figure 17. Gating strategy for identification of intra-tumoral macrophages, B-cells and dendritic cells.

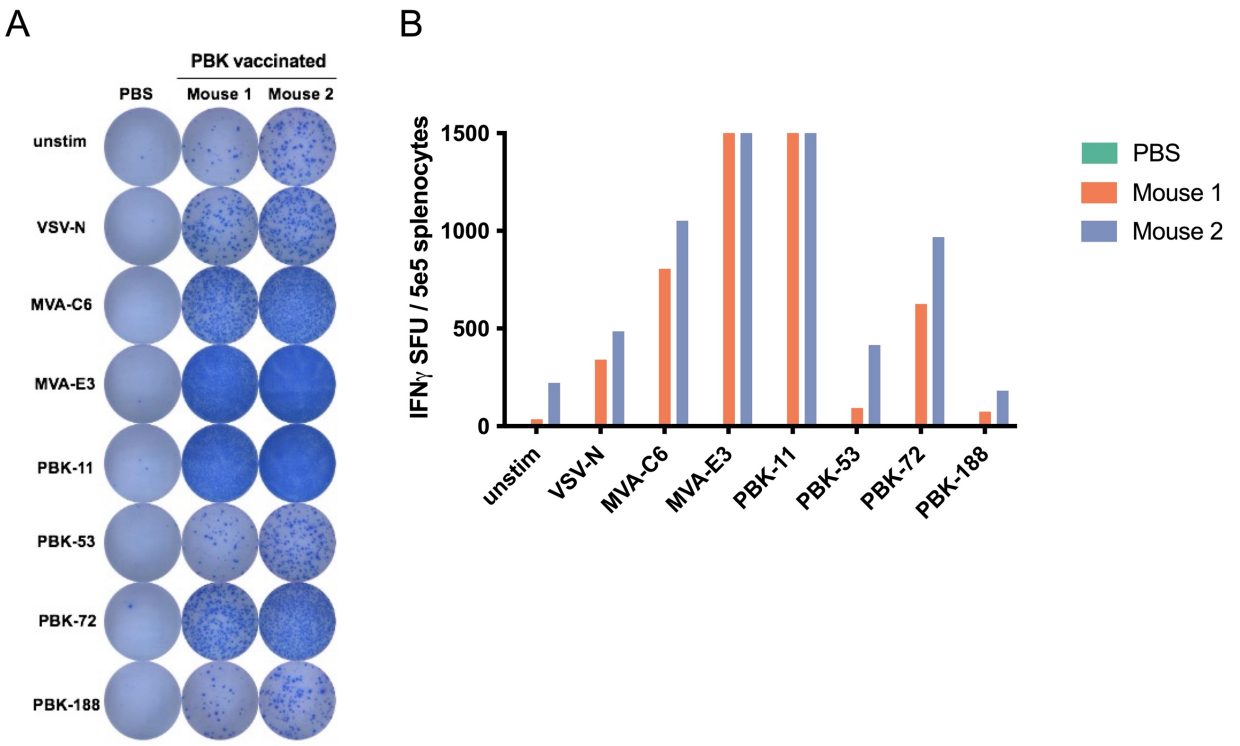

Supplemental Figure 18. Representative plates from ELISPOT assay. Splenocytes isolated from immunized mice were co-cultured with peptides for 24 hours. Graph of IFNγ spot forming units (SFU) per $5x10^5$ splenocytes (log 10 scale)

A

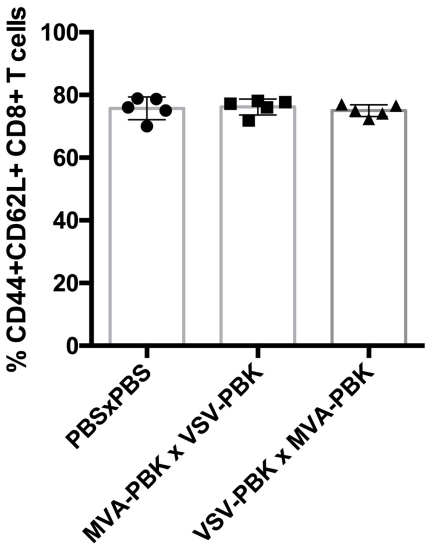

B

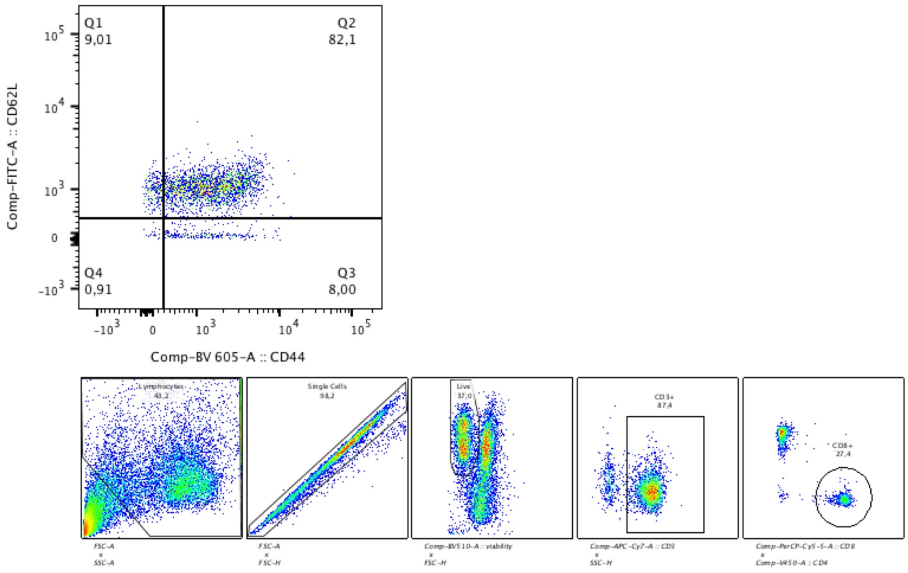

Supplemental Figure 19. (**A)** Percentage of CD44+CD62L+ T_{MEM} cells (**B)** Gating strategy for identification of memory T cells. Sample was gated on lymphocytes, single cells, live cells, CD3+, CD8+ and CD62L+CD44+.

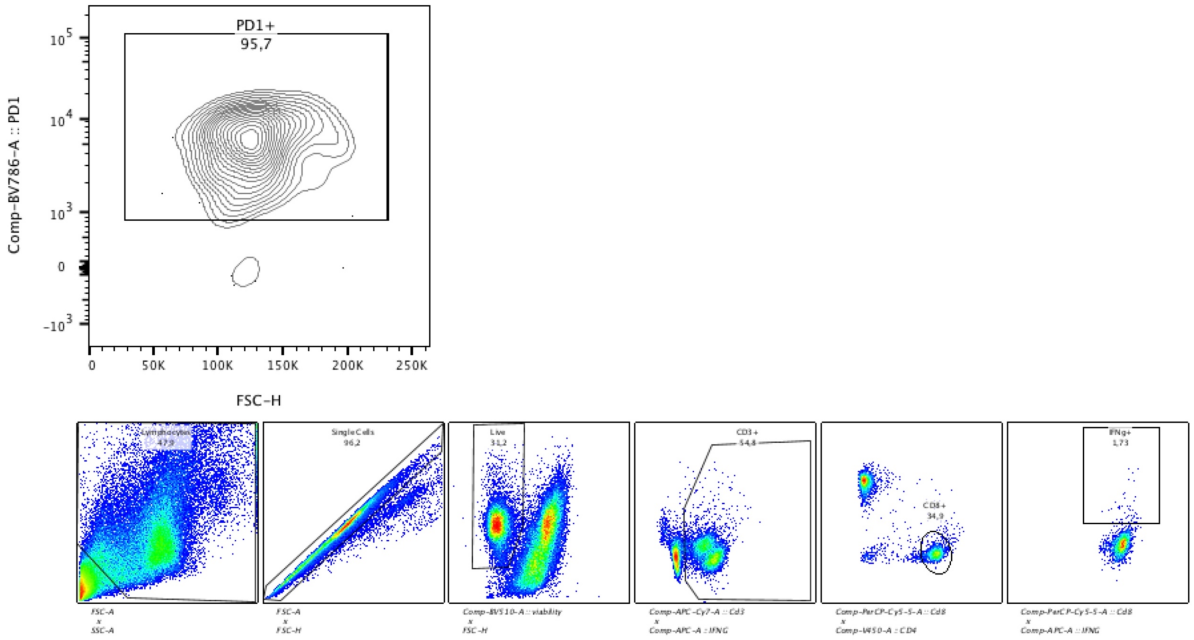

Supplemental Figure 20. Gating strategy to identify PD1+ antigen specific CD8+ T cells. Sample was gated on lymphocytes based on FSC and SSC, then single cells, live cells, CD3+, CD8+, IFNγ + and PD1+

Appendix III. Sequences

Nucleic acid sequencing of PBK encoded into DEC205, VSVΔ51 and MVA constructs:

ATGAAGCTAAGATTTAAAAAAAACCTTAATCACCCAAACATTATAGGGTATCATGCT
TTTACTGAAGCCAGTGATGGTAGTCTGTGCCTTGCTATGGAATATGGAGGTGAAAAG
TCTCTGAATGACTTAATAGAAGAGCAGAACAAAGACAGTGGAAGTCCTTTTCTAGC
AGCTGTAATTCTCAGAGTTGCTTTATACATGGCCAGACGCCTAAAGTATCTGCATCA
AGAAAAGAAGCTGCTTCATGTAGACATAAAGTCTTCAAATGTTGTGATTAAAGGTG
ATTTTGAAACAATTAAAATCTGTGATGTAGGAGTCTCTCTGCCGTTGGATGAAAATA
TGACTGTGACTGATCCTGAGGCCTGTTGTATTGGACCTGAGCCATGGAAACCCAAGG
AACCGTTGGAAGAAAATGGCATCATTACTGACAAGGCAGATATGTTTGGTTTTGGCC
TTACTCTGTGGGAAATGATGACTTTATGTATTCCACACATCAATCTTCCAGATGATG
ATGTTGATGAAGATGCAACCTTTGATGAGAGTGACTTCGATGATGAAGCATATTATG
CAGCTCTGGGGACAAGGCCATCCATCAACATGGAAGAGCTGGATGAATCCTACCAG
AAAGGTCATTGA

Truncated amino acid PBK sequence encoded in DEC205, VSVΔ51 and MVA:

MKLRFKKNLNHPNIIGYHAFTEASDGSLCLAMEYGGEKSLNDLIEEQNKDSGSPFLAAVI
LRVALYMARRLKYLHQEKKLLHVDIKSSNVVIKGDFETIKICDVGVSLPLDENMTVTDP
EACCIGPEPWKPKEPLEENGIITDKADMFGFGLTLWEMMTLCIPHINLPDDDVDEDATFD
ESDFDDEAYYAALGTRPSINMEELDESYQKGH

Molecular Therapy
Oncolytics
Original Article

Oncolytic Rhabdovirus Vaccine Boosts Chimeric Anti-DEC205 Priming for Effective Cancer Immunotherapy

Fanny Tzelepis,[1,7] Harsimrat Kaur Birdi,[1,2,7] Anna Jirovec,[1,2,7] Silvia Boscardin,[3,4] Christiano Tanese de Souza,[1] Mohsen Hooshyar,[1] Andrew Chen,[1] Keara Sutherland,[1,2] Robin J. Parks,[2,6] Joel Werier,[5] and Jean-Simon Diallo[1,2]

[1]Centre for Innovative Cancer Research, Ottawa Hospital Research Institute, Ottawa, ON, Canada; [2]Department of Biochemistry, Microbiology and Immunology, University of Ottawa, Ottawa, ON, Canada; [3]Laboratory of Antigen Targeting to Dendritic Cells, Department of Parasitology, University of São Paulo, São Paulo, Brazil; [4]Institute for Investigation in Immunology (iii)-INCT, São Paulo, Brazil; [5]Department of Surgery, The Ottawa Hospital, Ottawa, ON, Canada; [6]Regenerative Medicine Program, Ottawa Hospital Research Institute, Ottawa, ON, Canada

Prime-boost vaccination employing heterologous viral vectors encoding an antigen is an effective strategy to maximize the antigen-specific immune response. Replication-deficient adenovirus serotype 5 (Ad5) is currently being evaluated clinically in North America as a prime in conjunction with oncolytic rhabdovirus Maraba virus (MG1) as a boost. The use of an oncolytic rhabdovirus encoding a tumor antigen elicits a robust anti-cancer immune response and extends survival in murine models of cancer. Given the prevalence of pre-existing immunity to Ad5 globally, we explored the potential use of DEC205-targeted antibodies as an alternative agent to prime antigen-specific responses ahead of boosting with an oncolytic rhabdovirus expressing the same antigen. We found that a prime-boost vaccination strategy, consisting of an anti-DEC205 antibody fused to the model antigen ovalbumin (OVA) as a prime and oncolytic rhabdovirus-OVA as a boost, led to the formation of a robust antigen-specific immune response and improved survival in a B16-OVA tumor model. Overall, our study shows that anti-DEC205 antibodies fused to cancer antigens are effective to prime oncolytic rhabdovirus-boosted cancer antigen responses and may provide an alternative for patients with pre-existing immunity to Ad5 in humans.

INTRODUCTION

As knowledge of the important role played by the immune system in preventing tumor growth in healthy individuals has expanded over the last decades, immunotherapy has emerged as a viable treatment option for cancer.[1] One form of immunotherapy that has gained recent regulatory approval employs oncolytic viruses (OVs). OVs are live, replicating viruses selected or genetically modified to preferentially target and kill cancer cells while leaving healthy cells relatively unharmed.[2] This is possible owing to the fact that cancers exhibit many characteristics that are conducive to successful viral replication, such as resistance to apoptosis, increased nucleotide synthesis, and an impaired antiviral response.[3] OVs elicit their anti-cancer effects through multiple mechanisms and following tumor cell lysis and immunogenic cell death, can trigger anti-cancer immune responses.[4] In addition to Imlygic, an intratumorally delivered oncolytic herpes simplex virus 1 (HSV-1) strain approved for treatment of late-stage melanoma, many different viruses have been clinically evaluated for their potential as OVs, including many that can be delivered intravenously (i.v.), such as (but not limited to) measles virus,[5] coxsackie virus,[6] and rhabdoviruses, like vesicular stomatitis virus (VSV) and the closely related Maraba virus (MG1).[7] Additional attenuating genetic modifications are generally introduced into OVs in order to increase their safety profile. For example, oncolytic rhabdoviruses are attenuated by deletion of the matrix protein in VSV (termed VSVΔ51) and mutation of components of the matrix and glycoproteins in MG1.[8] In addition, OVs can be genetically manipulated to encode proteins that either help to establish a productive infection of cancer cells or encode cytokines and/or immunogenic antigens, such as cancer antigens.

It is known that OVs can elicit *in situ* cancer vaccine effects and relieve local immunosuppression through the induction of immunostimulatory cytokines. In this environment, dendritic cells (DCs) can phagocytose dead/dying infected tumor cells and prime an anti-tumor as well as antiviral immune response in the draining lymph node.[9] However, the heterogeneous nature of cancer has resulted in limited efficacy of OVs as monotherapies and has steered researchers to investigate combinations of these biologics with other therapies that not only enhance OV infection of tumors but also enable anti-tumor immune responses.[10,11]

Typical vaccination regimens are generally not limited to a single dose and can be made more effective by multiple immunizations. This can involve the administration of additional homologous (matched

Received 15 January 2020; accepted 9 October 2020;
https://doi.org/10.1016/j.omto.2020.10.007.

[7]These authors contributed equally to this work.

Correspondence: Jean-Simon Diallo, Centre for Innovative Cancer Research, Ottawa Hospital Research Institute, 501 Smyth Road, C3128, Ottawa, ON K1H8L6, Canada.
E-mail: jsdiallo@ohri.ca

vaccine) or heterologous (unmatched vaccine) doses.[12] In the context of cancer vaccines, it has been recently shown that a heterologous prime-boost strategy, where an initial priming dose of an adenovirus virus encoding a cancer antigen is administered, followed by a boosting dose of an oncolytic rhabdovirus encoding the same antigen, can be effective to eradicate tumors.[13] This strategy has been shown to induce robust and long-term effector T cell responses[14,15] and is currently undergoing clinical evaluation for multiple antigens and indications (ClinicalTrials.gov: NCT02285816, NCT02879760, NCT03618953, and NCT03773744).

As a boosting component, oncolytic rhabdoviruses are thought to be uniquely effective because in addition to infecting tumor and breaking local immunosuppression, they efficiently, but nonproductively, infect splenic B cells, which provides an additional source for antigen presentation to DCs, resulting in secondary expansion of T cells.[16]

To prime the oncolytic rhabdovirus boost, current clinical trials employ a nonreplicating adenovirus serotype 5 (Ad5) vector expressing a shared cancer antigen (e.g., MAGE-A3, ClinicalTrials.gov: NCT02285816). Questions regarding the importance of vector seropositivity were raised recently following Merck's failed phase II clinical trial of a trivalent human immunodeficiency virus (HIV) vaccine delivered in an Ad5 vector.[17] Indeed, Ad5 seropositivity is sometimes an exclusion criterion in vaccine and gene-therapy clinical trials employing this vector.[18] Approximately 30%–40% of the North American population is seropositive for Ad5, and this proportion approaches an 85% average globally, posing a potential limitation to the widespread use of Ad5 as a priming vector for the oncolytic rhabdovirus heterologous prime-boost cancer immunotherapy strategy.[19–21]

DEC205 is a C-type lectin endocytic receptor highly expressed on certain DC subtypes.[22] Chimeric antibodies specific to DEC205 fused with an antigen of interest (anti-DEC205 [aDEC205]) have been shown to be an effective strategy to target fused antigens directly to DCs, inducing robust cellular and humoral responses when combined with adjuvants.[23,24] To overcome potential issues with Ad5 and other viruses that could be used as priming vectors but that may have the potential to be affected by pre-existing immunity, we hypothesized that chimeric aDEC205 antibodies could provide an effective alternative. In this study, we modeled and evaluated the impact of pre-existing immunity on Ad5-based priming. As proof of concept, we also evaluated a heterologous prime-boost vaccine strategy employing aDEC205-ovalbumin (OVA) as the priming agent, followed by a boost with OVA-expressing oncolytic rhabdoviruses in an experimental model of OVA-expressing B16 melanoma.

RESULTS

Pre-existing Immunity to Wild-Type Ad5 (WTAd5) Impairs Generation of a SIINFEKL-Specific Immune Response to Recombinant Ad5-SIINFEKL (rAd5-SIINFEKL)

We hypothesized that pre-existing immunity to WTAd5 may negatively affect priming of the immune response induced by rAd5-expressing antigens. To investigate this, we evaluated the capacity of Ad5 encoding the OVA epitope rAd5-SIINFEKL to generate an antigen-specific immune response in mice with pre-existing immunity to WTAd5. To model pre-existing immunity, we immunized naive C57BL/6 mice with 10^{10} plaque-forming units (PFU) of the WTAd5 virus. After 35 days, mice were administered 10^8 PFUs rAd5-SIINFEKL intramuscularly (i.m.) (Figure 1A). Generation of anti-adenovirus neutralizing antibodies (AdNAbs) in sera of preimmunized mice 40 days postadministration of WTAd5 was confirmed by neutralization assay and was elevated in preimmunized mice (Figure 1B). SIINFEKL-specific $CD8^+$ T cell responses were measured 10 days after rAd5-SIINFEKL immunization, the peak time of the adaptive immune response elicited by adenovirus vectors.[25] We observed a statistically significant decrease from 10% to approximately 5% of splenic SIINFEKL-specific $CD8^+$ T cells, depicted by $H2K^b$-SIINFEKL pentamer staining, from preimmunized mice compared to control phosphate-buffered saline (PBS) mice (Figures 1C and 1D). To assess $CD8^+$ T cell functionality, splenocytes from preimmunized mice and PBS mice were restimulated with SIINFEKL peptide *in vitro* and followed by intracellular cytokine staining (ICS) for interferon (IFN)-γ and tumor necrosis factor (TNF)-α. Again, there was a reduction from an average of 6% to 2% of IFN-γ- and TNF-α-producing $CD8^+$ T cells specific to SIINFEKL detected in the splenocytes from preimmunized mice compared to control PBS (Figures 1E and 1F). Together, these results indicate that modeled pre-existing immunity to WTAd5 limits the generation of SIINFEKL-specific cellular responses following rAd5-SIINFEKL immunization in C57BL/6 mice.

Production and Characterization of aDEC205-OVA

Impaired SIINFEKL-specific immune responses following rAd5-SIINFEKL immunization of C57BL/6 mice modeling pre-existing immunity led us to consider employing an alternative priming agent that would be better able to overcome pre-existing immunity to WTAd5 and other potential alternative viral vectors. Several studies have shown the ability of chimeric aDEC205 antibodies fused to antigens, such as OVA (aDEC205-OVA) or tumor antigens, to elicit strong antigen-specific immune responses in mice when administered with an adjuvant.[26,27] To evaluate the use of antigen-fused aDEC205 antibodies as alternative priming agents for heterologous boosting with Oncolytic rhabdovirus (ORV) vectors, we used aDEC205 fused to the model antigen OVA.

To generate the aDEC205 antibodies used in this study, human embryonic kidney (HEK)293T cells were cotransfected with plasmids containing the mouse aDEC205-kappa light chain and the aDEC205 heavy chain fused to the full OVA protein sequence at the carboxyl terminus (or no antigen as a control [aDEC205-empty]). The recombinant antibodies produced following transient transfection in HEK293T cell were purified on protein G Sepharose columns.

The resulting antibodies were characterized by western blot using anti-immunoglobulin G (IgG) antibodies on SDS-PAGE under reducing conditions (Figure 2A). Figure 2A shows that heavy and light chains of the purified recombinant antibodies had the expected size for both the fused antibody (Ab) aDEC205-OVA (~95 kDa and 25 kDa, respectively) and control antibody aDEC205-empty (50 kDa

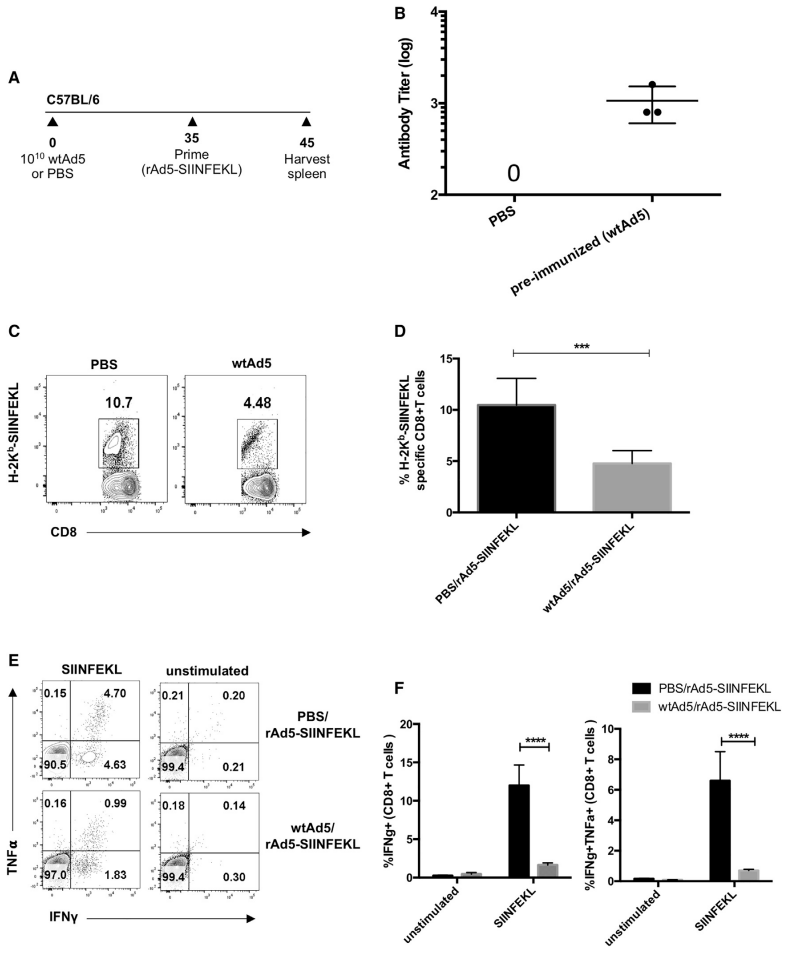

Figure 1. Comparing the SIINFEKL-Specific T Cell Response after i.m. Injection of Priming Agent Recombinant Adenovirus Expressing the SIINFEKL Transgene (rAd5-SIINFEKL) in Mice Modeling Pre-existing Immunity to WTAd5

(A) Naive C57BL/6 mice were injected i.m. on day 0 with 10^{10} PFUs of WTAd5 (n = 7) or PBS (n = 5). After 35 days, mice were injected i.m. with rAd5-SIINFEKL. (B) Anti-adenovirus neutralizing antibody (AdNAbs) titers in mouse sera (n = 3) were determined by neutralization assay, 40 days after administration of WTAd5.10 days after prime, the representative gating (C) and total percentage of (D) SIINFEKL-specific $CD8^+$ T cells in the spleen was determined by H2-K^b-SIINFEKL pentamer staining.The representative gating (E) and percentage of (F) OVA-specific T cells producing IFN-γ and TNF-α in the spleen was evaluated by flow cytometry. Briefly, splenocytes were stimulated *in vitro* with MHC-I epitope (SIINFEKL) for 5 h, subsequently stained for intracellular production of IFN-γ and TNF-α, and assessed by flow cytometry. ***$p < 0.001$ and ****$p < 0.0001$ (two-way ANOVA).

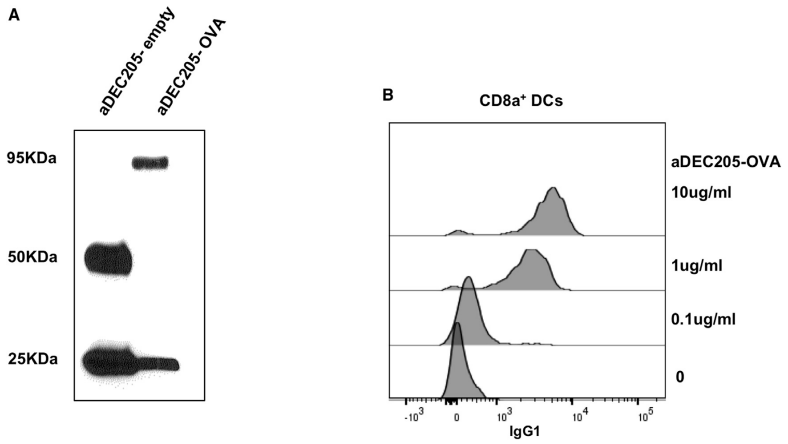

Figure 2. Production and Characterization of aDEC205-OVA

(A) aDEC205-OVA and aDEC205-empty were generated by transfection of 293T cells *in vitro* and subsequent purification of the antibody. (A) Final antibody product was reduced by β-mercaptoethanol and verified by immunoblotting for the heavy and light chains. aDEC205-empty shows a heavy chain at 50 kDa and light chain at 25 kDa. aDEC205-OVA shows the heavy chain linked with OVA at 95 kDa, indicating the presence of OVA antigen and a light chain at 25 kDa. (B) A binding assay was performed to verify effective binding of aDEC205-OVA to the DEC205 receptor on $CD11c^+CD8^+$ dendritic cells (DCs) isolated from murine splenocytes. aDEC205-OVA is probed with an anti-IgG1-APC antibody and detected by flow cytometry. The histogram overlay depicts high binding of aDEC205-OVA to $CD11c^+CD8^+$ DCs at concentrations of 10 μg/mL and 1 μg/mL and low binding at 0.1 μg/mL.

and 25 kDa, respectively). The capacity of the aDEC205-OVA and aDEC205-empty antibodies to bind to its receptor on the surface of splenic DCs $CD11c^+CD8a^+$ was confirmed with a binding assay.[28] Incubation of splenocytes from naive C57BL/6 mice with different concentrations of aDEC205-OVA (0.1, 1, or 10 μg/mL) resulted in a dose-dependent binding (Figure 2B) on the surface of splenic $CD11c^+CD8a^+$ DCs (gating strategy shown in Figure S1) expressing the DEC205 receptor. These results indicate that aDEC205-OVA and aDEC205-empty were successfully purified from culture supernatants and that aDEC205-OVA and aDEC205-empty (Figure S2) retain binding capacity to the DEC205 receptor as expected.

aDEC205-OVA Administered via Intraperitoneal (i.p.) and i.v. Routes Generates Cellular Immune Responses against SIINFEKL

Several studies demonstrated the influence of the route of immunization on immune response and disease outcome.[29] To determine which route of aDEC205-OVA administration leads to the most potent T cell response systemically, we immunized naive C57BL/6 mice i.p. or i.v. with 10 μg aDEC205-OVA or aDEC205-empty, both in combination with 50 μg poly(I:C) and 50 μg anti-CD40. SIINFEKL-specific T cells were evaluated by flow cytometry at 10 and 21 days postimmunization (Figure 3A; gating strategy shown in Figure S3). ICS, after *in vitro* restimulation of lymphocytes with the SIINFEKL peptide, showed that i.v. and i.p. routes of administration elicited statistically similar percentages of IFN-γ- and TNF-α-producing $CD8^+$ T cells in the lung and spleen of mice immunized with aDEC205-OVA at days 10 and 21 postimmunization (Figures 3B–3D; Figure S4). Additionally, staining with the $H2K^b$-SIINFEKL pentamer showed statistically similar percentages of SIINFEKL-specific $CD8^+$ T cells at day 21 in the spleen and lung of mice immunized with aDEC205-OVA when comparing i.v. and i.p. routes of administration (Figures 3E; Figure S4). As expected, no SIINFEKL-specific $CD8^+$ T cells were detected in the spleen or lungs of animals immunized with control aDEC205-empty. These results indicate that either route of administration elicits a strong anti-SIINFEKL primary immune response. Ultimately, to model a preferred route of administration in humans, we proceeded to administer aDEC205-OVA i.v. for the remainder of this study.

aDEC205-OVA Overcomes Barriers Posed by Pre-existing Immunity and Generates Cellular and Humoral Immunity against OVA

We next evaluated the ability of aDEC205-OVA to overcome pre-existing immunity to WTAd5 in a C57BL/6 murine model. To model pre-existing immunity, all naive C57BL/6 mice were immunized with WTAd5 35 days prior to the injection of priming agents (Figure 4A). As previously observed, AdNAbs were detected by a neutralization assay in mouse sera 40 days postadministration of WTAd5 and were elevated in preimmunized mice around time of prime

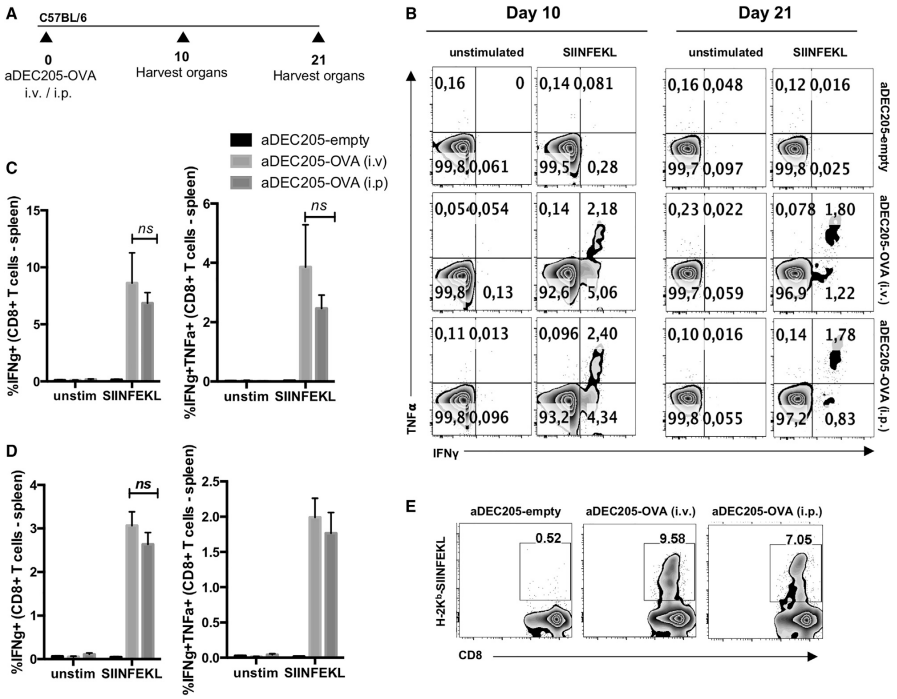

Figure 3. aDEC205-OVA Administered i.v. or i.p. Elicits OVA-Specific T Cells in the Spleen of Immunized Mice

(A) Naive C57BL/6 mice were primed with 10 μg of aDEC205-OVA or aDEC205-empty + 50 μg poly(I:C) + 50 μg anti-CD40 i.v. or i.p. The percentage of SIINFEKL-specific T cells producing IFN-γ and TNF-α in the spleen (B) on day 10 (C) and on day 21 (D) was evaluated by flow cytometry. (E) Quantification of SIINFEKL-specific T cells by pentamer staining (H-2K^{b}-SIINFEKL) was also assessed in the spleen by flow cytometry at day 21 postinjection. p value was considered nonsignificant (ns) when >0.05 (two-way ANOVA).

(Figure 1B). Pre-existing immunity to WTAd5 did not affect priming with aDEC205-OVA; approximately 9% of SIINFEKL-specific CD8^{+} T cells were observed in the spleen of preimmunized mice and control PBS mice 10 days after prime (Figures 4B and 4C). Furthermore, a similar percentage of splenic IFN-γ- and TNF-α-producing CD8^{+} T cells specific to SIINFEKL was also detected by intracellular staining (Figures 4D and 4E). Together with Figure 1, these results suggest that adjuvanted aDEC205 is an effective prime in the face of pre-existing immunity to WTAd5.

Heterologous Boosting of aDEC205-OVA Prime with Rhabdovirus-Encoding OVA Potentiates a Cellular and Humoral Immune Response

Priming with Ad5 encoding a cancer antigen, followed by boosting with ORV vectors, such as MG1 or VSV, expressing the same antigen, induces strong antigen-specific responses, providing survival benefit in various tumor models.[11–15] Therefore, we tested the ability of the combination aDEC205-OVA prime and MG1-OVA boost in the generation of a SIINFEKL-specific T cell response. To this end, naive C57BL/6 mice were primed (i.v.) with 10 μg aDEC205-OVA or aDEC205-empty, both in combination with 50 μg poly(I:C) and 50 μg anti-CD40 and boosted (i.v.) 14 days later with 10^{8} PFUs of MG1-OVA or 10 μg aDEC205-OVA with 50 μg poly(I:C) and 50 μg anti-CD40 or PBS. 7 and 14 days after boost, lymphocytes were harvested from the spleen and lung and then stained with the H2K^{b}-SIINFEKL pentamer. At days 7 and 14 postboost, the greatest expansion of SIINFEKL-specific T cells was observed in the spleen (Figures 5A–5E) and lungs (Figure S5) of animals boosted with MG1-OVA. Similar results were obtained using VSV-OVA (Figures S6A and S6B). Although boost with aDEC205-OVA expanded the

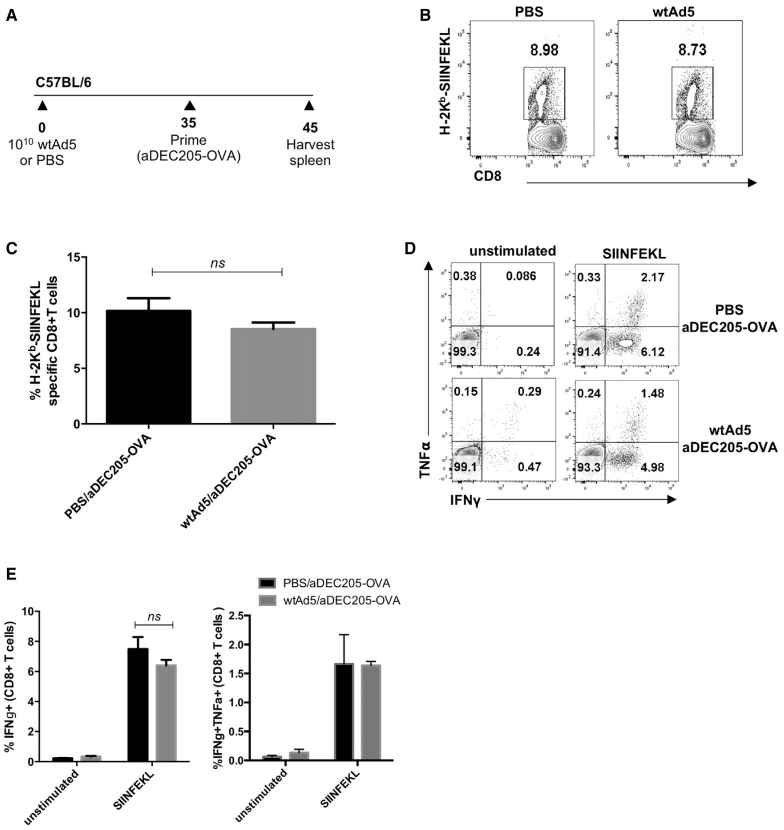

Figure 4. Pre-existing Immunity to Adenovirus Does Not Affect an Immune Response Elicited by aDEC205-OVA Prime

(A) Naive C57BL/6 mice were injected i.m. on day 0 with 10^{10} PFUs of WTAd5 or PBS. (B and C) After 35 days, mice were injected i.v. with 10 μg of aDEC205-OVA + 50 μg poly(I:C) + 50 μg anti-CD40. 10 days after priming, the representative gating (B) and percentage of (C) SIINFEKL-specific $CD8^+$ T cells in the spleen was determined by H2-K^b-SIINFEKL pentamer staining. The representative gating (D) and percentage of (E) SIINFEKL-specific T cells producing IFN-γ and TNF-α in the spleen was also evaluated by ICS and flow cytometry. p value was considered nonsignificant when >0.05 (two-way ANOVA).

antigen-specific cells compared to the group only primed with aDEC205-OVA, the level of expansion was significantly lower compared to MG1-OVA. Humoral immunity was also assessed using mouse sera to quantify OVA-specific IgG by ELISA. The combination of aDEC205-OVA/MG1-OVA prime-boost generated the highest anti-OVA antibody titers compared to other combinations and control groups (Figure 5F). Immunization with aDEC205-OVA/VSV-OVA prime-boost generated similar antibody titers compared to aDEC205-OVA/MG1-OVA prime-boost at day 7 postboost (Figure S6C).

Heterologous Prime-Boost Vaccine with aDEC205-OVA and Rhabdovirus-Encoding OVA Confers a Survival Advantage in Tumor-Bearing Mice

We next evaluated the therapeutic efficacy of the aDEC205-OVA/MG1-OVA prime-boost vaccine in an experimental model of lung

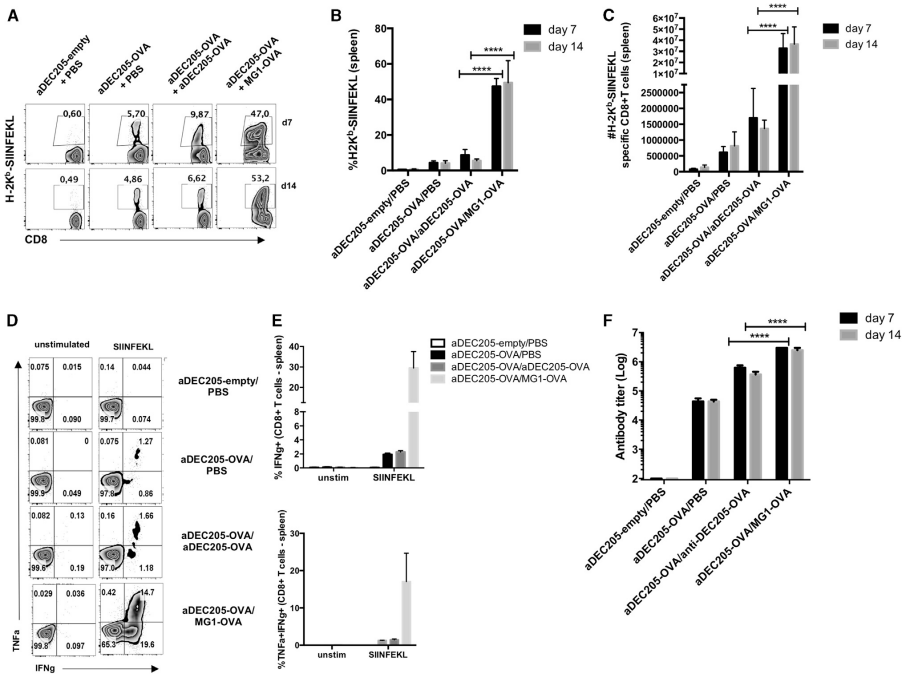

Figure 5. Induction of a Potent Cellular and Humoral OVA-Specific Immune Response after aDEC205-OVA Prime and MG1-OVA Boost

C57BL/6 mice were immunized i.v. with 10 μg of aDEC205-OVA or aDEC205-empty + 50 μg poly(I:C) + 50 μg anti-CD40 at day 0. 14 days later, mice were immunized with a boosting dose of PBS, 10 μg aDEC205-OVA i.v. + 50 μg poly(I:C) + 50 μg anti-CD40, or 10^8 PFUs of MG1-OVA. Spleens were harvested 7 and 14 days following boost to evaluate cellular immune response to prime-boost regimens by flow cytometry (A). The percentage (B) and total number of (C) SIINFEKL-specific $CD8^+$ T cells were determined by H2-K^b-SIINFEKL pentamer staining. At day 14, the representative gating (D) percentage of (E) splenic IFN-γ- and TNF-α-producing $CD8^+$ T cells in response to *in vitro* stimulation with 5 μM SIINFEKL peptide was evaluated. (F) The titers of anti-OVA antibodies in the sera of mice were determined by ELISA at day 7 and day 14 after boost. These results are representative of two independent experiments. ****$p < 0.0001$ (two-way ANOVA).

metastasis. Briefly, 3×10^5 B16-OVA cells were injected i.v. in C57BL/6 mice, and different primes were administered 5 days post-B16-OVA tumor implantation (Figure 6A). Generation of SIINFEKL-specific T cell responses was evaluated by H2-K^b-SIINFEKL pentamer staining of blood 7 days after boost. The heterologous prime-boost combination employing aDEC205-OVA or rAd5-OVA as a prime generated the greatest percentage of circulating antigen-specific T cells. Interestingly, whereas different routes of administration of the aDEC205-OVA prime (i.v. versus i.p.) did not significantly impact priming responses (Figure 3), there was a trend for a higher magnitude of a SIINFEKL-specific $CD8^+$ T cell response generated after prime with aDEC205-OVA administered i.v. compared to aDEC205-OVA prime administered i.p. (Figures 6B and 6D). In general, all OVA-targeted heterologous prime-boost regimens led to improved survival of tumor-bearing mice, with rAd5-OVA/MG1-OVA and aDEC205-OVA/MG1-OVA regimens being the most effective (30% complete remission). The administering of a prime-boost of aDEC205-OVA/VSV-OVA also resulted in the generation of greater SIINFEKL-specific $CD8^+$ T cells and improved survival of tumor-bearing mice (Figures S6B, S6D, and S6E). Cured mice were rechallenged with a subcutaneous injection of 2×10^6 B16-OVA cells (data not shown); no mice previously cured by any prime-boost regimen developed tumors, thus confirming that anti-SIINFEKL responses were long lasting and conferred protection against recurrent tumors.

DISCUSSION

Cancer immunotherapy has emerged as a promising alternative to conventional cancer treatments. Therapeutic strategies that actively

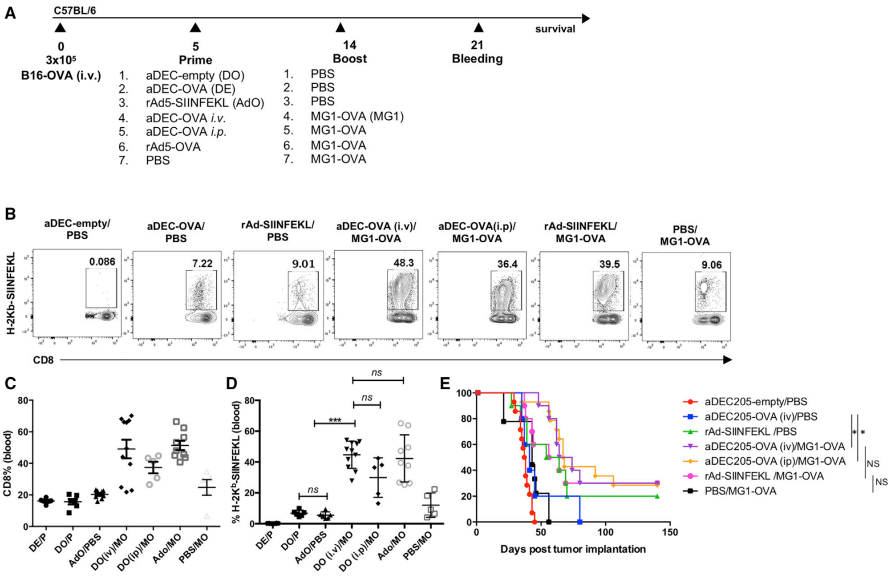

Figure 6. Therapeutic Efficacy of an aDEC205/OVA Prime-Boost Vaccine

(A) Schematic representation of immunization schedule. Briefly, C57BL/6 mice received 3 × 10^5 B16-OVA cells i.v. At day 5, mice were immunized i.v. or i.p. with 10 μg of aDEC205-OVA or aDEC205-empty + 50 μg poly(I:C) + 50 μg anti-CD40, 10^8 rAd5-SIINFEKL, or PBS. At day 14, mice were immunized with a boosting dose of either PBS or 10^8 MG1-OVA. (B–D) At day 21 saphenous (saph) bleeds were performed to assess the percentage, by flow cytometry (B), of bulk-circulating $CD8^+$ T cells (C) and SIINFEKL-specific $CD8^+$ T cells (D), the latter determined by H2-K^b-SIINFEKL pentamer staining. p value was considered nonsignificant when >0.05; ***p < 0.001 (one-way ANOVA). (E) Mice were monitored for survival 140 days post-B16-OVA implantation. Data from three independent survival experiments are pooled. p value was considered nonsignificant when >0.05; *p < 0.05 (log-rank Mantel-Cox).

stimulate the immune system to reject tumors have grown to include diverse platforms, including immune-modulating antibodies,[30] small molecules,[31,32] as well as genetically engineered bacteria,[33] cells,[34] and viruses.[7] OVs are attracting increasing interest as multi-mechanistic platforms for immunotherapy, owing, in part, to the recent approval of Imlygic for the treatment of melanoma and to the possibility of combining OVs with antibodies targeting immune checkpoints.[35] Indeed, it is increasingly recognized that OVs have significant potential as part of combination therapy regimens.[36]

In this study, we have further explored one such combination strategy consisting of a heterologous prime-boost, where the priming and boosting vectors share a similar tumor antigen and where the boosting vector is an oncolytic rhabdovirus.[37] This is a strategy that is now under phase I/II clinical evaluation using a nonreplicating Ad5 as a priming vector and oncolytic MG1 as a boosting vector. In contrast with repeat dosing with the same vector (homologous vaccination), this heterologous prime-boost approach has been shown to skew the immune response from antiviral to anti-tumor, promoting long-lasting anti-tumor immunity.[12,38] The secondary immunization with rhabdovirus, which preferentially infects tumors, not only induces oncolysis but also boosts the primary anti-tumor adaptive immune response and breaks immune tolerance.[8]

Although nonreplicating Ad5 is an effective and well-validated vector for vaccination, pre-existing immunity to Ad5, resulting from prior exposure to WT adenoviruses in humans, can potentially limit its effectiveness in clinical trials.[16,17] Indeed, we found that administration of rAd5-SIINFEKL in preimmunized mice led to both significantly lower percentages of SIINFEKL-specific $CD8^+$ T cells (Figures 1C and 1D) and a reduction in their functionality (Figures 1E and 1F).

As an alternative to Ad5, we demonstrate here, in line with other studies, that i.p. or i.v. administration of aDEC205-OVA generates antigen-specific and functionally robust anti-SIINFEKL T cells, as well as humoral immunity toward OVA.[22,25,39] However, as a standalone vaccination agent, we observed that aDEC205-OVA did not perform as well as rAd5-SIINFEKL in terms of controlling

B16-OVA tumors (Figure 6E) and generating activated (IFN-γ^+, TNF-α^+), SIINFEKL-specific $CD8^+$ T cells, even though the numbers of SIINFEKL-specific T cells were similar with both primes (Figure 6B). This difference could relate to dosing inequivalence between aDEC205 relative to Ad5, however something that is difficult to establish, owing to differences in how immune responses are initiated with the two vaccination methods. However, the dose of aDE205-OVA used in this study is within the range of the human equivalent dose of what is being evaluated in clinical trials employing aDEC205 (ClinicalTrials.gov: NCT01834248 and NCT01127464).[40,41] In comparison, Ad5 was administered at a higher human equivalent dose than what is administered in current clinical trials, further illustrating the potential of aDEC205 over Ad5. Additionally, pre-existing immunity to WTAd5, as evidenced by the presence of AdNAbs (Figure 1B), strongly decreased the ability of rAd5-SIINFEKL to produce an immune response against the SIINFEKL antigen but predictably bore no impact on the ability of aDEC205-OVA to generate functional anti-SIINFEKL $CD8^+$ T cells.

Consistent with other studies, we found that heterologous boosting with an oncolytic rhabdovirus, such as MG1-OVA, amplifies antigen-specific immunity in the spleen at days 7 and 14 to a higher extent than homologous boosting, for example, with aDEC205-OVA (Figure 5; Figure S5).[15,36] All heterologous regimens tested conferred a survival advantage in B16-OVA-bearing mice (Figure 6), and in this regard, primes using chimeric aDEC205 or Ad5 were essentially equivalent. This suggests that aDEC205 chimeric antibodies are a feasible alternative to Ad5 in the context of heterologous prime-boost with an oncolytic rhabdovirus. In addition to overcoming pre-existing immunity, which may be a barrier when using certain viral priming vectors, chimeric aDEC205 antibodies can provide additional practical advantages, including, but not limited to, ease of manufacturing, storage, and the possibility of repeat dosing. This last point is a notable limitation for viral vectors encoding antigens, which generally induce an antiviral immune response after the first dose.

Vaccines employing DCs loaded *ex vivo* with tumor lysate or major histocompatibility complex class I (MHC-I) peptides for re-administration to patients have been studied for decades and have been shown to generate robust memory $CD8^+$ T cell responses.[42] Following research in the 1990s on antigen-loaded DC vaccines, many clinical trials carried out to this end have been unable to achieve significant clinical responses.[43,44] Objective response rates for a range of DC vaccines loaded with antigens, such as tyrosinase, gp100, MART-1, and MAGE-A3, and autologous peptides in melanoma patients did not exceed 5%–10%.[45] With the consideration of limitations and logistical challenges in producing DC vaccines, DC targeting using chimeric antibodies, like aDEC205, may be more feasible for treating a diverse population of patients.[46] However, as observed in this study (Figure 6E), chimeric aDEC205 antibodies may be insufficient as standalone anti-cancer vaccines.

One key feature of chimeric aDEC205 antibodies is that they deliver a specific antigen directly to DCs, which in turn, present antigen and activate $CD4^+$ T cells, as well as cross present antigen to $CD8^+$ T cells. However, this approach is also not without limitations. For example, there can be antibody/protein engineering challenges restricting the choice of antigen and how many antigens can be fused to a given aDEC205 antibody. This can be somewhat addressed by using more restricted epitopes in tandem or using multiple different chimeric antibodies.

Another consideration for use of chimeric aDEC205 antibodies is the requirement for an adjuvant.[47] In our study, we found that aDEC205-OVA, administered with poly(I:C) and anti-CD40 adjuvants, was effective in generating anti-OVA responses in mice; however, whereas anti-CD40 antibodies (that target the costimulatory receptor CD40 on DCs to induce their maturation) are highly effective in mice, they have displayed severe toxicity in human cancer immunotherapy trials.[48,49] Although this regimen was selected for modeling purposes in mice, we expect adjuvants that are amenable to human use and that have been used in clinical trials (e.g., poly(I:C) stabilized with polylysine and carboxymethylcellulose [poly ICLC] Hiltonol) to be similarly effective in combination with aDEC205.[50] Indeed, many human-compatible adjuvants are known and available and routinely used in the context of cancer vaccines. These include, but are not limited to, alum, poly(I:C), CpG, lipopolysaccharide (LPS), T helper (Th)1-specific cytokines, and growth factors, like Flt3L, important for the development of classical DCs.[40,51] These adjuvants, cytokines, and growth factors may be further combined. For example, CDX-301, a soluble recombinant human (rhu)Flt3L, has been used in combination with poly ICLC in the context of a phase II human trial, testing an aDEC205-NY-ESO-1 melanoma vaccination strategy.[52]

Altogether, our study indicates that a vaccine consisting of an aDEC205-OVA prime, followed by a rhabdovirus boost, is a promising alternative to the current heterologous prime-boost that employs Ad5-OVA as a priming agent. To our knowledge, this study is the first of its kind to showcase a combination of the well-studied aDEC205 antibody in combination with an OV. Additional studies in other tumor models and antigenic targets will be necessary to assess the applicability of this novel approach to a broad range of disease models.

MATERIALS AND METHODS

Cell Lines

HEK 293T cells, kindly donated by the Oncolytic Virus Manufacturing Facility (OVMF; Ottawa, Canada) for antibody production and purification, were cultured in HyQ high-glucose Dulbecco's modified Eagle's medium (HyClone), supplemented with 10% ultra-low IgG fetal bovine serum (FBS; Gibco), 5% penicillin/streptomycin (pen-strep; Gibco), and 5% L-glutamine (Gibco). B16-F10-OVA cells, kindly gifted by Dr. Yonghong Wan (McMaster University), were cultured in Roswell Park Memorial Institute (RPMI; HyClone), supplemented with 10% FBS, pen-strep, 1 M HEPES buffer, and 50 μg/mL geneticin sulfate (G148 sulfate) (Gibco). All cell lines were incubated at 37°C in a 5% CO_2 humidified incubator.

All cells were tested by PCR and Hoechst staining to ensure that they are free of mycoplasma contamination.

Mice

6- to 8-week-old female C57BL/6J mice were obtained from Charles River Laboratories. All animals were handled in strict accordance with good animal practice and approved by the appropriate committee in collaboration with the Office of Animal Ethics and Compliance.

Antibody Production and Purification

The pcDNA plasmids expressing the heavy-chain aDEC205, aDEC205-OVA, and aDEC205-empty and the light-chain DEC205-kappa sequences were generated by Dr. Silvia Boscardin (University of São Paulo). The plasmid DNA was individually transformed in competent DH5-α, and DNA was purified using the QIAGEN Plasmid Maxi Kit (catalog [Cat.] 12165). Transfection of 90% confluent HEK293T cells in 150 mm tissue-culture dishes, collection of antibody from culture supernatant, and antibody purification were performed as previously described.[53]

Peptides

Peptides corresponding to the immunodominant epitope of OVA (SIINFEKL) that binds to H-2K^b were synthesized by New England Peptide (lot number 3001-1/48-21) and have >95% purity.

Tissue Processing

SIINFEKL-specific T cell responses were measured in blood, spleen, and lung. Briefly, saphenous bleeds of mice from hindlimb were performed, and blood (70–100 μL) was collected in sterile heparin tubes. Red blood cells were lysed using ammonium-chloride-potassium (ACK) lysis buffer. Spleens were excised from sacrificed mice and filtered through a 100-μm plastic cell strainer (Fisherbrand; 352360, 22-363-549) for cell collection. The cell viability of the resulting white blood cells was determined using Trypan blue staining. Lungs were also excised from sacrificed mice after lung perfusion and dissociated using the Lung Dissociation Kit-Mouse (Miltenyi Biotec; 130-095-927), according to the manufacturer's instructions. Upon resuspension in R10 buffer (RPMI, 10% FBS), the cells from blood, spleen, and lung were counted, and 1×10^6 cells per condition were stained for flow cytometry.

Immunoblotting

After aDEC205-OVA antibody quantification by the NanoDrop ND-1000 spectrometer, 1 μg of antibody was run on NuPAGE Novex 4%–12% Bis-Tris precast gels (Thermo Fisher Scientific) under reducing conditions using the XCell SureLock Mini-Cell System (Thermo Fisher Scientific) and transferred to nitrocellulose membranes (Hybond-C; Bio-Rad). Blots were blocked with 2% milk and probed with a goat anti-mouse peroxidase-conjugated antibody (1:2,000) (Jackson ImmunoResearch Laboratories). Bands were visualized using the SuperSignal West Pico Chemiluminescent substrate (Thermo Fisher Scientific).

ELISA

Murine serum was collected from blood for detection of OVA-specific antibodies. Briefly, blood (500 μL) from immunized mice was collected in sterile, 1.5 mL Eppendorf tubes. Collected blood was centrifuged for 10 min at 2,000 × *g*, and the resulting serum in the supernatant was collected and frozen at −20°C for downstream use. Murine serum samples were evaluated for presence of OVA-specific antibodies by ELISA for all groups. 96-well enzyme immunoassay (EIA)/radioimmunoassay (RIA) microplates (Corning; Cat. CLS3590) were coated with albumin (Sigma-Aldrich; A5503-1G) at a concentration of 2 ng/μL in PBS and incubated overnight at 4°C. Plates were washed twice with PBS-Tween 20 0.02% and blocked with blocking buffer (PBS-Tween 20 0.02%, 5% nonfat milk, and 1% BSA) for 1 h at room temperature (RT). Blocking buffer was removed, and serum dilutions (1:500–1:1,000,000 dilution in PBS-Tween 20 0.02%, 5% nonfat milk, and 0.25% BSA) were added to wells and incubated for 2 h at RT. Plates were washed three times with PBS-Tween 20 0.02%, and horseradish peroxidase (HRP)-AffiniPure goat anti-mouse IgG (Jackson ImmunoResearch), diluted 1:4,000, was added to wells and incubated for 1 h at RT. Plates were washed six times with PBS-Tween 20 0.02%, developed with substrate solution (R&D Systems; Cat. DY99), and incubated for 20 min in the dark (RT); development was stopped by addition of 2 N sulfuric acid, and absorbance was read at 510 nm on a Multiskan Ascent plate reader (Thermo LabSystems).

Neutralization Assay

A neutralization assay was performed to quantify the amount neutralizing antibodies against WTAd5, present in serum samples of preimmunized murine, and is based on the ability of serum antibodies to block adenovirus infection of A549 cells. Adenovirus used carries the firefly luciferase (Fluc) reporter gene, E1 deletion, and cytomegalovirus (CMV) promoter. 2-fold serum dilutions (1:100; 1:200; 1:400; 1:800; 1:1,600; 1:3,200; 1:6,400; 1:12,800; 1:25,600; 1:51,200; 1:102,400) were tested. In 96-well flat-bottom plates, the Ad-Fluc virus (MOI 100) was combined with different serum dilutions and incubated for 1 h at 37°C. Contents of this plate were transferred to a 96-well flat-bottom plate, previously seeded with 2×10^5 A549 cells per well, washed 3× with PBS, and incubated for 48 h at 37°C. To read plate, luciferin was added at a final concentration of 2 mg/mL luciferin per well and imaged/read by the Biotek Synergy Mx Microplate Reader. The antibody neutralizing unit (NU) was defined as the minimum serum dilution required to achieve at least an 80% reduction in luciferase activity, which was assumed to correlate directly to an inhibition of vector infection.

Mouse Tumor Model and Injections

B16-OVA lung tumors were established in 8-week-old female C57BL/6 mice by i.v. injection of 3×10^5 cells in 100 μL PBS. For adenovirus injections, mice were anesthetized with 5% isoflurane. WTAd5 (10^{10} PFUs) and rAd5-SIINFEKL (10^8 PFUs) were administered i.m. in 50 μL PBS. For aDEC205 injections, a solution containing 10 μg of aDEC205, 50 μg poly(I:C), and 50 μg anti-CD40 ligand (CD40L) in 150 μL of PBS was administered either i.v. or i.p. Oncolytic

rhabdoviruses (MG1-OVA and VSVΔ51-OVA) were administered i.v. in 100 μL of PBS.

Detection of Antigen-Specific T Cell Responses

OVA-specific T cell responses were measured 7 days and 14 days postboost in blood, spleen, and lung. Splenocytes and lung-resident lymphocytes were isolated and stained for the presence of SIINFEKL-specific T cells using a H-2K^b-SIINFEKL pentamer. For SIINFEKL-specific CD8$^+$ T cell *in vitro* restimulation, 1×10^6 splenocytes and lung-resident lymphocytes were incubated in RPMI medium, supplemented with 10% FBS and 5% pen-strep containing 5 μM of SIINFEKL peptide and brefeldin A (Golgi plug) for 4 h. ICS was performed as described below.

Virus Preparation

The adenoviruses were made using standard techniques.[54] The Indiana serotype of VSV (VSVΔ51 or VSVΔ51-OVA) and the Brazilian MG1 (or MG1-OVA) were used throughout this study and were propagated in Vero cells. VSVΔ51-expressing and MG1-expressing OVA are recombinant derivatives of VSVΔ51 and MG1, described previously.[55] All viruses were propagated on Vero cells and purified on 5%–50% OptiPrep (Sigma) gradient, and all virus titers were quantified by the standard plaque assay on Vero cells, as previously described.[56]

Antibody Binding Assay

A flow cytometry-based binding assay was performed for evaluation of aDEC205-OVA and aDEC205-empty binding specificity to the target DEC205 receptor on DCs. Bulk splenocytes were isolated from spleens of naive C57BL/6J mice. Red blood cells were lysed, and 5×10^6 bulk splenocytes were incubated with graded concentrations of antibody (0.1 μg/μL, 1 μg/μL, and 10 μg/μL) in a 96-well plate for 45 min (4°C). After incubation, cells were stained for flow cytometry.

Flow Cytometry

After processing the tissues as described above, cells were then stained with the FVS780 viability dye (BD Biosciences, San Jose, CA) PBS for 15 min at RT. Following washes, cells were incubated with anti-CD16/32 in 0.5% BSA/PBS at 4°C to block nonspecific antibody interaction with Fc receptors. Subsequently, the following protocols were used for staining.

Staining for Antibody Binding Assay

Anti-CD11c-phycoerythrin (PE)-Cy7, anti-MHC-I-PE, anti-CD8-PE-CF594, anti-IgG-allophycocyanin (APC), anti-CD3-fluorescein isothiocyanate (FITC), and anti-CD19-FITC antibodies were added to cells and incubated for 30 min (4°C).

Staining for ICS

First, 1×10^6 cells were incubated with antibodies targeting T cell surface markers CD3-AF700 and CD8-PE-CF594 for 30 min (4°C). Cells were washed twice with fluorescence-activated cell sorting (FACS) buffer. Next, the mouse Cytofix/Cytoperm Plus (BD Bioscience) was used for permeabilization and ICS. Cells were incubated with Cytofix for 20 min to permeabilize cells for ICS (4°C). Cells were washed twice with PermWash and incubated with anti-IFN-γ-BV650 and anti-TNF-α-AF647 diluted in PermWash for 30 min (4°C).

Staining for OVA-Specific T Cells/Pentamer Staining

Cells were washed with FACS buffer. In a 96-well plate, 3 μL of H-2K^b-SIINFEKL pentamer-APC (Proimmune) in 50 μL of FACS buffer was added per well and incubated for 10 min (RT) in the dark. Cells were washed twice with FACS buffer and stained with fixable viability stain for 30 min (4°C). Subsequently, the cells were washed with FACS buffer and incubated with anti-CD16/32 in FACS buffer for 5 min (4°C). Next, cells were stained with anti-CD8-PE-CF594 and anti-CD3-AF700 for 30 min (4°C)

After staining, cells were washed with FACS buffer and fixed in 1% paraformaldehyde. Cells were acquired on Becton Dickinson (BD) flow cytometry (Fortessa), and analyses were performed using FlowJo software version (v.)9.

VSV-OVA Cloning and Rescue

Phagemid cloning vector, also known as BlueScribe SK (pBSSK)-VSVΔ51, plasmid-containing viral genome, was used to construct VSVΔ51-OVA. In brief, the OVA gene was PCR amplified from pcDNA expressing aDEC205-OVA using the following primers: forward: 5′-AATTCTCGAGATGGGCTCCATCG-3′ and reverse: 5′-CATCGCTAGCTCACTACAGATCCTC-3′. PCR amplicon was digested by XhoI and NheI and cloned into the multiple cloning site (MCS) of pBSSK-VSVd51 between G and L open reading frames (ORFs). Positive clones were screened by restriction digestion mapping and verified by sequencing.

Statistics

Statistical significance was calculated using Student's t test or one-way or two-way ANOVA test, using Tukey's multiple comparison test, as indicated in the figure legends. The log rank (Mantel-Cox) test was used to determine significant differences in plots for survival studies. Error bars represent standard error of the mean. Significance is based on a p value <0.05. Statistical analyses were performed using GraphPad Prism 6.0 and Excel.

SUPPLEMENTAL INFORMATION

Supplemental Information can be found online at https://doi.org/10.1016/j.omto.2020.10.007.

AUTHOR CONTRIBUTIONS

F.T. conceived the project. F.T. and J.-S.D. designed the study. All authors participated in the acquisition, analysis, and/or interpretation of data and have read and approved the final manuscript. A.J., H.K.B., and J.-S.D. drafted the manuscript with editorial contributions from F.T. S.B. provided plasmids and protocols. C.T.d.S. and A.C. performed all animal work. M.H. and K.S. constructed and rescued viral vectors. R.J. P. provided adenovirus. J.-S.D. supervised the study.

CONFLICTS OF INTEREST

The authors declare no competing interests.

ACKNOWLEDGMENTS

We thank Dr. Brian Lichty (McMaster University) for providing the recombinant adenovirus encoding the epitope SIINFEKL (rAd5-SIINFEKL). We thank Turnstone Biologics for providing Maraba MG1 constructs. J.-S.D. is supported by the Canadian Institute for Health Research (CIHR) through a new investigator award in Infection and Immunity. J.-S.D. holds grants from the Terry Fox Research Institute (INI-147824). This project was supported by BioCanRx (FY18/CAT17) and Valerie's Flutter Foundation, as well as by the Canadian Cancer Society (grant 705952) and Canadian Institutes of Health Research–Institute of Cancer Research (grant 705952). F.T. was supported by a BioCanRx Travel Exchange Award. H.K.B. and A.J. were supported by the MITACS Accelerate Canadian Partnership in Immunotherapy Manufacturing Excellence PhD Internships.

REFERENCES

1. Strausberg, R.L. (2005). Tumor microenvironments, the immune system and cancer survival. Genome Biol. *6*, 211.
2. Russell, S.J., Peng, K.W., and Bell, J.C. (2012). Oncolytic virotherapy. Nat. Biotechnol. *30*, 658–670.
3. Ilkow, C.S., Swift, S.L., Bell, J.C., and Diallo, J.-S. (2014). From scourge to cure: tumour-selective viral pathogenesis as a new strategy against cancer. PLoS Pathog. *10*, e1003836.
4. Gujar, S., Bell, J., and Diallo, J.S. (2019). Snapshot: cancer immunotherapy with oncolytic viruses. Cell *176*, 1240–1240.e1.
5. Russell, S.J., and Peng, K.W. (2009). Measles virus for cancer therapy. Curr. Top. Microbiol. Immunol. *330*, 213–241.
6. Miyamoto, S., Inoue, H., Nakamura, T., Yamada, M., Sakamoto, C., Urata, Y., Okazaki, T., Marumoto, T., Takahashi, A., Takayama, K., et al. (2012). Coxsackievirus B3 is an oncolytic virus with immunostimulatory properties that is active against lung adenocarcinoma. Cancer Res. *72*, 2609–2621.
7. Chiocca, E.A., and Rabkin, S.D. (2014). Oncolytic viruses and their application to cancer immunotherapy. Cancer Immunol. Res. *2*, 295–300.
8. Brun, J., McManus, D., Lefebvre, C., Hu, K., Falls, T., Atkins, H., Bell, J.C., McCart, J.A., Mahoney, D., and Stojdl, D.F. (2010). Identification of genetically modified Maraba virus as an oncolytic rhabdovirus. Mol. Ther. *18*, 1440–1449.
9. Lichty, B.D., Breitbach, C.J., Stojdl, D.F., and Bell, J.C. (2014). Going viral with cancer immunotherapy. Nat. Rev. Cancer *14*, 559–567.
10. Zamarin, D., Ricca, J.M., Sadekova, S., Oseledchyk, A., Yu, Y., Blumenschein, W.M., Wong, J., Gigoux, M., Merghoub, T., and Wolchok, J.D. (2018). PD-L1 in tumor microenvironment mediates resistance to oncolytic immunotherapy. J. Clin. Invest. *128*, 1413–1428.
11. Selman, M., Rousso, C., Bergeron, A., Son, H.H., Krishnan, R., El-Sayes, N.A., Varette, O., Chen, A., Le Boeuf, F., Tzelepis, F., et al. (2018). Multi-modal potentiation of oncolytic virotherapy by vanadium compounds. Mol. Ther. *26*, 56–69.
12. Lu, S. (2009). Heterologous prime-boost vaccination. Curr. Opin. Immunol. *21*, 346–351.
13. Pol, J.G., Zhang, L., Bridle, B.W., Stephenson, K.B., Rességuier, J., Hanson, S., Chen, L., Kazdhan, N., Bramson, J.L., Stojdl, D.F., et al. (2014). Maraba virus as a potent oncolytic vaccine vector. Mol. Ther. *22*, 420–429.
14. Bridle, B.W., Boudreau, J.E., Lichty, B.D., Brunellière, J., Stephenson, K., Koshy, S., Bramson, J.L., and Wan, Y. (2009). Vesicular stomatitis virus as a novel cancer vaccine vector to prime antitumor immunity amenable to rapid boosting with adenovirus. Mol. Ther. *17*, 1814–1821.
15. Le Boeuf, F., Selman, M., Son, H.H., Bergeron, A., Chen, A., Tsang, J., Butterwick, D., Arulanandam, R., Forbes, N.E., Tzelepis, F., et al. (2017). Oncolytic Maraba Virus MG1 as a Treatment for Sarcoma. Int. J. Cancer *141*, 1257–1264.
16. Bridle, B.W., Nguyen, A., Salem, O., Zhang, L., Koshy, S., Clouthier, D., Chen, L., Pol, J., Swift, S.L., Bowdish, D.M.E., et al. (2016). Privileged antigen presentation in splenic B cell follicles maximizes T cell responses in prime-boost vaccination. J. Immunol. *196*, 4587–4595.
17. Sekaly, R.P. (2008). The failed HIV Merck vaccine study: a step back or a launching point for future vaccine development? J. Exp. Med. *205*, 7–12.
18. Barnes, E., Folgori, A., Capone, S., Swadling, L., Aston, S., Kurioka, A., Meyer, J., Huddart, R., Smith, K., Townsend, R., et al. (2012). Novel adenovirus-based vaccines induce broad and sustained T cell responses to HCV in man. Sci. Transl. Med. *4*, 115ra1.
19. Mast, T.C., Kierstead, L., Gupta, S.B., Nikas, A.A., Kallas, E.G., Novitsky, V., Mbewe, B., Pitisuttithum, P., Schechter, M., Vardas, E., et al. (2010). International epidemiology of human pre-existing adenovirus (Ad) type-5, type-6, type-26 and type-36 neutralizing antibodies: correlates of high Ad5 titers and implications for potential HIV vaccine trials. Vaccine *28*, 950–957.
20. Nwanegbo, E., Vardas, E., Gao, W., Whittle, H., Sun, H., Rowe, D., Robbins, P.D., and Gambotto, A. (2004). Prevalence of neutralizing antibodies to adenoviral serotypes 5 and 35 in the adult populations of The Gambia, South Africa, and the United States. Clin. Diagn. Lab. Immunol. *11*, 351–357.
21. Saxena, M., Van, T.T.H., Baird, F.J., Coloe, P.J., and Smooker, P.M. (2013). Pre-existing immunity against vaccine vectors–friend or foe? Microbiology (Reading) *159*, 1–11.
22. Trombetta, E.S., and Mellman, I. (2005). Cell biology of antigen processing in vitro and in vivo. Annu. Rev. Immunol. *23*, 975–1028.
23. Bonifaz, L., Bonnyay, D., Mahnke, K., Rivera, M., Nussenzweig, M.C., and Steinman, R.M. (2002). Efficient targeting of protein antigen to the dendritic cell receptor DEC-205 in the steady state leads to antigen presentation on major histocompatibility complex class I products and peripheral CD8+ T cell tolerance. J. Exp. Med. *196*, 1627–1638.
24. Moriya, K., Wakabayashi, A., Shimizu, M., Tamura, H., Dan, K., and Takahashi, H. (2010). Induction of tumor-specific acquired immunity against already established tumors by selective stimulation of innate DEC-205(+) dendritic cells. Cancer Immunol. Immunother. *59*, 1083–1095.
25. Yang, T.C., Dayball, K., Wan, Y.H., and Bramson, J. (2003). Detailed analysis of the CD8+ T-cell response following adenovirus vaccination. J. Virol. *77*, 13407–13411.
26. Bonifaz, L.C., Bonnyay, D.P., Charalambous, A., Darguste, D.I., Fujii, S., Soares, H., Brimnes, M.K., Moltedo, B., Moran, T.M., and Steinman, R.M. (2004). In vivo targeting of antigens to maturing dendritic cells via the DEC-205 receptor improves T cell vaccination. J. Exp. Med. *199*, 815–824.
27. Dudziak, D., Kamphorst, A.O., Heidkamp, G.F., Buchholz, V.R., Trumpfheller, C., Yamazaki, S., Cheong, C., Liu, K., Lee, H.W., Park, C.G., et al. (2007). Differential antigen processing by dendritic cell subsets in vivo. Science *315*, 107–111.
28. Mukherjee, G., Geliebter, A., Babad, J., Santamaria, P., Serreze, D.V., Freeman, G.J., Tarbell, K.V., Sharpe, A., and DiLorenzo, T.P. (2013). DEC-205-mediated antigen targeting to steady-state dendritic cells induces deletion of diabetogenic CD8$^+$ T cells independently of PD-1 and PD-L1. Int. Immunol. *25*, 651–660.
29. Zhang, P., Andorko, J.I., and Jewell, C.M. (2017). Impact of dose, route, and composition on the immunogenicity of immune polyelectrolyte multilayers delivered on gold templates. Biotechnol. Bioeng. *114*, 423–431.
30. Scott, A.M., Allison, J.P., and Wolchok, J.D. (2012). Monoclonal antibodies in cancer therapy. Cancer Immun. *12*, 14.
31. Liu, M., Wang, X., Wang, L., Ma, X., Gong, Z., Zhang, S., and Li, Y. (2018). Targeting the IDO1 pathway in cancer: from bench to bedside. J. Hematol. Oncol. *11*, 100.
32. Zhao, Y., and Adjei, A.A. (2014). The clinical development of MEK inhibitors. Nat. Rev. Clin. Oncol. *11*, 385–400.
33. Liang, K., Liu, Q., Li, P., Luo, H., Wang, H., and Kong, Q. (2019). Genetically engineered Salmonella Typhimurium: Recent advances in cancer therapy. Cancer Lett. *448*, 168–181.

34. Miliotou, A.N., and Papadopoulou, L.C. (2018). CAR T-cell therapy: a new era in cancer immunotherapy. Curr. Pharm. Biotechnol. *19*, 5–18.

35. Zamarin, D., Holmgaard, R.B., Subudhi, S.K., Park, J.S., Mansour, M., Palese, P., Merghoub, T., Wolchok, J.D., and Allison, J.P. (2014). Localized oncolytic virotherapy overcomes systemic tumor resistance to immune checkpoint blockade immunotherapy. Sci. Transl. Med. *6*, 226ra32.

36. Phan, M., Watson, M.F., Alain, T., and Diallo, J.S. (2018). Oncolytic viruses on drugs: achieving higher therapeutic efficacy. ACS Infect. Dis. *4*, 1448–1467.

37. Bridle, B.W., Stephenson, K.B., Boudreau, J.E., Koshy, S., Kazdhan, N., Pullenayegum, E., Brunellière, J., Bramson, J.L., Lichty, B.D., and Wan, Y. (2010). Potentiating cancer immunotherapy using an oncolytic virus. Mol. Ther. *18*, 1430–1439.

38. Pol, J.G., Acuna, S.A., Yadollahi, B., Tang, N., Stephenson, K.B., Atherton, M.J., Hanwell, D., El-Warrak, A., Goldstein, A., Moloo, B., et al. (2018). Preclinical evaluation of a MAGE-A3 vaccination utilizing the oncolytic Maraba virus currently in first-in-human trials. Oncoimmunology *8*, e1512329.

39. Mahnke, K., Guo, M., Lee, S., Sepulveda, H., Swain, S.L., Nussenzweig, M., and Steinman, R.M. (2000). The dendritic cell receptor for endocytosis, DEC-205, can recycle and enhance antigen presentation via major histocompatibility complex class II-positive lysosomal compartments. J. Cell Biol. *151*, 673–684.

40. Miller, G., Pillarisetty, V.G., Shah, A.B., Lahrs, S., and DeMatteo, R.P. (2003). Murine Flt3 ligand expands distinct dendritic cells with both tolerogenic and immunogenic properties. J. Immunol. *170*, 3554–3564.

41. Nair, A.B., and Jacob, S. (2016). A simple practice guide for dose conversion between animals and human. J. Basic Clin. Pharm. *7*, 27–31.

42. Tacken, P.J., de Vries, I.J., Torensma, R., and Figdor, C.G.G. (2007). Dendritic-cell immunotherapy: from ex vivo loading to in vivo targeting. Nat. Rev. Immunol. *7*, 790–802.

43. Nestle, F.O., Alijagic, S., Gilliet, M., Sun, Y., Grabbe, S., Dummer, R., Burg, G., and Schadendorf, D. (1998). Vaccination of melanoma patients with peptide- or tumor lysate-pulsed dendritic cells. Nat. Med. *4*, 328–332.

44. Hsu, F.J., Benike, C., Fagnoni, F., Liles, T.M., Czerwinski, D., Taidi, B., Engleman, E.G., and Levy, R. (1996). Vaccination of patients with B-cell lymphoma using autologous antigen-pulsed dendritic cells. Nat. Med. *2*, 52–58.

45. Lesterhuis, W.J., Aarntzen, E.H.J.G., De Vries, I.J.M., Schuurhuis, D.H., Figdor, C.G., Adema, G.J., and Punt, C.J.A. (2008). Dendritic cell vaccines in melanoma: from promise to proof? Crit. Rev. Oncol. Hematol. *66*, 118–134.

46. Caminschi, I., Maraskovsky, E., and Heath, W.R. (2012). Targeting dendritic cells in vivo for cancer therapy. Front. Immunol. *3*, 13.

47. Kato, M., McDonald, K.J., Khan, S., Ross, I.L., Vuckovic, S., Chen, K., Munster, D., MacDonald, K.P.A., and Hart, D.N.J. (2006). Expression of human DEC-205 (CD205) multilectin receptor on leukocytes. Int. Immunol. *18*, 857–869.

48. Wen, P.Y., Reardon, D.A., Armstrong, T.S., Phuphanich, S., Aiken, R.D., Landolfi, J.C., Curry, W.T., Zhu, J., Glantz, M., Peereboom, D.M., et al. (2019). A Randomized Double-Blind Placebo-Controlled Phase II Trial of Dendritic Cell Vaccine ICT-107 in Newly Diagnosed Patients with Glioblastoma. Clin. Canc. Res. *25*, 5799–5807.

49. Vonderheide, R.H., Flaherty, K.T., Khalil, M., Stumacher, M.S., Bajor, D.L., Hutnick, N.A., Sullivan, P., Mahany, J.J., Gallagher, M., Kramer, A., et al. (2007). Clinical activity and immune modulation in cancer patients treated with CP-870,893, a novel CD40 agonist monoclonal antibody. J. Clin. Oncol. *25*, 876–883.

50. Bowen, W.S., Svrivastava, A.K., Batra, L., Barsoumian, H., and Shirwan, H. (2018). Current challenges for cancer vaccine adjuvant development. Expert Rev. Vaccines *17*, 207–215.

51. Anandasabapathy, N., Feder, R., Mollah, S., Tse, S.W., Longhi, M.P., Mehandru, S., Matos, I., Cheong, C., Ruane, D., Brane, L., et al. (2014). Classical Flt3L-dependent dendritic cells control immunity to protein vaccine *211*, 1875–1891.

52. Bhardwaj, N., Pavlick, A.C., Ernstoff, M.S., Hanks, B.A., Albertini, M.R., Luke, J.J., Yellin, M.H., Keler, T., Davis, T.A., Crocker, A., et al. (2016). A Phase II Randomized Study of CDX-1401, a Dendritic Cell Targeting NY-ESO-1 Vaccine, in Patients with Malignant Melanoma Pre-Treated with Recombinant CDX-301, a Recombinant Human Flt3 Ligand. J. Clin. Oncol. *34*, 9589, 9589.

53. Henriques, H.R., Rampazo, E.V., Gonçalves, A.J.S., Vicentin, E.C., Amorim, J.H., Panatieri, R.H., Amorim, K.N.S., Yamamoto, M.M., Ferreira, L.C.S., Alves, A.M.B., and Boscardin, S.B. (2013). Targeting the non-structural protein 1 from dengue virus to a dendritic cell population confers protective immunity to lethal virus challenge. PLoS Negl. Trop. Dis. *7*, e2330.

54. Ross, P.J., and Parks, R.J. (2009). Construction and characterization of adenovirus vectors. Cold Spring Harb. Protoc. *2009*, pdb.prot5011.

55. Stojdl, D.F., Lichty, B.D., tenOever, B.R., Paterson, J.M., Power, A.T., Knowles, S., Marius, R., Reynard, J., Poliquin, L., Atkins, H., et al. (2003). VSV strains with defects in their ability to shutdown innate immunity are potent systemic anti-cancer agents. Cancer Cell *4*, 263–275.

56. Diallo, J.S., Vähä-Koskela, M., Le Boeuf, F., and Bell, J. (2012). Propagation, purification, and in vivo testing of oncolytic vesicular stomatitis virus strains. Methods Mol. Biol. *797*, 127–140.

Appendix V – Curriculum Vitae

ANNA JIROVEC

EDUCATION

University of Ottawa, Ottawa, ON

PhD, Microbiology and Immunology **September 2017 – September 2023**
Supervisor: Dr. Jean Simon Diallo
Thesis Title: *Development of a novel prime-boost immunotherapy for dedifferentiated liposarcoma*

Honours Bachelor of Science, Biopharmaceutical Sciences **2013 – 2017**

WORK EXPERIENCE

The Ottawa Hospital Research Institute - Centre for Innovative Cancer Research
PhD Researcher **September 2017 – September 2023**

- Led, designed, and executed several research projects including: 1) Pre-clinical evaluation of an innovative oncolytic virus and dendritic cell targeting vaccine for its application in cancer immunotherapy 2) Immune profiling, and novel target identification and validation in a rare human cancer 3) Pre-clinical implementation of novel cancer targets in vaccine strategies
- Fostered multidisciplinary collaborations with leading sarcoma physicians to enhance translational research outcomes.
- Highly trained in: Cell culture; Cell-based assays (cell viability, proliferation, cytotoxicity assays, cell migration & invasion); Immune assays (ELISA, ELISPOT and multi-colour flow cytometry); Development of standard operation procedures (SOPs); Data management and analysis

Public Health Agency of Canada – National Advisory Committee on Immunization (NACI) Secretariat
Junior Analyst **May 2021 - May 2023**

- Provided immunological expertise and technical analysis to members of the NACI Secretariat during public health emergencies, including COVID-19 and Monkeypox.
- Conducted critical evaluation and provided comprehensive review and analysis of COVID-19 related literature regarding vaccine safety, efficacy, and immunogenicity and communicated findings to key stakeholders to inform federal COVID-19 vaccine recommendations
- Key contributor to an extensive review of literature assessing the likelihood and impact of developing novel mRNA vaccines for current vaccine preventable diseases and pathogens without authorized vaccines in Canada
- Key technical support to two systematic reviews titled “Immunocompromised status as a risk for severe outcomes from COVID-19 in children and adolescents” and “Efficacy, effectiveness and immunogenicity of a reduced HPV vaccination schedule” (unpublished, for internal use only). Performed title/abstract screening, full-text screening, assessing risk of bias using Cochrane-2, data extraction and conflict resolution.

The Ottawa Hospital Research Institute - Centre for Innovative Cancer Research
Research Assistant **May 2017 – August 2017**

- Generated recombinant therapeutic antibody and evaluated its therapeutic efficacy in a murine model of melanoma
- Techniques used: restriction cloning, PCR, Western Blot, cell culture, cell transfection, column antibody purification, animal handling, animal tissue processing, flow cytometry (sample preparation, acquisition and analysis), immunohistochemistry

PUBLISHED MANUSCRIPTS

1. Alluqmani N, **Jirovec A**, Taha Z, Varette O, Chen A, Serrano D, Maznyi G, Khan S, Forbes N, Arulanandam R, Auer RC, Diallo JS. Vanadyl Sulfate-enhanced oncolytic virus immunotherapy mediates the antitumor immune response by upregulating the secretion of pro-inflammatory cytokines and chemokines. *Front Immunol*. 2022;13. doi.org/10.3389/fimmu.2022.1032356

2. Crupi MJF, Taha Z, Janssen TJA, Petryk J, Boulton S, Alluqmani N, **Jirovec A** *et al.* Oncolytic virus driven T-cell-based combination immunotherapy platform for colorectal cancer. *Front Immunol*. 2022;13. Doi:10.3389/fimmu.2022.1029269
3. Taha Z, Arulanandum R, Maznyi G, Godbout E, Carter-Timofte M, Kurmasheva N, Reinert L, Chen A, Crupi M, Boulton S, Laroche G, Phan A, Rezaei R, Alluqmani N, **Jirovec A**, *et al*. Identification of FDA-approved bifonazole as a SARS-CoV-2 blocking agent following a bioreporter drug screen. *Mol Ther*. 2022;30(9):2998-3016. doi:10.1016/j.ymthe.2022.04.025
4. Birdi HK*, **Jirovec A***, Cortés-Kaplan S*, Werier J, Nessim C, Diallo JS, Ardolino M. Immunotherapy for sarcomas: new frontiers and unveiled opportunities. *J Immunother Cancer*. 2021; 9:e001580. doi: 10.1136/jitc-2020-001580
5. Tzelepis F*, Birdi HK*, Jirovec A*, Boscardin S, Tanese de Souza C, Hooshyar M, Chen A, Sutherland K, Parks R, Werier J, Diallo J-S. Oncolytic rhabdovirus vaccine boosts chimeric anti-DEC205 priming for effective cancer immunotherapy. *Molecular Therapy: Oncolytics* 2020;19:240-252 doi.org/10.1016/j.omto.2020.10.007.
6. Arulanandam R, Taha Z, Garcia V, Selman M, Chen A, Varette O, **Jirovec A**, Sutherland K, Macdonald E, Tzelepis F, Birdi H, Alluqmani N, Landry A, Bergeron A, Vanderhyden B, Diallo JS. The strategic combination of trastuzumab emtansine with oncolytic rhabdoviruses leads to therapeutic synergy. *Commun Biol.* 2020;3:254 doi: 10.1038/s42003-020-0972-7
7. Atherton MJ, Stephenson KB, Tzelepis F, Bakhshinyan D, Nikota JK, Son HH, **Jirovec A**, Lefebvre C, Dvorkin-Gheva A, Ashkar AA, Wan Y, Stojdl DF, Belanger EC, Breau RH, Bell JC, Saad F, Singh SK, Diallo JS, Lichty BD. Transforming the prostatic tumor microenvironment with oncolytic virotherapy. *Oncoimmunology.* 2018; e1445459 doi: 10.1080/2162402X.2018.1445459.

*Equal contribution

In Preparation:

1. **Jirovec A**, Flaman A, Godbout E, Serrano D, Werier J, Purgina B, Diallo JS. *Immune profiling of dedifferentiated liposarcoma and identification of novel antigens for targeted immunotherapy*

PRESENTATIONS

Oral Presentations

1. **Anna Jirovec**, Ashley Flaman, Bibianna Purgina, Fanny Tzelepis, Joel Werier, Jean-Simon Diallo. "Tumor Immune Profiling and Identification of Immunotherapeutic Targets in Dedifferentiated Liposarcoma" Toronto International Sarcoma Symposium, May 2023. Toronto, Canada.
2. **Anna Jirovec**, Ashley Flaman, Bibianna Purgina, Fanny Tzelepis, Joel Werier, Jean-Simon Diallo. "Tumor Immune Profiling and Identification of Immunotherapeutic Targets in Dedifferentiated Liposarcoma" COA, CORS & CORA Meeting, June 2022. Quebec City, Canada.
3. **Anna Jirovec**, Ashley Flaman, Bibianna Purgina, Fanny Tzelepis, Joel Werier, Jean-Simon Diallo. "Evaluation of Cancer-testis Antigens in Osteosarcoma and Dedifferentiated Liposarcoma as Targets for Immunotherapy" COA, CORS & CORA Virtual Meeting, June 2020.
4. **Anna Jirovec**, Fanny Tzelepis, Joel Werier, Jean-Simon Diallo. "Evaluation of Cancer-testis Antigens as Targets for Immunotherapy for Sarcoma" University of Ottawa BMI Seminar Day, February, 2019, Ottawa, Canada.
5. **Anna Jirovec**, Fanny Tzelepis, Joel Werier, Jean-Simon Diallo. "Evaluation of Cancer-testis Antigens as Targets for Immunotherapy for Sarcoma" Hans K. Uhthoff Research Day, Division of Orthopaedic Surgery of The Ottawa Hospital. April 2017, Ottawa, Canada.
6. **Anna Jirovec**, Fanny Tzelepis, Joel Werier, Jean-Simon Diallo. "Evaluation of Cancer-testis Antigens as Targets for Immunotherapy for Sarcoma" Ottawa Hospital Research Institute's Summer Student Seminar Series, July-August 2016, Ottawa, Canada.

Poster Presentations

1. **Anna Jirovec***, Ashley Flaman, Bibianna Purgina, Kristy Ng, Andrew Chen, Jean-Simon Diallo, Joel Werier "Tumor Immune Profiling and Identification of Immunotherapeutic Targets in Dedifferentiated Liposarcoma" Connective Tissue Oncology Society (CTOS), November 16-19, 2022, Vancouver, Canada

2. **Anna Jirovec***, Ashley Flaman, Bibianna Purgina, Fanny Tzelepis, Joel Werier, Jean-Simon Diallo "Evaluation of Cancer-testis Antigens in Osteosarcoma and Dedifferentiated Liposarcoma as Targets for Immunotherapy" OHRI Research Day, November 19th, 2020, Ottawa, Canada (virtual meeting)
3. **Anna Jirovec***, Ashley Flaman, Bibianna Purgina, Fanny Tzelepis, Joel Werier, Jean-Simon Diallo "Evaluation of Cancer-testis Antigens in Osteosarcoma and Dedifferentiated Liposarcoma as Targets for Immunotherapy" BioCanRx Summit for Cancer Immunotherapy, October 20-23 2019, Victoria, Canada
4. Ashley Flaman*, **Anna Jirovec**, Bibianna Purgina, Fanny Tzelepis, Joel Werier, Jean-Simon Diallo "Evaluation of Cancer-testis Antigens in Osteosarcoma and Dedifferentiated Liposarcoma as Targets for Immunotherapy" Connective Tissue Oncology Society (CTOS), November 13-16, 2019, Tokyo, Japan.
5. **Anna Jirovec***, Ashley Flaman, Bibianna Purgina, Fanny Tzelepis, Joel Werier, Jean-Simon Diallo "Evaluation of Cancer-testis Antigens in Osteosarcoma and Dedifferentiated Liposarcoma as Targets for Immunotherapy" OHRI Research Day, November 7th 2019, Ottawa, Canada
6. **Anna Jirovec***, Fabrice Le Boeuf, Mohammed Selman, Anabel Bergeron, Andrew Chen, Fanny Tzelepis, Rozanne Arulanandam, John C. Bell, Joel Werier, Hesham Abdelbary, Jean-Simon Diallo. "Oncolytic Immunotherapy for the Treatment of Bone and Soft Tissue Sarcoma" BMI Poster Day, May 3rd, 2018, Ottawa, Canada.
7. **Anna Jirovec***, Fabrice Le Boeuf, Mohammed Selman, Anabel Bergeron, Andrew Chen, Fanny Tzelepis, Rozanne Arulanandam, John C. Bell, Joel Werier, Hesham Abdelbary, Jean-Simon Diallo. "Oncolytic Immunotherapy for the Treatment of Bone and Soft Tissue Sarcoma" Toronto International Sarcoma Symposium, June 7-8 2018, Toronto, Canada
8. **Anna Jirovec***, Fabrice Le Boeuf, Mohammed Selman, Anabel Bergeron, Andrew Chen, Fanny Tzelepis, Rozanne Arulanandam, John C. Bell, Joel Werier, Hesham Abdelbary, Jean-Simon Diallo. "Oncolytic Immunotherapy for the Treatment of Bone and Soft Tissue Sarcoma" Connective Tissue Oncology Society (CTOS), November 2017, Hawaii, US.
9. **Anna Jirovec*,** Fanny Tzelepis, Joel Werier, Jean-Simon Diallo "Evaluation of Cancer-testis Antigens as Targets for Immunotherapy for Sarcoma" BioCanRx Summit for Cancer Immunotherapy, October 27-30, 2018, Banff, Canada
10. **Anna Jirovec*,** Fanny Tzelepis, Joel Werier, Jean-Simon Diallo "Evaluation of Cancer-testis Antigens as Targets for Immunotherapy for Sarcoma" Keystone's Cancer Immunotherapy: Combinations, March 23-27, 2018, Montréal, Canada.
11. **Anna Jirovec***, Fabrice Le Boeuf, Mohammed Selman, Anabel Bergeron, Andrew Chen, Fanny Tzelepis, Rozanne Arulanandam, John C. Bell, Joel Werier, Hesham Abdelbary, Jean-Simon Diallo. "Oncolytic Immunotherapy for the Treatment of Bone and Soft Tissue Sarcoma" Ottawa Hospital Research Institute (OHRI) Research Day, November 7, 2017, Ottawa, Canada.
12. **Anna Jirovec*,** Fanny Tzelepis, Joel Werier, Jean-Simon Diallo "Evaluation of Cancer-testis Antigens as Targets for Immunotherapy for Sarcoma" University of Ottawa's Biopharmaceutical Sciences Honour's Presentation, April 29, 2017, Ottawa, Canada.

AWARDS AND SCHOLARSHIPS

- Mitacs Accelerate CanPRIME PhD Internship (total award value $80,000), May 2019-April 2023
- Admission Scholarship – Graduate Studies, University of Ottawa ($15,000 yearly), 2017-2022
- Travel Award – Poster Presentation, BioCanRx's Summit for Cancer Immunotherapy, 2018
- 2017 BioCanRx Summer Studentship Award, BioCanRx, ($6,000), 2017
- Dean's Honour List, University of Ottawa, 2017
- Third Place Winner, Upper Division - Scinapse USCC National Case Competition, 2016
- IgNITE Case Competition Finalist - Project Pulse Spark Conference, 2016
- Admission Scholarship – Undergraduate Studies, University of Ottawa, ($1,000), 2013

LEADERSHIP & COMMUNITY INVOLVEMENT

First Aid Provider - Canadian Ski Patrol **May 2018 – September 2019**

Work with a team of volunteers to provide on-site advanced first aid to patients at local snow resorts and off-hill events.

Volunteer - Rattle Me Bones **September 2017 – September 2019**

Work with a team of volunteers to organize and advertise the yearly Rattle Me Bones Run. Communicate the importance of basic scientific research to race participants and donors.

Volunteer - Let's Talk Science **September 2017 – September 2018**
Deliver STEM learning activities in both school and community settings. Involved in the Let's Talk Science Cancer Symposium.

Club President and Co-Founder - University of Ottawa Tennis Club **September 2015 – September 2017**
Student club promoting the game of tennis among students, staff, alumni and members of the community. As club president, managed club committee members, handled club finances, actively reached out to potential sponsors to obtain funding, organized and provided structured weekly practices to club members.